

The focus of this book is on the naval submarine body form design and related hydrodynamic effects. This book can help us to optimize the body form such as bow, stern, sailing, L/D ratio et.al. for minimizing the hydrodynamic resistance. Parallel middle body submarines are studied here. The safe and calm depth for earning fully submerged conditions, away from free surface effect and ocean waves are studied too. In this section, some new important criteria for evaluating the seakeeping performance of a naval submarine are presented. The specifications and advantages of the innovative plan and patent of "Moon-Korol" system for minimizing the wave effects on submarine motions at snorting depth are discussed. The wall effect due to moving a submarine close to the sea bottom or a torpedo inside a torpedo tube on the lift and resistance forces is evaluated too.

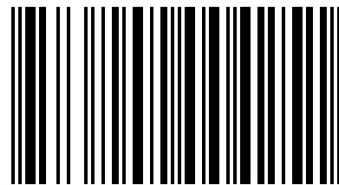
Naval Submarine Body Form Design



Mohammad Moonesun
Yuri Korol

Naval Submarine Body Form Design and Hydrodynamics

M.Moonesun: B.Sc: Naval Architecture and Marine Engineering - Amir Kabir University of Technology (Iran Poly technique University) (1998-2002). M.Sc: Marine Engineering/ Sharif University of Technology-Iran (2002-2004). PhD student: National University of Shipbuilding (NUOS)- Ukraine (2013-2017).



978-620-2-00425-1

Moonesun, Korol

 **LAMBERT**
Academic Publishing

**Mohammad Moonesun
Yuri Korol**

Naval Submarine Body Form Design and Hydrodynamics

**Mohammad Moonesun
Yuri Korol**

**Naval Submarine Body Form Design
and Hydrodynamics**

LAP LAMBERT Academic Publishing

Imprint

Any brand names and product names mentioned in this book are subject to trademark, brand or patent protection and are trademarks or registered trademarks of their respective holders. The use of brand names, product names, common names, trade names, product descriptions etc. even without a particular marking in this work is in no way to be construed to mean that such names may be regarded as unrestricted in respect of trademark and brand protection legislation and could thus be used by anyone.

Cover image: Provided by the author

Publisher:

LAP LAMBERT Academic Publishing

is a trademark of

International Book Market Service Ltd., member of OmniScriptum Publishing Group

17 Meldrum Street, Beau Bassin 71504, Mauritius

Printed at: see last page

ISBN: 978-620-2-00425-1

Copyright © Mohammad Moonesun, Yuri Korol

Copyright © 2017 International Book Market Service Ltd., member of OmniScriptum Publishing Group

All rights reserved. Beau Bassin 2017



Mohammad Moonesun



Yuri Korol

Dedication

We would like to dedicate this work to:

my wife and my family

Yuri

my parents, my wife, Saman and Aseman

Mohammad

and to

All peoples who try for better human life!

Acknowledgement

We started our study about submarine hydrodynamics in 2002 by experimental activities in towing tanks of Iran and Ukraine.

A long-term friendly partnership has taken place between the University of Admiral Makarov of Ukraine and the universities of Iran.

In 2013, Mohammad Moonesun began his study as a Ph.D. student under supervision of Prof. Yuri Korol.

Over the course in four years, several modeling was carried out using the CFD method, and along with that, the towing tank of Admiral Makarov University was used to validate the results.

The researches and the achievements of IHSS (Iranian Hydrodynamic Series of Submarine) which are used in this book, has always been welcomed by Iran's Defense Research Organization.

Our focus in this book is optimizing the body form design of PMB (parallel middle body) submarine by minimizing its resistance.

We thank our friends who helped us to complete this research. Each of them gains 3% of the scientific score of this book: Hosein Dalayeli, Asghar Mahdian, Valeri Nikrasov, Anna Brazhko, Mehran Javadi, Alexander Ursolov, Firouz Ghasemzade, Alexi Yastreba, Alexander Bandarinko, Olha Korneliuk.

Table of Contents

Chapter 1: General concepts for submersible body form	23
1-1- Introduction	23
1-2- Main operational property of naval submarine	26
1-3- Specification of models for CFD Analysis	28
1-4- Provisions of Analysis.....	29
1-5- Analysis of Results.....	31
1-6- Discussion and Conclusion	34
References	36
Chapter 2:	38
Principles of Naval Submarine Shape Form Design	38
2-1- Submarine Shape Coding.....	38
2-1-1- Coding in IHSS.....	38
2-1-2- Ratio L/D :	40
2-1-3- Ratio L_t/L :	41
2-1-4- Ratio L_m/L :	41
2-1-5- Sailing and its parameters:.....	42
2-1-6- Considered limitations in IHSS:	43
2-1-7- Some Samples for IHSS.....	43
2-2- A review on the bare hull form equations of submarine	46
2-2-1- Introduction.....	46
2-2-2- Some important factors in bare hull form design.....	47
2-2-3- Bare hull form equations.....	48
2-3- Power Series Optimization for Submarine bare hull Form	58
2-3-1- Specifications of the Models.....	58
2-3-2- CFD Method of Study.....	60
2-3-3- CFD Results Analysis	62
2-3-4- Review	64
References	65
Chapter 3: Submarine Bow Shape.....	69
3-1- Bow Shape Equations.....	69
3-1-1- Introduction.....	69
3-1-2- Some important factors in bow form design.....	70
3-1-3- Bow form equations.....	71
3-1-4- Specifications of the models for CFD modeling	75
3-1-5- Preparations of CFD analysis.....	79
3-1-6- CFD Analysis.....	81
3-2- Bow Shape Model Test Results at surface motion.....	88
3-2-1-Equipments and Experimental Procedure	89

3-2-2-Results and Discussions.....	91
3-2-3- Investigation of flow.....	94
3-2-4- Review.....	98
References.....	101
Chapter 4: Submarine Stern Shape.....	103
4-1- General Bow Shape Analysis.....	103
4-1-1- Introduction.....	103
4-1-2- General Shapes for the Stern.....	103
4-1-3- Assumptions for the Models for CFD Analysis.....	108
4-1-4- CFD Method of Study.....	113
4-1-6- Review 1.....	118
4-2- Some more Detailed Optimizations.....	119
4-2-1- General Assumptions for the Models.....	119
4-2-2- CFD Result Analysis.....	122
4-2-3- Review 2.....	127
References.....	129
Chapter 5: Optimum L/D.....	130
5-1- Introduction.....	130
5-2- Assumptions for the Models.....	131
5-3- CFD Method of Study.....	132
5-4- CFD Analysis.....	133
5-5- Review.....	135
References.....	137
Chapter 6: Submarine Sailing Shape Design.....	138
6-1- Introduction.....	138
6-2- Specifications of the models.....	140
6-3- Preparations of CFD analysis.....	144
6-4- CFD Analysis.....	147
6-5- Review.....	152
References.....	153
Chapter 7: Engineering Estimation of Submerged Resistance of Submarine.....	154
References.....	156
Chapter 8:.....	157
Evaluation of Naval Submarine Sea keeping Criteria.....	157
8-1- Introduction.....	157
8-2-Ship and submarine sea keeping behavior comparison.....	158
8-3- Sea keeping performance values.....	164
8-4- Review.....	166
References.....	167
Chapter 9: Surfaced Resistance of Submarine.....	169
9-1- Wave making system in submarines at surface condition.....	169
9-2- A review study about critical Froude number in wave making resistance diagram.....	171

9-2-1- Introduction.....	171
9-2-2- Range of Froude number in submarines.....	174
9-2-3-Wave making principles in submarine.....	175
9-2-4- CFD Method.....	177
9-2-5- Experimental Method.....	181
9-2-6- Analytical formula Method.....	182
9-2-7- Review 1.....	183
9-3- Added Resistance of Submarine due to Deck Wetness at Surface Condition.....	185
9-3-1-Freeboard and reserve of buoyancy in submarines.....	185
9-3-2- Assumptions for the Model of CFD analysis.....	187
9-3-3- CFD Results at $h=0$	187
9-3-4- CFD results at $h=0.1m$	192
9-3-5- Review 2.....	193
References.....	195
Chapter 10:.....	196
Fully Submerged Depth for eliminating wave making resistance.....	196
10-1- Introduction.....	196
10-2- Main factors in near surface resistance.....	198
10-3- Assumptions for the Models.....	199
10-4- CFD Results and Analysis.....	202
10-5- Review.....	206
References.....	208
Chapter 11: Fully Submerged Depth at Waves.....	209
11-1- Minimum immersion depth for minimizing the submarine motions under regular waves.....	209
11-1-1- Introduction.....	209
11-1-2- CFD Method of Study.....	211
11-1-3-Specifications of Model.....	212
11-1-4- Domain and Boundary Conditions.....	212
11-1-5- Considered Conditions for Analyses.....	216
11-1-6-Results and Discussion.....	217
11-1-6-1-Method of Extracting the Results.....	217
11-1-6-2-Results.....	218
11-1-6-3-Discussion and Analysis.....	218
11-1-7- Review 1.....	219
11-2- Evaluation of Submarine Motions under Irregular Ocean Waves by Panel Method.....	220
11-2-1- Theory of the Study.....	220
11-2-2-The Model Specifications.....	221
11-2-3- Irregular wave spesifications and wave spectrum.....	223
11-2-4- Modeling by Panel Method and results.....	224
11-3- Moon-Korol system.....	232

References	235
Chapter 12:	238
Underwater Model Test of Submarine in Towing Tank.....	238
12-1- Scaling method for underwater hydrodynamic model test of submarine.....	238
12-1-1-Introduction.....	238
12-1-2- connection of model and strut.....	240
12-1-2-1- At deeply submerged depth	240
12-1-2-2- At snorkel depth.....	241
12-1-3- Case Study	242
12-1-4- Analysis and Conclusion.....	248
12-2- Technical notes on the near surface experiments of submerged submarine	249
12-2-1- Model	249
12-2-2- Strut.....	251
12-2-3- Towing Tank.....	252
12-2-4-Experimental results.....	253
12-2-4-1- At surface draft	253
12-2-4-2- At snorkel draft.....	254
12-2-5- Estimation of induced resistance by CFD method.....	255
12-2-6- Discussion	260
12-2-7- Review	262
References	264
Chapter 13: Bottom effect on the submarine moving close to the sea bottom.....	269
13-1- Introduction	269
13-2-Specifications of the Model.....	269
13-3- CFD Method of Study.....	270
13-4- Bottom effect on the pressure field around a submarine.....	273
13-5- CFD Results Analysis	274
13-6- Analysis of lift force.....	276
13-7- Analysis of resistance force.....	276
13-8- Review.....	278
References	279
Chapter 14: AUV Moving Inside a Water Pipeline.....	280
14-1- Axi-Symmetric Movement.....	280
14-1-1- Introduction.....	280
14-1-2- Specifications of the Model and pipe.....	282
14-1-3- CFD Method of Study.....	284
14-1-3-1- Condition "A"	285
14-1-3-2- Condition "B"	287
14-1-3-3- Condition "C"	287
14-1-4- CFD Results and Analysis	289
14-1-4-1- Condition "A" and "B"	290
14-1-4-2- Condition "C"	295

14-1-5- Review 1	295
14-2- Asymmetric Movement.....	296
14-2-1- Pressure variation.....	297
14-2-2- Review 2	301
References	304

List of Figures

Chapter 1: General concepts for submersible body form

Figure 1: Ghadir class midget submarine (cylindrical middle body)

Figure 2: Total resistance components for bare hull showing effect of change in L/D and prismatic coefficient

Figure 3: Components of resistance

Figure 4: General view of naval submarines operational trajectory

Figure 5: Cyclogram of each part of trajectory path

Figure 6: Situation of fuel capacity and battery charge in start and end of trajectory

Figure 7: Forms of six models

Figure 8: Mesh independency evaluations

Figure 9: Modeling of domain and models

Figure 10: Total resistance coefficients for six models

Figure 11: Pressure resistance coefficients for six models

Chapter 2: Principles of Naval Submarine Shape Form Design

Figure 1: general shapes of submarines

Figure 2: Defined parameters on the submarine geometry

Figure 3: different L/D in submarines and its variation effects on skin and form resistance for selection of optimum point

Figure 4: Dimension limitations in IHSS

Figure 5: Dimensions of the model in case 1 (IHSS.1001565-30108025)

Figure 6: Modeling of case 1 in the Flow Vision software

Figure 7: Dimensions of model in case 2 (IHSS.8336058)

Figure 8: Modeling of case 2 in the Flow Vision software

Figure 9: Parameters of DREA submarine hull

Figure 10: Coordinates on the bow and stern

Figure 11: Tail planes dimensions

Figure 12: Sail plane dimensions

Figure 13: Coordinates and parameters in submarine hull

Figure 14: Effect of n_f and n_a on hull geometry

Figure 15: SSG with sail and control surfaces

Figure 16: Hull form with coefficients of n_a , n_f

Figure 17: Coordinates and parameters in submarine hull

Figure 18: Myring profile

Figure 19: SUBOFF hull and coordinate

Figure 20: Hull form of SUBOFF

Figure 21: Sail form of SUBOFF

Figure 22: General configuration of the models

Figure 23: Configurations of Models

Figure 24: Mesh independency evaluations

Figure 25: (a) Domain and structured grid (b) Very tiny cells near the wall for boundary layer modeling and keeping y^+ about 30 (c) Quarterly modeling because of axis-symmetry

Figure 26: Resistance, resistance coefficients and Semnan coefficients of models

Chapter 3: Submarine Bow Shape

Figure 1: General arrangement of bow part of submarine

Figure 2: Evolution of bow shape of submarines

Figure 3: Parameters of DREA submarine hull

Figure 4: Coordinates and parameters in submarine hull

Figure 5: Coordinates and parameters in submarine hull

Figure 6: Hull form with coefficients of n_a , n_f

Figure 7: Myring profile

Figure 8: SUBOFF hull and coordinate

Figure 9: Configuration of models (stage A)

Figure 10: Configuration of models (stage B)

Figure 11: Mesh independency evaluations

Figure 12: (a) Domain and structured grid (b) Very tiny cells near the wall for boundary layer modeling and keeping y^+ about 30 (c) Quarterly modeling because of axis-symmetry

Figure 13: Pressure distribution over the body

Figure 14: Results of CFD analysis on different bow shape (stage A)

Figure 15: Results of CFD analysis on different bow shape (stage B)

Figure 16: Model setup in the towing tank

Figure 17: The Bows profiles; tango shape (A) and standard shape (B)

Figure 18: Variation of total drags versus Froude Number for tango and standard bows at trip conditions

Figure 19: Variations of total, residual and friction drags as function of Froude number in a two graph for Standard bow (First graph) and Tango bow (Second graph)

Figure 20: Variation of residual resistance coefficient with Froude number for two cases

Figure 21: Variations of hydrodynamic coefficients resistance by Froude number

Figure 22: Flow investigations of waves made by tango and standard bows in around the bow body in different Froude number

Figure 23: Trajectories of the waves from bow to stern of the model with the both types of bows at different velocities

Figure 24: Variations of the portion of the wave making resistance to the total resistance for the model

Chapter 4: Submarine Stern Shape

Figure 1: General arrangement of stern part (inside and outside of the pressure hull)

Figure 2: Reference coordinate and parameters

Figure 3: Several shapes of stern

Figure 4: patched circle in discontinuity area of connection

Figure 5: simple sterns without curvature

Figure 6: sterns that is formed by an ogive of circle

Figure 7: sterns with functional curvature according to the equations of the sections g-k.

Figure 8: (a) Domain and structured grid (b) Very tiny cells near the wall for boundary layer modeling and keeping y^+ about 30 (c) Quarter modeling because of axis-symmetry

Figure 9: pressure contour around the body

Figure 10: wetted area comparison in 14 models

Figure 11: Resistances and Coefficients for 14 models

Figure 12: General configuration of the models- Dimensions unit (m)

Figure 13: Configurations of parabolic models

Figure 14: Configurations of power series models

Figure 15: Configurations of Haack series models

Figure 16: pressure contour around the body

Figure 17: comparison of wetted area for 19 models

Figure 18: Variation of the total resistance, resistance coefficient and Semnan coefficient with K' for Parabolic stern

Figure 19: Variation of the total resistance, resistance coefficient and Semnan coefficient with n_a for Power series stern

Figure 20: Variation of the total resistance, resistance coefficient and Semnan coefficient with C for Haack series stern

Chapter 5: Optimum L/D

Figure1: Some examples of L/D for modern submarines

Figure 2: Resistance component for constant volume versus L/D

Figure 3: Some models with different L/D but constant volume

Figure 4: Structured grid with cubic cells around the cylindrical middle body submarine in the domain

Figure 5: (a) Very tiny cells near the wall for boundary layer modeling and keeping y^+ about 50 (b) Quarterly modeling because of axis-symmetry

Figure 6: Pressure resistance versus L/D variations

Figure 7: Viscose resistance versus L/D

Figure 8: Wetted area versus L/D

Figure 9: Optimum range for L/D for cylindrical middle body submarine

Figure 10: Resistance coefficients versus L/D

Figure 11: Schematic variations of resistance versus L/D

Chapter 6: Submarine Sailing Shape Design

Figure 1: Parameters of DREA submarine hull

Figure 2: Typical mast arrangement inside the sailing

Figure 3: General dimensions of the submarine as base model (A1,B1)

Figure 4: Configuration of models (stage A): changing the fore part of sailing

Figure 5: Configuration of models (stage B) : changing the after part of sailing

Figure 6: (a) Domain and structured grid (b) Very tiny cells near the wall for boundary layer modeling and keeping y^+ about 30 (c) Half modeling due to center plane-symmetry

Figure 7: Pressure distribution over the body

Figure 8: Results of CFD analysis on different sailing's frontal shape (stage A)

Figure 9: Results of CFD analysis on different sailing's aft shapes (stage B)

Chapter 8: Evaluation of Naval Submarine Sea keeping Criteria

Figure 1: Ideal, safe and unsafe draft for sonar efficiency (and hydroplanes) in snorkel condition

Figure 2: Main parameters in submarine architecture for improvement of snorkel mast flooding

Chapter 9: Surfaced Resistance of Submarine

Figure 1: Important factors in wave making resistance

Figure 2: Typical resistance curve for a ship, showing interference effects of waves

Figure 3: variations of wave resistance coefficient versus Froude number for ships

Figure 4: variations of wave resistance coefficient versus Froude number in several depth from sea surface for submarines

Figure 5: Wave making resistance of a tear drop shape submarine

Figure 6: Comparison of wave system in submarines and ships

Figure 7: General configuration of the model

Figure 8: (a) Domain and parts (b) structured grid and tiny cell around free surface (c) Very tiny cells near the wall for boundary layer modeling and keeping y^+ about 30 (d) pressure distribution upon the hull and fluid

Figure 9: Results of CFD analysis for wave making resistance

Figure 10: Variations of hydrodynamic coefficients resistance by Froude number

Figure 11: Comparison the center of bow wave in to the different bow shapes

Figure 12: Diagram of wave making resistance in snorkel depth

Figure 13: Estimation of critical Froude number in submarine

Figure 14: General form of interference of bow and stern waves in critical Froude numbers of A, B, C

Figure 15: Free board, deck and free flooding space in submarine

Figure 16: General configuration of the model

Figure 17: Up view and side view of free surface at $h=0$ m

Figure 18: Resistance versus Froude numbers in fully submerged condition

Figure 19: Resistance versus Froude numbers in free surface condition

Figure 20: Up view and side view of free surface at $h=0.1$ m

Chapter 10: Fully Submerged Depth for eliminating wave making resistance

Figure 1: Relative snorkel depth in naval submarines

Figure 2: General variations of total Resistance coefficient versus submergence depth

Figure 3: General variations of wave making resistance coefficient versus Froude number and depth of submergence

Figure 4: General configuration of the models

Figure 5: (a) Domain and structured grid (b) tiny cell around free surface (c) Very tiny cells near the wall for boundary layer modeling and keeping y^+ about 30 (d) Half modeling because of axis-symmetry and free surface variations

Figure 6: Diagrams of each part of resistance for Model-A

Figure 7: Variations of total resistance versus depth in Model-A

Figure 8: Diagrams of each part of resistance for Model-B

Figure 9: Variations of total resistance versus depth in Model-B

Figure 10: Milestone and Fully submergence depth in high and low Froude numbers

Chapter 11: Fully Submerged Depth at Waves

Figure 1: Orbital motion in waves

Figure 2: General configuration of the model Persia-110

Figure 3: Wave simulation by CFD tools (Flow-3D)

Figure 4: Linear wave definition

Figure 5: Evaluation of time history of pitch angle in 100 seconds for condition $h=D$

Figure 6: time history of pitch angle

Figure 7: gradient of RMS pitch versus submergence depth of submarine

Figure 8: General form of modeled naval submarine

Figure 9: 3D model with body lines in Maxsurf

Figure 10: Meshing the body in Panel Method

Figure 11: Dynamic simulation of submarine under non-linear wave (JONSWAP spectrum)

Figure 12: Polar diagram at several depths

Figure 13: RMS values of motions at different depths

Figure 14: Schematic of Moon-Korol snorting system

Figure 15: Inside arrangement of Snorting Buoy: ballast tank is used for floating the buoy and solid ballast (lead) for providing stability and upright standing

Chapter 12: Underwater Model Test of Submarine in Towing Tank

Figure 1: Schematic variations of the viscous pressure resistance coefficients versus Reynold's number

Figure 2: Schematic variations of the frictional resistance coefficients versus Reynold's number

Figure 3: Deeply submerged model test

Figure 4: Model test at snorkel condition

Figure 5: Other position of connections

Figure 6: Submarine model test in towing tank (Two strut arrangement)

Figure 7: Dimensions of the model in case 1

Figure 8: Modeling of case 1 in the Flow Vision software

Figure 9: The diagram of variations of total resistance coefficients versus Reynold's numbers in case 1

Figure 10: The diagram of variations of viscous pressure resistance coefficients versus Reynold's numbers in case 1

Figure 11: Dimensions of model in case 2

Figure 12: The diagram of variations of total resistance coefficients versus Reynold's numbers in case 2

Figure 13: The diagram of variations of viscous pressure resistance coefficients versus Reynold's numbers in case 2

Figure 14: Schematic shape of the test stand

Figure 15: The diagram of variations of resistance coefficients versus Reynold's numbers for model test in towing tank

Chapter 13: Bottom effect on the submarine moving close to the sea bottom

Figure 1: General configuration of the models

Figure 2: Mesh independency evaluations

Figure 3: (a) Domain and structured grid (b) Very tiny cells near the wall for boundary layer modeling and keeping y^+ about 30 (c) Half modeling because of symmetry

Figure 4: Pressure field around a submarine (far from the sea bottom)

Figure 5: Negative pressure (suction) area at the effect of the sea bottom

Figure 6: Variation of hydrodynamic coefficients versus distance from sea bottom

Figure 7: Fit the best curves to the variation of CL versus H^*

Part 14: AUV Moving Inside a Water Pipeline

Figure 1: Schematic of pipeline inspection System and sample AUV (PICTAN)

Figure 2: (a) Boundary layer and velocity distribution inside a pipe in laminar flow (b) Difference in laminar and turbulent flow

Figure 3: General configuration of the models

Figure 4: Cross section area of AUV and pipe (hatched area: water between AUV and pipe)

Figure 5: Condition A: (a) Domain and general dimensions (b) structured grid and Very fine cells near the wall for boundary layer modeling

Figure 6: Condition B: Free stream modeling (without pipe wall effects)

Figure 7: Condition C: Entrance length condition for $d/D=4$

Figure 8: Pressure variation in several ratios of d/D

Figure 9: Total resistance and pressure resistance of AUV in several different d/D and speed

Figure 10: The ratio of pressure resistance to total resistance

Figure 11: Ratio of total resistance to free stream resistance

Figure 12: Out of axis movement of the AUV inside the pipe

Figure 13: Out of axis modeling in Flow Vision

Figure 14: Pressure variation in several ratios of out of axis "e" for $d/D=4$ and $v=3\text{m/s}$

Figure 15: Diagram of hydrodynamic forces in $d/D=4$

Figure 16: Diagram of hydrodynamic forces in $d/D=12$

List of Tables

Chapter 1: General concepts for submersible body form

Table 1: Comparison of wetted surface area in circle and square cylinder

Table 2: Total resistance coefficients

Table 3: Pressure resistance coefficients

Table 4: Comparison between total resistance coefficients

Table 5: Comparison between pressure resistance coefficients

Chapter 2: Principles of Naval Submarine Shape Form Design

Table 1: Total resistance coefficient of case 1 by CFD method

Table 2: Total resistance coefficient of case 2 by CFD method

Table 3: Main Submarine Dimensions (meter)- IHSS.8891666-34167525

Table 4: Results of model test in towing tank

Table 5: Selected values for C_p and C_s

Table 6: Miring parameters for STD REMUS

Table 7: Main assumptions of models

Table 8: Specifications of 11 Models

Table 9: Resistance, resistance coefficients and Semnan coefficients of models

Chapter 3: Submarine Bow Shape

Table 1: Main assumptions of models

Table 2: Models of stage A

Table 3: Models of stage B according to Eq.2

Table 4: Resistance components of Models in stage (A)

Table 5: Resistance components of Models in stage (B)

Table 6: Specification of Models in stage (A)

Table 7: Specification of Models in stage (B)

Table 8: A summary of scale model characteristics

Chapter 4: Submarine Stern Shape

Table 1: Main assumptions of models

Table 2: specifications of 14 models

Table 3: Settings of the simulation

Table 4: Resistances and Coefficients for 14 models

Table 5: Main assumptions of the models

Table 6: specifications of 19 models

Table 7: Total resistance, resistance coefficient (based on wetted area surface) and Semnan coefficient of the models

Chapter 5: Optimum L/D

Table 1: Variations of wetted area versus L/D for a simple cylinder

Table 2: Main assumptions of models

Table 3: Resistance and resistance coefficient versus values of L/D

Chapter 6: Submarine Sailing Shape Design

Table 1: Main assumptions of models

Table 2: Models of Stage A (bow shapes)

Table 3: Models of stage B (stern shapes)

Table 4: Settings of the simulation

Table 5: Resistance components of Models in stage (A)

Table 6: Resistance components of Models in stage (B)

Table 7: Specifications for Models in stage (A)

Table 8: Specification of Models in stage (B)

Chapter 9: Surfaced Resistance of Submarine

Table 1: Maximum Froude number in some naval submarines

Table 2: Wave system around a submarine

Table 3: Main assumptions of models

Table 4: Main assumptions of models

Table 5: Added frictional resistance due to deck wetness

Chapter 10: Fully Submerged Depth for eliminating wave making resistance

Table 1: Main assumptions of models

Table 2: Simulation depth of Models

Table 3: Resistance of Model-A in several depths

Table 4: Resistance of Model-B in several depths

Chapter 11: Fully Submerged Depth at Waves

Table 1: Settings of simulation

Table 2: Considered conditions for analyses

Table 3: RMS values for considered conditions

Table 4: Comparison between Strip theory and Panel method

Table 5: mass distribution of the simulated model

Table 6: hydrostatic properties of the model

Table 7: Characteristics of JONSWAP irregular wave

Table 8: descriptions of surfaced or submerged depth

Table 9: Sample result at snorkel depth and encountered wave angle of 180

Table 10: Results for the main headings of 0, 90 and 180 degrees

Chapter 12: Underwater Model Test of Submarine in Towing Tank

Table 1: Total resistance coefficient of case 1 by CFD method

Table 2: Viscous pressure resistance coefficient of case 1 by CFD method

Table 3: Total resistance coefficient of case 2 by CFD method

Table 4: Viscous pressure resistance coefficient of case 2 by CFD method

Table 5: Main Submarine Dimensions (meter)

Table 6: Results of model test in towing tank

Table 7: Considered conditions for analyses in two drafts: surface draft and near surface

Table 8: Resistance in depth of 100mm

Table 9: Settings of CFD simulation

Table 10: Comparison of resistance

Table 11: Initial CFD results of resistance

Table 12: Modified CFD results of resistance

Table 13: Modified experimental results

Chapter 13: Bottom effect on the submarine moving close to the sea bottom

Table 1: Settings of the simulation

Table 2: Values of resistance and lift in distance from sea bottom

Part 14: AUV Moving Inside a Water Pipeline

Table 1: Description of considered conditions

Table 2: Settings of the simulation (inside the pipe)

Table 3: Values of total resistance and pressure resistance

Table 4: Comparison of results for $d/D=4$

Chapter 1: General concepts for submersible body form

1-1- Introduction

There are some rules and concepts about submarines and submersibles body form design. There is an urgent need for understanding the basis and concepts of form design. Submarine form design, similar to the form design of other marine vehicles and ships, is strictly depended on the hydrodynamic. Submarines encounters limited energy source in the submerged navigation and because of that, the minimum resistance is vital for the design of submarine hydrodynamic. The technical concepts about submarine hydrodynamic design have widely been discussed in Ref. books[1-9] and Ref. papers [10-17].

In recent years, some extended studies have been performed by M.Mooneson and Y.Korol on the naval submarine body form design [18-21]. These studies are based on CFD and experimental methods. In addition, the form design is depended on the internal architecture and general arrangements of submarine. Related materials about general arrangement in naval submarines are presented in [1-5,22] and discussions about general form of submarines are found in [23-27]. Ref.[27] is a unique reference evaluating the resistance (drag) coefficient of general geometric shapes for submarines. Convergence between hydrodynamic needs and architecture requirements are vital for determination of overall form design of a submarine. Submarines have two major categories for hydrodynamic form: tear drop form and cylindrical middle body (Fig.1). Tear drop form has a lot of difficulties in construction and cost more than cylindrical shape, but it has unique advantages in hydrodynamics. The most real naval submarines and ROVs, such as the basic form in IHSS series, have cylindrical middle body form[28,29]. Gertler in 1950 reported the results of resistance experiments on a systematic series of 24 streamlined bodies of revolutions which led to the base of choice for Albacore submarine form. This study showed five important geometrical parameters: fineness ratio, prismatic coefficient, nose radius, tail radius and the position of maximum section (by maximum width at about a quarter length from the bow) [9]. The optimum value of C_{pr} is approximately 0.61 [2]. Figure 2 shows the effect of L/D and prismatic coefficient on the submarine resistance. In Collins submarine, C_{pr} is 0.8. In Albacore, C_{pr} is 0.65 with L/D of 7.723 [9]. Therefore, optimum L/D depends on the prismatic coefficient. Submarines have two modes of navigation: surfaced mode and submerged mode. In the surfaced mode of navigation, the energy source limitation is less than that for submerged mode. Therefore, the design base of required power for propulsion engines is the submerged mode for the real naval submarines. The focus on this chapter is on the resistance at fully submerge mode without free surface effects. The resistance of a submarine will have a major influence

on its highest possible speed and endurance. In addition, high resistance will affect the acoustic signature due to: 1) increased flow noise 2) the increased propulsion power to achieve the required speed [2]. The components of resistance of a submarine are similar to that of a ship. It is observed in Fig.3 that the magnitude of the components depends on the hull shape and proximity with the water surface [2]. The friction form resistance is produced because the flow velocity is not the same as that over a flat plate. In some places, it will be higher or lower. This is a very small component of resistance [2]. The form resistance is due to viscose pressure variations, which depended on the body form such as flow separation on the stern part. The induced resistance is due to the proximity of two bodies such as main hull and sailing or hydroplanes. The wave making resistance is zero for deeply submerged submarine. Basically, frictional resistance has the most important role in submarine resistance and is directly related to the wetted surface. The circular section has the lowest wetted surface compared with other section forms for a given contained volume. The reason is explained by an example in Tab.1. Because of that, for a given displacement, the wetted area of a tanker ship is more than a submarine. The block coefficient of a circular cylinder is: $C_B = \nabla / B.T.L = (\pi.R^2.L) / (2R.2R).L = \pi/4 = 0.785$. Therefore, the block coefficient of main hull of all submarines is less than 0.785 due to curvature of the bow and stern of a submarine.



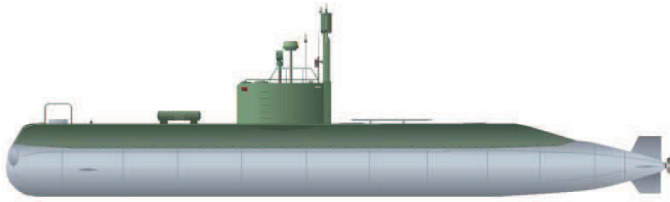


Figure 1: Ghadir class midjet submarine (cylindrical middle body)

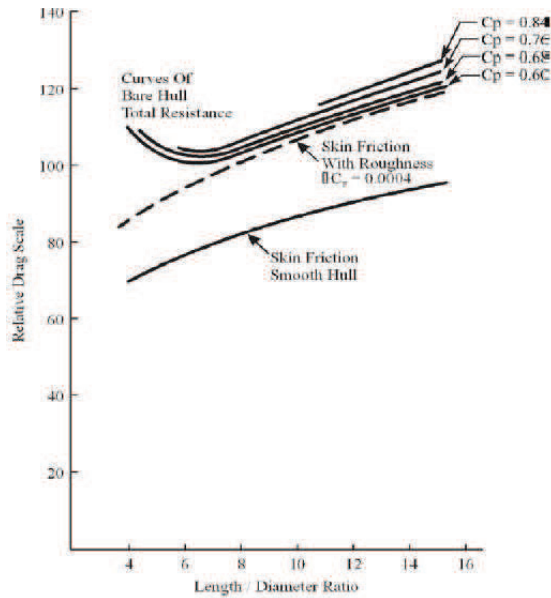


Figure 2: Total resistance components for bare hull showing effect of change in L/D and prismatic coefficient [32]

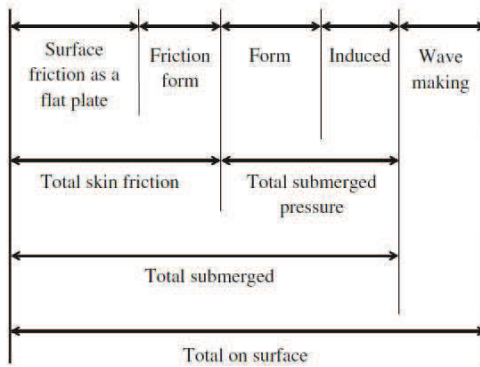


Figure 3: Components of resistance [2]

Table 1: Comparison of wetted surface area in circle and square cylinder

	L (m)	Section dim. (m)	Volume (m ³)	Wetted area (m ²)
circular cylinder	1	D= 1	0.785	3.14
square cylinder	1	a=0.886	0.785	3.55

1-2- Main operational property of naval submarine

There are some important properties which define the capabilities of naval submarines such as: IR (Indiscretion Ratio), noise level, timing in torpedo firing, maximum diving depth, duration, endurance, range (maximum distance of movement), maximum submerge speed, maximum surface speed, cruise speed (submerge economic speed) and number of carried torpedoes. Anyway, IR is the most important operational parameter for naval submarine and is the main difference between ship and submarine. The definition of IR is:

$$\text{Indiscretion Ratio} = \frac{\text{snorting time}(t1)}{\text{snorting time}(t1) + \text{submerged time}(t2)}$$

For ships, IR=1 and for ideal and nuclear submarines is near IR=0. This ratio for ordinary diesel-electric submarines is about 0.1 and for submarines

equipped with AIP system (such as fuel cell) is about 0.01–0.02. It is independent of the tonnage and dimensions of submarines. For estimating the snorting time (t_1), needs to know the total power includes hotel load and propulsion power. The parameter IR, covers some other parameters such as underwater cruise speed, range, duration, propulsion efficiency and resistance and power. The fewer amount of energy consumption, meant longer duration and range and better IR. Due to that, the minimizing the submerged resistance is very important. For better understanding the matter, the cyclogram of a naval submarine should be described. General operational trajectory of naval submarines has three parts: departure, patrol and return which constitute total range and duration (Fig.4).

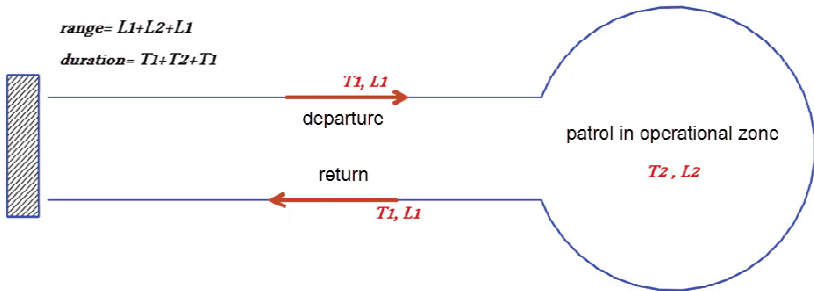


Figure 4: General view of naval submarines operational trajectory

Each part of movement includes movement in the submerged and snorkel depth. It is necessary to note that there is not "surface travel" at standard definition of submarine cyclogram because in real operational conditions, it is forbidden for naval submarines to surface navigate. The cyclogram of each part of the trajectory path is shown in Fig.5. The base submerged speed is cruise or economic speed. The maximum submerged speed is usually considered for emergency and escape conditions. For earning the maximum range and duration it is necessary to navigate at economic speed and optimum battery usage. The standard assumption for calculating the total energy storage and maximum achievable range and duration, is loading full fuel storage and full charged batteries at the start point on the port, and zero fuel storage and zero battery charge at the end point of travel (however, it is not acceptable in operational point of view to have zero energy storage) (Fig.6).

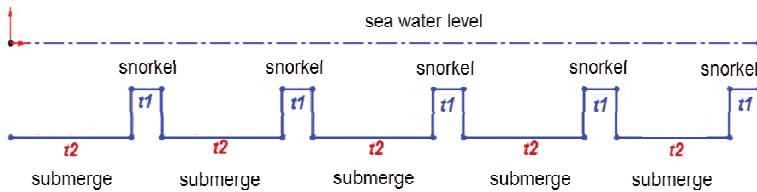


Figure 5: Cyclogram of each part of trajectory path

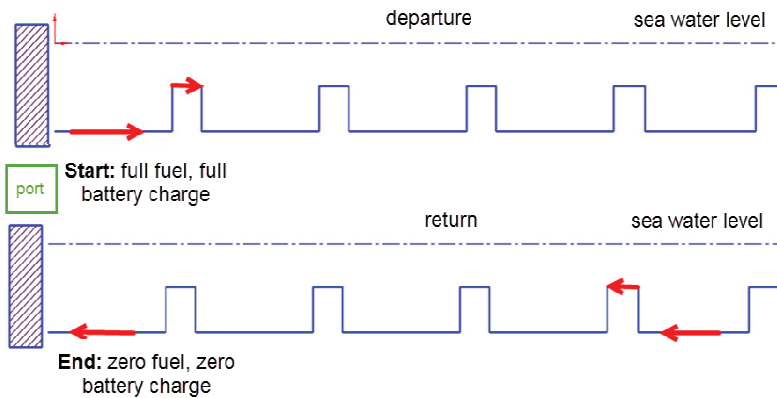


Figure 6: Situation of fuel capacity and battery charge in start and end of trajectory

1-3- Specification of models for CFD Analysis

In this section, the general forms of submersibles are studied for six models [21]. There are six models with torpedo shape without any appendages. For all models, according to Fig.7, there is a constant length equal to 10 meters, constant diameter equal to 2 meters and constant L/D equal to 5 but different volume. In all models, bow length is 2 meters, and stern length is 3 meters. Middle part is a cylinder with 5 meters length. Model 1 is a simple cylinder without a tapered bow and stern that shows the most resistance coefficient and the worst selection. Model 2 is a cylinder but with a conical stern. Model 3 is a cylinder but with an elliptical bow. Model 4 has a conical bow and stern.

Model 5 has an elliptical bow and conical stern such as today submarines. Model 6 is similar to Model 5 but with a curved stern instead of conical stern. This curvature is provided by sector of a circle with radius of 5 meters. This sector is tangent to the cylinder without any discontinuity.

1-4- Provisions of Analysis

This analysis is done by Flow Vision (V.2.3) software based on CFD method and solving the RANS equations. Generally, the validity of the results of this software has been done by several experimental test cases, and nowadays this software is accepted as a practicable and reliable software in CFD activities. For modeling these cases in this chapter, Finite Volume Method (FVM) is used. A structured mesh with cubic cell has been used to map the space around the submarine. For modeling the boundary layer near the solid surfaces, the selected cell near the object is tiny and very small compared to the other parts of domain. The turbulence model is K-Epsilon and y^+ is considered equal to 50. The considered flow is incompressible fluid (fresh water) in 20 degrees centigrade.

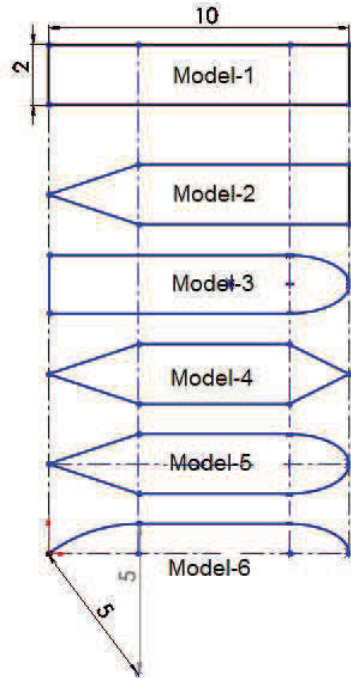


Figure 7: Forms of six models

For selecting the proper quantity of the cells, for one certain form (Model 6 with $v=1$ m/s), five different amount of meshes were selected and the results were compared insofar as the results remained almost constant after 0.4 millions meshes, and it shows that the results are independent of meshing (Fig.8).

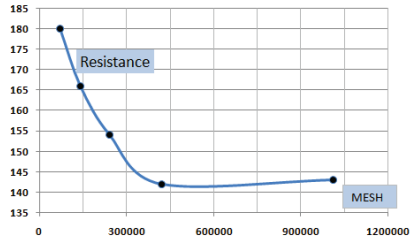


Figure 8: Mesh independency evaluations

In all modeling the mesh numbers are considered more than 0.6 millions. For the selection of suitable iteration, it was continued until the results were almost constant with variations less than one percent, which shows the convergence of the solution. All iterations are continued to more than one millions that are depended on the amount of meshes. In this domain, there are inlet (with uniform flow), Free outlet, Symmetry (in the four faces of the box) and Wall (for the body of submarine). Dimensions of cubic half domain are 50m length (equal to 5L), 4m beam (half beam equal to 4R) and 8m height (equal to 8R). Pay attention that because of Axi-symmetric form, the only half or quarter of a body can be modeled. Meanwhile, the study has shown that the half beam equal to 4R can be acceptable. Here, there are little meshes in far from the object. The forward distance of the model is equal to L and after distance is 3L in the total length of 5L (Fig.9). For validation of the results, there aren't any experimental results but according to Ref.[27,30], the resistance coefficient for simple cylinder is 0.89 and according to CFD results, it is earned 0.81. It shows 8.9% difference and error, which can be acceptable in numerical methods. The range of velocity for modeling is selected on the base of Reynolds number. Ref.[31] showed that resistance coefficients after Reynolds 5 millions remain almost constant. Because of that, the velocities are so selected that 3 points before 5 millions, one point on the 5 millions and others, after that can be shown on the diagrams. The velocities in m/s are: 0.02, 0.05, 0.1, 0.5, 0.7, 1, 2 and 3.

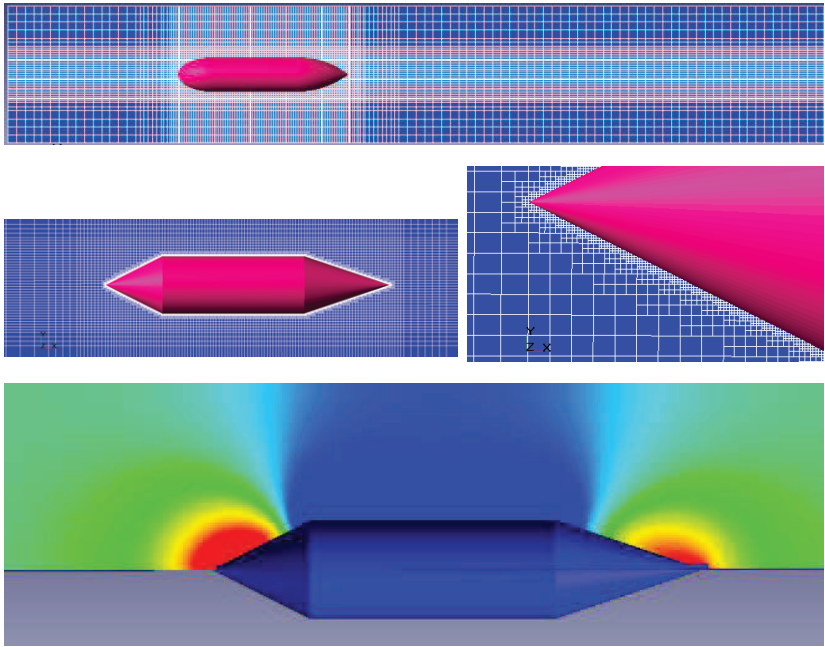


Figure 9: Modeling of domain and models

1-5- Analysis of Results

The total resistance is equal to summation of frictional and pressure resistance. In Flow Vision software, the total resistance and pressure resistance is presented. Frictional resistance is equal to total resistance minus pressure resistance. Similar to this subject relies on coefficients. In Fig.10, the diagrams of total resistance versus Reynolds number are presented for all six models. All resistance coefficients are based on cross section area equal to 3.14 square meters. Logically, the first model has the most resistance coefficient, and sixth model has a minimum coefficient but the amount of differences between models are important and considerable. Attention on these differences can show the logic of submarine form design. Now questions in these fields can be answered, for example: Why we cannot use sharp shape for submarines? Why the stern should be conical? Why the bow should be curved? Why the curved stern is better than simple conical stern? and so on.

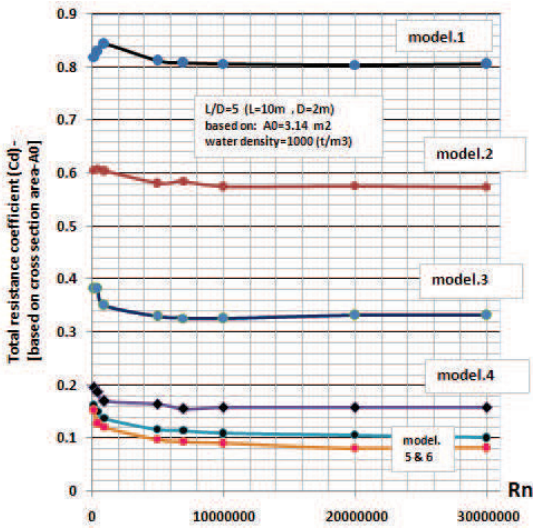


Figure 10: Total resistance coefficients for six models

Diagrams of the pressure resistance coefficients versus Reynolds numbers are presented in Fig.11. Pressure resistance is a function of the form of the object (submarine) so that it names "form resistance". Here, assumption is in viscid fluid. Viscosity effect is regarded in friction resistance. As mentioned before, all coefficients after Reynolds 5 millions are almost constant.

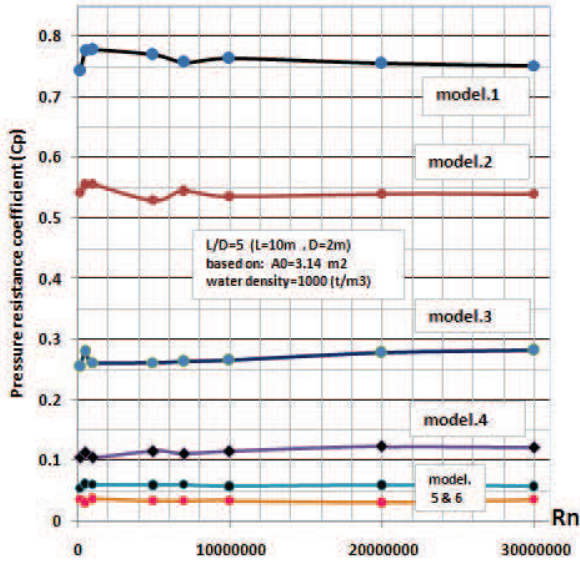


Figure 11: Pressure resistance coefficients for six models

For better comparison between the coefficients, all total and pressure resistance coefficients are presented in Tab.2&3.

Table 2: Total resistance coefficients

V (m/s)	Rn	Model-1	Model-2	Model-3	Model-4	Model-5	Model-6
0.02	200000	0.819	0.605	0.382	0.195	0.162	0.153
0.05	500000	0.829	0.606	0.382	0.188	0.150	0.127
0.1	1000000	0.843	0.604	0.350	0.169	0.138	0.120
0.5	5000000	0.812	0.581	0.329	0.164	0.117	0.097
0.7	7000000	0.808	0.584	0.326	0.155	0.114	0.093
1	10000000	0.807	0.575	0.326	0.158	0.109	0.090
2	20000000	0.805	0.576	0.331	0.158	0.105	0.081
3	30000000	0.806	0.574	0.332	0.159	0.101	0.082

Table 3: Pressure resistance coefficients

V (m/s)	Rn	Model-1	Model-2	Model-3	Model-4	Model-5	Model-6
0.02	200000	0.742	0.541	0.255	0.105	0.054	0.035
0.05	500000	0.776	0.555	0.280	0.114	0.061	0.031
0.1	1000000	0.778	0.557	0.262	0.106	0.060	0.036
0.5	5000000	0.770	0.530	0.262	0.116	0.059	0.034
0.7	7000000	0.757	0.545	0.264	0.111	0.060	0.034
1	10000000	0.764	0.535	0.266	0.116	0.058	0.034
2	20000000	0.756	0.540	0.278	0.123	0.059	0.031
3	30000000	0.752	0.540	0.283	0.123	0.057	0.036

1-6- Discussion and Conclusion

There are many huge different between the coefficients in model 1 and model 6. Ordinary form of today submarines are similar to model 6, and this model is selected as a base model. With comparing these results, it can be understood the concepts of form design of submarines. Table 4 shows the total resistance coefficients for all six models. Remember that L, D and then L/D for all models are constant. It shows that coefficient of model 1 is 10 times of model 6. By adding a conical stern in model 2, the resistance coefficient becomes 7.19 times of model 6 that means 28% lesser resistance from model 1. According to model 4, by adding a conical bow to model 2, the resistance becomes 80% fewer than model 2. It shows the important role of bow shape. By adding the elliptical bow to the simple cylinder, according to model 3, the resistance becomes 59% lesser than model 1. It shows that curved bow has a significant role in reducing the resistance. If the model has an elliptical bow with conical stern as model 5, the resistance coefficient becomes 70% fewer than model 3 and 88% fewer than model 1. Finally, the model 6, has the least resistance coefficient that shows the best design in the hull form.

Table 4: Comparison between total resistance coefficients

model	Ct	Times
Model-1	0.8	10
Model-2	0.575	7.19
Model-3	0.33	4.125
Model-4	0.16	2
Model-5	0.1	1.25
Model-6	0.08	1

Table 5: Comparison between pressure resistance coefficients

model	Cp	Times
Model-1	0.76	25.33
Model-2	0.54	18
Model-3	0.27	9
Model-4	0.12	4
Model-5	0.06	2
Model-6	0.03	1

Table 5 shows the comparison between pressure resistance coefficients. The intensities of variations of pressure resistance coefficients are more than viscose and total resistance. In conclusion, it can be concluded that:

- 1) Bow and stern of submarine should be tapered gradually (by comparison between models 1 and other models).
- 2) Sharp narrow bow isn't a good selection, but a blunt form such as an elliptical bow is recommended (by comparison between models 4 and 5).
- 3) Curved stern is better than conical stern (by comparison between models 5 and 6).
- 4) Effects of the bow on the resistance is strongly more than the effect of stern (by comparison between models 2 and 4).
- 5) Curved bow (such as elliptical) and curved stern (such as a sector of circle or parabolic) with cylindrical middle part can be good recommendation for submarines and submersibles (by comparison between models 6 and other models).

Nomenclature

L	overall length of hull	C_t	Total resistance coefficient
D	maximum diameter of the outer hull	C_p	Pressure resistance coefficient
R	maximum radius of the outer hull	C_{pr}	Prismatic coefficient
V	speed of water in m/s	C_f	Frictional resistance coefficient
A₀	Cross section area of model= 3.14 m ²	IHSS	Iranian Hydrodynamic Series of Submarines
R_n	Reynolds number	CFD	Computational Fluid Dynamics

References

- [1] Jackson H A, "Submarine Design Notes", (Massachusetts Institute of Technology).1982, pp. 520
- [2] Renilson, M., (2015), Submarine Hydrodynamics, Springer, pp.45-89.
- [3] Burcher R, Rydill L J, "Concept in submarine design", (The press syndicate of the University of Cambridge., Cambridge university press), 1998, pp. 295
- [4] A group of authorities, "Submersible vehicle system design", The society of naval architects and marine engineers, 1990.
- [5] Ulrich Gabler, "Submarine Design", Bernard & Graefe Verlag, 2000.
- [6] Y.N.Kormilitsin, O.A.Khalizev, "Theory of Submarine Design", Saint-Petersburg State Maritime Technology University, 2001
- [7] L.Greiner, "Underwater missile propulsion : a selection of authoritative technical and descriptive papers", 1968.
- [8] P.N.Joubert, "Some aspects of submarine design: part 1: Hydrodynamics", Australian Department of Defence, 2004.
- [9] P.N.Joubert, "Some aspects of submarine design: part 2: Shape of a Submarine 2026", Australian Department of Defence, 2004.
- [10] M.Moonesun, M.Javadi, P.Charmdooz, U.M.Korol, "evaluation of submarine model test in towing tank and comparison with CFD and experimental formulas for fully submerged resistance", Indian Journal of Geo-Marine Science, vol.42(8), December 2013, pp.1049-1056.
- [11] Mackay M, "The Standard Submarine Model: A Survey of Static Hydrodynamic Experiments and Semiempirical Predictions", Defence R&D Canada, June 2003
- [12] Roddy, R., 1990. "Investigation of the stability and control characteristics of several configurations of the DARPA SUBOFF model (DTRC Model 5470) from captive-model experiments". Report No. DTRC/SHD-1298-08, September.
- [13] Mohammad Moonesun, Yuri Mikhailovich Korol, Sajjad Ardeshiri, Asghar Mahdian4, Ataollah Gharechahi, Davood Tahvildarzade, Alexander Ursalov, Evaluation of Naval Submarine Seakeeping Criteria, Journal of Scientific and Engineering Research, 2015, 2(4):45-54.
- [14] Prester Timothy, "Verification of a Six-Degree of Freedom Simulation Model for the REMUS Autonomous Underwater Vehicle", University of California at Davis, 1994
- [15] Praveen.P.C, Krishnankutty.P, " study on the effect of body length on hydrodynamic performance of an axi-symmetric underwater vehicle", Indian Journal of Geo-Marine Science, vol.42(8), December 2013, pp.1013-1022.
- [16] K.N.S.Suman, D.Nageswara Rao, H.N.Das, G.Bhanu Kiran, "Hydrodynamic Performance Evaluation of an Ellipsoidal Nose for High Speed Underwater Vehicle", Jordan Journal of Mechanical and Industrial Engineering (JJMIE), Volume 4, Number 5, November 2010, pp.641-652.
- [17] J.K.Stenars, "Comparative naval architecture of modern foreign submarines", Massachusetts Institute, 1988.
- [18] Mohammad Moonesun, Yuri Mikhailovich Korol, Hosein Dalayeli, Davood Tahvildarzade, Mehran Javadi, Mohammad Jelokhaniyan, Asghar Mahdian, Optimization on Submarine Stern Design, Journal of Engineering for the Maritime Environment (Ins. Mechanical Engineering-Part M, SAGE), February 2016, pp.1-11.
- [19] Mohammad Moonesun1, Yuri Mikhailovich Korol, Valeri A Nikrasov, Alexander Ursalov, Anna Brajhko, CFD analysis of the bow shapes of submarines, Journal of Scientific and Engineering Research, 2016, 3(1):1-16.

- [20] Mohammad Moonesun, Asghar Mahdian, Yuri Mikhailovich Korol, Mehdi Dadkhah, Mehrshad Moshref Javadi, Anna Brazhko, Optimum L/D for Submarine Shape, Indian Journal of Geo-Marine Sciences, Vol. 45(1), January 2016, pp. 38-43
- [21] Mohammad Moonesun, Asghar Mahdian, Yuri Mikhailovich Korol, Mehdi Dadkhah, Mehrshad Moshref Javadi, Concepts in Submarine Shape Design, Indian Journal of Geo-Marine Sciences, Vol. 45(1), January 2016, pp. 100-104.
- [22] M.Moonesun, P.Charmdooz, "General arrangement and naval architecture aspects in midget submarines", 4th International Conference on Underwater System Technology Theory and Applications 2012 (USYS'12), Malaysia.
- [23] Budiyo.A, " Advances in unmanned underwater vehicles technologies: modeling, control and guidance perspectives ", Indian Journal of Marine Science, vol.38(3), September 2009, pp.282-295.
- [24] J.M.Lee, J.Y.Park, B.Kim, H.Baek, , " Development of an Autonomous Underwater Vehicle IsiMI6000 for deep sea observation ", Indian Journal of Geo-Marine Science, vol.42(8), December 2013, pp.1034-1041.
- [25] Lisa Minnick, "A Parametric Model for Predicting Submarine Dynamic Stability in Early Stage Design", Virginia Polytechnic Institute and State University, 2006
- [26] D. Alemayehu, R.B.Boyle, E.Eaton, T.Lynch, J.Stepanchick, R.Yon," Guided Missile Submarine SSG(X)", SSG(X) Variant 2-44, Ocean Engineering Design Project, AOE 4065/4066, Virginia Tech Team 3 ,Fall 2005 – Spring 2006.
- [27] Hoerner, S.F., (1965), Fluid Dynamic Drag.
- [28] Iranian Defense Standard (IDS- 857), " Hydrodynamics of Medium Size Submarines", 2011
- [29] M.Moonesun, "Introduction of Iranian Hydrodynamic Series of Submarines (IHSS)", Journal of Taiwan Society of Naval Architects and Marine Engineers, Vol.33, No.3, pp.155-162, 2014, http://en.ustc.findplus.cn/search_list.html?h=articles&db=edselec&an=edselec.2-52.0-84908092928.
- [30] V.Streeter, E.Wylie, K.Bedford, "Fluid Mechanics", 9th edition, 1997
- [31] M.Monesun • Y.M.Korol, D.Tahvildarzade, M.Javadi, "Practical scaling method for underwater hydrodynamic model test of submarine", Journal of the Korean Society of Marine Engineering, Vol. 38, No. 10 pp. 1217~1224, 2014, <https://sites.google.com/site/jkosme76/archives/back-issues>.
- [32] E.Arentzen, P.E.Mandel, Naval Architectural Aspects of Submarine Design, SNAME, 1960.

Chapter 2:

Principles of Naval Submarine Shape Form Design

2-1- Submarine Shape Coding

2-1-1- Coding in IHSS

The principles of IHSS are explained in [1,2]. Standard series are very common practice in naval architecture engineering that causes easiness in the design process. Some of these series that contain body plans of ship and boat geometries are: 60, 62, 64, SSPA, NPL and NSMB that are without hydrodynamic specifications[3,4]. In addition, there are some series for propellers that contain propeller geometry and hydrodynamic coefficients (thrust and torque coefficients and open water efficiency) such as B-Wageningen, KCD, KCA and AU [4-9]. In aerospace engineering, NACA series are well known too. In all of these series, a special coding system is used, for example, in B-Wageningen series code B60-3 means a propeller with $A_E/A_0=0.6$ and 3 bladed. In the NACA series, for example, NACA0025, means a symmetric foil with the thickness to the chord ratio equal to 0.25. Using non dimensional ratios in these series assists to apply the existing data for each dimension of engineering projects. For extraction of these series, there are three main methods: 1) CFD 2) physical small model test 3) combination of model test and CFD.

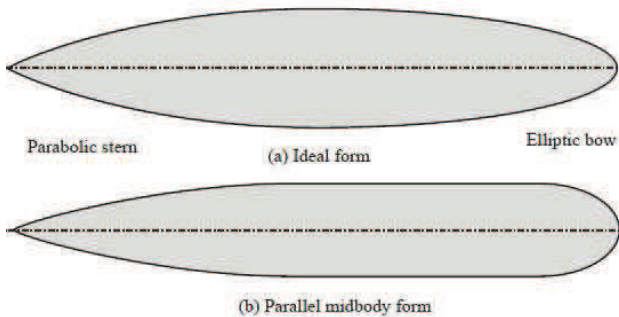


Figure 1: general shapes of submarines[10]

Despite much information about ships and boats, there is a little information about geometry and hydrodynamics characteristics of submarine as in references. References [10,11] present some information about general considerations of submarine hydrodynamics and references [12-18] contain some more details. General dimensions and general arrangements of submarines are described in [19-24]. Collective design information about submarine science such as dimensions, hydrodynamics and other aspects is presented in [25-29] as the main sources in naval submarine design. Iranian hydrodynamic series of submarines (IHSS) are presented for the first time in this book as a standard series. IHSS is starting the publication of some useful information about submarine hydrodynamics. IHSS is a new Simple and applicable instrument for hydrodynamic design of submarine specially beneficial for early stage designs. It uses a special 15 digit code for each submarine hull, and each code generally describes the geometry. Hydrodynamic shape of submarines has generally two types: tear drop shape as ideal form and parallel middle body shape (as shown in Fig.1)[10]. Tear drop shape has a parabolic stern and elliptic bow that is difficult for construction in large dimensions. The biggest cross section area is approximately 30-40% after of the bow[11]. In the parallel middle body shapes the main part of the hull is cylindrical and is easy to construction so that the most common shape of today submarines are similar to that [30]. In IHSS the base shape is parallel middle body shape that is made up of two main parts: main hull (bow, cylinder and stern) and conning tower or sailing on the main hull. Generally, other appendages such as hydroplanes, rudders, propeller and keel aren't considered in IHSS but rarely, in some cases may be used that are mentioned separately. Its reason is that the locations of appendages are very variable and can change the hydrodynamic results very much. In addition, none of them can't be considered as a base because it seriously depends on the design selections. For example, the fore hydroplane can be installed on the bow, cylinder part or on the bridge or not be installed at all [25-27]. Description of each submarine hull in IHSS is done by a 15 digit code that seven digits are related to the main hull, and eight digits are related to the dimensions and location of the conning tower. The coding is as below.

midgets less than 30 tons have a wide range between 5 and 22 [2,20]. Detailed information about L/D ratio is presented in reference [20].

2-1-3- Ratio L_f/L :

This parameter is an important factor for the variations of pressure, stagnation point and flow separation. L_f is the same entrance length in naval architecture and ship design. The greater bow length means lesser viscous pressure resistance. The ratio of L_f/L in parallel middle body submarines according to the statistical results are 0.1~0.3. Ratio L_f/D in reference [23] is mentioned 2.4. In reference [13] that supposed $L/D=8.75$ the ratio $L_f/D=1.75$ is suggested that means $L_f/L=0.2$. Therefore, the range $L_f/L=0.1\sim 0.3$ are a fair approximation.

2-1-4- Ratio L_m/L :

This parameter is mainly depended on the internal general arrangements of submarine and according to the statistical, result is varied on 0.25~0.6 in parallel middle body submarines.

The length of stern will be earned after bow and middle length thus this parameter doesn't enter in coding. The stern shape of submarines is parabolic or conical or combination of them but in IHSS, the stern is only considered conical. The conical length ratio according to the statistical results is varied on 0.3~0.45 and obtained from: $L_a/L = 1 - L_f/L - L_m/L$. Ratio L_a/D in reference [23] is mentioned 3.6. In reference [13] that supposed $L/D=8.75$ the ratio $L_a/D=3$ is suggested and means $L_a/L=0.34$. Therefore, the range $L_a/L=0.3\sim 0.45$ are a good approximation.

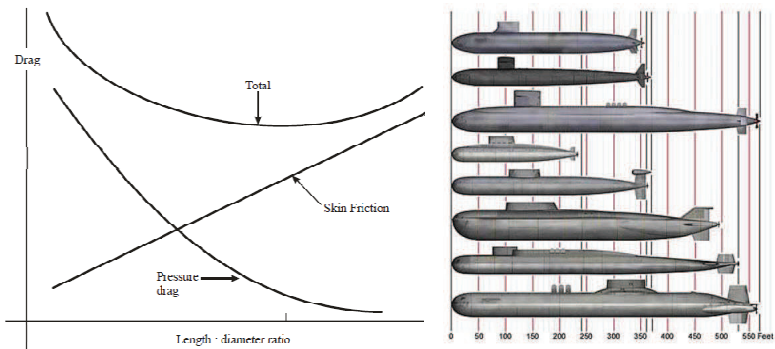


Figure 3: different L/D in submarines and its variation effects on skin and form resistance for selection of optimum point [24]

2-1-5- Sailing and its parameters:

Sailing (conning tower or sailing or bridge) is a big volume upon the hull by prismatic foil section shape that contains several objects such as: exit trunk, conning station, periscope mast, snorkel mast and many other masts. Sailing in hydrodynamic point of view is a harmful part that imposes huge pitching moments on the submarine, but it is an obligatory part for every submarine. Several parameters of the sailing that are considered in IHSS are described below.

Sailing distance from the bow end: This distance is shown as L_{tc}/L ratio and has very different and variable quantity in submarines. The internal arrangement has the main role in this parameter. In the small and medium submarine, the sailing is intended to the middle because it must be above the control room for easy access to the masts and in these submarines, the control room is usually located in the middle of pressure hull. In large SSBN atomic submarines, vertical ballistic missile launchers are located in the middle part of the hull. Then the sailing position has two types: forward or after of launchers. In most of them, the sailing is located forward. This ratio according to the statistical results in small and medium submarines varies between 0.3-0.4, and in large SSBN in first case is about 0.2~0.25 and in second case is 0.5~0.55.

Sailing length: The sailing length is mainly depended on the quantities of masts that are situated tandem longitudinally. The ratio of sailing length to the total length (L_c/L) in small and medium submarines is about 0.15~0.2 and in large submarines is about 0.1~0.15. On the other hand, in small and medium submarines $L_c/D=1.3\sim 2.5$ and in large submarines $L_c/D=0.8\sim 1.8$ could be regarded. In reference [13] the ratio $L_c/D=1.5$ is suggested.

Sailing height: The sailing height is essentially depended upon the height of the masts. There are two types of masts: telescope and permeate type. Telescope masts can be retracting and seating on the hull in several stages and in multi-layers. The permeate masts can permeate and lowered inside the pressure hull. In first type, the smaller height and wider beam of the sailing are

provided and in second type, the higher height and lesser wide is established. In terms of other, the higher height of the sailing means more depth in snorkel and periscope depth that is a positive feature in operational aspect of view. Thus, a logical height of the sailing with considering all parameters must be available. According to the statistics, the ratio of sailing height to the hull diameter (h_c/D) is about 0.45~0.9. The lesser height of the sailing means the lesser aspect ratio (AR) of sailing foil, and then the minimum AR means the minimum snap roll. Snap roll is annoying oscillatory movements. The values $AR=0.2\sim 1.1$ can be a fair estimation. In reference [13], $AR=0.57$ is used.

Sailing foil section: In all sailings, the prismatic section is a foil so that it has minimum hydrodynamic resistance. For preventing asymmetric lateral lifts the foil must be symmetrical. In IHSS, the selected foil is symmetrical NACA00 such as NACA0025. In reference [13] NACA0020 is used.

2-1-6- Considered limitations in IHSS:

The geometries of submarines that are considered in IHSS as first steps are mentioned in Fig 4.

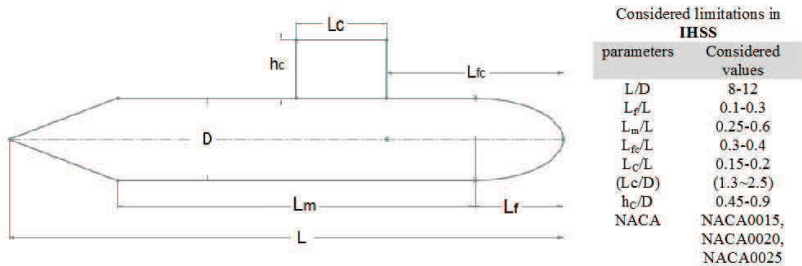


Figure 4: Dimension limitations in IHSS

2-1-7- Some Samples for IHSS

Sample 1: CFD analysis for a submarine

This analysis is done by Flow Vision software based on CFD method. The dimensions of the submarine are presented in Figure 5 and the modeling in Flow Vision is shown in Figure 6. Wetted area is 29.27 m^2 and the specifications of fresh water are considered. According to Iranian Hydrodynamic Series of Submarines (IHSS) the code of this shape is: IHSS.1001565-30108025. Therefore, the foil section of the sailing is

NACA0025. Architecture and general arrangements have a very important role in the selection of the hydrodynamic shape. Results are presented in Table 1 and Fig 7.

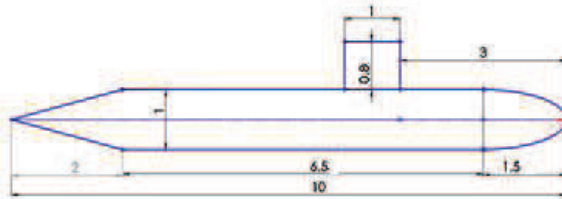


Figure 5: Dimensions of the model in case 1 (IHSS.1001565-30108025)

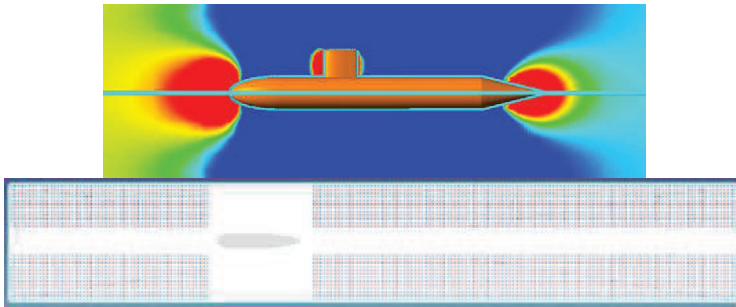


Figure 6: Modeling of case 1 in the Flow Vision software

Table 1: Total resistance coefficient of case 1 by CFD method

V (m/s)	Resistance (N)	Re	Cd
1	182.5	10000000	0.012470106
1.5	305.17	15000000	0.009267585
2	524.84	20000000	0.008965494
2.5	800.91	25000000	0.008756105
3	1136	30000000	0.008624682
5	2742	50000000	0.007494363
7	5544	70000000	0.007730978
9	9309	90000000	0.007852814
11	13738	110000000	0.007757922
13	18995	130000000	0.007679976
15	25034	150000000	0.007602475
17	31951	170000000	0.007554294

Sample 2: CFD analysis for a torpedo

The specifications of the model are shown in Figure 7 and the modeling in Flow Vision is presented in Figure 8. All modeling conditions are as mentioned in case 1. Wetted area is 7.87 m^2 and the specifications of fresh water are considered. According to Iranian Hydrodynamic Series of Submarines (IHSS) the code of this shape is: IHSS.8336058.

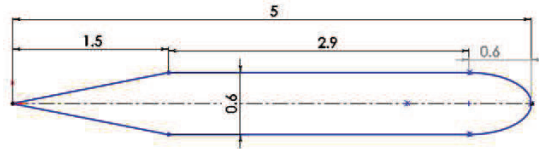


Figure 7: Dimensions of model in case 2 (IHSS.8336058)

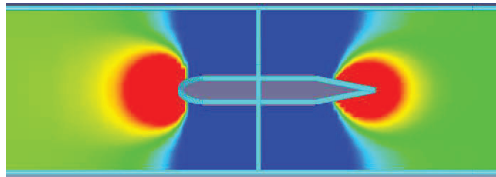


Figure 8: Modeling of case 2 in the Flow Vision software

Results is presented in Table 2.

Table 2: Total resistance coefficient of case 2 by CFD method

V (m/s)	Resistance (N)	Re	Cd
0.05	0.092	250000	0.00935197
0.2	1.33	1000000	0.008449809
0.5	6.78	2500000	0.006891995
1	23.83	5000000	0.006055909
2	89.1	10000000	0.005660737
4	342	20000000	0.00543202
6	756	30000000	0.005336722
8	1297	40000000	0.005150095
10	1970	50000000	0.005006353
12	2836	60000000	0.005004941
14	3803	70000000	0.004930892
16	4950	80000000	0.004913834
18	6250	90000000	0.004902191
20	7595	100000000	0.004825286
26	13124	130000000	0.004933723

Sample 3: model test in towing tank

According to Ref.[2], experiments were conducted in the marine laboratory of Isfahan University of Technology (IUT) in Iran. This submarine relies to code

IHSS.8891666-34167525. Characteristics and results are presented in Table &4.

Table 3: Main Submarine Dimensions (meter)- IHSS.8891666-34167525

L	D	L _F	L _m	L _{fc}	L _C	H _C	NACA00	L/D	L _F /L	L _m /L	L _{fc} /L	L _C /L	h _C /D
(m)	(m)	(m)	(m)	(m)	(m)	(m)							
32	3.6	5	21	10.8	5.1	2.7	25	8.89	0.16	0.66	0.34	0.16	0.75

Table 4: Results of model test in towing tank

V (m/s)	Re	Cd
0.2	200000	0.0065
0.5	500000	0.004293
0.6	600000	0.004119
0.7	700000	0.004201
0.8	800000	0.004177
0.9	900000	0.004047
1	1000000	0.004
1.1	1100000	0.003999
1.2	1200000	0.004011
1.3	1300000	0.003949
1.4	1400000	0.003883
1.5	1500000	0.003842

2-2- A review on the bare hull form equations of submarine

2-2-1- Introduction

Refs [10,11, 30-39] are the main references that describe the notes of naval submarine shape design with regarding the hydrodynamic aspects. Some studies about submarine hull form design with minimum resistance by CFD method is done in Ref [1-10] by M.Moonesun and colleagues. In Refs [26], there are the basis of submarine shape selection with all aspects such as general arrangement, hydrodynamic, dynamic stability, flow noise and sonar efficiency. Ref.[29] contains a lot of scientific materials about naval submarine hull form and appendages design with hydrodynamic considerations. Special discussions about naval submarine shape design are presented in Iranian Hydrodynamic Series of Submarines (IHSS)[1,2]. In Ref[17,18] some case study discussions about the hydrodynamic effects of the bow shape and overall length of the submarine by CFD method are presented. Defence R&D Canada, suggested a hull form equation for bare hull, sailing

and appendages [13,40] as the name of "DREA standard model". Refs.[23,24,41] presents an equation for teardrop hull form with the limitations of their coefficients, but the main source of their equation is presented in Ref.[42], and the simulation of the hull form with different coefficients is presented in Ref.[19]. Another equation for torpedo hull shape is presented in Ref[16]. Formula "Myring" as a famous formula for axisymmetric shapes is presented in Ref.[43]. Extensive experimental results about hydrodynamic optimization of teardrop or similar shapes are presented in Ref.[44] as a main reference book in the field of the selection of aerodynamic and hydrodynamic shapes based on experimental tests. A collective experimental study about the shape design of the bow and stern of the underwater vehicles is presented in Ref [45] that is based on the underwater missiles but the most parts of this book, is practicable in naval submarine shape design. Other experimental studies on the several teardrop shapes of submarines are presented in Ref.[46]. In Refs[47,48], all equations of hull form, sailing and appendages are presented with experimental and CFD result for SUBOFF project.

2-2-2- Some important factors in bare hull form design

Bare hull, is an outer hydrodynamic shape that envelopes the pressure hull. For a well judgment and the best selection of bare hull form, the most important factors in bare hull form design are counting as: 1) minimum submerged resistance: the ratio L/D and bow shape are the important factors. Demand for minimum resistance in submerged navigation is versus surfaced navigation but in submarine resistance calculation, the main criterion is the submerged mode. Optimization of submarine shape, based on minimum resistance is represented in Refs.[49,50] with a logical algorithm. Optimization of shape based on minimum resistance in snorkel depth is shown in Ref.[30]. Optimization of shape in surface condition (such as ships) is not regarded because in new modern submarines with using high storage batteries or nuclear storage or fuel cells, there isn't any need to surfacing, and air suction is done by snorkel mast in snorkel depth. 2) general arrangement demands specially for D . 3) enough volume for providing sufficient buoyancy according to given weight. 4) minimum flow noise specially around sonar and acoustic sensors. 5) minimum cavitation around the propeller. 6) suitable for single hull or twin hull: in a single hull submarine, there is almost cylindrical

pressure hull, and hydrodynamic envelope, there is only in the bow and stern parts. In twin hull submarine, hydrodynamic envelope (light hull), envelopes the pressure hull, totally. The shape demands of these two kinds of hull are different. There are two main parameters, which affect the submarine shape design: resistance and volume. The coefficient that can describe both parameters is "Semnan" coefficient:

$$\text{Semnan coefficient } (K_{SN}) = \frac{(\text{Volume})^{\frac{1}{3}}}{\text{Resistance Coefficient}} \quad (1)$$

This coefficient can be named "Hydro-Volume efficiency" because it counts both resistance and volume. For this coefficient, the more values mean the better design. In some cases, a shape has minimum resistance but has a little volume in a given constant length. Thus it can't be a good selection.

2-2-3- Bare hull form equations

As mentioned in "Introduction", there are several sources about equations of bare hull form, which will be presented here.

A) According to Refs.[13,40]: The equations are presented as "DREA Model" that is shown in Fig.9 and includes the specification of bare hull and appendages.

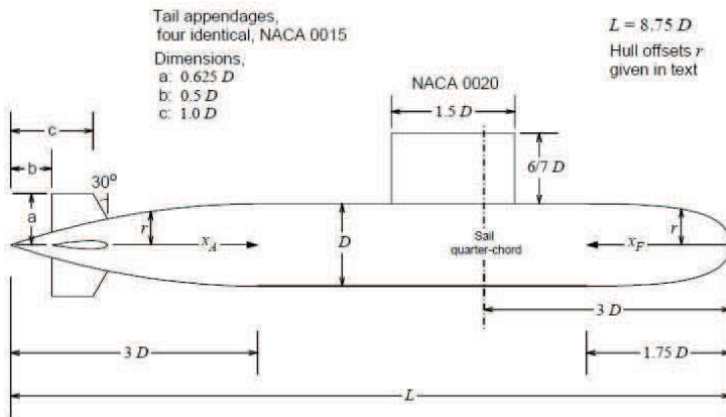


Figure 9: Parameters of DREA submarine hull [13]

The DREA model is specified in three sections; bow, midbody and tail. The fineness is $L/D=8.75$ so that bow length is equal to $1.75D$ and midbody length is $4D$ and stern length is $3D$. Axisymmetric profile of bow is:

$$\frac{r}{D} = 0.8685\sqrt{\frac{x_F}{D}} - 0.3978\frac{x_F}{D} + 0.006511\left(\frac{x_F}{D}\right)^2 + 0.005086\left(\frac{x_F}{D}\right)^3 \quad (1)$$

Middle body is a cylinder and axisymmetric parabolic profile of stern is:

$$\frac{r}{D} = \frac{1}{3}\left(\frac{x_A}{D}\right) - \frac{1}{18}\left(\frac{x_A}{D}\right)^2 \quad (2)$$

All parameters are shown in Fig.1 [13]. These equations are rewritten to another face in Ref.[40] as a function of length but by the same dimension relations ($L/D=8.75$). For bow with the length equal to $0.2L$ ($0 < x/L < 0.2$), the equation is:

$$\frac{r_1(x)}{L} = \frac{D}{L} \left[2.56905\sqrt{\frac{x}{L}} - 3.48055\frac{x}{L} + 0.49848\left(\frac{x}{L}\right)^2 + 3.40732\left(\frac{x}{L}\right)^3 \right] \quad (3)$$

Coordinate is shown in Fig.10. The middle body part, is a cylinder part and equation is ($0.2 < x/L < 1-3D/L$):

$$\frac{r_2(x)}{L} = \frac{D}{2L} \quad (4)$$

The stern part with the length equal to $3D$, the equation is ($1-3D/L < x/L < 1$):

$$\frac{r_3(x)}{L} = \frac{D}{2L} - \frac{L}{18D} \left[\frac{x}{L} - \left(1 - \frac{3D}{L}\right) \right]^2 \quad (5)$$

Alternate stern profile by using $x'=L-x$ and $0 < x'/D < 3$:

$$\frac{r_3(x')}{D} = \frac{1}{2} - \frac{1}{18} \left(3 - \frac{x'}{D} \right)^2 \quad (6)$$

Appendages are specified as: all appendages have four digit NACA foils, which hydrofoil thickness profile is given by:

$$\frac{y_c}{c} = \pm \frac{t}{c} \left[1.4845\sqrt{\frac{x}{c}} - 0.63\frac{x}{c} - 1.758\left(\frac{x}{c}\right)^2 + 1.4215\left(\frac{x}{c}\right)^3 - 0.5075\left(\frac{x}{c}\right)^4 \right] \quad (7)$$

Where the "c" is local chord length and t/c is the maximum thickness to the chord ratio. The leading edge is at $x=0$ and the trailing edge, which has non zero thickness is at $x=c$. Tail planes are four identical rudder and stern plane appendages in a symmetrical "+" configuration (Fig.11). The sections are the flat tip NACA0015 thickness profile ($t/c=0.15$). Propeller hub, is at aft three percent of hull. For sail, there is rectangular planform, flat tip, NACA0020 thickness profile ($t/c=0.2$). Sail planes (Fig.12) are flat tips, NACA0015 thickness profile ($t/c=0.15$).

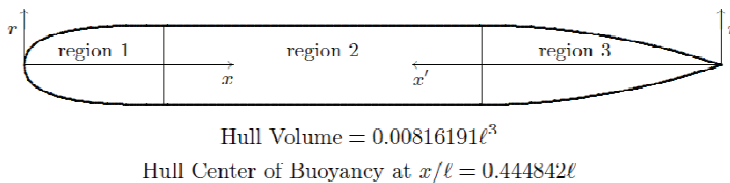


Figure 10: Coordinates on the bow and stern [40]

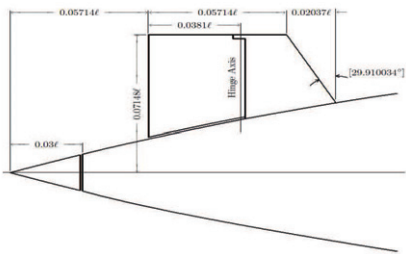


Figure 11: Tail planes dimensions [40]

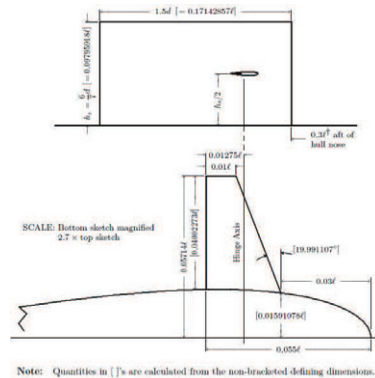


Figure 12: Sail plane dimensions [40]

B) According to Refs.[19,23,24,41,42]: The equations are presented as "Hull Envelope Equation". The envelope is first developed as a pure tear drop shape with the forward body comprising 40 percent of the length and the after body comprising the remaining 60 percent [41]. The forward body is formed by revolving an ellipse about its major axis and is described by the following equation:

$$Y_f = R \left[1 - \left(\frac{X_f}{L_f} \right)^{n_f} \right]^{1/n_f} \quad (8)$$

The after body is formed by revolving a line around axis and is described by:

$$Y_a = R \left[1 - \left(\frac{X_a}{L_a} \right)^{n_a} \right] \quad (9)$$

The quantities Y_a and Y_f are the local radius of the respective body of revolution with X_a and X_f describing the local position of the radius along the body (Fig.13). If the parallel middle body is added to the envelope, then cylindrical section with a radius equal to the maximum radius of the fore and after body is inserted in between them. The local radii represent the offsets for drawing the submarine hull and also determine the prismatic coefficient for the hull section. The prismatic coefficient (C_p) is a hull form parameter for fullness and is the ratio of volume of the body of revolution divided by the volume of a right cylinder with the same maximum radius. For an optimum shape, the fore and after bodies will have different values for C_p . C_p is used to determine the total hull volume by the following relation:

$$Volume = \frac{\pi D^2}{4} \left[3.6 D C_{pa} + \left(\frac{L}{D} - 6 \right) D + 2.4 D C_{pf} \right] \quad (10)$$

Where the added term $(L/D-6)D$ accounts for the for the volume of the parallel middle body where $C_p=1$. The surface area for the body can be described by the following relation:

$$Wetted Surface = \pi D^2 \left[3.6 D C_{sa} + \left(\frac{L}{D} - 6 \right) D + 2.4 D C_{sf} \right] \quad (11)$$

Surface coefficient (C_s), describes the ratio of the surface area of the body to the surface area of a cylinder with the same maximum radius. The factors n_f and n_a in equations, describe the "fullness" of the body by affecting the

curvature of the parabolas. Table 5 lists some representative values for n_f and n_a along with their resultant C_p and C_s . Figure 15 illustrates the effect of varying n_f and n_a on the hull geometry [41].

Table 5: Selected values for C_p and C_s

n_f (n_a)	Fore body				After body			
	2.0	2.5	3.0	3.5	2.0	2.5	3.0	3.5
C_p	.6667	.7493	.8056	.8443	.5333	.5954	.6429	.6808
C_{sf}	.7999	.8590	.8952	.9200	.6715	.7264	.7643	.7934

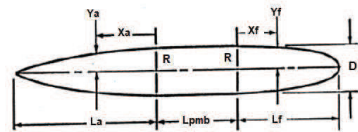
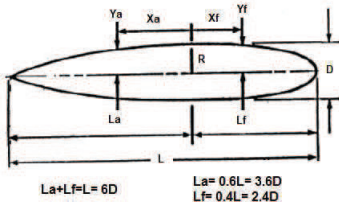


Figure 13: Coordinates and parameters in submarine hull

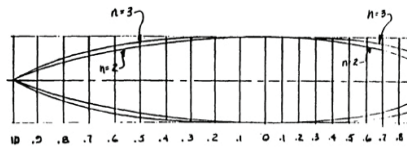


Figure 14: Effect of n_f and n_a on hull geometry

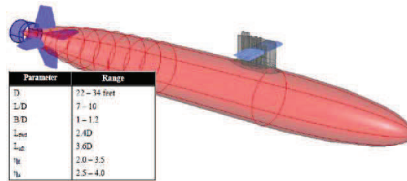


Figure 15: SSG with sail and control surfaces [16]

The range of these parameters, regarded for sample, represented in Fig.15. The simulation of the hull form with different coefficients is presented in Fig.16. These equations are rewritten to another face in Refs.[23,50,51] for another coordinate origin (Fig.17), and the shape optimization is done for snorkeling in snorkel depth.

$$r_a = R \left(1 - \left(\frac{L_a - x}{L_a} \right)^{n_a} \right) \quad (12)$$

$$r_f = R \left(1 - \left(\frac{(x - L_a - L_c)}{L_f} \right)^{n_f} \right)^{2/n_f} \quad (13)$$

C) **According to Refs.[19,43]:** The equations are presented as "Myring Equations" for earning minimum resistance and many submarines, AUVs and UUVs are designed according to these equations such as REMUS [19] which describes a body contour with a minimal drag coefficient for a given fineness ratio (maximum length to the maximum diameter). The parameters "a,b,c,d,θ" are shown in Fig.18. Parameter "n" is an exponential parameter which can be varied to give different body shapes. These equations assume an origin at the nose of the vehicle. Nose shape is given by the modified semi-elliptical radius distribution.

$$r(\Xi) = \frac{1}{2} d \left[1 - \left(\frac{\Xi + a_{offset} - a}{a} \right)^2 \right]^{\frac{1}{n}} \quad (14)$$

Tail shape is given by the equation:

$$r(\Xi) = \frac{1}{2} d - \left[\frac{3d}{2c^2} - \frac{\tan \theta}{c} \right] (\Xi - l)^2 + \left[\frac{d}{c^3} - \frac{\tan \theta}{c^2} \right] (\Xi - l_f)^3 \quad (15)$$

Where the forward body length is:

$$l_f = a + b - a_{offset} \quad (16)$$

Table 6 gives the dimensionalized "Myring" parameters.

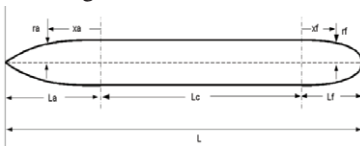


Figure 17: Coordinates and parameters in submarine hull

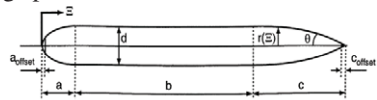


Figure 18: Myring profile

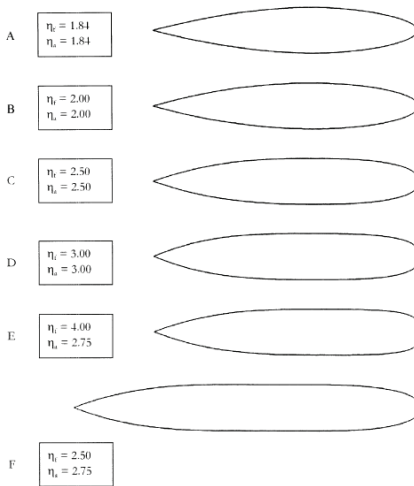


Figure 16: Hull form with coefficients of n_a , n_f [20]

Parameter	Value	Units	Description
a	+1.91e-001	m	Nose Length
a_{offset}	+1.65e-002	m	Nose Offset
b	+6.54e-001	m	Midbody Length
c	+5.41e-001	m	Tail Length
c_{offset}	+3.68e-002	m	Tail Offset
n	+2.00	n/a	Exponential Coefficient
θ	+4.36e-001	radians	Included Tail Angle
d	+1.91e-001	m	Maximum Hull Diameter
l_f	+8.28e-001	m	Vehicle Forward Length
l	+1.33e+000	m	Vehicle Total Length

Table 6: Myring parameters for STD REMUS [19]

D) According to Refs.[48,49]: The equations are presented as "SUBOFF Model" from Defence Advanced Research Project Agency (DARPA) that is shown in Fig.19 with coordinate location. Two geometrically identical models designed to a linear scale ratio of 24 with detailed equations and shape specifications for computer programming and modeling in CFD and experimental model test [47]. Extensive hydrodynamic results are presented in Ref.[28].

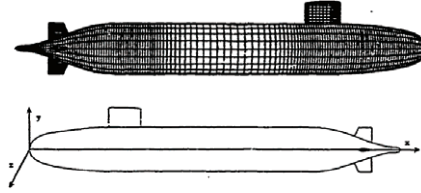


Figure 19: SUBOFF hull and coordinate [47]

The two SUBOFF models differ only in the location of surface pressure taps. Each model component is described by equation giving either the axial and radial values for an axisymmetric component and all units in equation are in feet. The model has overall length of 14.291667 ft (4.356 m) and maximum diameter of 1.666667 ft (0.508 m). Dimensions of model and equations to define the axisymmetric hull are:

Forebody Length = 3.333333 ft (1.016 m)
Parallel Middle Body Length = 7.3125 ft (2.229 m)
Afterbody Length = 3.645833 ft (1.111 m)
Aft Perpendicular at $x = 13.979167$ ft (4.461 m)
Total Body Length = 14.291666 ft (4.356 m)
Maximum Body Diameter = 1.666667 ft (0.508 m)
$\lambda = (\text{full/model})$ Scale Ratio = 24

Bow equation in $0 < x < 3.333$ (ft) is:

$$r = R \{ 1.126395101x(0.3x - 1)^4 + 0.442874707x^2(0.3x - 1)^3 + 1 - (0.3x - 1)^4(1.2x + 1) \}^{1/2.1} \quad (17)$$

Parallel middle body is a cylinder in $3.333 < x < 10.645833$ (ft). Stern equation in $10.645833 < x < 13.979167$ (ft) is:

$$r_s = R \left\{ r_h^2 + r_h K_o \xi^2 \left(20 - 20r_h^2 - 4r_h K_o - \frac{1}{3} K_i \right) \xi^3 + (-45 + 45r_h^2 + 6r_h K_o + K_i) \xi^4 + (36 - 36r_h^2 - 4r_h K_o - K_i) \xi^5 + \left(-10 + 10r_h^2 + r_h K_o + \frac{1}{3} K_i \right) \xi^6 \right\}^{1/2} \quad (18)$$

$$r_h = 0.1175 \quad K_0 = 10 \quad K_1 = 44.6244 \quad (19)$$

$$\xi = \frac{13.979167 - x}{3.333333} \quad , x \text{ in feet}$$

The equation of stern cap in $13.979167 < x < 14.291667$ (ft) is:

$$r_{se} = 0.1175 R [1 - (3.2x - 44.733333)^2]^{1/2} \quad (20)$$

The profile of each part is as Fig.20.

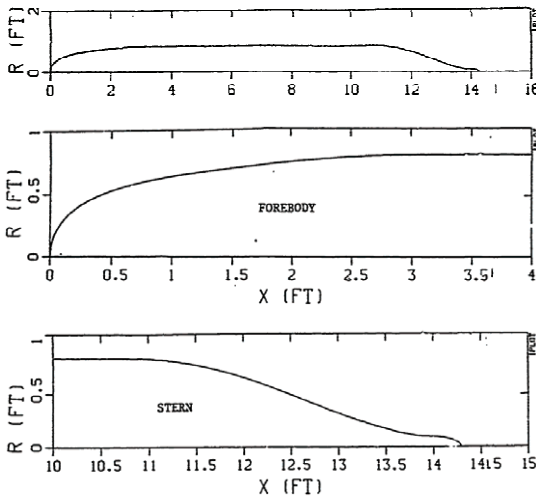


Figure 20: Hull form of SUBOFF [47]

The sail is defined by 4 sections: fore body, parallel middle body, after body and cap (Fig.21). Its main dimensions are:

Sail Forebody Length = 0.325521 ft (0.99m)
Sail Parallel Middle Body Length = 0.200521 ft (0.061m)
Sail Afterbody Length = 0.682292 ft (0.208m)
Total Sail Length = 1.208333 ft (0.368m)
Span of Sail with Uniform Profile = 0.674479 ft (0.206 m)
Z_{max} = One-Half the Maximum Sail Thickness = 0.109375 (0.033m)

Sail fore body equation is:

$$Z_1 = Z_{max} [2.094759(A) + 0.2071781(B) + (C)]^{1/2} \quad (21)$$

$$A = 2D (D - 1)^4$$

$$B = 1/3 (D^2)(D - 1)^3$$

$$C = 1 - (D - 1)^4(4D + 1)$$

$$D = 3.072 \cdot (x - 3.032986)$$

Sail parallel middle body equation is:

$$Z_1 = Z_{max} = 0.109375 \text{ ft} = 1.3125 \text{ inch} \quad (22)$$

Sail aft body equation is:

$$Z_1 = 0.1093750 [2.238361 (E(E - 1)^4) + 3.106529 (E^2(E - 1)^8) + (1 - (E - 1)^4(4E + 1))] \quad (23)$$

$$E = (4.241319 - x)/0.6822917 \quad (24)$$

Sail is closed at top with an ellipsoid that names "Sail cap" and is defined as:

$$Z_2 = [Z_1^2 - (2(y - 1.507813))^2]^{1/2} \quad (25)$$

Z_1 was defined previously as a function of x . The intersection of hull and sail is:

$$[R_{HS}(x)]^2 = y^2 + Z_1^2 \quad (26)$$

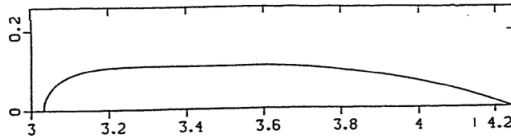


Figure 21: Sail form of SUBOFF [47]

2-3- Power Series Optimization for Submarine bare hull Form

2-3-1- Specifications of the Models

The base model that considered here, is an axis-symmetric body similar to torpedo, without any appendages because in this study, only bare hull effect on resistance, wants to be studied. It helps to quarterly CFD modeling of the body and saving the time. The bow and stern form in each model, change with the n_f and n_a . Middle part is a cylinder. In this section, 19 models are studied. The 3D models and its properties are modeled in Solid Works (Fig.22). For evaluating the hydrodynamic effects of bare hull, the lengths of stern, middle, bow and total length are constant. The L/D ratio is constant too, because the maximum diameter is constant. Therefore, every model has different volume and wetted surface area. The Tab.7 contains these assumptions. The specifications of all 11 models are presented in Tab.8.

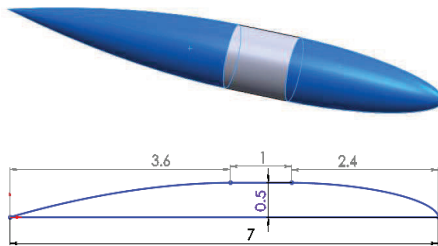


Figure 22: General configuration of the models

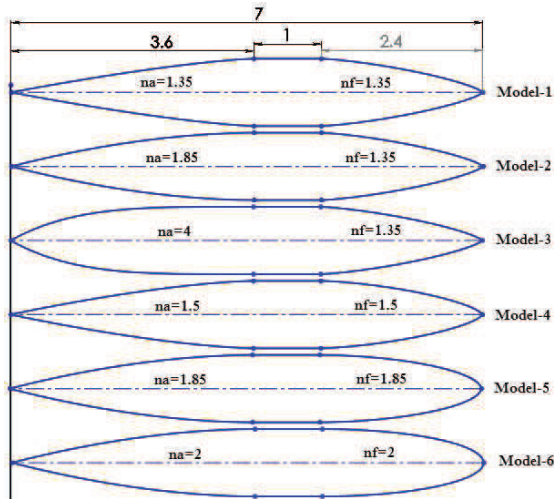
Table 7: Main assumptions of models

v (m/s)	L_t (m)	L_f (m)	L_m (m)	L_a (m)	D (m)	L_t/D	A_0 (m ²)
10	7	2.4	1	3.6	1	7	3.14

Table 8: Specifications of 11 Models

Model	specification of Model	Aw	V
1	nf=1.35, na=1.35	14.6	2.89
2	nf=1.35, na=1.85	15.45	3.15
3	nf=1.35, na=4	17.18	3.71
4	nf=1.5, na=1.5	15.22	3.07
5	nf=1.85, na=1.85	16.37	3.43
6	nf=2, na=2	16.57	3.49
7	nf=2.5, na=2.75	18.03	3.96
8	nf=3, na=3	18.55	4.13
9	nf=3.5, na=3.5	19.1	4.31
10	nf=4, na=2.75	18.76	4.19
11	nf=4, na=4	19.53	4.44

Wetted surface area (A_w) is used for the resistance coefficient and the total volume is used for "Semnan" coefficient. Total volume is different and is represented in fourth column. In addition, for CFD modeling in all models, velocity is constant and equal to 10 m/s. This velocity is selected so that the Reynolds number be more than five millions because in ref.[42] it was proved that total resistance coefficient after Reynolds of five millions can be remained constant. Configurations of all models are represented in Fig.23. In every model, the coefficients, n_f and n_a change. The coefficient n_f , varies the bow form, and n_a , varies the stern form.



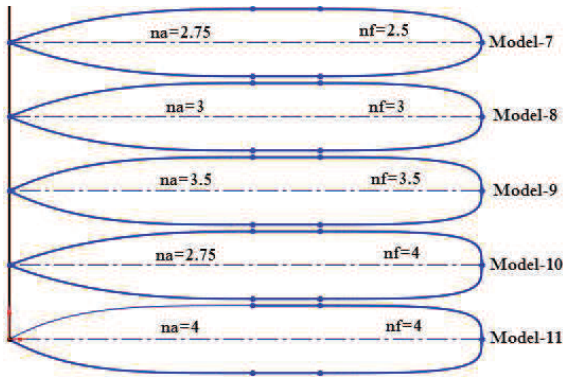


Figure 23: Configurations of Models

2-3-2- CFD Method of Study

This analysis is performed by Flow Vision (V.2.3) software based on CFD method and solving the RANS equations. Generally, the validity of the results of this software has been done by several experimental test cases, and nowadays this software is accepted as a practicable and reliable software in CFD activities. For modeling these cases in this chapter, Finite Volume Method (FVM) is used. A structured mesh with cubic cell has been used to map the space around the submarine. For modeling the boundary layer near the solid surfaces, the selected cell near the object is tiny and very small compared to the other parts of domain. For selecting the proper quantity of the cells, for one certain model ($n_f=1.35$, $n_a=1.35$) and $v=10\text{m/s}$, seven different amount of meshes were selected and the results were compared insofar as the results remained almost constant after 1.1 millions meshes, and it shows that the results are independent of meshing (Fig.24). In all modeling the mesh numbers are considered more than 1.2 millions.

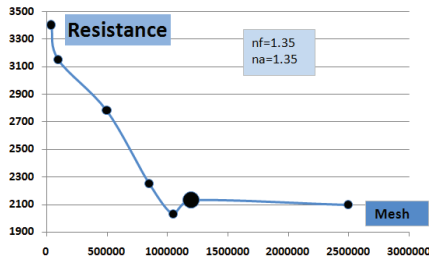
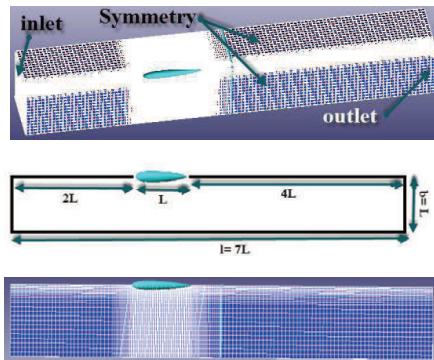


Figure 24: Mesh independency evaluations

For the selection of suitable iteration, it was continued until the results were almost constant with variations less than one percent, which shows the convergence of the solution. All iterations are continued to more than one millions. In this domain, there is inlet (with uniform flow), Free outlet, Symmetry (in the four faces of the box) and Wall (for the body of submarine). Dimensions of cubic domain are 49m length (equal to $7L$), 7m beam and 7m height (equal to L or $7D$). Pay attention to that only quarter of the body is modeled because of axis-symmetric shape, and the domain is for that. Meanwhile, the study has shown that the beam and height equal to $7D$ in this study can be acceptable. Here, there are little meshes in far from the object. The forward distance of the model equals to $2L$ and after distance is $4L$ in the total length of $7L$ (Fig.25). The turbulence model is K-Epsilon and y^+ is considered equal to 30. The considered flow is incompressible fluid (fresh water) in 20 degrees centigrade and constant velocity of 10 m/s.



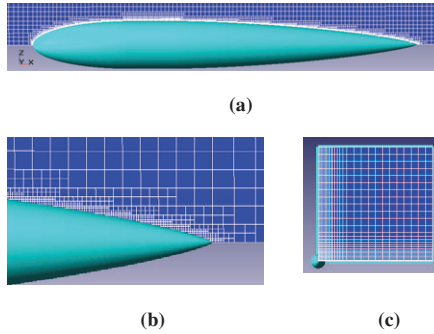


Figure 25: (a) Domain and structured grid (b) Very tiny cells near the wall for boundary layer modeling and keeping y^+ about 30 (c) Quarterly modeling because of axis-symmetry

2-3-3- CFD Results Analysis

The results of analysis are represented in Tab.9 and Fig.26. According to these results, total resistance increases with an increase in fullness of body and coefficients of n_f and n_a .

Table 9: Resistance, resistance coefficients and Semnan coefficients of models

Model	R	Ct*10000	Semnan Coef./10
1	2128	29.15	48.85
2	2220	28.74	50.99
3	2456	28.59	54.12
4	2236	29.38	49.45
5	2512	30.69	49.12
6	2584	31.19	48.61
7	3012	33.41	47.33
8	3388	36.53	43.90
9	3696	38.70	42.03
10	3812	40.64	39.65
11	3944	40.39	40.67

Resistance coefficient (based on the wetted area surface), similar to resistance diagram, has an upward trend with numbers of models, but there is a local minimum value for Model 3 ($n_f=1.35$, $n_a=4$). It means that, for constant wetted surface area, the bare hull form of $n_f=1.35$ and $n_a=4$, has the best results and

minimum resistance. For selecting a good shape form of submarine, enough volume should be provided, thus Semnan coefficient is very important.

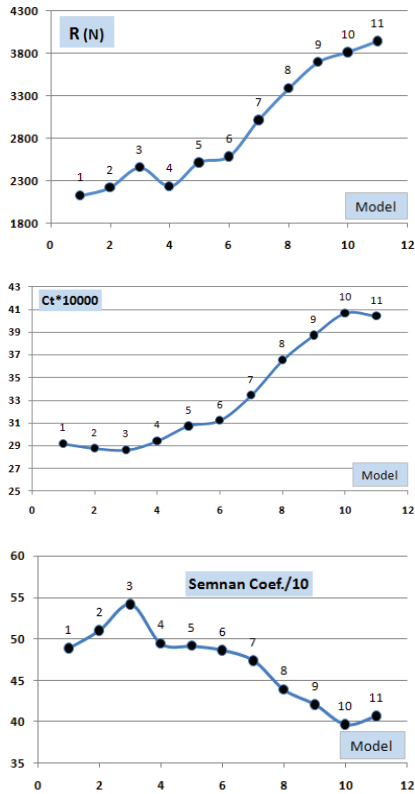


Figure 26: Resistance, resistance coefficients and Semnan coefficients of models

According to last diagram of Fig.26, Semnan coefficient diagram, has a downward trend but there is a local maximum point in Model 3, that shows a good form of this model. It seems that Model 3 ($n_f=1.35$, $n_a=4$), be a good selection, because it has a maximum value in Semnan coefficient and a minimum value in the resistance coefficient that shows the best condition and ideal form. However, in real naval submarines, the form of Model 3, cannot be a good selection because of sharpness of bow shape and internal arrangements

problems. For better arrangement in the bow and stern, the blunt, thick and bulky form is ideal. For hydrodynamic form, more the thin form is ideal, thus in hydrodynamic point of view, Model 3 has the best form.

2-3-4- Review

Submarine bare hull form selection is a very important stage in submarine design. There are several parameters which take part in the form design such as: minimum resistance (hydrodynamic notes), general arrangement, sufficient volume for providing enough buoyancy, minimum flow noise, minimum cavitation around the propeller, suitable for single hull or twin hull. Hydrodynamic and minimizing resistance has a unique and important role in naval submarine form design, because it causes to more speed, more duration at the depth of the water and thus, more range of navigation. According to the studies of this chapter, the Model 3 by $n_f=1.35$ and $n_a=4$, has the best results. These diagrams show that, the blunter and thick form (more value of n_f and n_a), causes a steep increase in resistance coefficient values. The exact needed values of n_f and n_a , depend on the other parameters of design, which mentioned above.

Nomenclature

L	overall length of hull	C_t	Total resistance coefficient
D	maximum diameter of the outer hull	C_p	Pressure resistance coefficient
R	maximum radius of the outer hull	C_{pr}	Prismatic coefficient
V	speed of water in m/s	C_f	Frictional resistance coefficient
A₀	Cross section area of model= 3.14 m ²	IHSS	Iranian Hydrodynamic Series of Submarines
R_n	Reynolds number	CFD	Computational Fluid Dynamics

References

- [1] Iranian Defense Standard (IDS- 857), " Hydrodynamics of Medium Size Submarines", 2011
- [2] M.Moonsun, "Introduction of Iranian Hydrodynamic Series of Submarines (IHSS)", Journal of Taiwan Society of Naval Architects and Marine Engineers, Vol.33, No.3, pp.155-162, 2014,
http://en.ustc.findplus.cn/search_list.html?h=articles&db=edselc&an=edselc.2-52.0-84908092928.
- [3] Rawson K J, Tupper E C, "Basic Ship Theory", (Jordan Hill., Oxford), 2001, pp. 731
- [4] Lewis Edward V, "Principles of Naval Architecture, Second Revision, Volume II • Resistance, Propulsion and Vibration", The Society of Naval Architects and Marine Engineers (SNAME), 1988
- [5] Moonesun M, "Handbook of Naval Architecture Engineering", (Kanoon Pajohesh., Isfahan), 2009, pp.1003
- [6] Bertram V, "Practical Ship Hydrodynamics", (Elsevier Ltd., UK), 2000, pp. 369
- [7] ITTC (23th International Towing Tank Conference), Recommended procedures and guidelines- Sample Work Instructions Calibration of Load Cells, (2002) 7.6-02-09.
- [8] ITTC (23th International Towing Tank Conference), Recommended procedures and guidelines-Model Manufacture Ship Models, (2002) 7.5-01-01-01.
- [9] ITTC (23th International Towing Tank Conference), Recommended procedures and guidelines Testing and Extrapolation Methods- Resistance Uncertainty Analysis, (2002) 7.5-01-01-01.
- [10] P.N.Joubert, "Some aspects of submarine design: part 1: Hydrodynamics", Australian Department of Defence, 2004.
- [11] P.N.Joubert, "Some aspects of submarine design: part 2: Shape of a Submarine 2026", Australian Department of Defence, 2004.
- [12] M.Moonsun, M.Javadi, P.Charmdooz, U.M.Korol, "evaluation of submarine model test in towing tank and comparison with CFD and experimental formulas for fully submerged resistance", Indian Journal of Geo-Marine Science, vol.42(8), December 2013, pp.1049-1056.
- [13] Mackay M, "The Standard Submarine Model: A Survey of Static Hydrodynamic Experiments and Semiempirical Predictions", Defence R&D Canada, June 2003
- [14] Roddy, R., 1990. "Investigation of the stability and control characteristics of several configurations of the DARPA SUBOFF model (DTRC Model 5470) from captive-model experiments". Report No. DTRC/SHD-1298-08, September.
- [15] M.Moonsun, U.M.Korol, V.O.Nikrasov, S.Ardeshiri, D.Tahvildarzade, " Proposing New Criteria for Submarine Seakeeping Evaluation", 15th Marine Industries Conference (MIC2013), Kish Island, 2013.
- [16] Prester Timothy, " Verification of a Six-Degree of Freedom Simulation Model for the REMUS Autonomous Underwater Vehicle", University of California at Davis, 1994

- [17] Praveen.P.C, Krishnankutty.P, " study on the effect of body length on hydrodynamic performance of an axi-symmetric underwater vehicle", *Indian Journal of Geo-Marine Science*, vol.42(8), December 2013, pp.1013-1022.
- [18] K.N.S.Suman, D.Nageswara Rao, H.N.Das, G.Bhanu Kiran, "Hydrodynamic Performance Evaluation of an Ellipsoidal Nose for High Speed Underwater Vehicle", *Jordan Journal of Mechanical and Industrial Engineering (JJMIE)*, Volume 4, Number 5, November 2010, pp.641-652.
- [19] J.K.Stenars, "Comparative naval architecture of modern foreign submarines", Massachusetts Institute, 1988.
- [20] M.Moonesun, P.Charmdooz, "General arrangement and naval architecture aspects in midget submarines", 4th International Conference on Underwater System Technology Theory and Applications 2012 (USYS'12), Malaysia.
- [21] Budiyo.A, " Advances in unmanned underwater vehicles technologies: modeling, control and guidance perspectives ", *Indian Journal of Marine Science*, vol.38(3), September 2009, pp.282-295.
- [22] J.M.Lee, J.Y.Park, B.Kim, H.Baek, , " Development of an Autonomous Underwater Vehicle IsiMI6000 for deep sea observation ", *Indian Journal of Geo-Marine Science*, vol.42(8), December 2013, pp.1034-1041.
- [23] Lisa Minnick, "A Parametric Model for Predicting Submarine Dynamic Stability in Early Stage Design", Virginia Polytechnic Institute and State University, 2006
- [24] D. Alemayehu, R.B.Boyle, E.Eaton, T.Lynch, J.Stepanchick, R.Yon," Guided Missile Submarine SSG(X)", SSG(X) Variant 2-44, Ocean Engineering Design Project, AOE 4065/4066, Virginia Tech Team 3 ,Fall 2005 – Spring 2006.
- [25] Jackson H A, "Submarine Design Notes", (Massachusetts Institute of Technology).1982, pp. 520
- [26] Bucher R, Rydill L J, "Concept in submarine design", (The press syndicate of the University of Cambridge., Cambridge university press), 1998, pp. 295
- [27] A group of authorities, "Submersible vehicle system design", The society of naval architects and marine engineers, 1990.
- [28] Ulrich Gabler, "Submarine Design", Bernard & Graefe Verlag, 2000.
- [29] Y.N.Kormilitsin, O.A.Khalizev, "Theory of Submarine Design", Saint-Petersburg State Maritime Technology University, 2001
- [30] M.Moonesun, M.Javadi, P.Charmdooz, U.M.Korol, "Evaluation of submarine model test in towing tank and comparison with CFD and experimental formulas for fully submerged resistance", *Journal : Indian Journal of Geo-Marine Science*, vol.42(8), December 2013, pp.1049-1056, <http://nopr.niscair.res.in/handle/123456789/25467>.
- [31] M. Moonesun, Y.M. Korol, A. Brazhko, " CFD analysis on the equations of submarine stern shape", *Journal of Taiwan Society of Naval Architects and Marine Engineers*, Vol.34, No.1, pp.21-32, 2015.
- [32] M.Javadi, M.D.Manshadi, S.Kheradmand, M.Moonesun, "Experimental investigation of the effect of bow profiles on resistance of an underwater vehicle in free surface motion",

Journal of Marine Science and Application-Springer, No.14, Jan 2015, http://link.springer.com/article/10.1007/s11804-015-1283-0?sa_campaign=email/event/articleAuthor/onlineFirst.

- [33] M.Moonesun, Y.M.Korol, H.Dalayeli, D.Tahvildarzade, M.Javadi, M.Jelokhanian, "Power Series Optimization for Submarine Bare Hull Form", Turkish Journal of Engineering, Science and Technology (TUJEST), vol.3, No.1, pp.11-19, 2015.
- [34] Moonesun.M, Korol.Y.M, Dalayeli.H, CFD analysis on the bare hull form of submarines for minimizing the resistance, International Journal of Maritime Technology (IJMT), Vol.3, 2014, p.1-13.
- [35] Mohammad Moonesun, Yuri Mikhailovich Korol, Hosein Dalayeli, Davood Tahvildarzade, Mehran Javadi, Mohammad Jelokhaniyan, Asghar Mahdian, Optimization on Submarine Stern Design, Journal of Engineering for the Maritime Environment (Ins. Mechanical Engineering-Part M, SAGE), February 2016, pp.1-11.
- [36] Mohammad Moonesun, Yuri Mikhailovich Korol, Valeri A Nikrasov, Alexander Ursalov, Anna Brazhko, CFD analysis of the bow shapes of submarines, Journal of Scientific and Engineering Research, 2016, 3(1):1-16.
- [37] Mohammad Moonesun, Asghar Mahdian, Yuri Mikhailovich Korol, Mehdi Dadkhah, Mehrshad Moshref Javadi, Anna Brazhko, Optimum L/D for Submarine Shape, Indian Journal of Geo-Marine Sciences, Vol. 45(1), January 2016, pp. 38-43
- [38] Mohammad Moonesun, Asghar Mahdian, Yuri Mikhailovich Korol, Mehdi Dadkhah, Mehrshad Moshref Javadi, Concepts in Submarine Shape Design, Indian Journal of Geo-Marine Sciences, Vol. 45(1), January 2016, pp. 100-104.
- [39] M. Moonesun, A. Mahdian, Y.M. Korol and A. Brazhko, Out of Axis Movement of an AUV inside a Water Pipeline, The Journal of Engineering Research (TJER), Vol. 14, No. 1, (2017) 10-22
- [40] Christopher Baker, "Estimating Drag Forces on Submarine Hulls", Defence R&D Canada, September 2004, pp.131
- [41] Grant.B.Thomson,"A design tool for the evaluation of atmosphere independent propulsion in submarines", Massachusetts Institute of Technology, 1994, pp.191-193
- [42] Jackson.H.A, CAPT.P.E, "Submarine Parametrics", Royal institute of naval architects international symposium on naval submarines, London, England, 1983.
- [43] D.F.Myring, "A Theoretical study of body drag in subcritical axisymmetric flow", 1976
- [44] S.F.Hoerner, "Fluid Dynamic Drag", 1965.
- [45] L.Greiner, "Underwater missile propulsion : a selection of authoritative technical and descriptive papers ", 1968.
- [46] E.V.Denpol, "An estimation of the normal force and the pitching moment of 'Teardrop' underwater vehicle", 1976.
- [47] N.C.Groves, T.T.Haung, M.S.Chang, "Geometric Characteristics of DARPA SUBOFF model", David Taylor Research Centre, 1989.

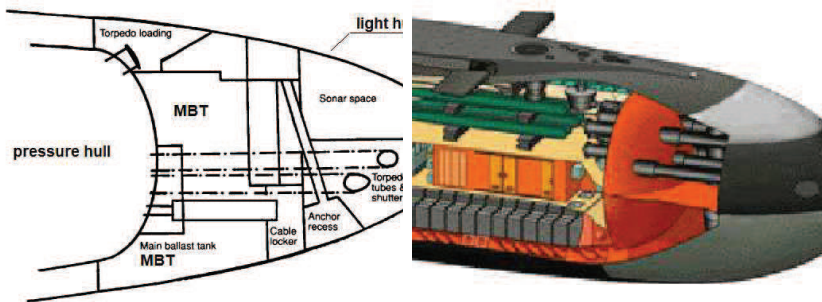
- [48] Roddy, R., 1990. "Investigation of the stability and control characteristics of several configurations of the DARPA SUBOFF model (DTRC Model 5470) from captive-model experiments". Report No. DTRC/SHD-1298-08, September.
- [49] Jerome S. Parsons, Raymond E. Goodson, Fabio R. Goldschmied, "Shaping of Axisymmetric Bodies for Minimum Drag in Incompressible Flow", J. HYDRONAUTICS, VOL.8, NO. 3, pp:100-108, JULY 1974.
- [50] Brenden Matthews, "Design and Development of UUV", University of New South Wales, Australian Defence Force Academy, School of Engineering and Information Technology Canberra, Thesis Report, 2010.
- [51] Volker Bertram, Alberto Alvarez "Hull Shape Design of a Snorkeling Vehicle".

Chapter 3: Submarine Bow Shape

3-1- Bow Shape Equations

3-1-1- Introduction

Bow of submarine, plays some roles in submarine hydrodynamic design, specially stagnation point (location and pressure) that forms the boundary layer on the overall of the body. The focus of this chapter is on the resistance at fully submerge mode without free surface effects. In addition to the hydrodynamic, the shape of the bow, depends on the internal architecture and arrangements inside the bow part.

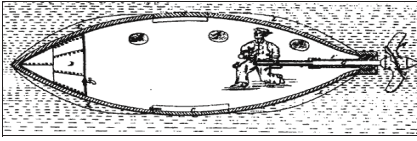


Typical bow arrangement [1]

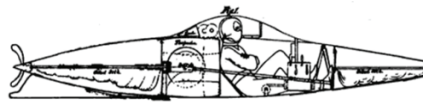
Kilo class bow arrangement

Figure 1: General arrangement of bow part of submarine

Figure 1 shows a usual internal arrangement inside the bow part of submarine that limits and forms the shape of the bow. Related materials about general arrangement in naval submarines are presented in Refs.[1,2]. According to Fig.1, the bow part, is composed of pressure hull (fore compartment) and light hull. The light hull, is a steel hull with a small thickness (compare to the pressure hull) that can be formed easily. The curvature of the bow shape should be acceptable for arranging all equipment with reasonable clearance for accessibility and repairing. The most part of the bow is occupied by main ballast tank (MBT) which needs a huge volume inside the bow but doesn't affect the bow shape because only the absolute volume is important.



Ogive shape bow- Philips submarine (1852)



Conic shape bow- J.Holland (1874)



Ship shape bow- German submarine (U-Boat) (1941)



Conic-elliptic bow- Astute Class Nuclear Submarine (1977)



Elliptic bow shape- Le Terrible class submarine (2010)



An over view

Figure 2: Evolution of bow shape of submarines

Passive sonar occupies a big volume that is vital for submarine navigation, therefore, can strongly affect the bow shape. Several torpedo tubes, are the next essential elements for arranging inside the bow. The resultant shape, should have the minimum resistance. The focus of this chapter is on the curvature of the bow for minimizing the resistance. Figure 2 shows some bow shape of submarines.

3-1-2- Some important factors in bow form design

For a well judgment and the best selection of bow form, the most important factors in the bare hull form design are counting as: 1) minimum flow noise especially around sonar and acoustic sensors. 2) minimum submerged resistance 3) general arrangement demands especially for Main Ballast Tanks

(MBT) and torpedo tube arrangement. The focus of this book is on the curvature and the shape of the bow for minimizing the resistance.

3-1-3- Bow form equations

As mentioned in "Introduction", there are several sources about equations of bow form, which will be presented here. Extensive hull form equations of submarine are presented in Ref.[31].

A) According to Refs.[3,4]: The equations are presented as "DREA Model" that is shown in Fig.3 and includes the specification of bare hull and appendages. The DREA model is specified in three sections; bow, midbody and tail. The fineness is $L/D=8.75$ so that bow length is equal to $1.75D$ and midbody length is $4D$ and stern length is $3D$. Axisymmetric profile of the bow is:

$$\frac{r}{D} = 0.8685 \sqrt{\frac{x_F}{D}} - 0.3978 \frac{x_F}{D} + 0.006511 \left(\frac{x_F}{D}\right)^2 + 0.005086 \left(\frac{x_F}{D}\right)^3 \quad (1)$$

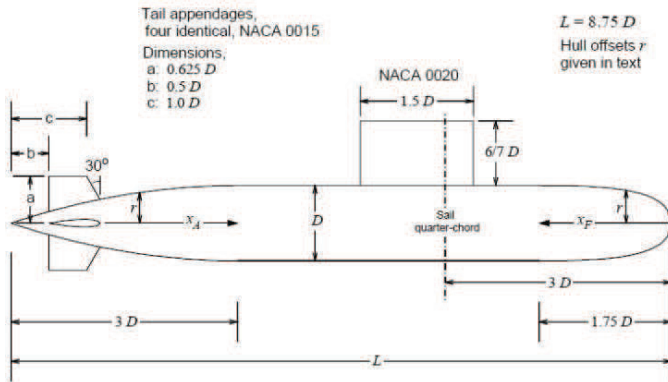


Figure 3: Parameters of DREA submarine hull [3]

B) According to Refs.[5-9]: The equations are presented as "Hull Envelope Equation". The envelope is first developed as a pure tear drop shape with the fore body comprising 40 percent of the length and after body comprising the remaining 60 percent [6]. The forward body is formed by revolving an ellipse about its major axis and is described by the following equation:

$$Y_f = R \left[1 - \left(\frac{X_f}{L_f} \right)^{n_f} \right]^{1/n_f} \quad (2)$$

The quantity Y_f is the local radius of the respective body of revolution with X_f describing the local position of the radius along the body (Fig.4). For $n_f=2$; the bow shape profile is an elliptic form, and for $n_f=1$; the bow profile is a conical form. If a parallel middle body is added to the envelope, then cylindrical section with a radius equal to the maximum radius of the fore and after the body is inserted in between them.

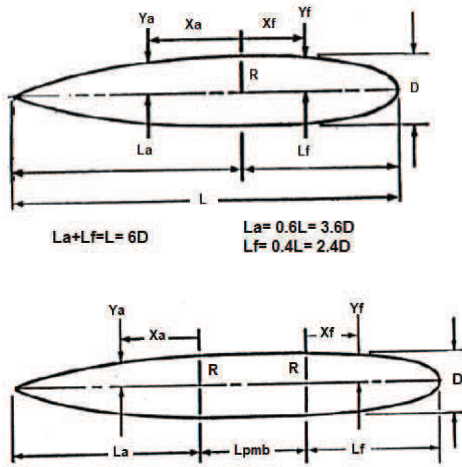


Figure 4: Coordinates and parameters in submarine hull

This equation is rewritten to another face in Refs.[6,10,11] for another coordinate origin (Fig.5), and the shape optimization is done for snorkeling in snorkel depth.

$$r_f = R \left(1 - \left(\frac{(x - L_a - L_c)}{L_f} \right)^{n_f} \right)^{1/n_f} \quad (3)$$

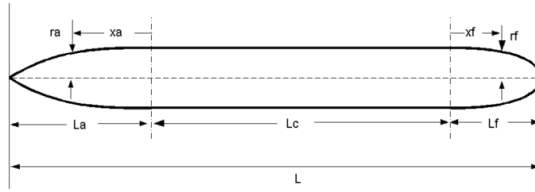


Figure 5: Coordinates and parameters in submarine hull

The simulation of the hull form with different coefficients is presented in Fig.6.

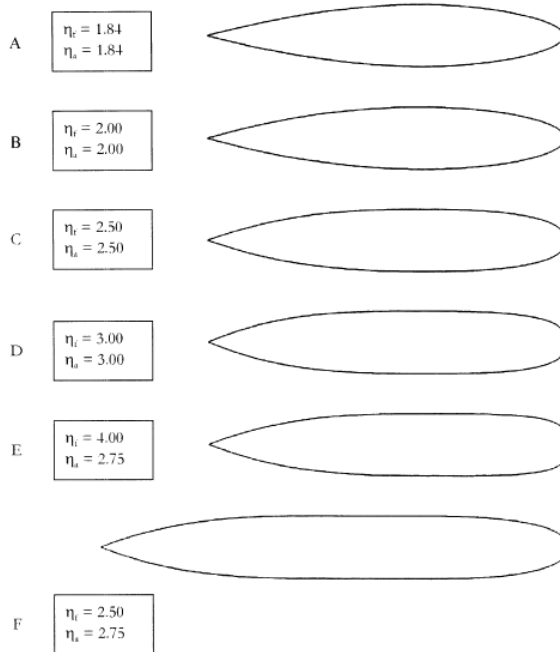


Figure 6: Hull form with coefficients of η_a , η_f [9]

C) According to Refs.[12,13]: The equations are presented as "Myring Equations" for earning minimum resistance, and many submarines, AUVs and UUVs are designed according to these equations such as REMUS [12] which

describes a body contour with a minimal resistance coefficient for a given fineness ratio (maximum length to the maximum diameter). The parameters "a,b,c,d,θ" are shown in Fig.7. Parameter "n" is an exponential parameter which can be varied to give different body shapes. These equations assume an origin at the nose of the vehicle. Nose shape is given by the modified semi-elliptical radius distribution.

$$r(\Xi) = \frac{1}{2} d \left[1 - \left(\frac{\Xi + a_{\text{offset}} - a}{a} \right)^2 \right]^{\frac{1}{n}} \quad (4)$$

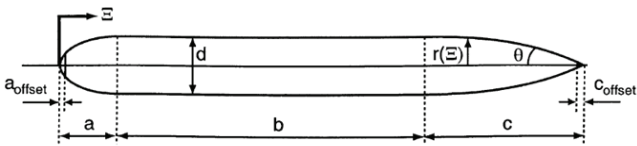


Figure 7: Myring profile

D) According to Refs.[14,15]: The equations are presented as "SUBOFF Model" from Defence Advanced Research Project Agency (DARPA) that is shown in Fig.8 with coordinate location. Two geometrically identical models are designed to a linear scale ratio of 24 with detailed equations and shape specifications for computer programming and modeling in CFD and experimental model test [15]. Extensive hydrodynamic results are presented in Ref.[16].

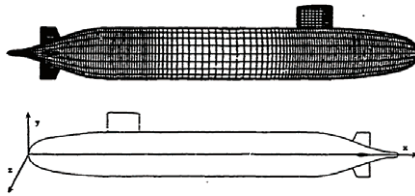


Figure 8: SUBOFF hull and coordinate [15]

Bow

in $0 < x < 3.333$ (ft) is:

equation

$$r = R \left[1.126395101x(0.3x - 1)^4 + 0.442874707x^2(0.3x - 1)^2 + 1 - (0.3x - 1)^4(1.2x + 1) \right]^{1/2.1} \quad (5)$$

3-1-4- Specifications of the models for CFD modeling

The base model that considered here, is an axis-symmetric body similar to torpedo, without any appendages because in this study, only bow effect on resistance, is wanted to be studied. It helps to quarterly CFD modeling of the body and saving the time. The stern is conical and middle part is a cylinder, but bow part is different for each model. In this chapter, 19 models are studied. The 3D models and its properties are modeled in Solid Works. There are three main assumptions:

Assumptions 1: For evaluating the hydrodynamic effects of the bow, the length of the bow is unusually supposed large. It helps that the effects of the bow be more visible.

Assumptions 2: The shapes of the stern and middle part are constant in all models. Stern shape is a conical shape, and middle shape is a cylindrical shape.

Assumptions3: For providing more equal hydrodynamic conditions, the total length, bow, middle and stern lengths are constant. The diameter is constant too. Thus, L/D is constant in all models. These constant parameters, provide equal form resistance with except the bow shape which varies in each model. Then, the effects of bow shape, can be studied. Therefore, every model has different volume and wetted surface area.

Dimensions and speed of all models are mentioned in Tab.1.

Table 1: Main assumptions of models

V (m/s)	L (m)	L _r (m)	L _m (m)	L _a (m)	D (m)	L/D	bow shape
10	6	3	1	2	1	6	Different for each model

The analysis is performed in two stages: Stage A) General shapes of the bow for understanding the basis and principles of submarine bow design. Stage B) Bow shape based on the Eq.2 for different values of n_f . This equation is a well-known and well practice equation, that covers a wide range of bow forms. The specifications of all models are represented in Tab.2,3. In Tab.2, there is modeling of stage A, and Tab.3 included modeling of stage B. In addition, for CFD modeling in all models, velocity is constant and equal to 10 m/s that results in Reynold's number of more than 60 millions. This Reynolds is suitable for turbulence modeling because M.Moonesun, in Ref.[17] proved that total resistance coefficient after Reynolds of five millions can be supposed constant.

Table 2: Models of stage A

	bow shape profile	Aw	A0	volume
A1	ogive	12.77	0.785	2.58
A2	ogive- capped with circle	13.19	0.785	2.67
A3	conic	11.16	0.785	2.09
A4	conic caped with elliptic	14.41	0.785	3.03
A5	ship shape	13.85	0.785	2.49
A6	hemisphere	15.8	0.785	3.53
A7	elliptical	13.87	0.785	2.88
A8	DREA form (according to Eq.1)	15.19	0.785	3.33

The forms of these models are shown in Fig.9. In the model A1, bow is an ogive shape, consist of an ogive section of a circle so that be tangent to the cylinder. Model A2 is an ogive shape that is capped by a circle. This shape is usual in small wet submarines. Model A3 has a conic bow that is not usual in submarines but for understanding that, why this bow is not applicable in today submarines, are represented. Model A4, has a conical bow that is capped by an elliptic so that, the elliptic and conic are tangent together. Model A5, has a ship shape bow with a vertical sharp edge. This shape of the bow is unusual in today submarines because this bow shape is efficient for ships and free surface of water. This bow has minimum resistance in surfaced navigation but has a large amount of resistance in submerged navigation. It was usual in old submarines because those had a little battery storage and then, the most time of navigation had performed at the surface, and only for attacking had gone to submerged mode of navigation for a restricted time. Models A6 and A7 have a hemispherical and elliptical bow. Hemispherical bow is not a common practice bow but elliptical bow, is the most usual form of the bow. Most of the equations that mentioned above, are similar to elliptical bow, for example, in Eq.2, for $n_f=2$, the bow shape profile is an elliptic form. Model A8 is designed according to Equation.1 for DREA submarine. The configurations of these models are presented in Fig.3.

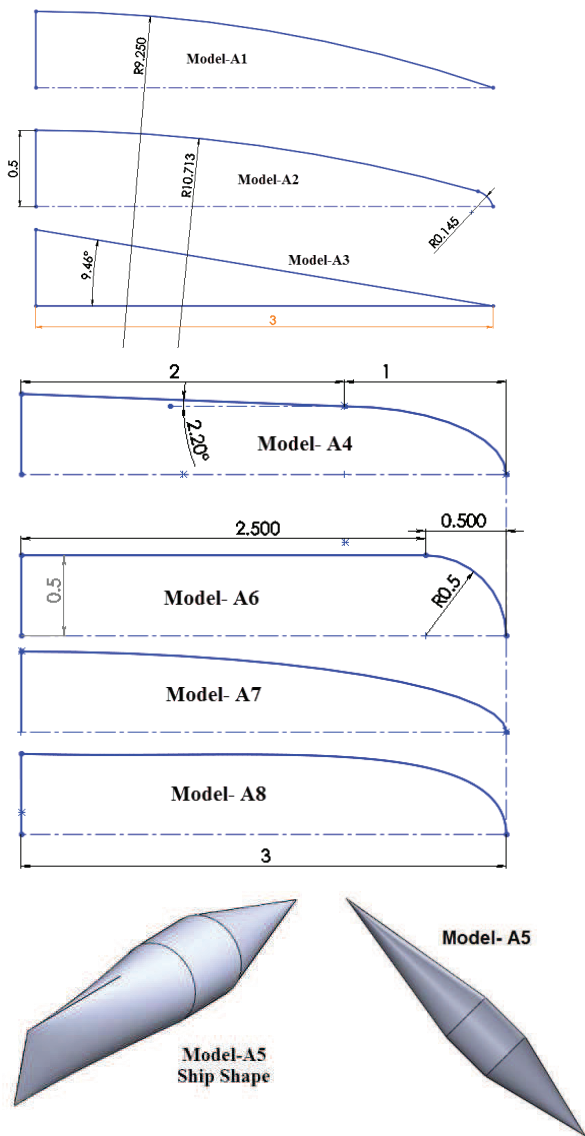


Figure 9: Configuration of models (stage A)

Table 3: Models of stage B according to Eq.2

	nf	Aw	A0	volume
B1	1	11.16	0.785	2.09
B2	1.15	11.79	0.785	2.26
B3	1.35	12.48	0.785	2.45
B4	1.5	12.9	0.785	2.58
B5	1.65	13.25	0.785	2.68
B6	1.75	13.45	0.785	2.75
B7	1.85	13.63	0.785	2.8
B8	2	13.87	0.785	2.88
B9	2.5	14.48	0.785	3.08
B10	3	14.87	0.785	3.21
B11	4	15.36	0.785	3.37
B12	5	15.64	0.785	3.46

In Tab.3, some profiles of the bow are presented, based on Equation (2). As showed in Fig.10, the values of nf , can be varied between 1.8~4 but for better understanding the effect of nf , the range of 1~5 are considered. For $n_f=2$, the bow shape profile is an elliptic form, and for $n_f=1$, the bow profile is a conical form. Increasing in nf is equivalent to increase in wetted surface area and enveloped volume. The configurations of these models are presented in Fig.10.

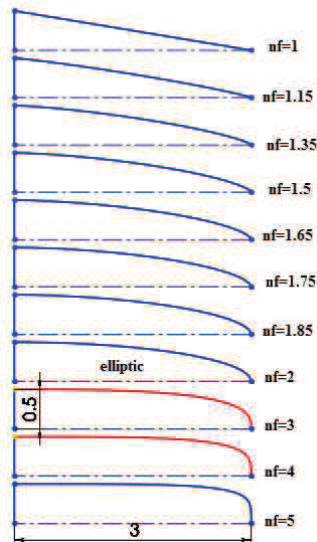


Figure 10: Configuration of models (stage B)

3-1-5- Preparations of CFD analysis

This analysis is performed by Flow Vision (V.2.3) software and FVM method. Transition of laminar layer to the turbulent layer in boundary layer at the bow, and flow separation is a very important factor in resistance calculations. Two significant parameters in CFD, for modeling the boundary layer, are Y^+ and mesh numbers, which should be selected correctly. For selecting the proper quantity of the cells, for one certain model (Model.A7) and $v=10\text{m/s}$, eight different amount of meshes were selected and the results remained almost constant after 1.2 millions meshes, and it shows that the results are independent of meshing (Fig.11). In all modeling the mesh numbers are considered more than 1.7 millions.

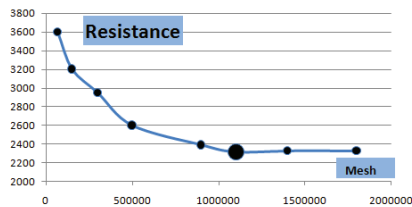
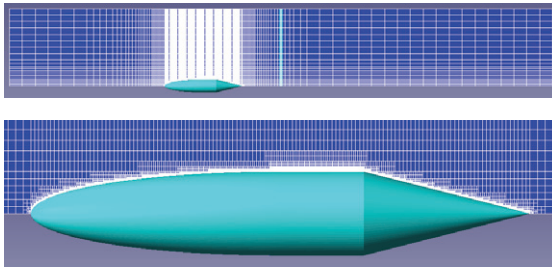
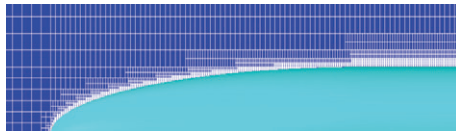


Figure 11: Mesh independency evaluations

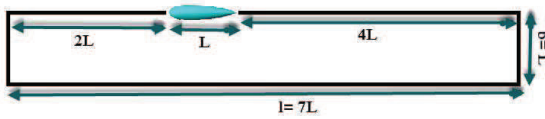
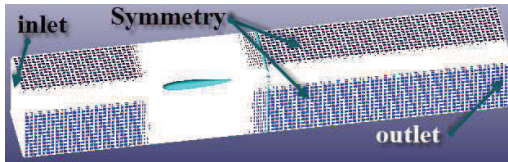
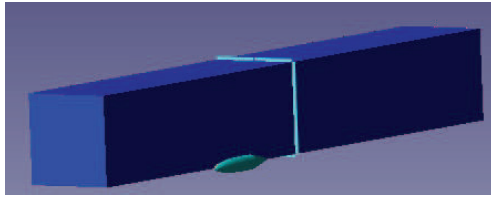
For the selection of suitable iteration, it was continued until the results were almost constant with variations less than one percent, which shows the convergence of the solution. All iterations are continued to more than one millions. In this domain, there is inlet (with uniform flow), Free outlet, Symmetry (in the four faces of the box) and Wall (for the body of submarine). Dimensions of cubic domain are 42m length (equal to $7L$), 6m beam and 6m height (equal to L or $6D$). Only quarter of the body is modeled because of axis-symmetric shape, and the domain is for that. Meanwhile, the study has shown that the beam and height equal to $6D$ in this study can be acceptable. Here, there are little meshes in far from the object. The forward distance of the model equals to $2L$ and after distance is $4L$ and the total length of $7L$ (Fig.12). The turbulence model is K-Epsilon and y^+ is considered equal to 30. The considered flow is incompressible fluid (fresh water) in 20 degrees centigrade and constant velocity of 10 m/s.



(a)



(b)



(c)

Figure 12: (a) Domain and structured grid (b) Very tiny cells near the wall for boundary layer modeling and keeping y^+ about 30 (c) Quarterly modeling because of axis-symmetry

3-1-6- CFD Analysis

In this chapter, the main goal is estimation of the resistance. The total resistance of a fully submerged submarine is composed of frictional resistance and viscous pressure resistance, but there is not wave resistance. The frictional resistance depends on the wetted area, and viscous pressure resistance depends upon the form of the object. Here, for optimization of the bow shape, both of these resistances are needed because in a given length, by changing the bow shape, the wetted area and the form will be changed. These values are presented in Tab.4 and Tab.5.

Table 4: Resistance components of Models in stage (A)

bow shape	R	Rvp	Rf	Rvp/R
ogive	1948	292	1656	15.0
ogive-circle	2036	348	1688	17.1
conic	1944	452	1492	23.3
conic-elliptic	2416	608	1808	25.2
ship shape	2488	660	1828	26.5
hemisphere	3280	1360	1920	41.5
elliptical	2336	620	1716	26.5
canadian form	2624	800	1824	30.5

Table 5: Resistance components of Models in stage (B)

nf	Rt	Rvp	Rf	Rvp/Rt (%)
1	1944	452	1492	23.3
1.15	1820	276	1544	15.2
1.35	1876	284	1592	15.1
1.5	1952	316	1636	16.2
1.65	2060	344	1716	16.7
1.75	2200	452	1748	20.5
1.85	2264	500	1764	22.1
2	2196	424	1772	19.3
2.5	2388	556	1832	23.3
3	2724	872	1852	32.0
4	3052	1204	1848	39.4
5	3368	1512	1856	44.9

Pressure resistance depends upon the pressure distribution over the body, and pressure distribution depends upon the form. The more uniform pressure distribution meant lesser resistance. The pressure distribution for several shapes is presented in Fig.13. Ships shape bow, is not a good design for fully submerged condition (without free surface), thus, it can be seen in Fig.13-a,

that high pressure area encompassed the most parts of the bow. It causes the high value of resistance. Hemispherical bow is a blunt and thick bow. Therefore, there is a highly intense high pressure area at the tip of the bow, as shown in Fig.13-b. It causes a greatly high value of resistance. The elliptical bow, as shown in Fig.13-c, has almost uniform distribution of pressure, which can result in lesser value of resistance. The pressure on the hull will be imposed upon the volume of fluid about it, as shown in Fig.13-c.



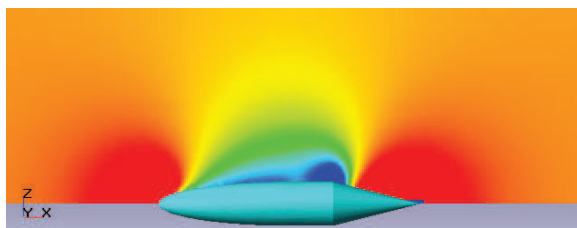
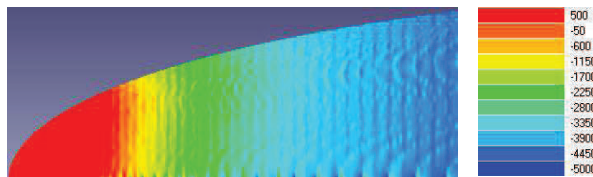
(a) Model A-5: ship shape bow



(b) Model A-6: hemisphere bow



(c) Model A-7: elliptical bow



(d) Contours of pressure and related values

Figure 13: Pressure distribution over the body

The results of CFD analysis in stage "A" is presented in Tab.6 and diagrams of Fig.14.

Table 6: Specification of Models in stage (A)

bow shape	Rt	Aw	Cd*1000	Cv*100
ogive	1948	12.77	33.90	2.07
ogive-circle	2036	13.19	34.30	2.12
conic	1944	11.16	38.71	2.38
conic-elliptic	2416	14.41	37.26	2.31
ship shape	2488	13.85	39.92	2.71
hemisphere	3280	15.8	46.13	2.83
elliptical	2196	13.87	35.18	2.17
DREA	2624	15.19	38.39	2.35

In table 6, C_d , is resistance coefficient based on wetted area (A_w) but C_v , is resistance coefficient based on $(\text{volume})^{2/3}$ that can describe the effect of earned volume in every shape. The formula is:

$$C_v = \frac{R}{0.5 \cdot \rho \cdot v^2 \cdot V^{\frac{2}{3}}} \quad (6)$$

As mentioned before, another important coefficient that can describe both parameters is "Semnan" coefficient so as:

$$\text{Semnan coefficient } (K_{sn}) = \frac{(\text{Volume})^{\frac{1}{3}}}{\text{Resistance Coefficient}} \quad (7)$$

This coefficient can be named "Hydro-Volume" efficiency, because it counts both resistance and volume. For this coefficient, the bigger values meant the better design. In some cases, a shape has minimum resistance but has a little volume in a given constant length. Thus it can't be a good selection (such as Model A3 and A5). These diagrams are presented in Fig.14. According to this Figure 14-a and b, conic bow shape has the least values of wetted area and volume but hemispherical bow shape, has the most values of them. In Fig.14-c, resistance diagram, it is obvious that in a given length, hemispherical bow has the most values, and conic bow has the least values. Resistance coefficient based on wetted area is shown in Fig.14-d, which shows, hemisphere bow and ship shape bows have the most (worst) values. ogive bow has the least (best) value and elliptical and conic elliptical bows, have the middle values of the resistance coefficients. Resistance coefficient based on volume (Fig.14-e) shows that, the hemisphere and ship shape bows have the most (worst) values, and ogive bow has the least (best) value. Finally, the Fig.14-f, represents the

best criterion for judging between the bow shapes. This figure shows that ogive shape has the most efficiency and conic, hemisphere and ship shape bow, have the least (worst) values. Now we can select a good bow shape. As shown in Fig.14, the bow shapes of conic, hemisphere and ship shape, are the worse selection in resistance and volume point of view. Hemisphere bow has the most values of resistance coefficient and resistance, while provides a good space for architecture but Fig.14-f, showed that hemisphere bow can't be a good selection.

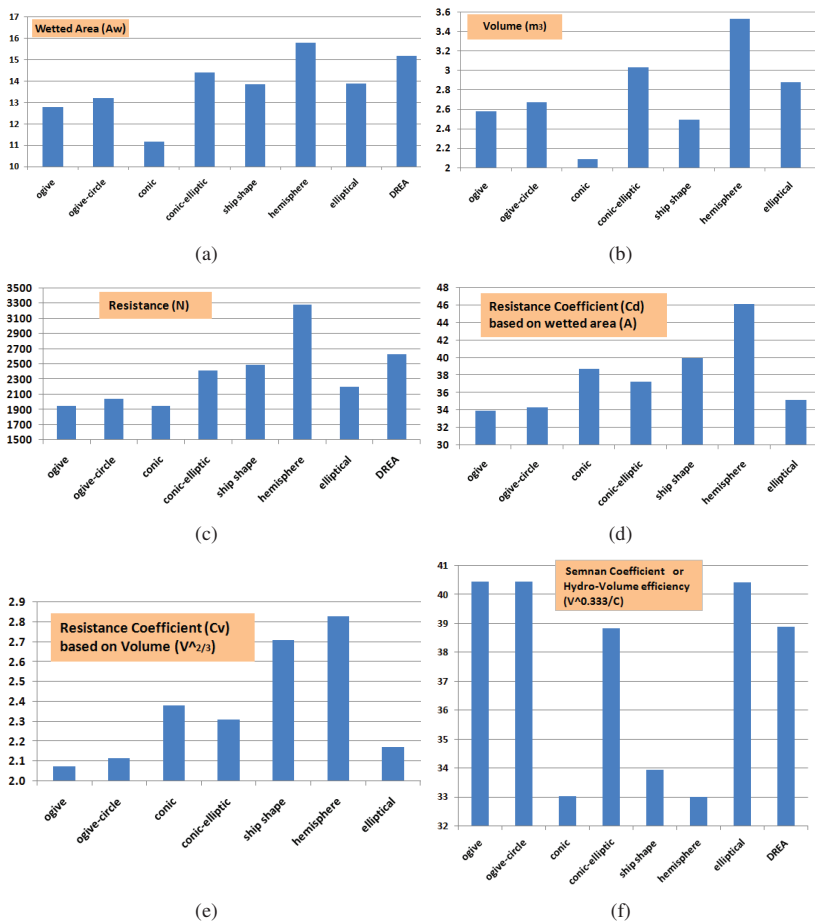


Figure 14: Results of CFD analysis on different bow shape (stage A)

Conic shape results in the minimum values of resistance and middle values of resistance coefficients but has the minimum volume in a given length; then conic bow can't be a good selection, as it was shown in Fig.14-f with minimum efficiency. Ship shape bow has high values of resistance coefficient and resistance with low value of volume. Therefore it has a very low efficiency in Fig.14-f, and is rejected for selection. Ogive and ogive capped with the hemisphere, have the minimum values of resistance coefficients and low values of resistance. Ogive bow seems to have a good condition in resistance aspect of view but isn't a good selection because it has low values of volume. This bow has steep frontal curvature that isn't a good configuration for arranging the sonar and torpedo tubes at the front of really naval submarines. Thus ogive bow is rejected despite the maximum values of efficiency in Fig.14-f and minimum values of the resistance coefficients. Finally, three remained bows can be discussed as a good selection: elliptical, conic elliptical and DREA form. These three bows have almost similar results. DREA form has more resistance and resistance coefficient compare to other two bows, but has better efficiency in Fig.14-f, thus can be a good selection. Generally elliptically bows are recommended. The result of CFD analysis in stage "B" is presented in Tab.7 and diagrams of Fig.15.

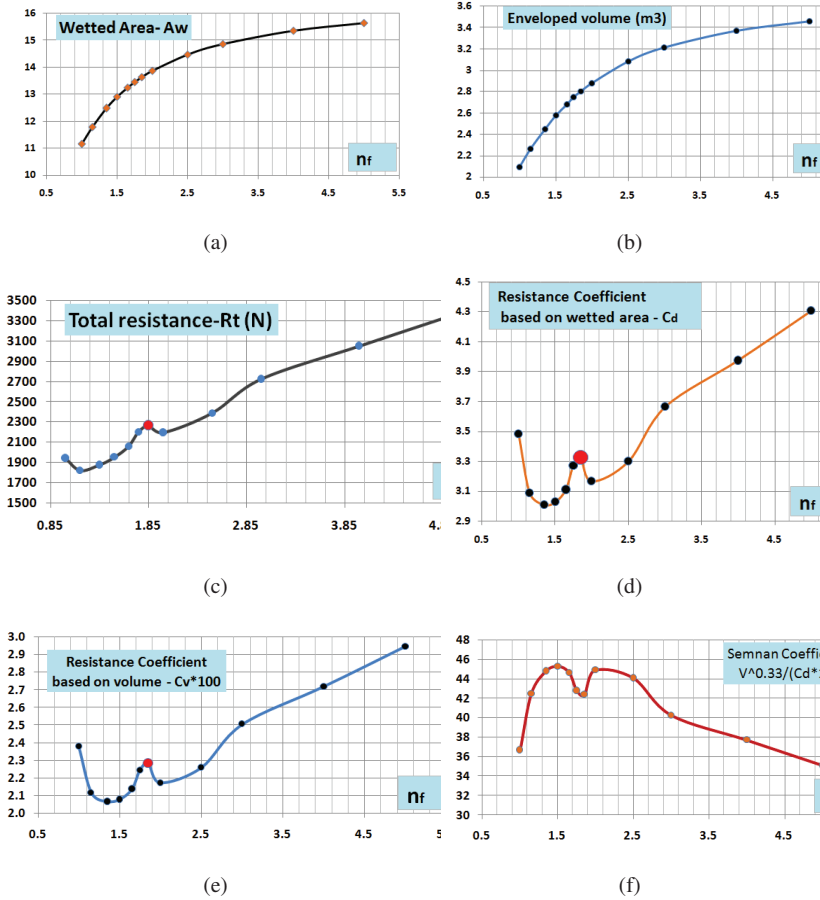


Figure 15: Results of CFD analysis on different bow shape (stage B)

The focus on this stage, is on the Equation.2 by variation in the values of n_f . This equation, covers a wide variety of bow profiles, thus the focus of this chapter in stage B, is concerned to it. As showed in Fig.15, the values of n_f , can be varied between 1.8~4 but for better understanding the effect of n_f , the range of 1~5 are considered. For $n_f=2$, the bow shape profile is an elliptic form, and for $n_f=1$, the bow profile is a conical form. Increasing in n_f is

equivalent to increase in wetted surface area and enveloped volume. In this chapter, the range of $n_f=1.35\sim 2$ are studied more because this range has some extremum points. The variations after $n_f=2$, is approximately linear, and the values less than $n_f=1.35$ aren't common practice in naval submarines. An overview on the results shows that, in this range, $n_f=1.85$ has maximum resistance and resistance coefficient, and minimum efficiency coefficient that means the worst results. The total resistance diagram shows that $n_f=1.15$ has minimum value and $n_f=1.85$ has the most value. Bow shape according to $n_f=1.15$, is a sharp bow that is unsuitable in architecture point of view. Diagrams in Fig.15-d and 15-e, that are resistance coefficients, which show that $n_f=1.35$ has the minimum (best) values, and $n_f=1.85$ has the maximum (worst) values. Diagram "f" in Fig.15 is the most important parameter for judging between them. This diagram shows that around $n_f=1.65$ and 2.5, there are local maximum points, which meant good selections for design, especially in $n_f=2.5$ that has maximum hydro-volume efficiency (Semnan coefficient). Values around $n_f=1.75\sim 1.85$, show the local minimum points which must be avoided in design.

Table 7: Specification of Models in stage (B)

nf	Rt	Aw	Cd*1000	V/(Cd*10)	Cv*100
1	1944	11.16	3.484	59.99	2.38
1.15	1820	11.79	3.087	73.20	2.11
1.35	1876	12.48	3.006	81.49	2.07
1.5	1952	12.9	3.026	85.25	2.08
1.65	2060	13.25	3.109	86.19	2.14
1.75	2200	13.45	3.271	84.06	2.24
1.85	2264	13.63	3.322	84.28	2.29
2	2196	13.87	3.167	90.95	2.17
2.5	2388	14.48	3.298	93.38	2.26
3	2724	14.87	3.664	87.62	2.51
4	3052	15.36	3.974	84.80	2.72
5	3368	15.64	4.307	80.34	2.95

According to these diagrams, some formulas can be fitted to them. The formula of relation between resistance coefficient (Cd) and n_f is:

For $1.15 < n_f < 2$:

$$C_d = (-11.85.n_f^4 + 70.31.n_f^3 - 153.73.n_f^2 + 146.62.n_f - 48.48) * 10^{-3} \quad (8)$$

3-1-7- Review

In this chapter, a study of the equations of bow form of submarines and CFD analysis on them, has been performed. These are the most famous equations in submarine form design. For a well judgment and the best selection of the bow form, the most important factors in bow form design must be counted such as: minimum flow noise specially around sonar and acoustic sensors, minimum submerged resistance and general arrangement and volume demands. The focus of this chapter is on the CFD analysis of submerged resistance by Flow Vision software. This study has shown that:

- 1) "Semnan Coefficient" can be presented as a important parameter in submarine shape design that counts both parameters: resistance coefficient and volume. It can be named "hydro-volume efficiency".
- 2) Conic bow and ship shape bow aren't a good design because of high values of resistance coefficients and very low values of hydro-volume efficiency.
- 3) Simple hemispherical bow isn't a good selection in design because of high values of resistance coefficients and the least value of hydro-volume efficiency. This form is not recommended at all.
- 4) Ogive bow shape has a good result in resistance coefficient and hydro-volume efficiency, but this shape isn't a common practice in really naval submarines because of many difficulties in internal arrangements of the bow.
- 5) Elliptical bow and other shapes similar to that, have the best acceptable results in resistance coefficients and hydro-volume efficiency. This shape of the bow, is highly recommended.
- 6) The coefficients around $nf=1.75\sim 1.85$ may have the worse results, but the coefficients around $nf=1.65$ and 2.5 are good selections for design, especially in $nf=2.5$ that has maximum hydro-volume efficiency.

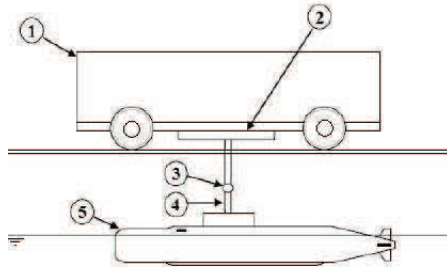
3-2- Bow Shape Model Test Results at surface motion

The extended report of this section is presented in [18]. Flow measurement around a model ship with propeller and rudder for the design of hull forms with better resistance and propulsive performance (Zhang 2012)(Van and Kim, 2006) [3], The bow wave breaking and the viscous interaction of stern wave study by simulating the free-surface flows (Seung-Hyun Kwag)(Kwag 2000) [4] and Shape optimization of bow bulbs with minimum wave-making resistance based on Rankine source method. Optimum hull shape of an underwater vehicle moving near the surface was studied by Alvarez(Alvarez,

Bertram et al. 2009) [21]. Suman designed and tested an ellipsoidal head, to evaluate the functionality for improved hydrodynamic performance of an underwater vehicle [22]. The designed vehicle having ellipsoidal heads of different major to minor axes ratio is fabricated and tested experimentally to validate the computational results. The result shows that the hydrodynamic performance of the vehicle can be improved with ellipsoidal profile head in submerged conditions. Numerical study on control effectiveness of a high-speed underwater vehicle with cruciform stern configuration using a computational fluid dynamics approach was done by Kim [23]. The calculation of the control derivatives of the underwater vehicle is validated by comparison with the experimental results of towing tank tests. The numerical results show that the force derivatives of the vehicle are over predicted by about 5% and the moment derivatives of the vehicle are over-predicted by about 10%.

3-2-1-Equipments and Experimental Procedure

Experiments were conducted in the towing tank which has 108(m) length, 3 (m) width and 2.2 (m) depth. The basin is equipped with a trolley that able to operate in 0.05-6 m/s speed with ± 0.02 m/s accuracy. The trolley is moved by two 7.5 KW electromotor. The trolley is controlled via a wireless system from control room of the lab. The system prepared with proper frequency encoder, i.e., 500 pulses in minutes, which decreases the uncertainty of measurements. A three degree of freedom dynamometer is used for force measurements. The dynamometer was calibrated by calibration weights [19]. Data are recorded via an accurate data acquisition system. The dynamometer equipped with 100 N load cells that has 1 percent uncertainty. An amplifier set are used to raise signals of load cells and to reduce the noise sensitivity of the system. All data are filtered to eliminate the undesirable accelerating parts of the motion data, Primary and terminative motion of trolley. The data presented within this chapter for each point is an average of several towing tank runs [20]. For each run, at least 750 samples in 15 seconds were collected and ensemble averaged. Schematic of the model and the overall test set up is shown in Figure 16.



Trolley; 2. Dynamometer; 3. Change trim angle mechanism; 4. Strut; 5. Model

Figure 16: Model setup in the towing tank

As indicated, the main purpose of the present work is to explore the effect of bow shape on the hydrodynamic behavior, i.e., residual and total resistance of a submarine in surface motions. The experiment conducted with a submarine model that is made by wood according to ITTC recommendations [25-29]. For bow effect study on total resistance, two bows with same length are manufactured. Figure 17 shows the profiles of bows. Profile A and B are tango and standard bow shape respectively. Table 8 provides a summary of the scale model characteristics.

Table 8: A summary of scale model characteristics

Length	2110 mm
Maximum Diameter	233 mm
Length of each bows	390 mm
Draft	183 mm
Mass	32 kg



Figure 17: The Bows profiles; tango shape (A) and standard shape (B)

3-2-2-Results and Discussions

In order to investigate the effects of bow profile on hydrodynamic performance of the vehicle, total resistance of the model is measured in a range of Froude numbers. Figure 18 shows the variation of forces acting on the model versus Froude number for tango and standard bow profiles.

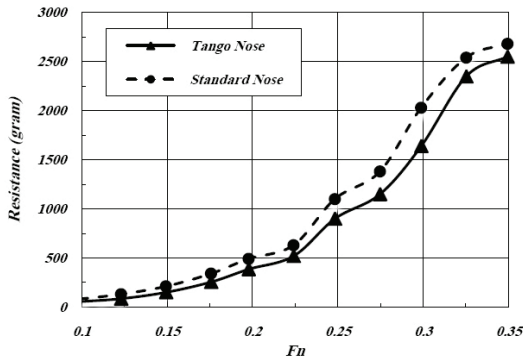


Figure 18: Variation of total resistances versus Froude Number for tango and standard bows at trip conditions

The figure clearly shows that the total resistance increases with Froude number. Figure 18 shows that after critical Froude number ($F_n=0.22$), the trend of total resistance decline with sharp slope, but before this Froude number, the trends of results progress such as a straight line and the variations are limited. Additionally, at the low Froude number ($0.098 < F_n < 0.22$), difference between total resistances caused by tango and standard bows are low (less than 1.08 N). However, at higher Froude numbers ($0.22 < F_n < 0.3$), the amount of total resistance for Standard bow is higher than that of Tango bow. Maximum difference is 3.82 N that observed at F_n of 0.3 where total

resistance of model with standard and tango bows is 16.08 and 19.91 respectively. At $Fr=0.22$, total resistance increases suddenly this means that critical Froude number of this vehicle is 0.22. The total resistance is the sum of friction resistance and residual resistance. Figure 19 shows the variations of these types of resistance as function of Froude number in a two graph for two bows. Figure shows that all types of resistances increase by Froude numbers.

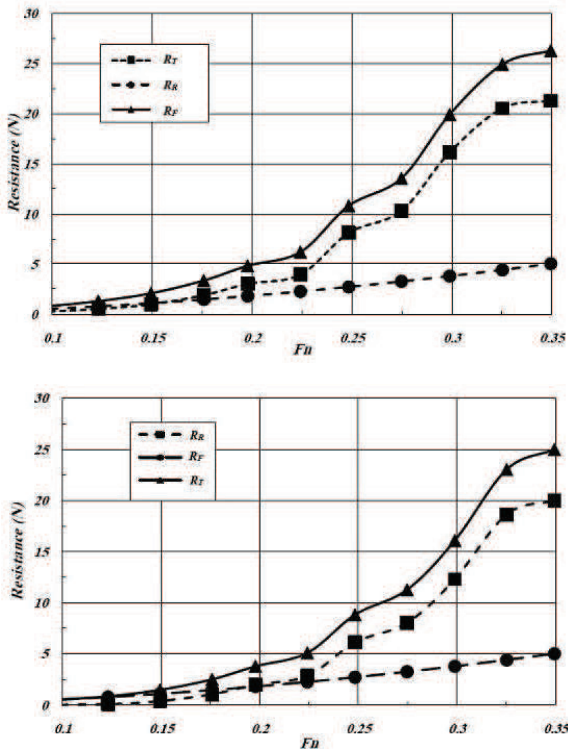


Figure 19: Variations of total, residual and friction resistances as function of Froude number in a two graph for Standard bow (First graph) and Tango bow (Second graph)

By inspection on the Figure, one can find that in $Fr=0.22$, there is a rapid augmentation in the total resistance. In low Froude numbers, friction resistance is main part of the total resistance. The result shows that for the model with tango bow at $Fr=0.098$, the residual resistance is 4 percent of total

resistance But for model with standard bow at the same Froude number, residual resistance is 33 percent of total resistance. In this Froude number and for both bows, friction resistance is the biggest component of submarine total resistance. By increasing Froude number to 0.197, residual resistance to total resistance ratio for tango and standard bows is 52% and 62% respectively. In Froude number between 0.3 to 0.325 residual resistances is major component of total resistance for two bows.

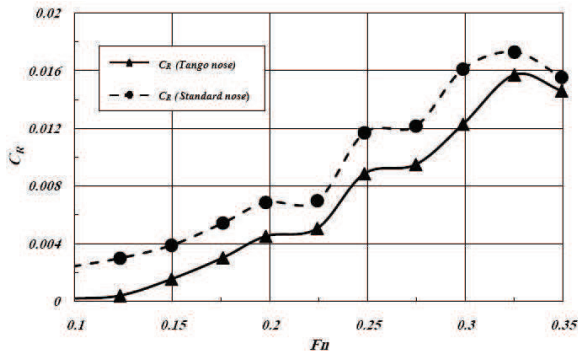


Figure 20: Variation of residual resistance coefficient with Froude number for two cases

On the other hand, the friction resistance is not a strong function of Froude number for two cases. The friction resistance depends on model dimensions and its wetted area. The length of the model and its wetted surface for the tango and standard bows are the same. Thus, the friction resistance coefficients for two types of bows are nearly the same. Using measured data of total and calculated friction resistance it is possible to find residual resistance. Fig.20 shows the variations of the residual resistance coefficient against Froude number for two bows. The findings show that the quantity of the residual resistance coefficient of the standard bow is more than tango shape. It is evident that there are many humps showing undesirable interactions and hallow points mentioned to the desirable interaction between bow and stern waves on the graph. One may conclude that residual resistance coefficient depends on shape of the submarine bow robustly.

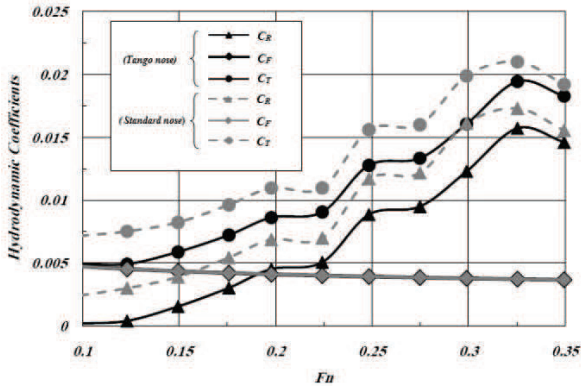


Figure 21: Variations of hydrodynamic coefficients resistance by Froude number

Fig.21 shows the variation of total, residual and friction resistance coefficients as a function of Froude number for two bows. The graph shows that the friction coefficient for two bows is the same. Other coefficients for standard bow are bigger than the tango bow, leading to higher total resistance for submarine with standard bow. Hump and hollow points for two bows are the same which shows that the hump and hollow points don't depend on bow shape and depend on model length. According to the graph, Frictional resistance coefficient over range of the study is limited. However, the residual resistance coefficient for two bows increases by Froude number. At $Fn=0.22$, residual resistance coefficient behaves like total resistance and has a sharp increase around this critical Froude number.

3-2-3- Investigation of flow

Investigation of Flow pattern is a significant method for fluid studies. The ability to see flow patterns around an underwater vehicle under experimental investigations often gives insight into design and optimization process. Here, the investigation of flow experiments is performed to realize the fluid physics on and around the model with different bows. Fig.22 shows the wave product by both of bow shapes at different velocities.

Submarine with Tango Nose Profile



Submarine with Standard Nose Profile

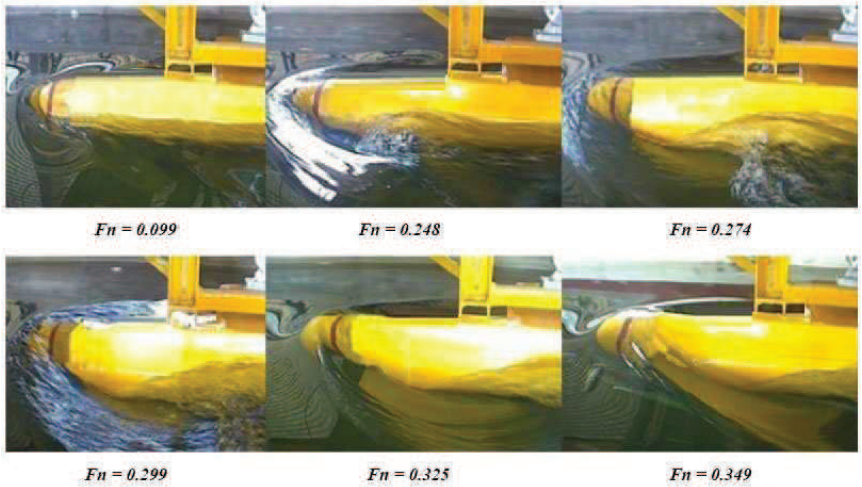


Figure 22: Flow investigations of waves made by tango and standard bows in around the bow body in different Froude number

All patterns are obtained by a high resolution camera fixed on the trolley. Fig.23 show the waves made by bows at bow area of the model extended from wave crest due to high pressure stations.

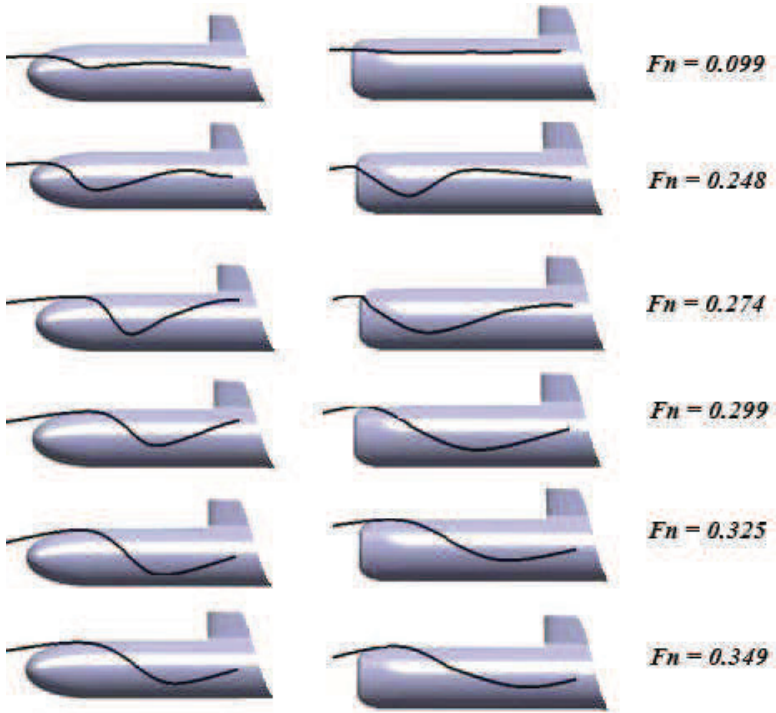


Figure 23: Trajectories of the waves from bow to stern of the model with the both types of bows at different velocities

The wave in aft and forward portion of shoulder involves in low pressure stations and extended from waves depth. The height of waves depended on values of velocities, and it increases for higher velocities. It is evident that at $F_n=0.099$ the heights of waves are very minute for both bows. For the tango bow, with an increase the Froude number to 0.248, the first wave crest appears at the tip of the bow where the distance between first crest to the next crest is nearly equal to the length of the bow. At higher Froude number, the wave height from the bow and the distance between the initial crest to the next, is

more than that of lower Froude numbers. Further, at $Fn=0.274$, the waves will be collected on the top of the submarine bow. In higher Froude number (0.299 and 0.325); water covers a part of the bow. Finally in $Fn=1.59$, water covers all of bow and some part of the deck. The similar results for the standard bow for $Fn=0.099$ to $Fn=1.59$ are indicated in Figure 9. One can find that the physics are almost such as the tango case but the distance between two crests is less than the tango bow and interferences of the waves are dissimilar. In order to investigate the effect of waves on hydrodynamic performance of the vehicle consider N , semi period number (equation 9). It is seen that for $N=1$, the bow wave started with crest and extended to wave depth of stern that can produce an undesired interference and increases the amount of wave resistance due to amplifying a low pressure region. A different phenomenon occurs for $N=2$. In this case, the waves move to the stern with the same behavior, i.e. with the crest of the wave. In other words, the crest and the depth of the wave are neutralized or weakened in the stern due to a preferred interference. Therefore, the wave resistance may slightly change. One may conclude that the wave resistance will increase for odd values of N where it is almost fixed for even counterparts. The variation in the local curvatures in Fig.23 mentioned to interferences between the bow and stern waves. If one can cancel out these interferences, the waves follow a parabolic route without any local changing; moreover, the resistance increases with the raise of velocity. The trajectories of the waves from the bow to stern of the model with both types of bows at different velocities are shown in Figure 21. The results show that the tango shape bow has the main effect on the wave breakage and decreases the resistance of the model than the other bow shape. Furthermore, for higher velocities, the height and length of the waves will increase. The profiles of bow and the Froude number have a significant role in the resistance of the model. As the results, the tango shape bow creates desirable behavior for waves and reduces the resistance relatively to standard bow at the same Froude number. One may conclude that there are two reasons for resistance reduction due to decrease the height of the wave. Firstly, the reduction of wave height can decrease wave making resistance; secondary, wave height reduction shall prevent of production of wave in critical condition and undesirable interactions.

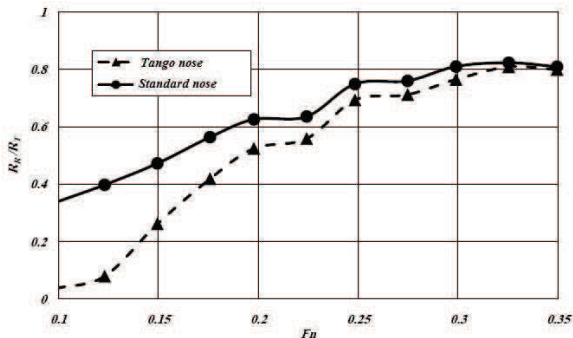


Figure 24: Variations of the portion of the wave making resistance to the total resistance for the model

Figure 24 shows variations of a portion of the wave making resistance to the total resistance for the model with different types of bows. The results clearly dictate that for lower velocities, there is a difference between the amount of this portion for tango and standard shapes of bows but at higher velocities, this portion has less dependency to the shape of the bow and is related to the length and the displacement volume of the submarine. This result shows that in low and middle Froude number ($F_n = 0.098-0.3$), height of wave caused by the tango bow is smaller than the standard bow. Therefore, tango bow is suitable for submarine in free surface motions.

3-2-4- Review

Experiments were performed to study the behavior of flow around a model of submarine with two types of bow shapes, i.e. tango and standard bows in free surface tests. The resistance components for different Froude numbers were considered. Finally, flow visualizations of wave fields around bows are done and wave field around two bows are compared. The Froude numbers were varied between 0.099 and 0.349. The trim angle of the model is adjusted equal to zero for all Froude numbers. Blockage fraction for the model is fixed to 0.0053. The following conclusions are obtained in this investigation:

1) The residual resistance of the standard bow is extremely more than the tango bow in surface motion that caused more total resistance for the submarine. However, in high Froude, bow shape effect decreases and the total resistance depends on submarine's length and displacement

- 2) The results show that the role of residual resistance is over 80 percent of the total resistance in larger Froude numbers where the variations of the friction resistance with Froude number are slightly increased. Furthermore, the length of the model and wetted surface for the tango and standard bows are the same. Thus, the amount of friction resistance coefficients for two types of bows are closely near.
- 3) The patterns of flow from visualization show that the waves made by bows at bow and stern areas of the model extended from wave crest due to high pressure stations. While, the waves in aft and forward portion of shoulder involves in low pressure stations and extended from waves depth. The height of waves depended on values of velocities and it increases for higher velocities. Furthermore, for the standard bow, the distance between two crests is less than the tango bow and interferences of the waves are dissimilar.
- 4) Finally, the profiles of the bow and the Froude number have a significant role in the resistance of the model. Here, the tango shape bow creates desirable behavior for waves and causes the least resistance relatively to standard bow at a same Froude number.

5) Nomenclature

A		Cross section area of towing tank (m^2)
a		Cross section area of model (m^2)
	A0	Cross section area (m^2)
	Aw	Wetted surface area (m^2)
C_f		Friction resistance coefficient
	Cd	Resistance coefficient based on wetted area
	Cv	Resistance coefficient based on volume
C_T		Total resistance coefficient
C_W		wave resistance coefficient
C_{vp}		Viscous resistance coefficient
C_R		Residual resistance coefficient
	D	Maximum hull diameter (m)
h		Combined wave height (m)
ha		Stern (aft) wave height (m)
hf		Bow (fore) wave height
ITTC		International Towing Tank Conference
	K_{sn}	Semnan coefficient
	La	Length of stern (m)
	Lf	Length of bow (m)
	Lm	Length of middle part (cylindrical) (m)
L		Maximum hull length (m)
LOA		Length overall (maximum length) (m)
LBP		Length between perpendiculars (m)
LWL		Level waterline length
LCP		Length of center of pressure
N		Semi period number
	n_f	Bow coefficient in Eq.2
	n_a	Stern coefficient
R		Resistance or drag (N)
Re		Reynolds number
	Rt	Total resistance in (N)
	r (Y)	Radial coordinate of hull (m)
S		Wetted surface area (m^2)
	x	Longitudinal coordinate of hull (m)
	v	velocity in (m/s)
V		Speed of model (m/s)
λ		Wave length (m)
ρ		Water density (kg/m^3)

References

- [1] Burcher R, Rydill L J, "Concept in submarine design", (The press syndicate of the University of Cambridge., Cambridge university press), 1998, pp. 295
- [2] M.Moonesun, P.Charmdooz, "General arrangement and naval architecture aspects in midget submarines", 4th International Conference on Underwater System Technology Theory and Applications 2012 (USYS'12), Malaysia.
- [3] Mackay M, "The Standard Submarine Model: A Survey of Static Hydrodynamic Experiments and Semiempirical Predictions", Defence R&D Canada, June 2003, pp.30
- [4] Christopher Baker, "Estimating Drag Forces on Submarine Hulls", Defence R&D Canada, September 2004, pp.131
- [5] D. Alemayehu, R.B.Boyle, E.Eaton, T.Lynch, J.Stepanchick, R.Yon," Guided Missile Submarine SSG(X)", SSG(X) Variant 2-44, Ocean Engineering Design Project, AOE 4065/4066, Virginia Tech Team 3 ,Fall 2005 – Spring 2006, pp.11-12.
- [6] Lisa Minnick, "A Parametric Model for Predicting Submarine Dynamic Stability in Early Stage Design", Virginia Polytechnic Institute and State University, 2006, pp.52-53.
- [7] Grant.B.Thomson,"A design tool for the evaluation of atmosphere independent propulsion in submarines", Massachusetts Institute of Technology, 1994, pp.191-193
- [8] Jackson.H.A, CAPT.P.E, "Submarine Parametrics", Royal institute of naval architects international symposium on naval submarines, London, England, 1983.
- [9] J.K.Stenars, "Comparative naval architecture of modern foreign submarines", Massachusetts Institute, 1988, pp.91.
- [10] Brenden Matthews, "Design and Development of UUV", University of New South Wales, Australian Defence Force Academy, School of Engineering and Information Technology Canberra, Thesis Report, 2010.
- [11] Volker Bertram, Alberto Alvarez "Hull Shape Design of a Snorkeling Vehicle".
- [12] Prestero Timothy, "Verification of a Six-Degree of Freedom Simulation Model for the REMUS Autonomous Underwater Vehicle", University of California at Davis, 1994, pp.14-15.
- [13] D.F.Myring, "A Theoretical study of body drag in subcritical axisymmetric flow", 1976
- [14] E.V.Denpol, "An estimation of the normal force and the pitching moment of 'Teardrop' underwater vehicle", 1976.
- [15] N.C.Groves, T.T.Haung, M.S.Chang, "Geometric Characteristics of DARPA SUBOFF model", David Taylor Research Centre, 1989.
- [16] Roddy, R., 1990. "Investigation of the stability and control characteristics of several configurations of the DARPA SUBOFF model (DTRC Model 5470) from captive-model experiments". Report No. DTRC/SHD-1298-08, September.
- [17] M.Moonesun, Y.M.Korol, D.Tahvildarzade ,M.Javadi, " Practical solution for underwater hydrodynamic model test of submarine", Journal of the Korean Society of Marine Engineering, 2014.
- [18] M.Javadi, M.D.Manshadi, S.Kheradmand, M.Moonesun, "Experimental investigation of the effect of bow profiles on resistance of an underwater vehicle in free surface motion", Journal of Marine Science and Application-Springer, No.14, Jan 2015,

[http://link.springer.com/article/10.1007/s11804-015-1283-](http://link.springer.com/article/10.1007/s11804-015-1283-0?sa_campaign=email/event/articleAuthor/onlineFirst)

[0?sa_campaign=email/event/articleAuthor/onlineFirst.](http://link.springer.com/article/10.1007/s11804-015-1283-0?sa_campaign=email/event/articleAuthor/onlineFirst)

- [19] Bao-ji Zhang (2012). Shape optimization of bow bulbs with minimum wave-making resistance based on Rankine source method. *Journal of Shanghai Jiaotong University*, 17(1), 65-69.
- [20] Kwag SH (2000). Bow wave breaking and viscous interaction of stern wave. *Journal of Mechanical Science and Technology*, 14(4), 448-455.
- [21] Alvarez A, Bertram V, Gualdesi V (2009). Hull hydrodynamic optimization of autonomous underwater vehicles operating at snorkeling depth. *Jordan Journal of Ocean Engineering*, 36(1), 105–112.
- [22] Suman KNS, Nageswara D, Das HN, Bhanu Kiran G (2010). Hydrodynamic Performance Evaluation of an Ellipsoidal Nose for a High Speed under Water Vehicle. *Jordan Journal of Mechanical and Industrial Engineering*, 4(5), 641 – 652.
- [23] Kim H, Cho H (2011). Numerical study on control derivatives of a high-speed underwater vehicle. *Journal of Mechanical Science and Technology*, 25(3), 759–765.
- [24] S.F.Hoerner, "Fluid Dynamic Drag", 1965.
- [25] ITTC (2002). Recommended procedures and guidelines- Sample Work Instructions Calibration of Load Cells. 23th International Towing Tank Conference, 7.6-02-09.
- [26] ITTC (2002). Recommended procedures and guidelines Testing and Extrapolation Methods- Resistance Uncertainty Analysis. 23th International Towing Tank Conference, 7.5-01-01-01.
- [27] ITTC (2002), Recommended procedures and guidelines-Model Manufacture Ship Models. 23th International Towing Tank Conference, 7.5-01-01-01.
- Rae WH, Pope A (1999). *Low-Speed Wind Tunnel Testing*, third edition, Canada, 609-649.
- [28] ITTC (2002), Recommended procedures and guidelines- Resistance Test, 23th International Towing Tank Conference, 7.5-02-02-01.
- [29] ITTC (2002), Recommended procedures and guidelines- Density and Viscosity of Water. 23th International Towing Tank Conference, 7.5-02-01-03.

Chapter 4: Submarine Stern Shape

4-1- General Bow Shape Analysis

4-1-1- Introduction

According to Fig.1, stern part, being composed of pressure hull (end compartment) and light hull. The slope of the stern shape should be acceptable for arranging all equipment with reasonable clearance for accessibility and repairing. The most part of the stern is occupied by main ballast tank (MBT) which needs a huge volume inside the stern. The more length of stern is equal to the better hydrodynamic conditions, and worse condition for the length of the motor shaft. There are several suggestions for the stern length such as IHSS and [3], but another important subject, is the curvature and the shape of the stern specially in the light hull part. The focus of this chapter is on the curvature and the shape equation of the stern.

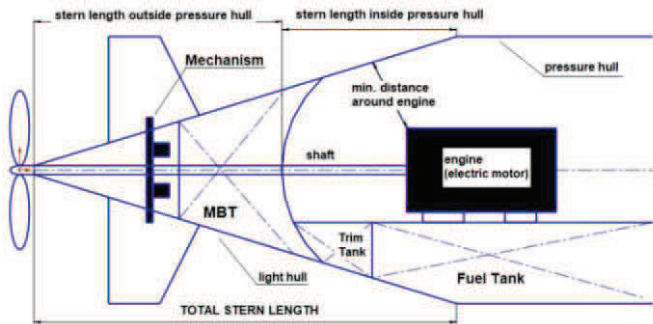


Figure 1: General arrangement of stern part (inside and outside of the pressure hull)

4-1-2- General Shapes for the Stern

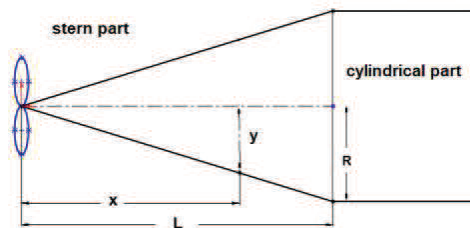


Figure 2: Reference coordinate and parameters

Reference coordinates and parameters are shown in Fig.2. The full body of revolution of the stern is formed by rotating the profile around the centerline (CL). Note that the equations describe the 'perfect' shape meanwhile, in practice, the end of stern is often blunted or truncated for manufacturing or installing the shaft and propeller (as shown in Fig.1). The equations of curvatures are presented in [4,5].

a) Conical: This shape is very usual and common stern in submarines. This shape is often chosen for its ease of manufacture, and is also a bad selection for its resistance characteristics. The sides of a conical profile are straight lines, so the diameter equation is simply: $y=x.R/L$. Cones are sometimes defined by their half angle, ϕ (Fig.3-a):

$$\phi = \arctan\left(\frac{R}{L}\right) \quad \text{and} \quad y = x \cdot \tan(\phi)$$

b) Spherically blunted cone: In most applications, a conical stern is often blunted by capping it with a segment of a sphere or cut vertically because the shaft exit, bearings and couplings, needs some distance before the end of the cone (Fig.3-b). The tangency point where the sphere meets the cone can be found from:

$$x_t = \frac{L^2}{R} \sqrt{\frac{r_n^2}{R^2 + L^2}} \quad y_t = \frac{x_t R}{L}$$

r_n is the radius of the spherical nose cap. The center of the spherical nose cap can be found from:

$$x_0 = x_t + \sqrt{r_n^2 - y_t^2}$$

$$x_a = x_0 - r_n$$

c) Bi-conic: This stern includes from two cones with different slope with length and radius of L_1, R_1, L_2, R_2 and thus: $L = L_1 + L_2$ (Fig.3-c) :

$$0 \leq x \leq L_1 : \quad y = \frac{x R_1}{L_1}$$

$$\phi_1 = \arctan\left(\frac{R_1}{L_1}\right) \quad \text{and} \quad y = x \tan(\phi_1)$$

$$L_1 \leq x \leq L : \quad y = R_1 + \frac{(x - L_2)(R_2 - R_1)}{L_2}$$

$$\phi_2 = \arctan\left(\frac{R_2 - R_1}{L_2}\right) \quad \text{and} \quad y = R_1 + (x - L_1) \tan(\phi_2)$$

d) Tangent ogive: The profile of this shape is formed by a segment of a circle such that the body is tangent with the curve of the stern at its base; and the base is on the radius of the circle (Fig.3-d). The popularity of this shape is largely due to the ease of constructing its profile. The radius of the circle that forms the ogive is called the ogive radius, ρ , and it is related with the length and base radius of the stern as expressed by the formula:

$$\rho = \frac{R^2 + L^2}{2R}$$

The radius y at any point x , as x varies from 0 to L is:

$$y = \sqrt{\rho^2 - (L-x)^2} + R - \rho$$

The stern length, L , must be less than or equal to ρ . If they are equal, then the shape is a hemisphere.

e) Spherically blunted tangent ogive: According to Fig.3-e, a tangent ogive stern is often blunted by capping it with a segment of a sphere. The tangency point where the sphere meets the tangent ogive can be found from:

$$x_0 = L - \sqrt{(\rho - r_n)^2 - (\rho - R)^2}$$

$$y_c = \frac{r_n(\rho - R)}{\rho - r_n} \quad x_c = x_0 - \sqrt{r_n^2 - y_c^2}$$

r_n is the radius, and x_0 is the center of the spherical nose cap. And the apex point can be found from:

$$x_a = x_0 - r_n$$

f) Secant ogive: According to shape 3-f, this shape of stern is also formed by a segment of a circle, but the base of the shape is not on the radius of the circle defined by the ogive radius. The cylinder body will not be tangent to the curve of the stern at its base. The ogive radius ρ is not determined by R and L (as it is for a tangent ogive), but rather is one of the factors to be chosen to define the stern shape. If the chosen ogive radius of a secant ogive is greater than the ogive radius of a tangent ogive with the same R and L , then the resulting secant ogive appears as a tangent ogive with a portion of the base truncated.

$$\rho > \frac{R^2 + L^2}{2R} \quad \alpha = \arctan\left(\frac{R}{L}\right) - \arccos\left(\frac{\sqrt{L^2 + R^2}}{2\rho}\right)$$

Then the radius y at any point x as x varies from 0 to L is:

$$y = \sqrt{\rho^2 - (\rho \cos \alpha - x)^2} + \rho \sin \alpha$$

g) Elliptical: According to Fig.3-g, this shape of the stern is one-half of an ellipse, with the major axis being the centerline and the minor axis being the base of the stern. A rotation of a full ellipse about its major axis is called a prolate spheroid, so an elliptical stern shape would properly be known as a prolate hemispheroid. This is not a shape normally found in usual submarines. If R equals L , this is a hemisphere.

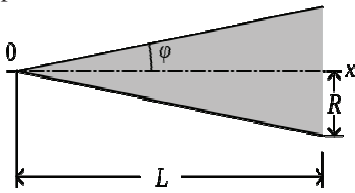
$$y = R \sqrt{1 - \frac{x^2}{L^2}}$$

h) Parabolic: This stern shape is not the blunt shape. The parabolic series shape is generated by rotating a segment of a parabola around an axis. This construction is similar to that of the tangent ogive, except that a parabola is the

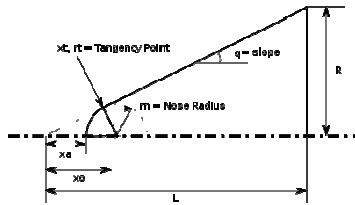
defining shape rather than a circle. Just as it does on an ogive, this construction produces a stern shape with a sharp tip (Fig.3-h).

$$\text{for } 0 \leq K' \leq 1: \quad y = R \left(\frac{2 \left(\frac{x}{L} \right) - K' \left(\frac{x}{L} \right)^2}{2 - K'} \right)$$

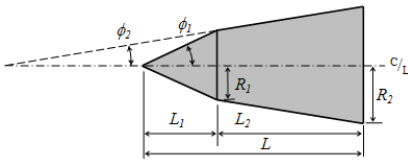
K' can vary anywhere between 0 and 1, but the most common values used for stern shapes are: $K'=0$ for a cone, $K'=0.5$ for a 1/2 parabola, $K'=0.75$ for a 3/4 parabola, $K'=1$ for a full parabola. For the case of the full Parabola ($K'=1$) the shape is tangent to the body at its base, and the base is on the axis of the parabola. Values of K' less than one, result in a slimmer shape, whose appearance is similar to that of the secant ogive. The shape is no longer tangent at the base, and the base is parallel to, but offset from, the axis of the parabola.



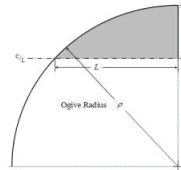
a) Conical stern



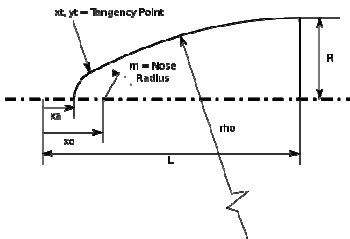
b) Spherically blunted cone



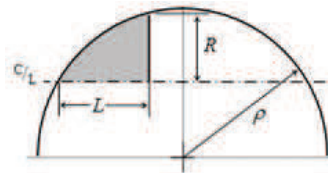
c) Bi-conic stern



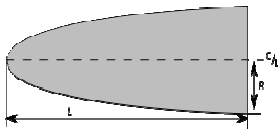
d) Tangent ogive stern



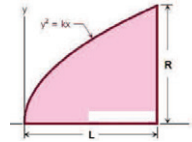
e) Spherically blunted tangent ogive stern



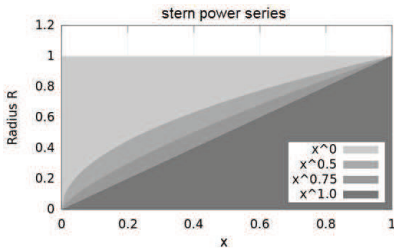
f) Secant ogive stern



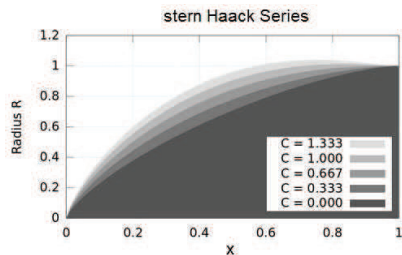
g) Elliptical stern



h) Parabolic stern



i) Power series for stern shape



j) Haack series for stern shape

Figure 3: Several shapes of stern [4,5]

i) Power series: According to Fig.3-i, the power series includes the shape commonly referred to as a "parabolic" stern, but the shape correctly known as a parabolic stern is a member of the parabolic series (described above). The power series shape is characterized by its (usually) blunt tip, and by the fact that its base is not tangent to the body tube. There is always a discontinuity at the joint between stern and body that looks distinctly non-hydrodynamic. The shape can be modified at the base to smooth out this discontinuity. Both a flat-faced cylinder and a cone are shapes that are members of the power series. The power series stern shape is generated by rotating the $y=R(x/L)^n$ curve about the x-axis for values of n less than 1. The factor n controls the bluntness of the shape. For values of n above about 0.7, the tip is fairly sharp. As n decreases towards zero, the power series stern shape becomes increasingly blunt. Then for n, it can be said: n=1 for a cone, n=0.75 for a 3/4 power, n=0.5 for a 1/2 power (parabola), n=0 for a cylinder.

$$0 \leq n \leq 1: \quad y = R \left(\frac{x}{L} \right)^n$$

j) Haack series: despite all the stern shapes above, the Haack Series shapes are not constructed from geometric figures. The shapes are instead mathematically derived for minimizing resistance. While the series is a continuous set of shapes determined by the value of C in the equations below, two values of C have particular significance: when C=0, the

notation LD signifies minimum drag for the given length and diameter, and when C=1/3, LV indicates minimum resistance for a given length and volume. The Haack series shapes are not perfectly tangent to the body at their base, except for a case where C=2/3. However, the discontinuity is usually so slight as to be imperceptible. For C>2/3, Haack stern bulge to a maximum diameter greater than the base diameter. Haack nose tips do not come to a sharp point, but are slightly rounded (Fig.3-j).

$$\theta = \arccos\left(1 - \frac{2x}{L}\right) \quad y = \frac{R}{\sqrt{\pi}} \sqrt{\theta - \frac{\sin(2\theta)}{2} + C \sin^2 \theta}$$

Where: C = 1/3 for LV-Haack and C = 0 for LD-Haack.

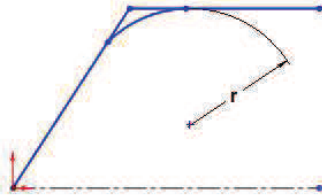


Figure 4: patched circle in discontinuity area of connection

k) Von Karman: The Haack series giving minimum drag for the given length and diameter, LD-Haack, is commonly referred to as the Von Karman or the Von Karman Ogive.

Patched Circle: In some cases which the connection between the cylinder and stern isn't fair with the sharp edge, a patched circle is used (Fig.4). The discontinuity at the joint between stern and cylinder body, looks strongly non-hydrodynamic that should be cured by a patched circle. This circle is tangent to both cylinder and stern.

4-1-3- Assumptions for the Models for CFD Analysis

The base model that considered here, is an axis-symmetric body similar to torpedo, without any appendages because in this study, only stern effect on resistance, wants to be studied. It helps to quarterly CFD modeling of the body and saving the time. The bow is elliptical and middle part is a cylinder but stern part is different. In this chapter, 14 models are studied. The 3D models and its properties are modeled in Solid Works. There are three main assumptions:

Assumptions 1: For evaluating the hydrodynamic effects of stern, the length of stern is unusually supposed large. It helps that the effects of stern be more visible.

Assumptions 2: The shape of bow and middle part are constant in all models. Bow shape is an elliptical shape and middle shape is cylindrical shape.

Assumptions 3: For providing more equal hydrodynamic conditions, the total length, bow, middle and stern lengths are constant. The diameter is constant too. Thus, L/D is constant in all models. These constant parameters, provide equal form resistance with except the stern shape and then the effects of stern shape, can be studied. Therefore, every model has different volume and wetted surface area.

Table 1: Main assumptions of models

v(m/s)	L_f (m)	L_t (m)	L_m (m)	L (m)	D(m)	L_f/D	stern shape
3	8	2	1	5	1	8	Axis-symmetric without appendages

The specifications of all 14 models are presented in Tab.2. In addition, for CFD modeling in all models, velocity is constant and equal to 3 m/s. This velocity is selected so that the Reynolds number be more than five millions.

Table 2: specifications of 14 models

MODEL	specification of stern	A0 (m2)	Aw (m2)	V (m3)
model 1-1	simple conic	3.14	16.1	3.14
model 1-2	conic with cut end	3.14	17.69	3.46
model 1-3	Spherically blunted cone	3.14	17.53	3.43
model 2	Bi-conic	3.14	18.46	3.77
model 3-1	Tangent ogive	3.14	18.74	3.93
model 3-2	Spherically blunted ogive	3.14	19.6	4.13
model 4	ogive - concave circle	3.14	13.48	2.61
model 5	elliptical	3.14	20.6	4.45
model 6-1	parabolic with $k'=0.5$	3.14	16.97	3.37
model 6-2	parabolic with $k'=0.75$	3.14	17.67	3.58
model 7-1	power series - $n=0.5$	3.14	18.71	3.8
model 7-2	power series - $n=0.75$	3.14	17.22	3.4
model 8-1	Haack series with $c=0$	3.14	18.47	3.8
model 8-2	Haack series with $c=0.333$	3.14	19.24	4.04

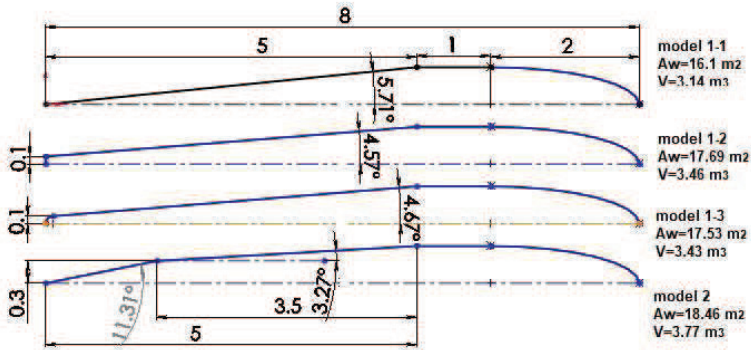


Figure 5: simple sterns without curvature

According to Fig.5, model 1-1 is the simplest stern shape that is supposed the base model for comparison with the results of other models for optimization. In most submarines, the stern is blunted cone because of shaft exit. Models 1-2 and 1-3 show two categories for this kind of blunting. The diameter of the blunting is depended on the shaft diameter and bearing thickness at the location of end part. Therefore, this diameter is small compare to the hull diameter. Model 2 in Fig.5 shows a bi-conic stern that contains two cones with different slopes. Usually the slope angle of first cone is bigger than the slope of second cone because the main reason of this arrangement is providing more space in the end part of submarine; inside the pressure hull or inside the light hull as showed in Fig.2. Usually, ordinary and small submarines have bi-conic arrangement in stern. Fig.5 shows the stern shapes without curvature that are cheap and easy to construction, especially for small submarines and ROVs and AUVs.

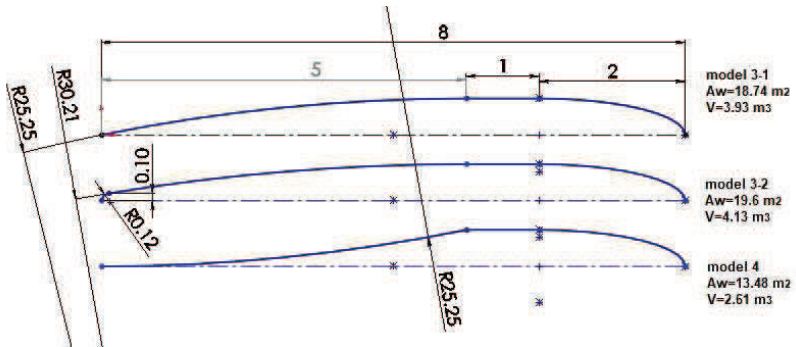


Figure 6: sterns that is formed by an ogive of circle

Fig.6 shows the sterns which are formed by an ogive of a circle. These shapes are almost easy to construction because the curvature of a circle in comparison to the other curvatures in Fig.6 is simpler. Model 3-1 is ideal tangent ogive with the radius of 25.25 meters. The radius of this circle must be so big that the ogive can be tangent to the cylinder part. For exit the shaft, Model 3-2 is more applicable that is a Spherically blunted tangent ogive. This model is formed by two ogives: one large ogive with radius of 30.21 meters and one small ogive with the radius of 0.12 meters for blunting the main ogive. Model 4 is formed by a concave ogive and hollow shape, that is rarely applicable. This shape is an unusual shape and is mentioned here, only for scientific comparison of the results of the concave and convex ogive.

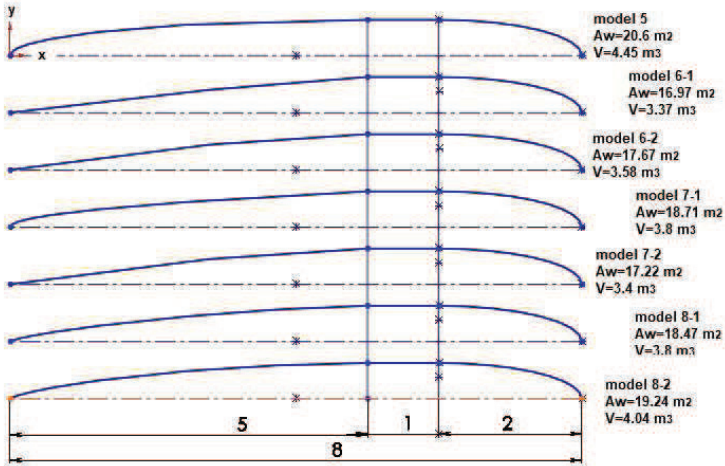


Figure 7: sterns with functional curvature according to the equations of the sections g-k.

In Fig.7, sterns with functional curvature are shown. All equations of these shapes are presented in the sections g-k. The construction of these models is usually complicated, complex, expensive and time consuming. Utilization of these forms is only affordable, if considerable hydrodynamic advantages could be earned. This chapter wants to answer this question. In the types that stern include pressure and light hull, forming the pressure hull according to these equations is very difficult because the thickness of the shell of pressure hull is very much. Therefore, only light hull can be formed by these functions. Model 5 is an elliptical shape that provides more volume in stern part of submarine but isn't so usual in design. Models 6-1 and 6-2 are parabolic shapes for $k=0.5$ and 0.75 . Models 7-1 and 7-2 are according to the power series for $n=0.5$ and 0.75 . Models 8-1 and 8-2 are according to Haack series for $n=0$ and 0.333 . There is a very little different between some of these models that can't be recognized with eyes such as Model 6-1 with Model 6-2. The wetted surface area and volume of each model are different to other models that these values are written beside the models.

4-1-4- CFD Method of Study

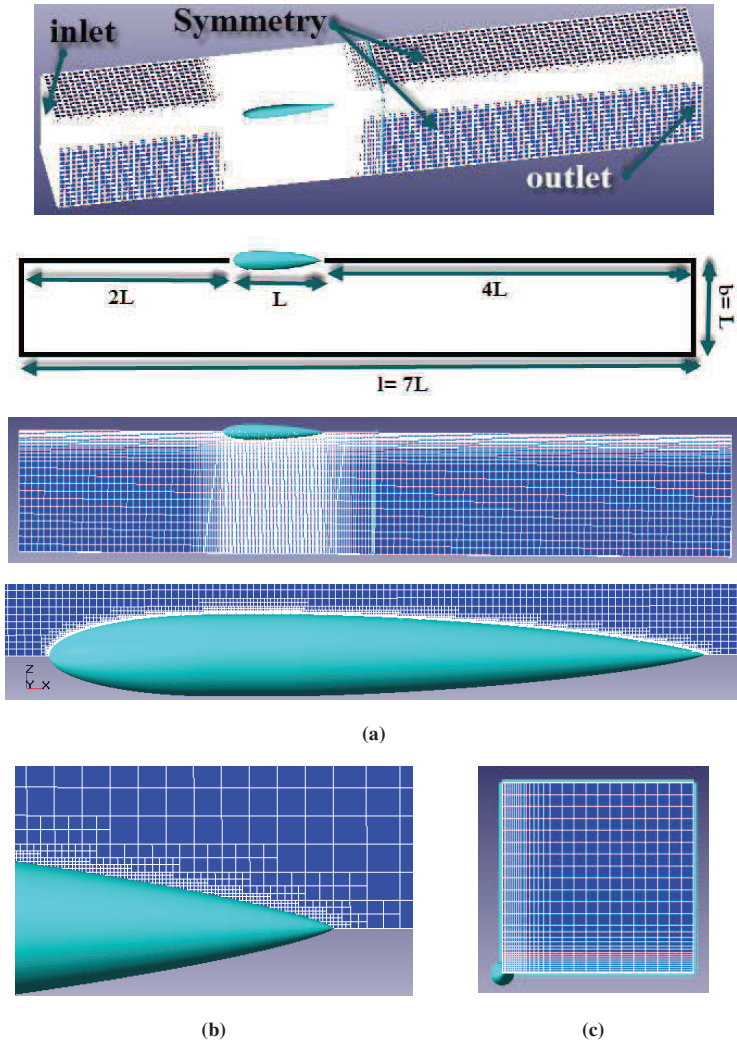


Figure 8: (a) Domain and structured grid (b) Very tiny cells near the wall for boundary layer modeling and keeping y^+ about 30 (c) Quarter modeling because of axis-symmetry

In all modeling the mesh numbers are considered more than 1.8 millions. For the selection of suitable iteration, it was continued until the results were almost constant with variations less than one percent, which shows the convergence of the solution. All iterations are continued to more than one millions. In this domain, there is inlet (with uniform flow), Free outlet, Symmetry (in the four faces of the box) and Wall (for the body of submarine). Dimensions of cubic domain are 56m length (equal to 7L), 8m beam and 8m height (equal to L or 8D). Pay attention to that only quarter of the body is modeled because of axis-symmetric shape, and the domain is for that. Meanwhile, the study has shown that the beam and height equal to 8D in this study can be acceptable. Here, there are little meshes in far from the object. The forward distance of the model is equal to 2L and after distance is 4L in the total length of 7L (Fig.8). The turbulence model is K-Epsilon, turbulent scale is considered 0.1m and y^+ is considered 30~100. The considered flow is incompressible fluid (fresh water) in 20 degrees centigrade and constant velocity of 3 m/s. Time step at each iteration, depends on the model length and velocity so here, time step is defined equal to 0.01 second i.e. the full model length is traversed at 2.67 second or 267 iterations. It is the minimum number of iterations. In this chapter, all models are performed by more than 1500 iterations. Settings of the simulation are collected in Tab.3.

Table 3: Settings of the simulation

Elements	Boundary conditions	Descriptions	
Domain	Box	conditions	Fully submerged modeling (without free surface)- quarter modeling- domain with inlet, outlet, symmetry and wall- Without heat transfer.
		dimensions	56*8*8 m- length before and after model=16 & 32 m
		grid	structured grid- hexahedral cells- tiny cell near wall- Meshes more than 1.5 millions.
		settings	Iterations more that 1500- Time step=0.01sec.
Fluid	-	Incompressible fluid- Reynolds number more than 24 millions- turbulent modeling: Standard k-ε- fresh water- tempreture:20 deg- $\rho=999.841 \text{ kg/m}^3$.	
Object	Wall	Bare hull of submarine- value $30 < y^+ < 100$ - roughness=0- no slip	
Input	Inlet	Velocity=3m/s- constant- normal (along x)- in 1 face	
Output	Free outlet	Zero pressure- in 1 face	
Boundaries	Symmetry	In 4 faces	

4-1-5- CFD Results Analysis

CFD analyses for all 14 models were done by Flow Vision software under the conditions that were mentioned above. All results are for fully submerged condition without free surface effects. Pressure distribution with viscosity effects, results in total resistance. Therefore, total resistance is the summation of pressure (form) resistance and viscous (frictional) resistance. Pressure contours around the body are shown in Fig.9 for sample for Model 3-1. Fore part of the object includes stagnation point and high pressure area. Middle part is low pressure area, but stern part is high pressure area. Non-uniform distribution of pressure on the body, results in pressure resistance. If the stern design be a stream lined form, the high pressure area in aft part is reduced and results in lower pressure resistance. In the other words, the better stern design, means the lesser pressure in stern part.

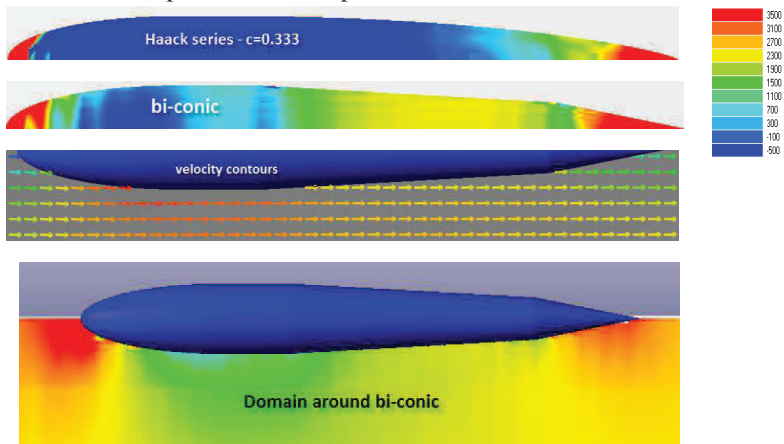


Figure 9: pressure contour around the body

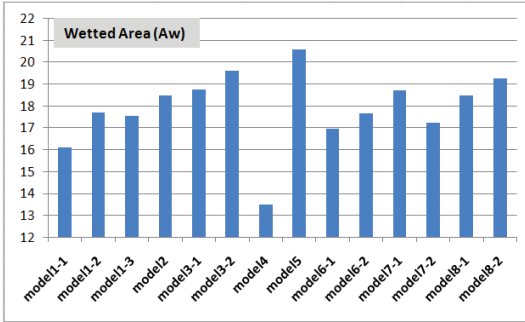


Figure 10: wetted area comparison in 14 models

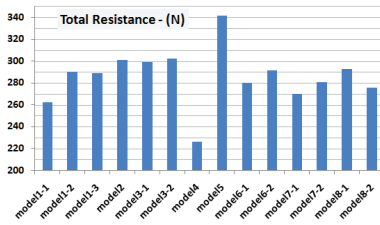
In viscous resistance, an important function is wetted area resistance. This parameter varies in all models, but cross section area is constant because the diameter is constant in all models. The amount of area was presented in Tab.2. The concave ogive shape (Model 4) results minimum and elliptical shape (Model 5) results in the maximum wetted area. Base on the area, two kinds of the resistance coefficient can be defined: 1- based on wetted area: $C_{d1} = R / 0.5\rho A_w v^2$ that is usually used for the frictional resistance coefficient. 2- based on cross section area: $C_{d0} = R / 0.5\rho A_0 v^2$ that is usually used for the pressure resistance coefficient. Here, for accounting on the effect of the wetted area on the coefficients, all coefficients are presented as a function of the wetted area. The amount of total resistance, pressure resistance and viscous resistance and their coefficients are presented in Tab.4. For better comparison, the diagrams of total resistance (Fig.11-a), pressure resistance (Fig.11-b), total resistance coefficient (Fig.11-c) and pressure resistance coefficient (Fig.11-d) are presented. In total resistance, wetted area coefficient is important. Therefore, according to Fig.11-a, the Model 4 has minimum and Model 5 has maximum resistance. Pressure resistance is a function of form efficiency. If the shape has streamed lined form without discontinuity and breaking, the pressure resistance will be minimum. In this study, an ideal stern form should have minimum resistance. It should be remembered that two main parameters there are here: 1-wetted area which affects the frictional resistance 2-general form which affects the pressure resistance by better distribution of

pressure on the body and avoiding low pressure area in the aft part of the body.

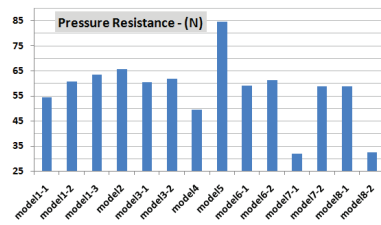
Table 4: Resistances and Coefficients for 14 models

MODEL	Rt	Rp	Rv	Ct*1000	Cp*1000	Cv*1000
Model 1-1	262	54.4	207.6	3.616	0.75086	2.865
Model 1-2	290.4	60.8	229.6	3.648	0.76377	2.884
Model 1-3	288.8	63.6	225.2	3.661	0.80624	2.855
Model 2	300.8	65.6	235.2	3.621	0.78970	2.831
Model 3-1	298.8	60.4	238.4	3.543	0.71623	2.827
Model 3-2	302	62	240	3.424	0.70295	2.721
Model 4	226.4	49.6	176.8	3.732	0.81767	2.915
Model 5	341.2	84.8	256.4	3.681	0.91478	2.766
Model 6-1	280	59.2	220.8	3.667	0.77522	2.891
Model 6-2	291.2	61.2	230	3.662	0.76967	2.893
Model 7-1	269.6	32	237.6	3.202	0.38007	2.822
Model 7-2	280.8	58.8	222	3.624	0.75881	2.865
Model 8-1	292.8	58.8	234	3.523	0.70745	2.815
Model 8-2	275.6	32.4	243.2	3.183	0.37422	2.809

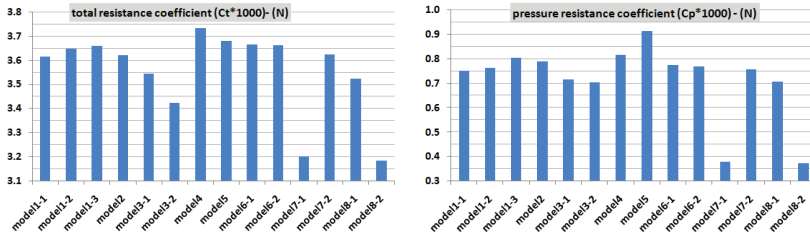
The Fig.11-b shows the pressure resistance diagrams that Model 7-1 (power series with $n=0.5$) and Model 8-2 (Haack series with $c=0.333$) have minimum pressure resistance but Model 5 (elliptical) has the maximum amount. The trends of resistance coefficients are different and to some extent, amazing.



(a): total resistance (N)



(b): pressure resistance (N)



(c): total resistance coefficient

(d): pressure resistance coefficient

Figure 11: Resistances and Coefficients for 14 models

According to Fig.11-c, the total resistance coefficients of Model 7-1 (power series with $n=0.5$) and Model 8-2 (Haack series with $c=0.333$) have minimum but Model 4 (ogive - concave circle) has the maximum amount. It means that, if the wetted area of all models be equal, Models 7-1 and 8-2 are the best designs, and the Model 4 is the worse design. Here the role of the wetted area is considerable. In Ogive with concave circle (concave ogive) shape, it was shown that, it has minimum total resistance but since its wetted area was minimum, then the total resistance coefficient was maximum. It is an amazing note in hydrodynamic design. Diagrams in Fig.11-d show that another time, Model 7-1 (power series with $n=0.5$) and Model 8-2 (Haack series with $c=0.333$) has minimum but Model 5 (elliptical stern) has a maximum pressure resistance coefficient. It means that, in form design aspect of view, Models 7-1 and 8-2 are the best designs, and the Model 4 is the worse design. Here the role of curvature and pressure distribution on the curvature is considerable. In some cases, providing a large volume for accommodating the MBT tanks or other devices inside the stern is important. Here, the criterion is providing more space and bigger volume. According to Tab.2 and Figs.11a and 11b, for a constant volume, it seems that elliptical stern (Model 5) be a bad design because of the high resistance result, but spherically blunted ogive (Model 3-2) be a better choice.

4-1-6- Review 1

In conclusion, the results of this study can be said as:

1- The hydrodynamic design of stern is important, but the results show that, its importance isn't comparable to the importance of the bow of submarine. This

comparison can be done by Ref.[20]. It seems that the hydrodynamic importance of the stern is not in resistance values but on the wake field. The quality of the inlet flow to the propeller will be shown in wake factor with considerable hydrodynamic consequences.

2- If the wetted area of all models be equal, stern shape with power series with $n=0.5$ and Haack series with $c=0.333$ are the best designs and the ogive - concave circle is the worse design (from Fig.11-c).

3- If the volume of all models be equal, it seems that elliptical stern be a bad design because of the high resistance results, but spherically blunted ogive be a better choice (from Tab.2 and Figs.11a and 11b).

4- If the stern length of all models be equal, stern shape of the concave ogive is the best design, and the elliptical stern is the worse design (from Fig.11-a). In practical point of view, Neither concave ogive, nor elliptical stern aren't so common practice. After that, it can be advised that, simple conic with any curvature is the best selection and three shapes of bi-conic, Tangent ogive, Spherically blunted ogive are the worse design. In real design of submarines, usually, the stern length supposes to be constant. Therefore, a simple conic shape of stern is a good advice with good hydrodynamic results, easy to construction and low in cost. It is the most important earning of this chapter.

4-2- Some more Detailed Optimizations

4-2-1- General Assumptions for the Models

Due to the effect of the stern on resistance is only intended to be studied in this study, the base model considered in this task is an axis-symmetric body (similar to torpedo) with no appendages. It helps model quarter of the body (in CFD model) and saves the time. The bow is elliptical and the middle part is cylindrical but the stern part is different.

In this section, 19 models are studied. The 3D models and their properties are modeled in Solid Works (Fig.12). There are three main assumptions:

Assumption 1: To evaluate the hydrodynamic effects of the stern, the length of the stern is unusually supposed larger than usual. It helps effects of the stern to be more visible.

Assumption 2: For all the models, the shapes of bow and middle part are assumed to be constant. The bow is elliptical and the middle part is cylindrical.

Assumption 3: To provide a more equal hydrodynamic condition, the total length and the lengths of a bow, middle part and stern are assumed to be constant. The fineness ratio (L/D) is constant as well according to the constant status of the maximum diameter. The assumed constant parameters provide an equal form of resistance except for the stern shape that varies in each model. Consequently, the effects of the stern shape can be analyzed and the models contained various volumes and wetted surface areas.

Table 5: Main assumptions of the models

v (m/s)	L_t (m)	L_f (m)	L_m (m)	L_a (m)	D (m)	L/D	A_0 (m ²)
10	8	2	1	5	1	8	3.14

The main assumptions of all considered models are reported in Tab.5. The specifications of all 19 models are presented in Fig.12 and reported in Tab.6.

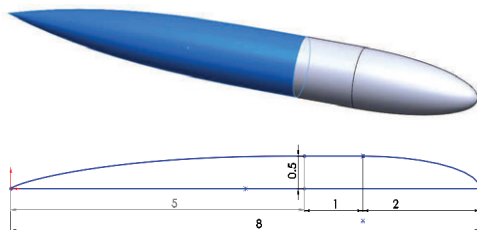


Figure 12: General configuration of the models-
Dimensions unit (m)

The wetted surface area (A_w) is used for the resistance coefficient and the total volume is used for "Semnan" coefficient. For all models, the volume of bow and cylinder is constant which is equal to 1.83 cubic meters but the total volumes are not the same. In addition, for CFD modeling in relation to all models, the velocity is assumed to be constant and equal to 10 m/s. In this study, the velocity is selected in which the Reynolds number could be more than five million.

Table 6: specifications of 19 models

MODEL	specification of stern	V(m3)
Model 1-1	parabolic with $k'=0.3$	3.26
Model 1-2	parabolic with $k'=0.5$	3.37
Model 1-3	parabolic with $k'=0.6$	3.45
Model 1-4	parabolic with $k'=0.75$	3.58
Model 1-5	parabolic with $k'=0.85$	3.7
Model 1-6	parabolic with $k'=1$	3.93
Model 2-1	power series - $n=1.5$	3.6
Model 2-2	power series - $n=1.65$	3.71
Model 2-3	power series - $n=1.85$	3.84
Model 2-4	power series - $n=2$ (Elliptic)	3.93
Model 2-5	power series - $n=3$	4.36
Model 2-6	power series - $n=4$	4.63
Model 2-7	power series - $n=5$	4.81
Model 2-8	power series - $n=6$	4.94
Model 2-9	power series - $n=8$	5.12
Model 3-1	Haack series with $c=0$	3.8
Model 3-2	Haack series with $c=0.15$	3.91
Model 3-3	Haack series with $c=0.333$	4.04
Model 3-4	Haack series with $c=0.666$	4.29

The configurations of all models including Parabolic models (models 1-1 to 1-6), power series models (models 2-1 to 2-9) and Haack series models (models 3-1 to 3-4) are displayed in Fig.13, Fig.14 and Fig.15, respectively.

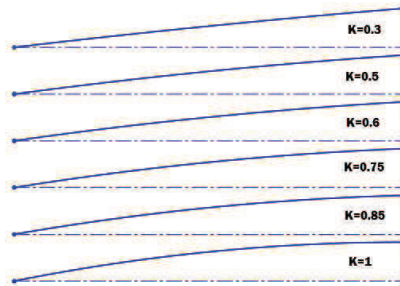


Figure 13: Configurations of parabolic models

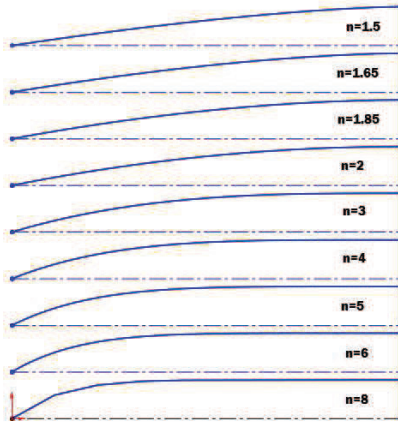


Figure 14: Configurations of power series models

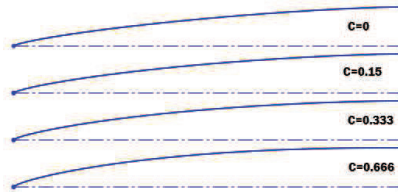


Figure 15: Configurations of Haack series models

4-2-2- CFD Result Analysis

CFD analyses were conducted for all 19 models by Flow Vision software under the above-mentioned conditions. All results are obtained at fully submerged mode with no regard of free surface effects. The total resistance takes the effects of Pressure distribution and viscosity into account. Therefore, the total resistance is the summation of pressure (form) resistance and viscose (frictional) resistance. Pressure contours around the body are shown in Fig.16 for sample for Model 1-1. The fore part of this object includes stagnation point and high pressure area. The middle part is low pressure area, but the stern part is high pressure area. The pressure distribution on the body is non-uniform. This leads to the pressure resistance. If the stern design can be conducted to a stream lined form, then the high pressure area in the aft part is reduced and

causes the lower pressure resistance. This means that the optimally designed stern results in a lesser pressure in the stern part.

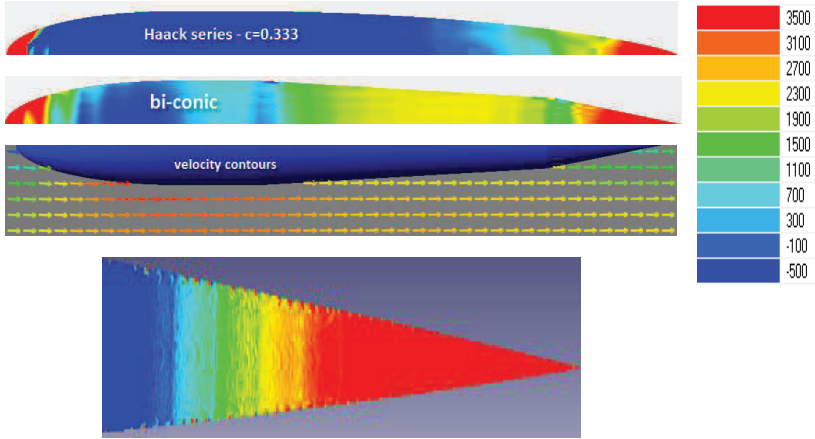


Figure 16: pressure contour around the body

In viscose resistance, an important parameter is the wetted area resistance. This parameter varies in all models but the cross- section area remains fixed, because the diameter is constant in all models. The values of the wetted area are reported in Tab.6. For better comparison, they are displayed in Fig.17 as well.

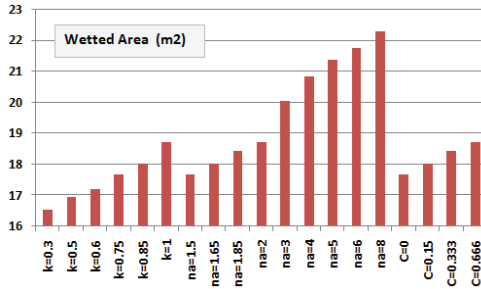


Figure 17: comparison of wetted area for 19 models

Based on the area, two kinds of the resistance coefficient can be defined: 1- Based on the wetted area: $C_{d1} = R / 0.5\rho A_w v^2$ that is usually used for the

frictional resistance coefficient. 2- Based on the cross-section area: $C_{ds} = R_f / 0.5\rho A_0 v^2$ that is usually used for the pressure resistance coefficient.

Here, for accounting on the effect of the wetted area on the coefficients, all coefficients are presented as a function of the wetted area. The amount of total resistance and resistance coefficient are presented in Tab.7. In this study, an ideal stern form should have minimum resistance. It should be remembered that here there are two main parameters as follows: 1- The wetted area which affects the frictional resistance. 2- The general form which affects the pressure resistance by better distribution of pressure on the body and avoiding low pressure area in the aft part of the body.

Table 7: Total resistance, resistance coefficient (based on wetted area surface) and Semnan coefficient of the models

MODEL	R_t (N)	C_t^*10000	$C_{semnan}/10$
Model 1-1	2472	29.87	37.71
Model 1-2	2510	29.60	39.01
Model 1-3	2528	29.38	39.97
Model 1-4	2577.2	29.19	41.28
Model 1-5	2614.8	29.02	42.44
Model 1-6	2692	28.78	44.49
Model 2-1	2688	30.44	39.73
Model 2-2	2716	30.16	40.91
Model 2-3	2760	29.95	42.13
Model 2-4	2808	30.02	42.65
Model 2-5	2940	29.36	46.40
Model 2-6	3024	29.04	48.53
Model 2-7	3120	29.21	49.24
Model 2-8	3220	29.61	49.28
Model 2-9	3460	31.07	47.85
Model 3-1	2780	31.48	40.27
Model 3-2	2824	31.36	41.16
Model 3-3	2868	31.12	42.31
Model 3-4	2960	31.64	43.18

The diagrams of the total resistance, resistance coefficient and Semnan coefficients corresponding to the Parabolic, power series and Haack series sterns are shown in Figs. 18, 19 and 20, respectively. In the Parabolic stern form, according to Fig. 18, the total resistance increases and the resistance coefficient decreases with increasing of K' . It means that, under the assumption of constant length, the fewer value of K' is better and, under the assumption of constant wetted surface area, the more value of K' is better. For having a better criterion, from the view point of naval architecture design, "Semnan" coefficient needs to be more for providing simultaneously both the

lesser value of resistance coefficient and the more value of enveloped volume. Here, the more value of K' means the more value of Semnan coefficient and the better condition as well. The equation of resistance coefficient is stated as Eqn.12:

$$C_t = -1.572(K') + 30.35 \quad (12)$$

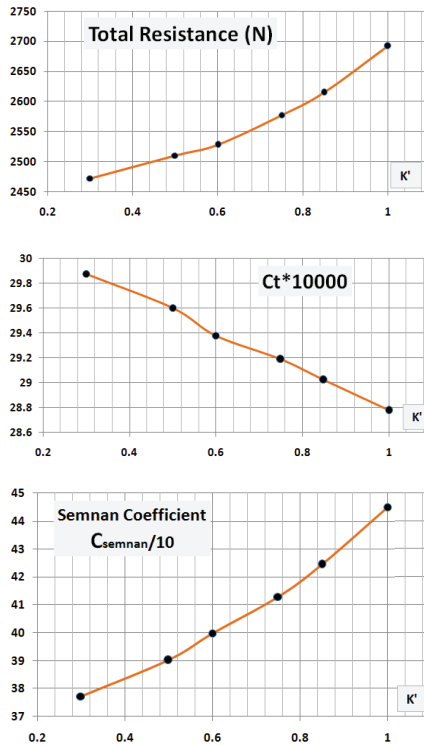


Figure 18: Variation of the total resistance, resistance coefficient and Semnan coefficient with K' for Parabolic stern

In the Power Series stern form, according to Fig. 19, the total resistance increases with increasing of n_a . The resistance coefficient diagram has two minimum points: a local minimum at $n_a=1.85$ and a global minimum at $n_a=4$. It means that, under the assumption of constant length, the lesser value of na is

better but, under the assumption of constant wetted surface area with regard to the resistance coefficient, the values of n_a around 4 are better. For this form, the Semnan coefficient has a maximum value around $n_a=5.6$ that shows the best selection regarding design process. In this regard, the equation of resistance coefficient for $2 < n_a < 8$ is as Eqn.13:

$$C_t = -0.01(n_a)^3 + 0.33(n_a)^2 - 2.11(n_a) + 33.03 \quad (13)$$

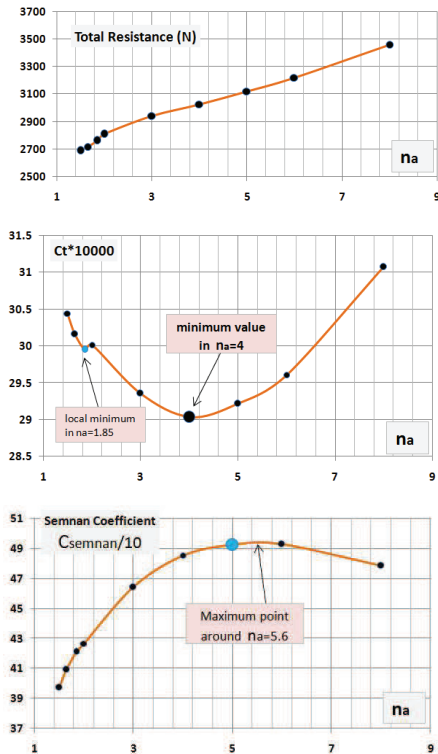


Figure 19: Variation of the total resistance, resistance coefficient and Semnan coefficient with n_a for Power series stern

In the Haack Series stern form, according to Fig.20, the total resistance increases with increasing of C . This variation is exactly linear. It means that, under the assumption of constant length, the lesser value of C is better but, under the assumption of constant wetted surface area with regard to the

resistance coefficient, the values of C around 0.3 are better. For this form, the Semnan coefficient increases with increasing of "C". In this regard, the equation of the resistance coefficient is as follows:

$$C_r = 30.9839 + 0.2066 \cos(9.176C + 0.1161) \quad (14)$$

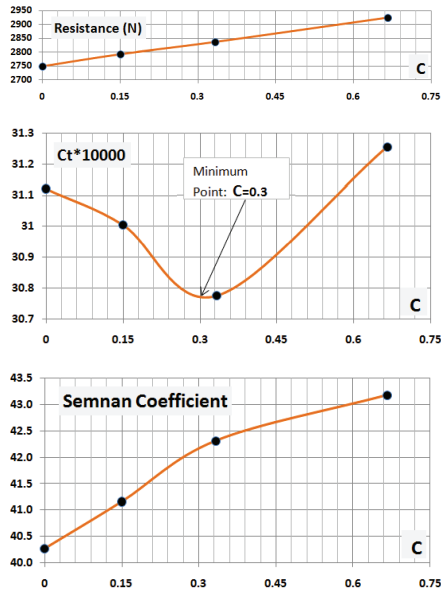


Figure 20: Variation of the total resistance, resistance coefficient and Semnan coefficient with C for Haack series stern

4-2-3- Review 2

In conclusion, the results of this study can be stated as follows:

1) In the Parabolic stern form, under the assumption of constant length, the value of $K'=0.3$ is a good selection but, under the assumption of constant wetted surface area, the stern form with $K'=1$ is the best design, because the maximum value of Semnan coefficient is achieved in this value.

2) In the Power Series stern form, under the assumption of constant wetted surface area, there are two minimum points around $n_a=1.85$ and 4 which offer good selections but, under the assumption of constant length, the stern form

with $n_a=5.6$ is the best design, because the maximum value of Semnan coefficient is achieved in this value.

3) In the Haack Series stern form, under the assumption of constant wetted surface area, the value of $C=0.3$ is a good selection because the minimum resistance coefficient is achieved in this value. Under the assumption of constant length, the stern form with $C=0.66$ is the best design because the more values of "C" is equal to the more values of Semnan coefficient.

4) A comparison between the three types of stern shapes, under the assumption of constant wetted surface area, indicates that the Haack series stern form has the worse result by the most value of resistance coefficient. The power series stern form, under the assumption of constant length, has the worse result by the most value of resistance. For providing more volume with the lesser resistance coefficient, based on the maximum value of Semnan coefficient, the power series stern form has the most value and offers the best result.

5) Finally, the best advice of this chapter for the stern form of submarine based on the diagrams of Semnan coefficients is "Power series" in the range of 4 to 6 for n_a .

Nomenclature

A0	cross section area ($3.14 \cdot D^2/4$) in m^2	IHSS	Iranian Hydrodynamic Series of Submarines
A _w	wetted area (outer area subject to the water) in m^2	MBT	Main Ballast Tank for providing reserve of buoyancy and ability to surfacing of submarine
D	diameter of the cylinder part (or) radius of the base of the stern	V	total volume of submarine in m^3
C _t	total resistance coefficient is shown in *1000	v	speed of submarine in m/s
C _p	pressure resistance coefficient is shown in *1000	R _t	Total resistance
C _v	viscous resistance coefficient is shown in *1000	R _p	pressure resistance
K _{sn}	Semnan Coefficient	R _v	viscous resistance
L _t	total length of submarine (m)	x	variable along the length. x varies from 0 to L
L	stern length of submarine (m)	y	is the radius at any point of the x
L _m	middle part length of submarine (m)	φ	half angle of stern cone
L _f	fore (bow) length of submarine (m)		

* Other parameters are described inside the text

References

- [1] M.Moonesun, Y.M.Korol, A.Brazhko, " CFD analysis on the equations of submarine stern shape", MIC2014 (16th Marine Industries Conference), Iran,2014.
- [2] M. Moonesun, Y.M. Korol, A. Brazhko, " CFD analysis on the equations of submarine stern shape",
Journal of Taiwan Society of Naval Architects and Marine Engineers, Vol.34, No.1, pp.21-32, 2015.
- [3] www.en.wikipedia.org/ the free encyclopedia
- [4] I.N. Bronshtein, K.A. Semendyayev, Gerhard Musiol, Heiner Mühlig, " Handbook of Mathematics", ISBN-13: 978-3540721215, 2007

Chapter 5: Optimum L/D

5-1- Introduction

This chapter is based on the studies of Ref.[1]. Submarines are encountered to limited energy in submerged navigation and because of that, the minimum resistance is vital in submarine hydrodynamic design. L/D parameter is an important hydrodynamic parameter that plays a unique role in submarine hydrodynamic design and minimizing resistance. Some studies about the effects of L/D on the resistance (drag) such as Ref [2,3]. In addition, the amount of L/D is depended on the internal architecture and general arrangements of submarine. Related materials about general arrangement in naval submarines. Convergence between hydrodynamic needs and architecture needs is vital for determination of L/D ratio. However, in hydrodynamic aspect of view, a hydrodynamic suggestion should be available. For large and small submarines, the L/D ratio can be the equal. It means that L/D is independent of tonnage of submarine. Ref [4,5] has presented some data about L/D in midget, small, medium and large naval submarines. Fig.1 shows some examples of L/D for modern submarines. Paying attention to that optimum L/D in hydrodynamic aspect of view may be different in architecture aspect of view. In real design processes all aspects should be regarded.

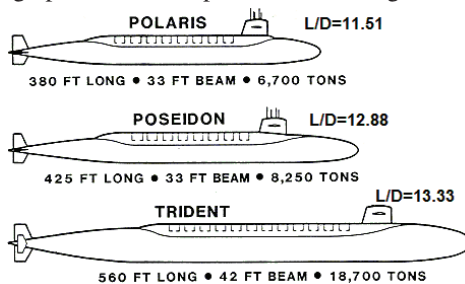


Figure1: Some examples of L/D for modern submarines

Submarines have two major categories for hydrodynamic shape: tear drop shape and cylindrical middle body shape. There is an optimum value of L/D for minimizing the resistance (Fig.2). With increasing the L/D, the form resistance decreases and skin friction resistance increases due to increase in wetted surface area. The Table.1 shows this concept by a sample for a simple cylinder. For tear drop shape, the optimum hydrodynamic L/D in Ref.[6] is mentioned equal to 7, in Ref.[7] equal to 6.6 and in Ref.[8] equal to 6~7, but they didn't have any suggestion for cylindrical middle body shapes. This

chapter wants to reply to this question because most real and naval submarines and ROV's have cylindrical middle body shape (Fig.1).

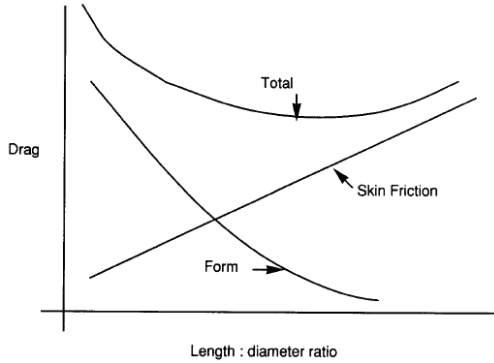


Figure 2: Resistance component for constant volume versus L/D [6]

Table 1: Variations of wetted area versus L/D for a simple cylinder

	L (m)	D (m)	Volume (m ³)	Wetted surface (m ²)
L/D=1	1	1	0.785	3.14
L/D=8	4	0.5	0.785	6.28

5-2- Assumptions for the Models

The base model that considered here, is an axis-symmetric body similar to torpedo, without any appendages because in this study, only L/D ratio wants to be studied. It helps to quarterly CFD modeling of the body and saving the time. The bow is elliptical and stern is conical. There are two main assumptions (Tab.2):

Assumptions 1: For evaluating the hydrodynamic effects of L/D, the total volume of shape is considered to be constant and only L/D ratios are changed. Here eleven models are modeled and in all models, total volume is equal to 5.89 m³. Base model is L/D=10, and other models are changed so that L/D varies with constant volume and because of that, the length amount has two decimal numbers. The 3D models and volume properties are modeled in Solid Works by try and error method.

Assumptions 2: For providing more equal hydrodynamic conditions, the bow and stern length are proportioned to the diameter. This constant proportion

provides equal form resistance with except L/D and then the effects of L/D can be studied. The bow length is equal to $1.5D$ and stern length is $3D$ in all models.

The L/D ratios for these 11 models are: 3.98, 5.48, 7.18, 7.98, 8.45, 10, 10.71, 11.53, 13.13, 13.88 and 15.15. For all models, above mentioned two assumptions are observed (Fig.3). In addition, for CFD modeling in all models, velocity is constant and equal to 2 m/s.

Table 2: Main assumptions of models

V (m^3)	v (m/s)	L_f	L_n	Object shape	Domain
5.89	2	$1.5D$	$3D$	Axi-symmetric	Quarterly modeled

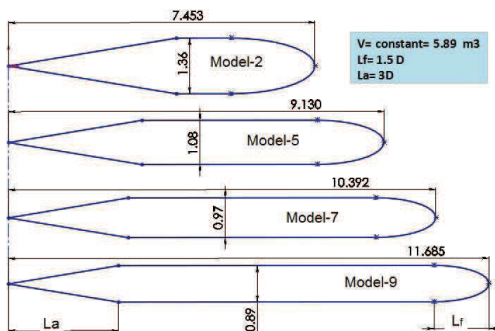


Figure 3: Some models with different L/D but constant volume

5-3- CFD Method of Study

In this domain, there are inlet (with uniform flow), Free outlet, Symmetry (in the four faces of the box) and Wall (for the body of submarine). Dimensions of cubic domain are 60m length (equal to $6L$), 3m beam and 3m height (equal to $6R$). Pay attention to that only quarter of the body is modeled because of axis-symmetric shape, and the domain is for that. Meanwhile, the study has shown that the beam and height equal to $3R$ can be acceptable. Here, there are little meshes in far from the object. The forward distance of the model is equal to $2L$ and after distance in at least $3L$ in the total length of $6L$ (Fig.4,5). The turbulence model is K-Epsilon and y^+ is considered equal to 50. The

considered flow is incompressible fluid (fresh water) in 20 degrees centigrade and constant velocity of 2 m/s.

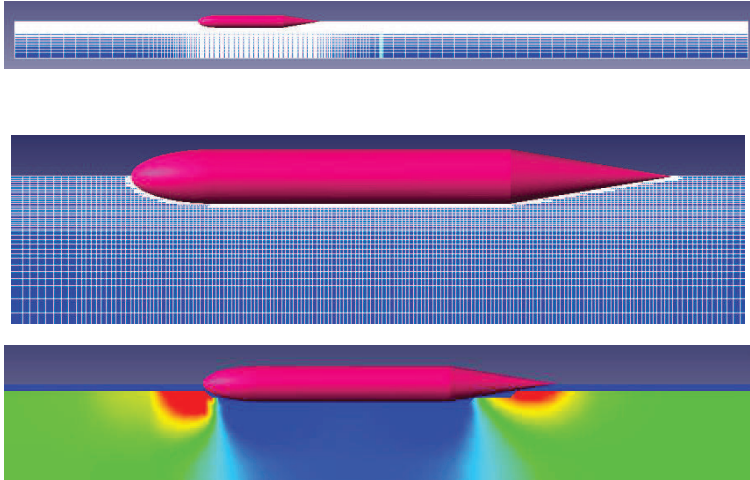


Figure 4: Structured grid with cubic cells around the cylindrical middle body submarine in the domain

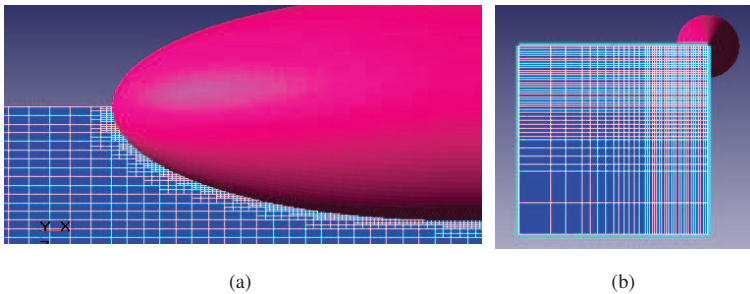


Figure 5: (a) Very tiny cells near the wall for boundary layer modeling and keeping y^+ about 50 (b) Quarterly modeling because of axis-symmetry

5-4- CFD Analysis

Some study is done about L/D hydrodynamic effects by CFD methods such as [2]. Analyses for all 11 models were done by Flow Vision (V.2.3) software. The results of pressure resistance and viscose resistance against L/D variations were presented in Fig.6&7. Pressure resistance diagram has a downward trend

with L/D. It means that increase in L/D causes a decrease in pressure resistance. The more L/D is equal to more stream-lined shape that fluid flow has more time for matching to the body. Frictional resistance diagram has an upward trend with L/D. It means that increase in L/D causes an increase in frictional resistance. The more L/D is equal to the more wetted area (Fig.8). Therefore, increase in L/D leads to increase in frictional resistance and decrease in pressure resistance.

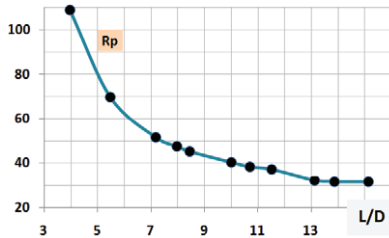


Figure 6: Pressure resistance versus L/D variations

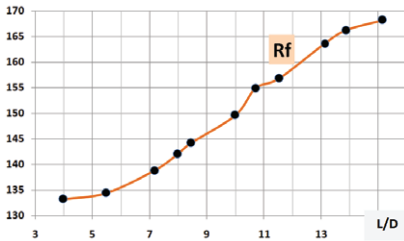


Figure 7: Viscose resistance versus L/D

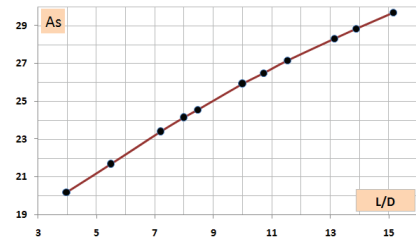


Figure 8: Wetted area versus L/D

These have vice versa and contrariwise trends. The total resistance is the summation of these two resistances then an optimum L/D or optimum range for L/D should be available. Figure 9 shows the optimum range for L/D for cylindrical middle body submarine. According to this diagram, the optimum range for L/D in cylindrical middle body submarines is 7~10. For tear drop shape, the optimum hydrodynamic L/D in several scientific references such as ⁷ is mentioned, equal to 7. The behaviors of resistance coefficients are wholly different. According to Tab.3 and Fig.10 the trends of resistance coefficients are downwards. Remember that in resistance formula ($R=0.5\rho.C_d.A.V^2$) an

important factor is wetted area that this parameter according to Fig.7 increases with L/D . Because of this subject, despite decrease in all resistance coefficients versus L/D , the total resistance diagram has downward and upward trends with the minimum range values (Fig.9).

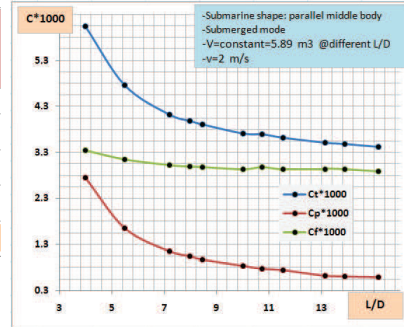
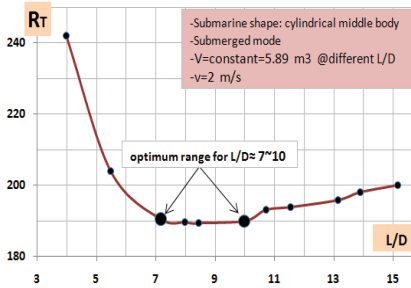


Figure 9: Optimum range for L/D for cylindrical middle body submarine

Figure 10: Resistance coefficients versus L/D

Table 3: Resistance and resistance coefficient versus values of L/D

L/D	R_t (N)	R_p (N)	$R_f = R_t - R_p$	A_s	V (m/s)	$C_t \cdot 1000$	$C_p \cdot 1000$	$C_f \cdot 1000$
3.98	242	108.8	133.2	20.21	2	5.987	2.692	3.295
5.48	204	69.6	134.4	21.67	2	4.707	1.606	3.101
7.18	190.4	51.6	138.8	23.38	2	4.072	1.104	2.968
7.98	189.6	47.6	142	24.12	2	3.930	0.987	2.944
8.45	189.36	45.2	144.16	24.56	2	3.855	0.920	2.935
10	190	40.4	149.6	25.92	2	3.665	0.779	2.886
10.71	193.2	38.32	154.88	26.5	2	3.645	0.723	2.922
11.53	194	37.2	156.8	27.16	2	3.571	0.685	2.887
13.129	196	32.4	163.6	28.32	2	3.460	0.572	2.888
13.88	198	31.8	166.2	28.84	2	3.433	0.551	2.881
15.15	200	31.8	168.2	29.7	2	3.367	0.535	2.832

5-5- Review

Main achievement of this chapter is the suggestion of $L/D=7\sim 10$ as the optimum range for cylindrical middle body submarine. Formerly, this range for tear drop shapes had been suggested $L/D=6\sim 7$. Other achievements of this chapter are so: 1) Pressure resistance decreases versus L/D but before optimum range, this decrease is steep. 2) Frictional resistance increases versus L/D but this variation is mild entirely. 3) All resistance coefficients (pressure, frictional and total) decrease versus L/D . 4) Wetted surface area increases versus L/D that causes an increase in frictional resistance despite decrease in

the resistance coefficient. Schematic variations are presented in Fig.11. All analyses for 11 models are done for constant volume but different L/D. The velocity is constant for providing Reynolds number of more than 5 millions that it means constant resistance coefficient, which is independent of the velocity.

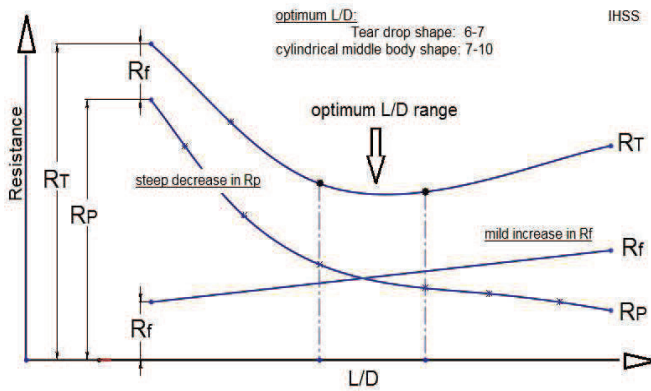


Figure 11: Schematic variations of resistance versus L/D

Nomenclature

L	overall length of hull	L_f	entrance length or bow length
D	maximum diameter of the outer hull	L_m	middle length or cylinder length
V	Volume of object (submarine) in m^3	L_a	aft length or stern length
v	Speed of water in m/s	IHSS	Iranian Hydrodynamic Series of Submarines

References

- [1] Mohammad Moonesun, Asghar Mahdian, Yuri Mikhailovich Korol, Mehdi Dadkhah, Mehrshad Moshref Javadi, Anna Brazhko, Optimum L/D for Submarine Shape, Indian Journal of Geo-Marine Sciences, Vol. 45(1), January 2016, pp. 38-43
- [2] Praveen.P.C, Krishnankutty.P, " study on the effect of body length on hydrodynamic performance of an axi-symmetric underwater vehicle", Indian Journal of Geo-Marine Science, vol.42(8), December 2013, pp.1013-1022.
- [3] K.N.S.Suman, D.Nageswara Rao, H.N.Das, G.Bhanu Kiran, "Hydrodynamic Performance Evaluation of an Ellipsoidal Nose for High Speed Underwater Vehicle", Jordan Journal of Mechanical and Industrial Engineering (JJMIE), Volume 4, Number 5, November 2010, pp.641-652.
- [4] M.Moonesun, P.Charmdooz, "General arrangement and naval architecture aspects in midget submarines", 4th International Conference on Underwater System Technology Theory and Applications 2012 (USYS'12), Malaysia.
- [5] Y.N.Kormilitsin, O.A.Khalizev, "Theory of Submarine Design", Saint-Petersburg State Maritime Technology University, 2001
- [6] Burcher R, Rydill L J, "Concept in submarine design", (The press syndicate of the University of Cambridge., Cambridge university press), 1998, pp. 295
- [7] Renilson, M., (2015), Submarine Hydrodynamics, Springer, pp.45-89.
- [8] P.N.Joubert, "Some aspects of submarine design: part 2: Shape of a Submarine 2026", Australian Department of Defence, 2004.

Chapter 6: Submarine Sailing Shape Design

6-1- Introduction

There are a number of concepts concerning submarine sailing (fin, conning tower, bridge, fairwater) shape design. Shape optimization, requires an understanding of the basic concepts of shape design. Sailing shape design is strictly depended upon on the hydrodynamic resistance as is observed in other marine vehicles and ships. Submarines encounter to limited energy supply in submerged navigation. This is why, the minimum resistance plays an essential role in the hydrodynamic design of a submarine. Due to the vertical and longitudinal location of the sailing, the resistance causes a huge undesirable longitudinal moment. This moment must be canceled out with hydroplanes, implying more resistance. Therefore, the better the hydrodynamic form the less resistant and the moment. A large sail may contribute up to 30% of total resistance [9]. Furthermore, the shape design is dependent upon the internal architecture and the general arrangements of the sailing. A penetrating periscope is major problem for determining the location of sailing because periscope should be at the top of the control room. The convergence between the hydrodynamic and architectural requirements is vital for the determination of the overall shape design of the sailing. The sailing is a vertical hydrofoil containing a few masts, a diver exit tank and a main hatch. Below, several shapes of the sailings are considered. The vertical section of the sailing is a symmetric foil such as NACA0030. The area inside the sailing is wetted except for the exit tank which contains the pressure hull. Hence the light hull of the sailing envelope renders it suitable and simple for every curvature forming. It needs to be pointed out that the sailing form design should be compatible with the overall submarine hydrodynamic shape design. The sailing, plays an important role in submarine hydrodynamic design, and the eddy vortex (horse shoe vortex) occurring on the hull which affects the total resistance of submarine. Refs [1, 2] are the main references for a naval submarine shape design having the hydrodynamic aspects of the sailing design and the masts inside the sailing. A general recommendation for the dimensions and the sailing location for DREA standard submarine hull is showing Fig. 1.

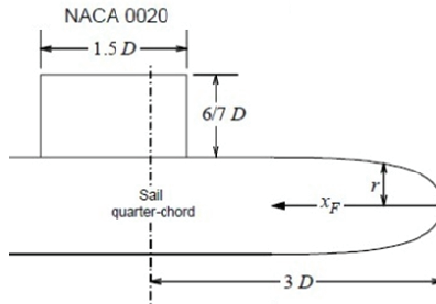
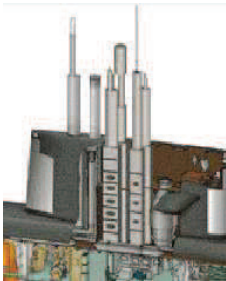
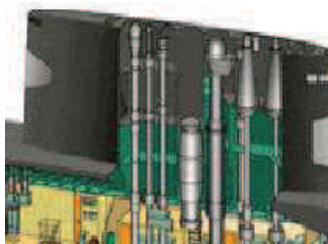


Figure 1: Parameters of DREA submarine hull [3]

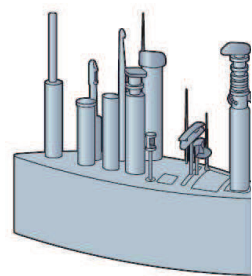
The present chapter focuses on the resistance of a fully submerge mode without considering free surface effects. Besides the hydrodynamics, the shape of the sailing depends upon the internal architecture and arrangements inside the sailing. Figure 2.a shows a typical masts arrangement inside the sailing. Figure 2.b shows the modern sailing setup of a German submarine, U212-A. This figure clearly demonstrates that in new modern sailings, the front and aft parts are not structured vertically. That is, they are inclined or curved to minimize the hydrodynamic resistance.



Amur class sailing arrangement



Kilo class sailing arrangement



Typical masts arrangement inside the sailing [1]



modern sailing configuration of German submarine U212-A



Akula class submarine: hydrodynamic sailing form

Figure 2: Typical mast arrangement inside the sailing

6-2- Specifications of the models

The base model considered here is an axisymmetric body submarine similar to that used in a torpedo, having a sailing that includes the horizontal section of a symmetrical NACA0030. This helps to halve the CFD modeling of the body and saving the time for analysis. The stern of submarine is conical, middle part is a cylinder and bow part is elliptical. In this chapter, 12 models with different sailing forms are studied. There are three main assumptions:

Assumptions 1: The shapes of the stern, bow and middle parts of submarine are constant in all models. Stern shape is a conical shape, middle shape is a cylindrical shape and bow shape is an elliptical shape.

Assumptions 2: For providing more equal hydrodynamic conditions, the total length, bow, middle and stern lengths of submarine are constant. The diameter is constant too. Thus, L/D of submarine hull is constant in all models. Height and width of sailing are also constant for all models. These constant parameters provide constant submarine hull shape resistance except the sailing shape which varies in each model. Next, the effects of the sailing form can be studied. Thus, each model has a different volume and a different wetted surface area.

Dimensions and speed for all models are provided in Tab.1 and Fig.3.

Table 1: Main assumptions of models

V	L	L _f	L _m	L _a	D	L/D	L _s	B _s	H _s
(m/s)	(m)	(m)	(m)	(m)	(m)		(m)	(m)	(m)
10	10	1	6	3	1	10	1,5	0,45	0,8

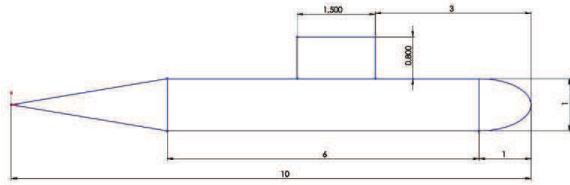


Figure 3: General dimensions of the submarine as base model (A1,B1)

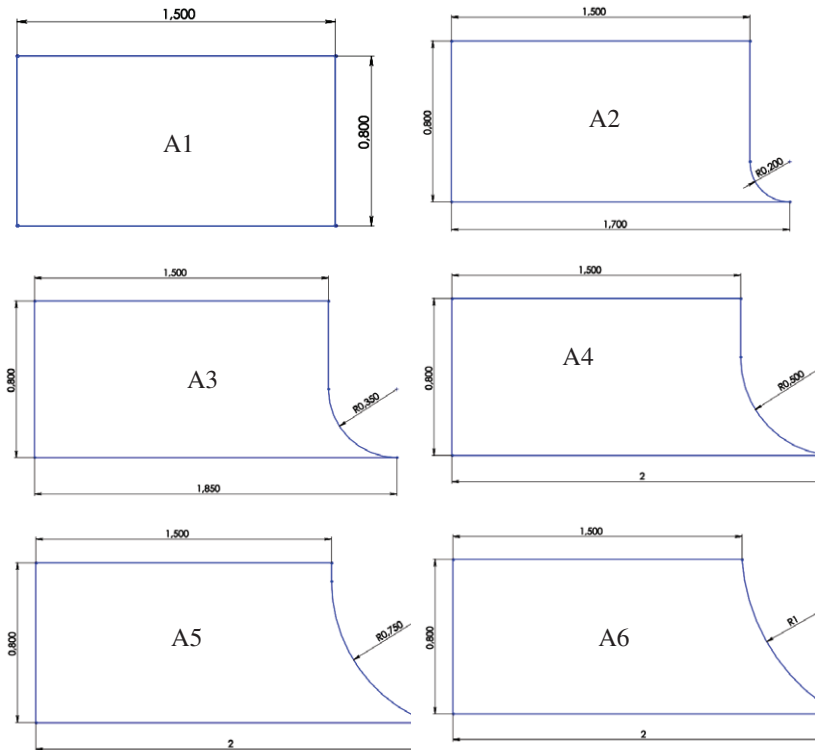
The analysis is performed in two stages: Stage A) Changing the front curvature and sailing radius having constant sailing after part. Stage B) Changing the line slope of the sailing after part having constant fore part. The specifications for all models are presented in Tab.2 and 3. In Tab.2, there is a modeling for Stage A, and Tab.3 included a modeling for Stage B. In addition, for CFD modeling in all models, the velocity is kept constant and equaling to 10 m/s resulting in Reynold's number of more than 15 million on the sailing. This Reynolds is suitable for turbulence modeling.

Table 2: Models of Stage A (bow shapes)

Sailing bow shape profile		Aw	A0
A1	without fillet	29.00	1.15
A2	fillet with r/D=0.2	28.98	1.15
A3	fillet with r/D=0.35	29.00	1.15
A4	fillet with r/D=0.5	29.01	1.15
A5	fillet with r/D=0.75	29.06	1.15
A6	fillet with r/D=1	29.11	1.15
A7	fillet with r/D=2	29.17	1.15
A8	inclined straight bow	29.23	1.15

The forms for these models are exhibited in Fig.4. All the models in Stage A have a straight vertical stern profile. In the model A1, the sailing bow is perpendicular to the main hull having no fillet. There are some fillets in the sailing front of models A2, A3 and A4. These fillets are tangent to the main

hull. Model A2, A3, and A4 have a fillet of 0.2, 0.3, and 0.5 m in the order mentioned. Model A5 has an arc profile with radius of 0.75 m, which arc is tangent to the vertical part of the sailing, but isn't tangent horizontally to the main hull since there is a limitation upon the sailing length. Models A6 and A7 have an arc which is not tangent to the vertical part not tangent to the main hull. Model A6 has a radius of arc of 1 m and model A7 has a radius of 2 m. Model A8 has a straight incline frontal profile corresponding to an arc with infinite radius. Models from A4 to A8 have an equal length of 2 m in the lower part of the sailing. All models have an upper length of 1.5 m for sailing.



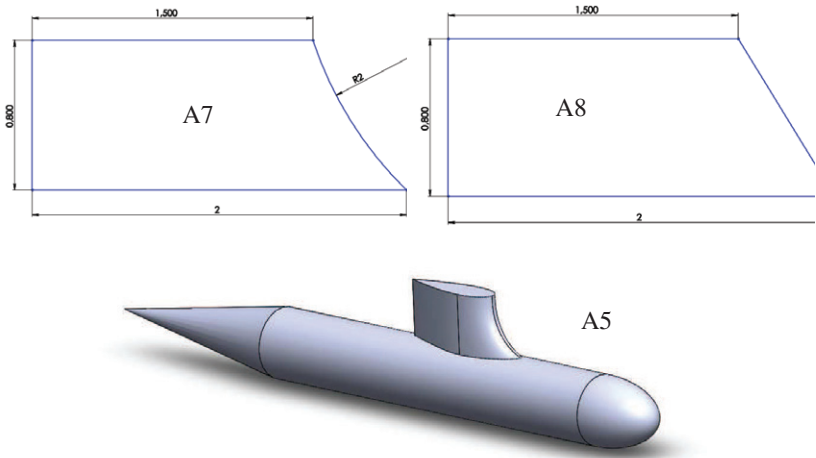


Figure 4: Configuration of models (stage A): changing the fore part of sailing

In Tab.3 and Fig.5, some profiles of the after part of the sailing are presented. As illustrated in Fig.5, the values of inclination angle of the sailing after edge vary between 90 and 145 degrees. For the 90° angle, the sailing after the profile is a vertical straight line. For models B2, B3, B4 and B5, the angles, in that order, are 105, 120, 135 and 145 degrees in the aft part with an inclined straight line.

Table 3: Models of stage B (stern shapes)

Sailing stern shape profile		Aw	A0
B1	without incline (90 deg)	11.16	1.15
B2	with incline of 105 deg	11.79	1.15
B3	with incline of 120 deg	12.48	1.15
B4	with incline of 135 deg	12.9	1.15
B5	with incline of 145 deg	13.25	1.15

Increasing the angle means an equivalent increase in wetted surface area and enveloped volume. The configurations related to each of these models are presented in Fig.5.

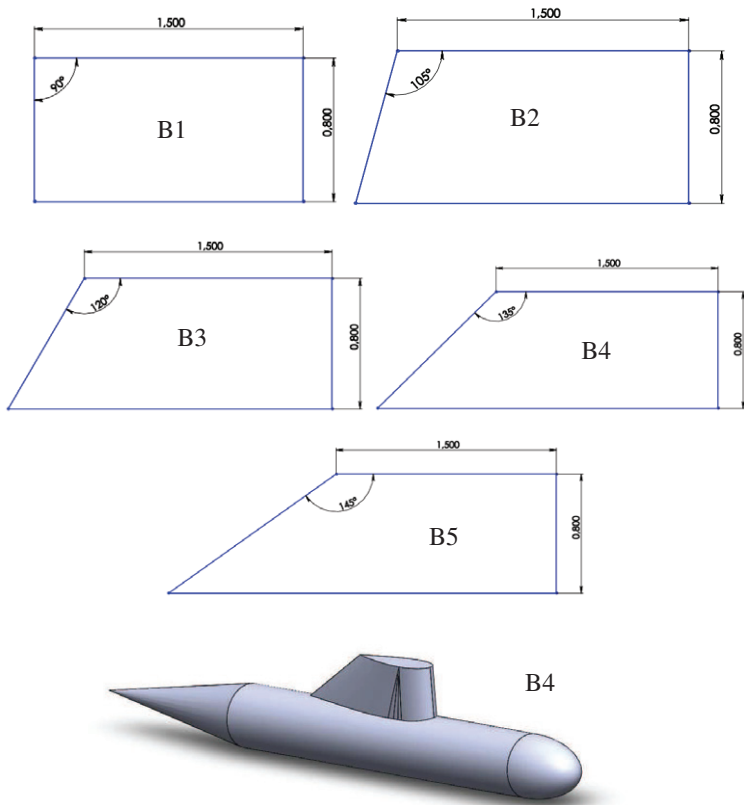
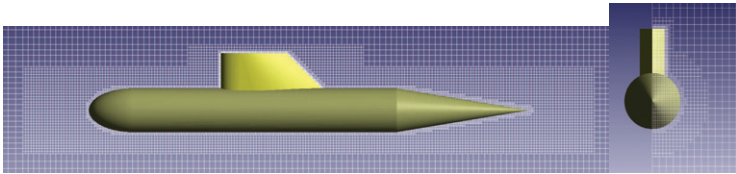
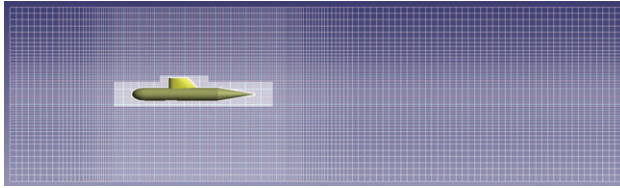


Figure 5: Configuration of models (stage B) : changing the after part of sailing

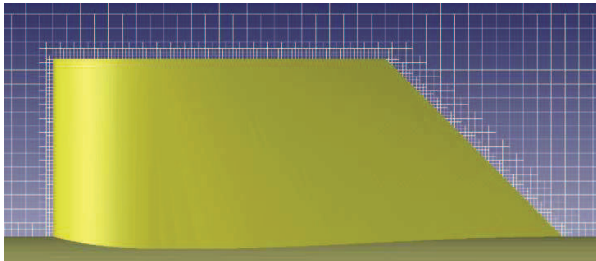
6-3- Preparations of CFD analysis

All calculations are performed on more than one millions computational fluid cells. In this domain, there is an inlet (having a uniform flow), free outlet (aft, starboard, top and bottom faces of the box), symmetry (central plane of submarine) and Wall (for the body of the submarine). The following are the cubic domain dimensions: length=50m (being equal to 5L), beam=7m (equaling 0.7L or 7D), and height=14m (equivalent to 1.4L or 14D). Only half of the body is modeled because of the central plane symmetry shape, the same applies on the domain. Meanwhile, this study has demonstrated that the beam

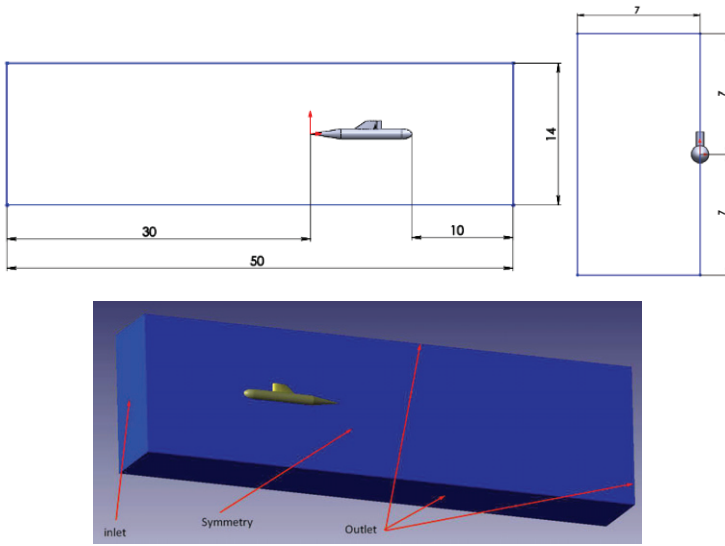
and the height equaling to $14D$ could be quite acceptable. Here, there are little meshes far from the object. The forward distance from the model equals L , the after distance is $3L$, and the total length being $5L$ (Fig.6). The turbulence model is K-Epsilon and y^+ is considered equivalent to 30. The intended flow selected for the analysis was that of an incompressible fluid of fresh water. Having a temperature of 15 degrees Celsius and a constant velocity of 10 m/s. Settings of the CFD simulation are abstracted in table 4.



(a)



(b)



(e)

Figure 6: (a) Domain and structured grid (b) Very tiny cells near the wall for boundary layer modeling and keeping y^+ about 30 (c) Half modeling due to center plane-symmetry

Table 4: Settings of the simulation

Elements	Boundary conditions	Descriptions
Domain	conditions	Fully submerged modeling (without free surface)- half modeling- domain with inlet, outlet, symmetry and wall- Without heat transfer.
	dimensions	length: $5L=L+L+3L$ (distance before: L - distance after: $3L$)- beam: $0.7L$ or $7D$ - height: $1.4L$ or $14D$
	grid	structured grid- hexahedral cells- fine cell near wall- Mesh numbers: more than 1.1 million
Fluid	settings	Iterations more that 700- Time step= 0.01 sec. Incompressible fluid (water)- turbulent modeling: Standard $k-\epsilon$ - fresh water- temperature: 20 deg- $\rho=999.841$ kg/m^3 .
Object	Wall	Submaribe- value $30 < y^+ < 100$ - roughness= 0 - no slip
Input	Inlet	Velocity= $10m/s$ - normal (along x)- in 1 face
Output	Free outlet	Zero pressure- in 4 face
Symmetry	Symmetry	In 1 faces

6-4- CFD Analysis

The main goal of the study is to estimate the resistance of a fully submerged submarine together with the sailing comprises frictional resistance and viscous pressure resistance, there is no wave resistance, however the frictional resistance depends on the wetted area, while the viscous pressure resistance is determined by the object. Here, to optimize of the sailing shape, both of these resistances are required since at a given length, by changing the shape of the sailing, the wetted area and the form will also change. These values are presented in Tab.5 and Tab.6.

Table 5: Resistance components of Models in stage (A) [N]

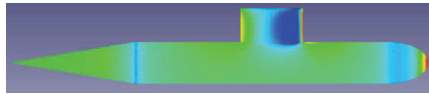
front shape		Rt	Rvp	Rf	Rvp/Rt
A1	without fillet	7074	3575	3498	50.5
A2	fillet with r/D=0.2	7000	3486	3514	49.8
A3	fillet with r/D=0.35	6950	3426	3525	49.3
A4	fillet with r/D=0.5	6935	3404	3530	49.1
A5	fillet with r/D=0.75	6854	3308	3545	48.3
A6	fillet with r/D=1	6760	3205	3555	47.4
A7	fillet with r/D=2	6646	3068	3579	46.2
A8	inclined straight bow	6456	2859	3597	44.3

Table 6: Resistance components of Models in stage (B) [N]

stern shape		Rt	Rvp	Rf	Rvp/Rt
B1	without incline (90 deg)	7074	3575	3499	50.5
B2	with incline of 105 deg	7047	3524	3523	50.0
B3	with incline of 120 deg	7025	3490	3535	49.7
B4	with incline of 135 deg	6982	3411	3571	48.9
B5	with incline of 145 deg	6934	3360	3574	48.5

Pressure resistance depends upon the pressure distribution over the body, and the pressure distribution depends upon the form. The more uniform the pressure distribution, the less the resistance. Logically, the after part of the sailing is a low pressure area and the front part is a high pressure one. The pressure distribution for several shapes is presented in Fig.7. the sailing form having a rectangular side view cannot be considered a good design. This can be seen in Fig.7-a, with an intense high pressure area at the front of the sailing and a low pressure at the after part, which cause a high rate of resistance. Increasing the radius of the curvature at front causes more smooth distribution of hydrodynamic pressure on the sailing along with less differences between

the minimum and the maximum pressure values, as is shown in Fig.7-b and 13-c. As mentioned above, the after part of the sailing is a low pressure area. The less the pressure at the after part, the more the pressure difference between the front and the after parts of the sailing. This causes more pressure resistance. Similarly, increasing the inclination angle of the after part of the sailing creates more smooth pressure distribution on the sailing. These are indicated in Fig.7-d and 7-e. These factors contribute to fewer values of resistance. As Fig.7-f shows, the volume of the surrounding liquid exerts a pressure on the hull.



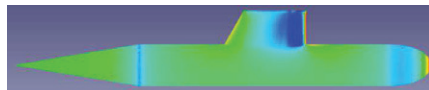
(a) Model A1 (B1): Initial sailing



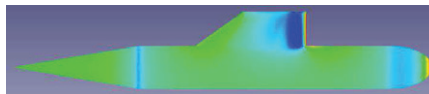
(b) Model A5: Sailing frontal radius of 0.75 m



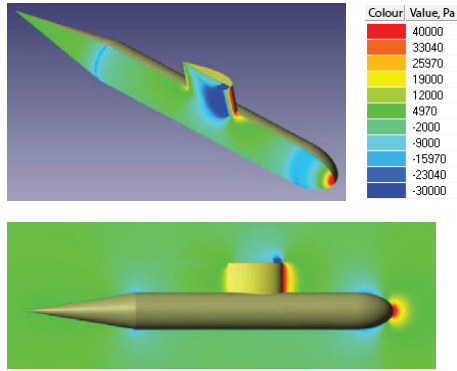
(c) Model A8: Inclined straight sailing frontal part



(d) Model B3: Sailing's aft angle of 120 degrees



(e) Model B5: Sailing's aft angle of 145 degrees



(f) pressure contours and relevant values

Figure 7: Pressure distribution over the body

The results of CFD analysis in stage "A" are presented in Tab.7 and the diagrams of Fig.8.

In table 7, C_d , is resistance coefficient based on the wetted area (A_w). The formula is thus stated as:

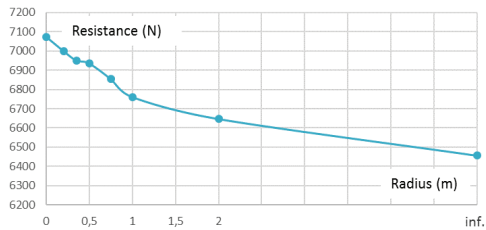
$$C_d = \frac{R_t}{0.5 \cdot \rho \cdot v^2 \cdot A_w} \quad (2)$$

Table 7: Specifications for Models in stage (A)

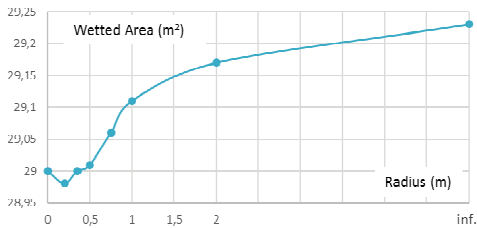
bow shape	Rt [KN]	A _w [m ²]	C _d *1000
A1	7074	29.00	4.878
A2	7000	28.98	4.831
A3	6950	29.00	4.793
A4	6935	29.01	4.781
A5	6854	29.06	4.717
A6	6760	29.11	4.645
A7	6646	29.17	4.557
A8	6456	29.23	4.417

It can be seen clearly from Figure 8-b-the resistance diagram-that by growing the radius, we can obtain less resistance. According to Figure 8-b, the shape of the sailing with a radius of 0.2 m has the least values of the wetted area but this will increase with an increase in the radius. The straight inclined bow shape has the maximum value of the wetted area. As for the resistance

coefficient based on the wetted area in Fig.8-c, one can infer that the greater the radius of the fillet the less the values of the resistance coefficient. However, bigger radii of the fillet give more space for gears in the sailing. At this stage we can select a proper sailing frontal shape. As shown in Fig.8, the front shape without the fillet of the sailing front is a worse selection in terms of resistance. Straight inclined bow shape has the minimum value of resistance, and thus, it can be the most suitable selection.



(a)



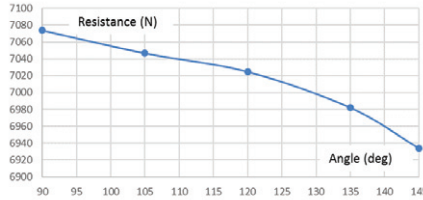
(b)



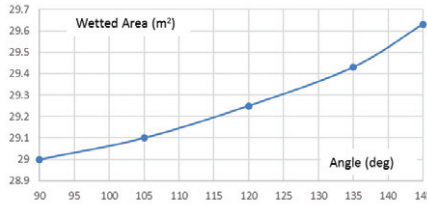
(c)

Figure 8: Results of CFD analysis on different sailing's frontal shape (stage A)

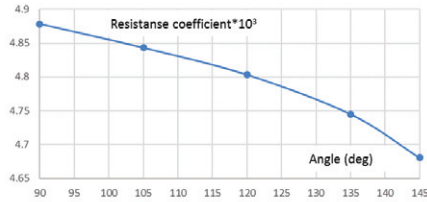
The result of CFD analysis in stage "B" is presented in Tab.8 and diagrams of Fig.9.



(a)



(b)



(c)

Figure 9: Results of CFD analysis on different sailing's aft shapes (stage B)

At stage B the focus is on the sailing aft shape by varying the values of inclination angle. As shown in Fig.9, the range of inclination angles of 90-145 degrees are considered. For the angel of 90 degrees, the sailing after edge profile is a vertical line, but for angles 105, 120, 135 and 145 degrees, the profile is an inclined one. Increasing the inclination angle is equivalent to increasing the wetted surface area and the enveloped volume. An overview of

the results reveals that, in this range, the angle of 90 degrees has the maximum resistance and resistance coefficient, as well as the minimum wetted area with the worst results. The total resistance diagram shows that the resistance is decreased with an increase in inclination angle. However, the greater angle values mean greater wetted surface area, a point inferred from Fig 9-b. Accordingly, the resistance coefficient decreases with an increase in the inclination angle, a fact displayed in Fig.9-c. The after shape conforming to 145 degrees, angle has the minimum value of total resistance and resistance coefficient, albeit maximum wetted surface area, thus it can be selected as a good choice.

Table 8: Specification of Models in stage (B)

After shape	Rt [KN]	Aw [m ²]	Cd*1000
B1	7074	11.16	4.878
B2	7047	11.79	4.843
B3	7025	12.48	4.803
B4	6982	12.9	4.745
B5	6934	13.25	4.680

Following these diagrams, one can fit them with some formulas. The relation between the resistance coefficient (Cd) and the inclination angle α can be formulated thus:

For $90 < \alpha < 145$:

$$C_d = -1.042 \cdot 10^{-6} \cdot \alpha^3 - 3.244 \cdot 10^{-4} \cdot \alpha^2 - 3.589 \cdot 10^{-2} \cdot \alpha - 6.241 \quad (2)$$

6-5- Review

The present research chapter explored a number of sailing shapes- front and aft part- executive the CFD analysis on these forms. The shapes considered in this study are the most common in the submarine sailings. The most crucial factor taken into consideration in the sailing shape is exhibiting the least amount of submerged resistance. The research focused on the CFD analysis of the submerged resistance utilizing flow vision software. Analyzing the date, the following emerged:

- 1) Greater radius of the sailing frontal fillet corresponds with fewer values of the resistance coefficient.
- 2) Resistance coefficient decreases with an increase in the inclination angle of the sailing aft edge.

- 3) Submarine resistance with an inclined sailing front (Model A8) displays less resistance-9.4 percent- compared with a straight vertical(Model A1).
- 4) Submarine resistance with an inclined sailing aft of 145 degrees (Model B5) exhibits less resistance-4.1 percent- if comparison with a straight vertical aft shape (Model B1).

References

- [1] P.N.Joubert, "Some aspects of submarine design: part 1: Hydrodynamics", Australian Department of Defence, 2004.
- [2] P.N.Joubert, "Some aspects of submarine design: part 2: Shape of a Submarine 2026", Australian Department of Defence, 2004.
- [3] Mackay M, "The Standard Submarine Model: A Survey of Static Hydrodynamic Experiments and Semiempirical Predictions", Defence R&D Canada, June 2003, pp.30

Chapter 7: Engineering Estimation of Submerged Resistance of Submarine

For calculation of submarine resistance at fully submerged condition, there are some engineering formulas based on experimental results with rather accurate results and small errors. These formulas could be applicable in conceptual and preliminary stage design.

These methods with model test method and CFD method can provide a suitable estimation of resistance. These results are not exactly equal and similar. By omission of diverged results, the final estimate can be exact and correct.

Method 1) this method is for calculation of bare hull resistance by several diagrams in Reference [1]: $C_T = C_f + C_{VP} + C_A$. In this method resistance coefficient can be extracted from these diagrams. Results of calculations by method 1 are in Table 1.

Method 2) this method is mentioned in Reference [2]. Conditions of use for this method are:

- Length to diameter ratio: $5 < L/D < 7$
- Depth of submergence more than 5 times of diameter: $h \geq 5D$

After these conditions, bare hull resistance can be calculated as these stages:

1- Calculation of the frictional resistance coefficient by ITTC-1957:

$$C_{F_o} = \frac{0.075}{(\log R_e - 2)^2}$$

2- Added resistance from surface roughness equal to 5 percent of C_F :

$$\delta C_F = 0.05 C_f$$

$$C_F = C_{F_o} + \delta C_F$$

3- Calculation of the form coefficient (K):

$$K = \left(\frac{D}{L}\right) + 1.5 \left(\frac{D}{L}\right)^3$$

4- Viscous pressure coefficient by:

$$C_{VP} = C_{Form} = K.C_{F_o}$$

5- Total resistance coefficient:

$$C_T = C_F + C_{VP}$$

6-Calculation of total resistance of bare hull:

$$R_T = \frac{1}{2} C_T \cdot \rho \cdot A \cdot V^2$$

That A is wetted surface area. Appendage resistance must be added up to results. Results of calculation by method 2 are shown in Table 1.

Method 3) this method is in Reference [3] by these stages for bare hull resistance:

1-frictional resistance by ITTC-1957

$$C_{F_o} = \frac{0.075}{(\log R_e - 2)^2}$$

2-total frictional resistance coefficient:

$$C_T = C_F \left(1 + 1.5 \left(\frac{D}{L} \right)^{1.5} + 7 \left(\frac{D}{L} \right)^3 \right)$$

3-calculation of total bare hull resistance:

$$R_T = \frac{1}{2} C_T \cdot \rho \cdot A \cdot V^2$$

That A is wetted surface area. Appendage resistance must be added to this amount. Results of calculations by method 3 are in Table 1.

Method 4) this method is either in Reference [3]. This method is similar to method 3 but a different way for calculate C_T This coefficient is:

$$C_T = C_F \left(3 \left(\frac{D}{L} \right) + 4.5 \left(\frac{D}{L} \right)^{0.5} + 21 \left(\frac{D}{L} \right)^2 \right)$$

That S is cross section area of submarine. Results of method 4 are presented in Table 1.

$$R_T = \frac{1}{2} C_T \cdot \rho \cdot S \cdot V^2$$

Table 1-Total Resistance of Main Submarine (KN)

V (knot)	method 1	method 2	method 3	method 4
1	0.36677514	0.30590877	0.2801496	0.5549127
2	1.35476246	1.09280212	1.0007824	1.9051925
3	2.91871624	2.30798527	2.1136407	4.0286747
4	5.03809373	3.92753338	3.5968143	6.861308
5	7.69959057	5.93595174	5.4361133	10.376349
6	10.893471	8.32190174	7.6211537	14.554213
7	14.6121165	11.0765105	10.14381	19.379562
8	18.8493033	14.1925298	12.997444	24.839863
9	23.5997927	17.6638582	16.176468	30.924559
10	28.8590756	21.4852444	19.676073	37.624564
11	34.6232042	25.6520906	23.492049	44.931916
12	40.8886748	30.1603163	27.620659	52.839551
13	47.6523432	35.0062596	32.058548	61.341124
14	54.9113617	40.1866041	36.80268	70.430891

References

- [1] R.K.Durcher, L.J.Rydill.1995.Concepts in Submarine Design. Cambridge university press
- [2] V.Bertram. 2000. Practical Ship Hydrodynamics
- [3] J.Pulmor.2001.Underwater Vehicle Design with Regard to Power plant Selection
- [4] H.A.Jackson.1980. Submarine Design Notes
- [5] K.J.Rawson, E.C.Tupper. 2001. Basic Ship Theory-Vol2
- [6] M.Moonesun.2009. Handbook of Naval Architecture Engineering

Chapter 8:

Evaluation of Naval Submarine Sea keeping Criteria

8-1- Introduction

The first step in the assessment of Seakeeping performance is usually to determine the wave spectrum for a seaway [1-3]. The emphasis is often on wave heights rather than wave periods, and information on directionality and wave spectrum forms is rare [4-6]. In seakeeping analysis, until design of RAO (Response Amplitude Operation) diagrams, there is not any need for design criteria but for extraction of SOE (Seakeeping Operating Envelope) polar diagrams[7,8] and submarine seaworthiness abilities, there is an urgent need for some clear and technical criteria according to the submarine technical specifications. The characteristics of submarine systems are presented in Refs.[9-13]. A knowledge about these systems is urgent for seakeeping performance evaluation. A simplified method of presenting the seakeeping performance of specific design is to plot a polar diagram[15,16]. In SOE diagrams the restrictions of submarine operations or Operability Index (O.I) in several sea states are evaluated. The seakeeping performance of a ship can either be predicted using computer codes or measured in a seakeeping basin [17]. Performing all expected missions in rough seas can be accepted for a ship as an indication for a good seakeeping [18]. Ship motions at sea have always been a problem for the naval architect [8]. Whilst the introduction of ride controls has somewhat reduced the severity of motions in some cases, there has been considerable interest in the underlying effect of hull form on the ship motions [18]. Ships are partially submerged objects with six degrees of freedom for their motion (with constraints related to its interaction with water)[19]. Seakeeping properties and motion of ships and submarines are different in several aspects of views [20,23]. The shape and navigation mode of submarines are very different from ships. Seakeeping performance index is a term used to assess the motion and dynamic effects for a given sea state, direction of heading angle and speed of transit[24]. Dynamic stability or capsizing of ships can also be investigated in detail as the cause-effect chain can be analyzed in a deterministic, repeatable wave train at different interaction positions [25,26]. Submarine can dive from the sea surface into the depth of sea in three conditions: surface, snorkel and submerge condition. In snorkel condition, the total volume of submarine is under the water surface but very near to the surface so that only snorkel mast is out of water. Snorkel mast causes suction of air for starting and operating of diesel engine and air compressor. Diesel engine causes batteries charging and air compressor can charge high pressure air capsules. After a restricted time, batteries and

capsules have been charged and diesel-generator and compressor are turned off and submarine is ready to dive and go to submerged condition. In submerged condition, submarine is fully submerged and is far from the sea surface and waves. In this situation, sea waves don't have any influence on the submarine motion so that seakeeping studies are ignored in submerged mode and are only evaluated for surface and snorkel condition. Static stability and GZ curve parameters in snorkel are very weak compared with the surface condition because water plane area is almost zero. Transverse and longitudinal metacentric height in snorkel mode is equal to each other and very smaller than the metacentric height in surface condition. Therefore, stability in snorkel condition is very weak and submarine is still under wave moment. It means more critical and sensible condition compared to surface condition because of minimum stability and strong wave heeling and pitching moments. Wave action in snorkel is less than surface waves because of more drafts and distance from the water surface, but it is considerable for snorkel stability condition. In this chapter, two conditions for seakeeping criteria are presented; surface and snorkel condition and each of them have three categories; 1. People 2. Mission systems 3. platform system (Lewis, 1989). People category is related to human health and performance for doing their duties. It is the same for surface and snorkel condition. Mission system is related to the operational systems that are urgent for doing the mission such as sonar search, battery charging and snorkeling. It is different for surface and snorkel condition because of that each mission is different. Platform systems are related to the general system and devices that must be kept safe and intact in the submarine life period such as diesel, generator, electric motor, piping and installation. It is different in surface and snorkel because some systems are turned off in each condition. According to these differences, different criteria must be regarded. This chapter, firstly, identifies the new proposed parameters that are based on authors' experiences on submarine design and data acquisition in sea trials. Other data are achieved from modeling in Paramarine and Flow Vision software. Hence some quantities are proposed for each parameter. Another part in this chapter is removing some parameters from twelve parameters of ships that are not belonged to submarines and are special for ships. The final step is providing a table of seakeeping criteria special for submarines that could be the basis of extraction of submarine SOE diagrams. The main reference of this chapter is Ref.[27].

8-2-Ship and submarine sea keeping behavior comparison

The performance of a hull form, both in calm and rough water is a major concern for the naval architect. No single parameter can be used to define the

seakeeping performance of a design. There are twelve parameters for ship seakeeping behavior according to table 1. (Lewis, 1989).

Table 1: Twelve seakeeping performance criteria for ships [8]

NO	Seaway performance criteria	Affected elements	Performance degradation
(a) Absolute Motion Amplitudes			
	Roll angle Pitch angle	People, Mission and Platform Systems	Personnel injury, reduced task proficiency and mission and hull system degradation
	Vertical displacement of points on flight deck	{ People Mission Systems	Injury to personnel handling aircraft, inability to safely launch or recover aircraft
(b) Absolute Velocities and Accelerations			
	Vertical acceleration Lateral acceleration	People and Mission Systems	Personnel fatigue, reduced task proficiency and mission system degradation
	Motion sickness incidence (MSI)	People	Reduced task proficiency
	Slam acceleration (vibratory, vertical)	People, Mission and Platform Systems	Personnel fatigue, injury, reduced task proficiency and mission and hull system degradation. Preclusion of towed sonar operation.
(c) Motions Relative to Sea			
	Frequency of slamming. (Simultaneous bow reimmersion & exceedance of a threshold vertical velocity)	{ Mission Systems Platform Systems	Hull whipping stresses and damage to sensors on the masts. Slamming damage to bottom forward hull structure
	Frequency of emergence of a sonar dome	Mission Systems	Reduced efficiency of sonar
	Frequency of deck wetness (submergence if the main deck forward)	{ People Mission Systems	Injury or drowning of personnel. Damage to deck-mounted equipment
	Probability of propeller emergence	Platform Systems	Damage to the main propulsion plant
(d) Motions relative to aircraft			
	Vertical velocity of aircraft relative to the flight deck	Mission Systems	Damage to aircraft landing gear and/or loss of aircraft

From table 1, some of these parameters are not related to submarine and must be omitted so as:

- 1- Vertical displacement of points on flight deck: It is according to criterion No.3 in table 1 and is omitted because the flight deck, there are not on a submarine.
- 2- Vertical velocity of aircraft relative to the flight deck: It is according to criterion No.12 in table 1 and is omitted because the flight deck, there is not on a submarine.

Frequency of deck wetness; according to criterion No.10 table 1 this parameter is also omitted because the submarine hull is cylindrical and completely watertight. Moreover, all devices on submarines hull are designed for sea water condition and in the depth of water. Thus deck wetness cannot cause any damage to submarine stability and devices. The shape with circular cross section such as a cylinder has constant stability parameters in all roll angles and also the range of stability in GZ curve for submarine is to 180 degrees. According to these conditions, deck wetness is not important for submarines and is omitted. Therefore, three criteria are removed from table 1, and other three criteria are added that are belonged to submarine:

1-Sonar acoustic deafness: Submarine in submerged and snorkel condition doesn't have radar detection and direct vision (maybe only periscope in snorkel depth). Several sonars are eyes of submarine that prevent damage to the fixed barriers and mobile objects. Criterion No.9 of table 1 is only concentrated on the emergence of the sonar dome, but this parameter is not sufficient and clear for submarine detection because in most conditions, sonar emergence doesn't occur, but sonar becomes deaf. Its reason is a high level of ambient noise because of sea waves and stiff motions of the bow. In high sea states, moving and breaking of wave produces some troublous noises. In this condition, submarine may clash to underwater hills and barriers and other submarines and ship. Submarine has several kinds of sonars such as active, passive, conformal, flank, back looking and towing sonar array. In bad sea conditions and high sea forces, submarine is in dangerous condition. For getting a safe condition, submarine must go into the depth of water so that ambient noise be suitable and all sonars be efficient. Main restriction in this seakeeping parameter is related to the situation of sonar and acoustic sensors. This criterion is important for both surface and snorkel condition, especially in snorkel depth that sonar must be applicable for detection. As shown in Fig.1, waves move near the sonar, and their effects can cause a reduction in sonar efficiency. There is an ideal or optimum sonar draft in calm water than the sonar efficiency is maximum. In operational sea state, there is a safe sonar navigation draft as shown in Fig.1. In this draft, sonar efficiency isn't ideal but

submarine can navigate safely. In high sea state, there is an unsafe sonar navigation draft which sonar efficiency is minimum, and it is dangerous condition for navigation at near the surface. This condition is important for forward hydroplanes too. As shown in Fig.1, location B for sonar and hydroplanes is better than location A as regarding wave ambient noise. This parameter presents as percentage. This percentage is the ratio of the time that sonar is deaf and the total time (that is regarded one hour or 60 minutes).

$$P_1(\%) = \frac{t_1(\text{time that sonar is deaf})}{t_0(\text{total time} = 60 \text{ min})}$$

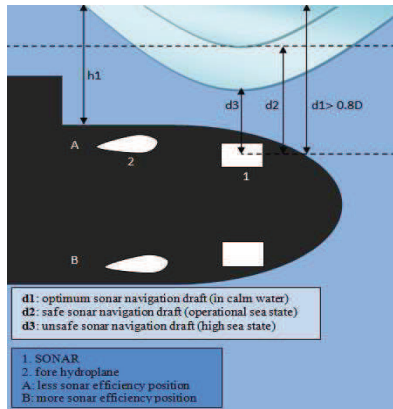


Figure 1: Ideal, safe and unsafe draft for sonar efficiency (and hydroplanes) in snorkel condition

2-Snorkel mast flooding: When a submarine is in snorkel depth, only snorkel mast is above the water surface for suction the atmosphere air (Fig.2). This mast has an automatic head valve. This head valve has a sensor that, if it is wetted, it will be closed immediately for preventing the water entrance to inside the submarine and preventing flooding and suffering damage to the diesel engine. The wetting of head valve is due to relative motion of sea wave and submarine as shown in Fig.2.

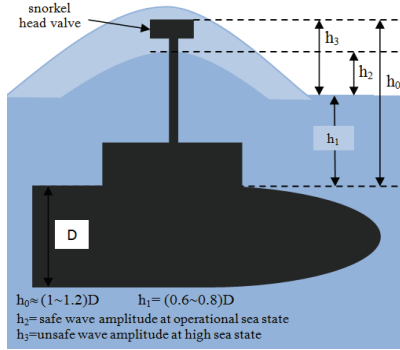


Figure 2: Main parameters in submarine architecture for improvement of snorkel mast flooding

Defined sea state for submarine operations is very important in snorkel condition. In Fig.4, the safe wave amplitude h_2 is related to standard sea state for submarine and h_3 is related to high sea states that causes a steep fall in snorkeling. For this reason, the automatic head valve will be interval opened and closed. There are two important parameters in submarine naval architecture design: the height h_0 is the usual height of snorkel mast from pressure hull and h_1 is a usual draft. Quantities are shown on Fig.2. All these parameters should be regarded with together. This interval action of head valve causes quick fall in the inlet air flux. As in snorkel depth, the diesel engine is turned on and consuming the air inside the hull, if the head valve be closed for long time, it will cause a quick fall of inside pressure or vacuum condition inside the pressure hull. Vacuum condition is very dangerous for human and machineries such as audience and breathing problems for human and water leakage into the pressure hull (because of intense pressure difference) and closing and jamming of the bulkhead door. Then the time of continuous operation of head valve is very important. This criterion is important only for snorkel condition and is presented by percentage as so:

$$P_2 (\%) = \frac{(t_0 - t_2)}{t_0} \times 100$$

t_2 : the time that head valve is open (in minutes), t_0 : the total time that is regarded 60 minutes.

Thus in this criterion, the wave height and sea force (sea state) is very important. Snorkel mast there is in ordinary diesel–electric submarine for air

intake and charging the batteries but in submarines that are equipped with air independent propulsion (AIP) system such as nuclear propulsion, this criterion is not important because they don't have snorkel mast.

3-Battery performance disruption: Submarines have 200 to 400 battery cells dependent upon the voltage level. Duty of these batteries is providing electric energy for propulsion (electric motor) and hotel load (lighting, air conditioning, etc.) then their continuous operation is vital. Sealed batteries are not influenced by submarine motions but non-sealed batteries such as lead-acid batteries are influenced by the submarine motions. Vertical accelerations on batteries and amplitude of roll and pitch motion are very effective on battery efficiency. For example, acid inside the battery is important for battery exercise and acid spillage cause battery disruption. Acid spillage can cause producing toxic gases and pressure hull corrosion and other damages to submarines. Thus battery performance is significant in submarine seakeeping behavior. This criterion is important both in surface and snorkel condition. This criterion is presented by percentage. This percentage defines as:

$$P_3(\%) = \frac{(t_0 - t_3)}{t_0} \times 100$$

t_3 : battery exercise in minutes. t_0 : total time (60 minutes).

Battery is important in diesel-electric submarines and is not significant for submarines that are equipped with AIP systems, and this criterion will be ignored. Thus after omitting three criteria (for ships) and adding three criteria (special for submarines), there will be twelve criteria for evaluation of submarine seakeeping behavior that is presented in table 2.

Table 2: Twelve seakeeping performance criteria for submarines

NO	Seaway performance criteria	Affected elements	Performance degradation
(a) Absolute Motion Amplitudes			
	Roll angle Pitch angle	People, Mission and Platform Systems	Personnel injury, reduced task proficiency and mission and hull system degradation
(b) Absolute Velocities and Accelerations			
	Vertical acceleration Lateral acceleration	People and Mission Systems	Personnel fatigue, reduced task proficiency and mission system degradation
	Motion sickness incidence (MSI)	People	Reduced task proficiency
	Slam acceleration	People, Mission	Personnel fatigue, injury, reduced

(vibratory, vertical)	and Platform Systems	task proficiency and mission and hull system degradation. Preclusion of towed sonar operation.
(c) Motions Relative to Sea		
Frequency of slamming. (Simultaneous bow reimmersion & exceedance of a threshold vertical velocity)	Mission Systems Platform Systems	Hull whipping stresses and damage to sensors on the masts. Slamming damage to bottom forward hull structure
Frequency of emergence of a sonar dome	Mission Systems	Reduced efficiency of sonar
Sonar acoustic deafness	Mission Systems	Reduced efficiency of sonar and detection abilities
Probability of propeller emergence	Platform Systems	Damage to the main propulsion plant
Batteries performance disruption	Mission Systems Platform Systems	Interruption in electric energy support, reduction in speed, acid spillage and damage to battery cell
Snorkel mast flooding	People, Mission and Platform Systems	Vacuum and pressure fall, audience and breathing problems, disruption in snorkeling, damage to diesel engine and compressor, water leakage

8-3- Sea keeping performance values

The hydrodynamic design based on clear definitions of operability requirements, and mission criteria have made sea keeping and maneuvering oriented design decisions easier through a quantitative description of performance throughout the design process. After introduction of sea keeping parameters of submarines, the values of each parameter can be determined. These are important for identifying safe and unsafe operating envelope or the polar diagrams of SOE. These suggested quantities are presented for two conditions; surface and snorkel (table 3).

Table 3: Quantities of sea keeping performance criteria for submarines in surface & snorkel condition

No	Seaway performance criteria	Surface condition	Snorkel condition
1	Roll angle (degree)	9.6	9.6
2	Pitch angle (degree)	1.5	2.5
3	Vertical acceleration (g)	0.25	0.2
4	Lateral acceleration (g)	0.1	0.1
5	Motion sickness incidence (MSI) (% in 2 hours)	20% in 2 hours	25% in 2 hours
6	Slam acceleration (vibratory, vertical) (g)	0.2	0.05
7	Frequency of slamming (Simultaneous bow re-immersion & exceeding of a threshold vertical velocity) (%)	3	0.5
8	Frequency of emergence of a sonar dome	60 in 1 hr	20 in 1 hr
9	Sonar acoustic deafness (%)	10	5
10	Probability of propeller emergence (%)	25	8
11	Batteries performance disruption (%)	5	5
12	Snorkel mast flooding (%)	-	25

By comparison between two conditions (surface and snorkel) it can be seen:

- 1- criterion of roll angle doesn't change in surface and snorkel because of constant relation between transverse stability and heeling moments.
- 2- Criterion of pitch angle is different between two conditions because of intensive fall of longitudinal metacentric height in snorkel condition and more motions.
- 3- Absolute vertical acceleration in snorkel is less than surface condition.
- 4- Absolute lateral acceleration is the same for two conditions.
- 5- Motion sickness incidence (MSI) in snorkel is more than the surface condition because of more intensive motions.
- 6- Usually, slamming loads are much larger than other wave loads. Slamming acceleration in snorkel is very less than surface because the draft in snorkel is more than surface condition. The snorkel draft is about two times of the surface draft.
- 7- Frequency of slamming in snorkel is very less than surface because of the same reason stated in criterion No.6.
- 8- Frequency of emergence of the sonar dome in snorkel is very less than surface because of the same stated in criterion No.6. Sonar dome is provided for passive sonar that is located at the front of hull, above or beneath the bow axis.
- 9- Sonar acoustic deafness and ambient noise in snorkel are less than surface condition because in snorkel draft, sonar has more distances from sea-surface waves.

- 10- Probability of propeller emergence in snorkel is lesser than the surface condition because of more draft, and more distance of propeller from the water surface.
- 11- Battery performance disruption is the same for both conditions.
- 12- Snorkel mast flooding is only important to snorkel condition and isn't significant in surface condition.

8-4- Review

For analyzing the sea keeping behavior of submarine and design of SOE polar diagram (that shows the safe and unsafe operation zone), some limitation and restrictions must be defined as sea keeping criteria. These criteria must be special for submarines because there is remarkable different between submarine and ship missions and machineries. Submarine has three conditions: surface, snorkel and submerge mode. For submerged mode, sea keeping criteria don't define because it is far from sea waves. In comparison with snorkel and surface condition, in some cases, snorkel is more critical and in other cases, surface parameters are critical. There are some obvious differences between snorkel and surface condition such as stability, draft, wave action, turn off/on machineries and their missions. Three parameters that are only for ship, are discussed and omitted and other additional three parameters that are special for submarine are identified and defined. Therefore, in this chapter twelve parameters were presented and suggested for submarine sea keeping analyzing.

Nomenclature

- p_1 Percentage of Sonar acoustic deafness
- p_2 Percentage of Snorkel mast flooding
- p_3 Percentage of Battery performance disruption
- t_0 total time that is regarded 60 minutes
- t_1 Sonar deafness time in minutes
- t_2 the time that head valve is open in minutes
- t_3 battery exercise in minutes

References

- [1] Kevin McTaggart , David Cumming, C.C. Hsiung, Lin Li , "Seakeeping of two ships in close proximity", Elsevier Science Ltd,2002.
- [2] S.K. Chakrabarti, "Offshore Structure Modeling, World Scientific", Singapore, 1994.
- [3] The Specialist Committee on Waves, "Final report and recommendations to the 23rd ITTC", Proceedings of the 23rd ITTC, vol. II, 2002.
- [4] Ming Li , "An optimal controller of an irregular wave maker", Elsevier Science Ltd, 2004.
- [5] Gabriele Bulian, Alberto Francescutto , Claudio Lugni, "Theoretical, numerical and experimental study on the problem of ergodicity and 'practical ergodicity' withan application to parametric roll in longitudinal long crested irregular sea", Elsevier Science Ltd,2005.
- [6] Sarioz, K. and Narli, E. , "Effect of Criteria on Seakeeping Performance Assessment", Elsevier Ireland Ltd, 2004.
- [7] Mynett A E, Keuning J A, "Ocean Wave Data Analysis and Ship Dynamics Dynamics of Marine Vehicles and Structures in Waves" , Elsevier Science Publishers B.V., 1991.
- [8] Lewis, E.V, "Principles of Naval Architecture (III)", SNAME, New Jersey ,1989.
- [9] Jackson H A, "Submarine Design Notes", (Massachusetts Institute of Technology).1982, pp. 520
- [10] Burcher R, Rydill L J, "Concept in submarine design", (The press syndicate of the University of Cambridge., Cambridge university press), 1998, pp. 295.
- [11] A group of authorities, "Submersible vehicle system design", The society of naval architects and marine engineers, 1990.
- [12] Ulrich Gabler, "Submarine Design", Bernard & Graefe Verlag, 2000.
- [13] Y.N.Kormilitsin, O.A.Khalizev, "Theory of Submarine Design", Saint-Petersburg State Maritime Technology University, 2001
- [14] Comstock .E, P.M. Covich , "Seakeeping Performance Design Program", NAVSEC Report 6136-75-2,1975.
- [15] Ramesvar.B et al, "Dynamic Of Marine Vehicles", Ocean Engineering ,A Wiley Series,1978.
- [16] G.J. Grigoropoulos, T.A. Loukakis, A.N. Perakis, "Seakeeping standard series for oblique seas (a synopsis)", Elsevier Science Ltd ,1999.
- [17] Sadık Ozum, Bekir Sener n, Huseyin Yilmaz, "A parametric study on seakeeping assessment of fast ships in conceptual design stage", Elsevier Science Ltd ,2011.
- [18] M.R. Davis , D.S. Holloway, "The influence of hull form on the motions of high speed vessels in head seas", Elsevier Science Ltd ,2003.
- [19] S. Esreban, J. M. Giron, B. Deanderson, J. M. Dela Cruz, "Fast Ships Models for Seakeeping Improvement Studies Using Flaps and T-Foil", Elsevier Science Ltd,2005.
- [20] M.Moonesun, U.M.Korol, V.O.Nikrasov, S.Ardehshiri, D.Tahvildarzade, "Submarine Seakeeping Evaluation", 15th Marine Industries Conference (MIC2013), Kish Island, 2013.
- [21] M.Moonesun, P.Charmdooz, "General arrangement and naval architecture aspects in midget submarines", 4th International Conference on Underwater System Technology Theory and Applications 2012 (USYS'12), Malaysia.
- [22] Chih-Chung Fang, Hoi-Sang, "ChanInvestigation of Seakeeping Characteristics of High-speed Catamarans in Waves", Journal of Marine Science and Technology, Taiwan, Vol. 12, No. 1, pp. 7-15 (2004)

- [23] Cheng-Neng Hwang, Joe- Ming Yang, "Design of Fuzzy Nonlinear Robust Compensator and its Application on Submarines", Journal of Marine Science and Technology, Taiwan, Vol. 11, No. 2, pp. 83-95 (2003)
- [24] V.I. Beena, V. Anantha Subramanian, "Parametric studies on seaworthiness of SWATH ships", Elsevier Science Ltd,2002.
- [25] G.F. Clauss, "Task-related wave groups for seakeeping tests or simulation of design storm waves", Elsevier Science Ltd, 1999.
- [26] Gregory J. Grigoropoulos, Dimitris S. Chalkias, "Hull-form optimization in calm and rough water", Elsevier Science Ltd, 2009.
- [27] Mohammad Moonesun, Yuri Mikhailovich Korol, Sajjad Ardeshiri, Asghar Mahdian4,Ataollah Gharechahi, Davood Tahvildarzade, Alexander Ursalov, Evaluation of Naval Submarine Seakeeping Criteria, Journal of Scientific and Engineering Research, 2015, 2(4):45-54.

Chapter 9: Surfaced Resistance of Submarine

9-1- Wave making system in submarines at surface condition

This chapter is based on references [1,2]. Submarines have two modes of navigation, a surface mode and a submerged mode. The wave-making resistance of a submarine is the net fore-and-aft force upon the body due to the fluid pressure acting normal to all parts of a hull, just as the frictional resistance that is the result of the tangential fluid forces. In the case of a deeply submerged submarine traveling at a constant speed far below the free surface, no waves are formed but the normal pressure varies along the length. In a non-viscous fluid, the net fore-and-aft force due to this variation would be zero. For a submarine that travels on or near the surface, however, the variation in pressure causes waves which change the distribution of pressure over the hull and produce the resultant net fore-and-aft force that is named the wave-making resistance. Wave making resistance should be of such a magnitude that the expended energy for moving the body would be equal to the energy that is necessary to maintain the wave system. The wave making resistance depends in a large measure upon the shapes adopted for the area curve, waterlines and transverse sections. Ship waves are believed to be due to Lord Kelvin idea (1904). He considered a single pressure point traveling in a straight line over the surface of the water, sending out waves. This consists of a system of transverse waves following behind the point, together with a series of divergent waves radiating from the point, the whole pattern being contained within two straight lines starting from the pressure point and making angles of 19 degrees and 28 minutes on each side of the line of motion[3]. The Kelvin wave pattern illustrates and explains many features of the wave system of ship or submarine. Near the bow of a ship or submarine, the most noticeable waves are a series of divergent waves that starts with a large wave at the bow and followed by others arranged on each side along a diagonal line. Between the divergent waves on each side of the body, transverse waves are formed having their crest lines normal to the direction of motion near the hull, bending back as they approach the divergent-system waves and finally coalescing with them. These transverse waves are most easily seen along the middle portion of a ship or submarine with parallel body or just behind a vehicle running at high speed. It is easy to see the general Kelvin pattern in such a bow system. Similar wave systems are formed at the shoulders, if any, and at the stern, with separate divergent and transverse patterns, but these are not always so clearly distinguishable because of the general disturbance already present from the bow system [3]. Since the wave pattern as a whole moves with the ship, the transverse waves are moving in the same direction as the ship at the same

speed V , and might be expected to have the length appropriate to free waves running on the surface at that speed, $L_w = 2\pi V^2/g$.

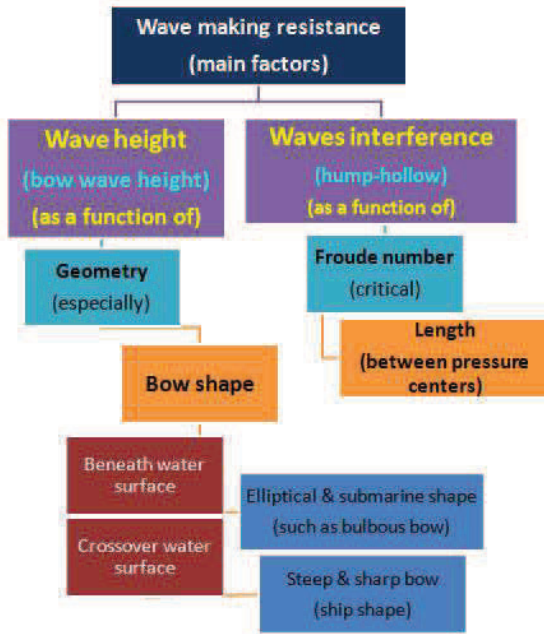


Figure1: Important factors in wave making resistance

Conventional naval submarines are periodically obliged to transit near the surface or, at the surface of water for surveillance and recovery affairs such as: intake fresh air, charge the high pressure air capsules and starting the diesel-generators for recharging the batteries. The process of charging the batteries is the most time-consuming task at near-surface depth or snorkel depth for usually 6 to 10 hours. This time depends on the specification of the electric power system and the battery storage system. Submarines have usually 220 to 440 battery cells that should be charged in the period of snorkeling. Minimizing the resistance of a submarine, moving close to the ocean surface, is very important, because a submarine must save the energy for earlier charging the batteries and lesser need to stay at snorkel depth. For every submersible, the more resistance is equal to the additional power requirement and thus the minor range and lesser duration of operation or endurance. In critical Froude numbers, wave making resistance can make up more than 50%

of the total resistance. Whenever a submarine ascends from the deep depth to the surface of water, the free surface effects cause a steep increase in the resistance because of the appearance of wave making resistance. The wave making system in ships and submarines is different because of differences in the bow shapes and Froude numbers. The rounded or elliptical bow shapes of submarines generate a high bow wave. An ideal bow form for free surface condition is a steep bow, such as ships, but for fully submerged condition without free surface effect, the suitable bow form is an elliptical shape with rounded nose, meanwhile this rounded bow is a very bad design in free surface condition. In surfaced mode of navigation, such as ships, the body interferes with the free surface of water. In surface mode in calm water, the wave making resistance is an important part of resistance that depends on the Froude number. Overall discussions about the wave making system (wave profile and resistance) in ships and surface vehicles are presented in many naval architecture engineering books such as Refs. [3-7]. A good evaluation and formulation have been presented in Ref.[4] for wave making resistance of submarine at surfaced mode. Other scientific materials about wave making in submarines are presented in Refs.[9-19]. Experimental formula for wave-making resistance achieved by submarine at snorkel depth (submerged depth just near the surface) is presented in Ref.[14]. This chapter is intended to evaluate the wave profile induced by submarine at surface condition and deck flooding occurred by the added wave-making due to the bow and the added frictional resistance caused by it.

9-2- A review study about critical Froude number in wave making resistance diagram

9-2-1- Introduction

In wave making resistance diagram, there are some hump and hollow that show the interference effects of the bow and stern waves. The related Froude numbers corresponding to the hollow and hump points are named "critical Froude numbers". As shown in Figure 1, the height of wave is a function of body shape, especially the bow shape, but the location of bow and stern wave is a function of Froude number, especially the value of "length" in Froude formula. Froude Number depends on the speed and length. In scientific references, the length term has different definitions, but it is usually considered as the distance between the pressure centers of the bow and stern. Because of that, the critical Froude numbers are different in ships and submarines. It notes that; $R_T = R_{f0} + R_R = R_f + R_w + R_{vp}$. Resistance coefficient for each component is equal to $C = R / (0.5 \rho A V^2)$. The focus of this chapter is on

finding out the hump and hollow of the wave making diagram and related critical Froude number. Figure 2, shows the total resistance coefficient for a model ship as a result of an experiment in towing tank [3]. The related Froude numbers are visible in Fig.2.

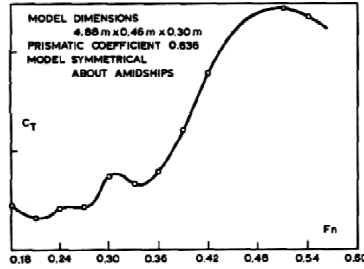


Figure 2: Typical resistance curve for a ship, showing interference effects of waves [1]

According to Ref. [6], the related length is defined as $L=0.9(LBP)$. Based on this assumption, the critical Froude numbers are shown in Figure 3.

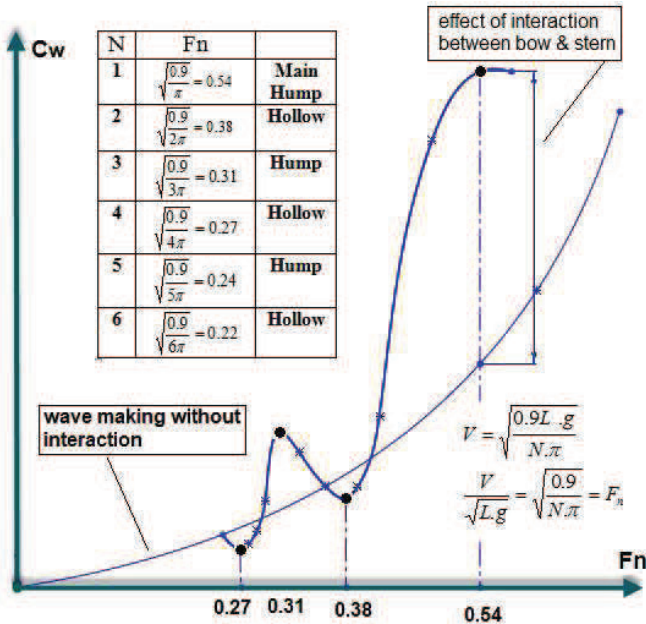


Figure 3: variations of wave resistance coefficient versus Froude number for ships

Regarding the wave making resistance, the first reference was presented in 1982, Ref. [18]. Figure 4 shows the variations of the wave resistance coefficient versus Froude number. In this diagram, two important factors, "L/D" and "depth of immerge" are considered. As shown in Figure 4, it is clear that the critical Froude numbers are the same in different depth of immerge. Moreover, the wave making resistance will decrease as the depth is increased until it disappears.

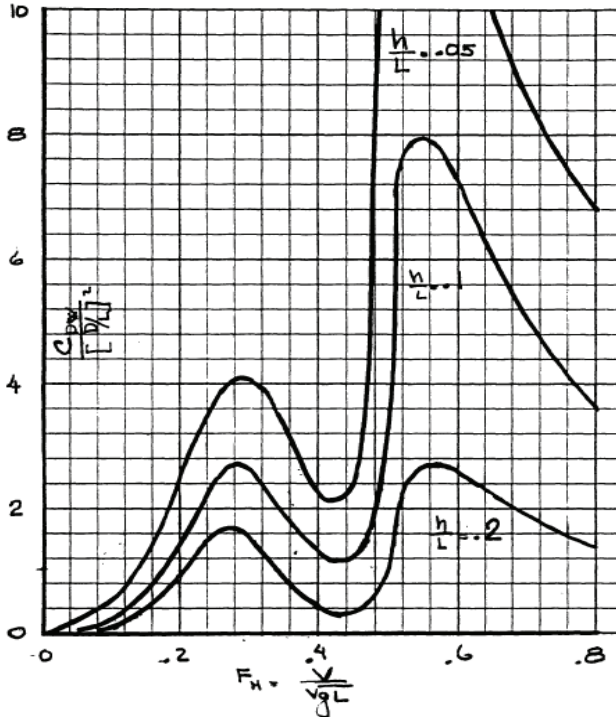


Figure 4: variations of wave resistance coefficient versus Froude number in several depth from sea surface for submarines [16, 18]

Figure 5 shows the wave resistance coefficient for a tear drop shape submarine by Boundary Element Method (BEM) [19]. The related Froude numbers are visible in Figure 5.

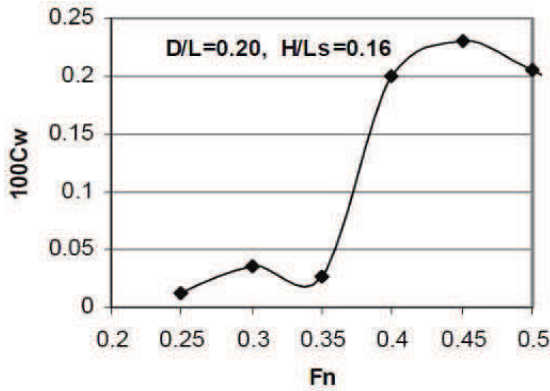


Figure 5: Wave making resistance of a tear drop shape submarine [19]

9-2-2- Range of Froude number in submarines

For estimating the range of the usual Froude number in submarines, statistical values have been collected (Tab.1). The usual range of the Froude number of naval submarines is 0.15~0.25 but for torpedoes and high speed UUVs can be more than 2. Submarine is a low-speed marine vehicle. As written in Tab.1, usually maximum surface speed is approximately 45~60% of maximum submerged speed, and by average of 55%. It means 55% loss speed, due to free surface effect and wave making resistance. On the other hand, the total resistance coefficient of surface condition is more than submerged condition. It can be described so, as the total power of submarine is constant, then: $P_{\text{submerge}}=P_{\text{surface}}=\text{constant}$, and $R = 0.5C_T \rho A V^2$ and $P=k.R.V$ then: $P=K.C_T.V^3$. For comparison between surface and submerged condition, it can be said:

$$C_{T1} \cdot V_1^3 = C_{T2} \cdot V_2^3 \quad (\text{or}) \quad \frac{C_{T2}}{C_{T1}} = \left(\frac{V_1}{V_2}\right)^3$$

If it be supposed that, the surface speed of a submarine be 50% of submerged speed, thus;

$$V_2=0.5V_1, \quad \frac{C_{T2}}{C_{T1}} = (2)^3 = 8$$

It meant that, total resistance coefficient in surface condition is 8 times the total resistance in submerged condition. If we suppose that frictional and form resistance are constant in snorkel depth and surface condition, then the wave

making resistance is seven times of them. It shows the huge effect of wave making resistance.

Table 1: Maximum Froude number in some naval submarines

Submarine Class	L (m)	Submerge speed (V1) (knot)	Surface speed (V2) (knot)	V2/V1 %	Fn
TRIUMPHANT	138	25	20	80	0.28
DELTA	167	24	14	59	0.18
TYPHOON	172	25	12	48	0.15
OSCAR II	144	32	16	50	0.22
COLLINS	78	20	10	50	0.19
DOLPHIN	57	20	11	55	0.24
GOTLAND	67	20	11	55	0.22
KILO	73	17	10	59	0.19
TUPI	67	24	10	42	0.20
VICTORIA	70	20	12	60	0.24
AKULA	110	33	10	30	0.16
U206	49	17	10	56	0.23
U209	64	22.5	11.5	51	0.24
Fateh	45	14	11	79	0.27
Torpedo	8	35	-	-	2.03

9-2-3-Wave making principles in submarine

In ships or submarines, at low speeds, the waves made by the vehicle are very small and the resistance is almost wholly viscous in character. Since the frictional resistance varies with a power of the speed (a bit less than 2), the coefficient of total resistance (C_T), when plotted to a base of Froude number, at first decreases by the increase of speed (Fig.2) and then with the increase in speed, the value of C_T begins to increase more and more rapidly. As Froude number approaches to 0.45, the resistance will vary with the sixth power of the speed (or more). However, this general form of the increase in C_T is usually accompanied by a number of humps and hollows in the resistance curve. As

the speed of the ship increases, the wave pattern will change in order to increase the length of the waves and alter the relative positions of their crests and troughs. In this process, there will be a succession of speeds when the crests of the two systems reinforce one another, separated by other speeds at which crests and troughs tend to cancel one another. The former condition leads to higher wave heights, the latter to lower ones, and as the energy of the systems depends upon the square of the wave heights, this means alternating speeds of higher and lower than average resistance. The humps and hollows in the C_T curve are due to the mentioned interference effects between the wave systems. Obviously, it is a good design practice, whenever possible, to ensure that the vehicle will be running under service conditions at a favorable speed. As will be seen later, the dependency of humps and hollows on Froude number is the subject that accounts for the close relationship between economic speeds and ship lengths [3]. The classification of resistance at the free surface condition is as: $R_T=R_p+R_f=(R_w+R_{VP})+R_f$. When a body travels through a fluid, the pressure field, varies over the body. While a body is moving in a stationary fluid, the waves travel at the same speed as the body. On the other hand, While a vehicle moves in a free surface, a part of dynamic energy will be lost in generating waves. At fully submerged depth, there is not a free surface. Thus, in relation to action and reaction system, the dynamic energy will be utilized for driving ahead. Indeed, the surface wave absorbs a part of energy. Obviously, the pressure fields at surface and submerged conditions are somewhat different. However, in this work, the fully submerged pressure field is considered for explaining the wave system. The wave system around a submarine is approximately according to Tab.2. Wave crest in bow tip and stern tail is expected, and wave trough between them.

Table 2: Wave system around a submarine

Part of bare hull	Location from bow tip (x/L)	Description
Bow tip	0~0.03	Stagnation point-very high pressure
Bow curvature	0.03~0.15	Very low pressure
cylinder	0.15~0.65	moderate pressure
Aft part (stern shoulder)	0.65~0.75	Low pressure
Tail of stern	0.75~1	High pressure

Because of essential differences in the shape of submarines and ships, the pressure field and wave system around the hull is very different. The minor wave height means the better form design and minor resistance. Wave crest at the bow of submarine is higher than the bow wave of a ship because of higher wave height. It means that sharp edge bow is better than elliptical bow in free surface condition. Because of submarines usually have a long conical stern that helps to gradual pressure variation, the amplitude of wave trough in the stern shoulder is less than the ship's one (Fig.6).

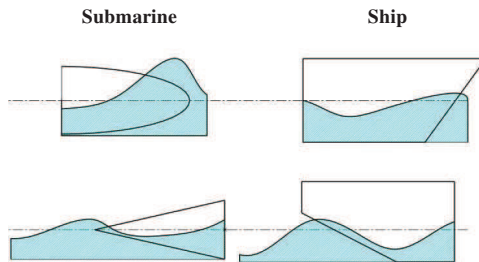


Figure 6: Comparison of wave system in submarines and ships

9-2-4- CFD Method

The base model considered in this work is an axis-symmetric body (similar to torpedo) without any appendages. It is because that the bare hull is only intended to be studied in this study. It helps to model half of the body (in CFD model) and saving the time. Here, one model at the draft of $0.7D$ is analyzed. The specifications of the model are presented in Tab.3 and Fig.7.

Table 3: Main assumptions of models

v (m/s)	Fn	L (m)	D (m)	L/D	S (m^2)
1.4~3.22	0.2~0.46	5	0.6	8.33	7.87

The speeds of the model's motions are so considered that the usual range of Froude numbers in submarines could be covered. Froude numbers less than 0.2 are not studied because, the wave height is so little, that wave making

resistance will be very little and there is not any hump and hollow in wave resistant coefficient diagram.

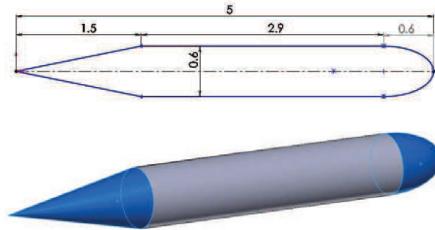
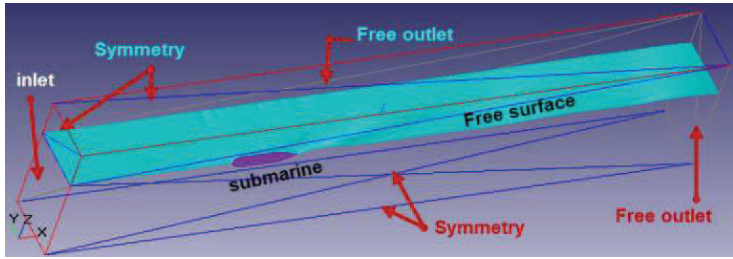
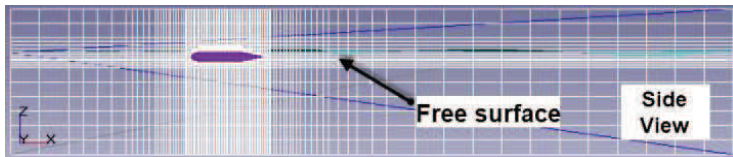


Figure 7: General configuration of the model

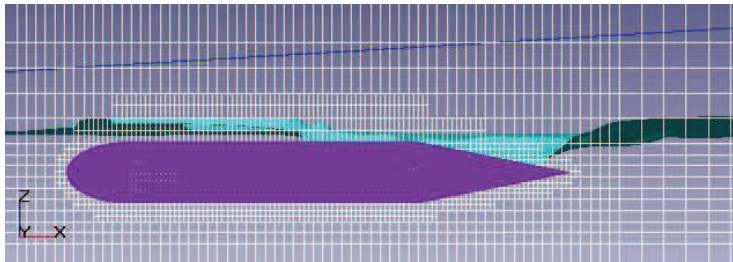
The domain as shown in Fig.8, has inlet (with uniform flow), Free outlet, Symmetry and Wall (for the body of submarine). Dimensions of cubic domain are 50m length (that frontal distance of the model is 12.5 m), 5m beam and 10m height (7m for water depth). Pay attention to that only half of the body is modeled because of axis-symmetric shape and symmetric flow. Therefore, the domain is modeled by half. The base model of analysis is "Free surface" with the method of "Volume of Fluid" and turbulence model is K-Epsilon and minimum y^+ is considered equal to 30. The considered fluid is fresh water at 20 degrees centigrade. Modeling of free surface is shown in Figure 8. The results of analysis are shown in Fig.9. This diagram shows the wave making resistance coefficient in the Froude number range 0.2-0.46. It is because of that the wave making effects in Froude numbers less than 0.2 are negligible, and ultimate value is so considered that can cover the hollow point of diagram. The first hump is happened in Froude number of 0.29, and hollow in Froude number of 0.4. The value of the wave resistance coefficient in the hump is more than two times the value in the hollow.



(a)

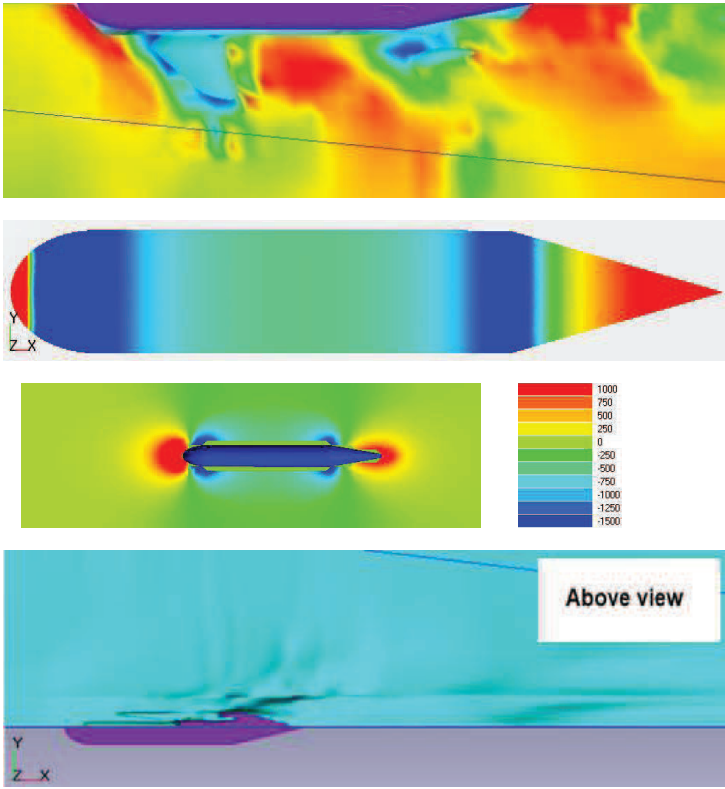


(b)



(c)





(d)

Figure 8: (a) Domain and parts (b) structured grid and tiny cell around free surface (c) Very tiny cells near the wall for boundary layer modeling and keeping y^+ about 30 (d) pressure distribution upon the hull and fluid

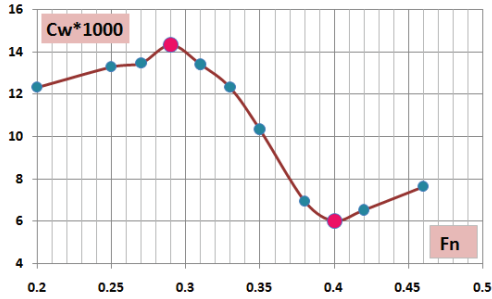


Figure 9: Results of CFD analysis for wave making resistance

9-2-5- Experimental Method

As mentioned before, an experiment was performed for two bow shapes. In this diagram, C_F is earned from ITTC-57 and other parts of resistance are gathered in C_R so as to satisfy equation $C_T = C_F + C_R$. These diagrams are plotted for two different bow shapes.

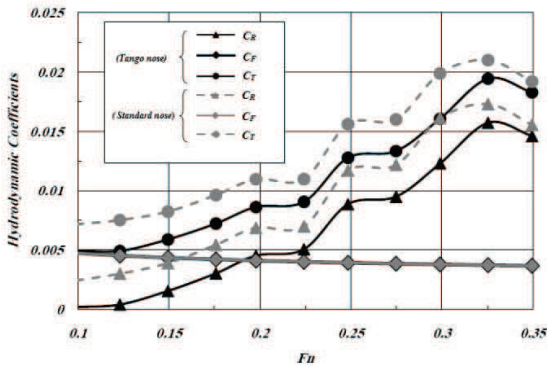


Figure 10: Variations of hydrodynamic coefficients resistance by Froude number

This diagram (Fig.10), shows a steep increase in the residual resistance coefficient in Froude numbers of 0.225 and 0.275, and variation after Froude numbers of 0.2 and 0.25 is approximately horizontal and mild. Therefore, it can be considered, Therefore, Froude numbers of 0.25 and 0.28 can be considered as hump and hollow points, respectively. As mentioned before,

interference of bow wave and stern wave, causes the creation of hump and hollow points in the resistance coefficient diagram of wave making or residual. The effect of bow wave is dominant. According to Figure 11, the location of bow wave in both types of the bow is approximately constant at a given Froude number.

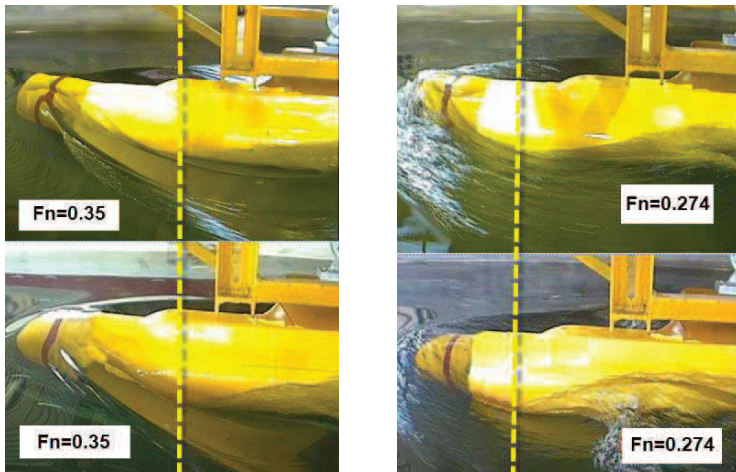


Figure 11: Comparison the center of bow wave in to the different bow shapes

9-2-6- Analytical formula Method

An approximate formula for estimating the wave resistance of submarines is presented in Ref.[15,16]. The length in this formula, is the length overall or maximum length of the hull (LOA). This formula is extracted from the experimental results on several models of submarines at snorkel depth. General shape of the submarine is "tear drop" or "Albacore" shape. The wave making resistance coefficient (C_{DW}), is the result of this formula as below:

$$F_n = \frac{V}{\sqrt{g \cdot LOA}} \quad (1)$$

$$C_{DW} = 561.3F_n^6 - 8812.6F_n^5 + 8148.4F_n^4 - 3454.3F_n^3 + 654.09F_n^2 - 40.235F_n + 0.2726 \quad (2)$$

(3
)

$$C_w = \frac{C_{DW}}{4 \left[\left(\frac{LOA}{D} \right) - 1.3606 \right] \left(\frac{LOA}{D} \right)^2}$$

For example, the diagram is plotted for $L/D=8.33$ in Fig.12 and critical points are marked on them.

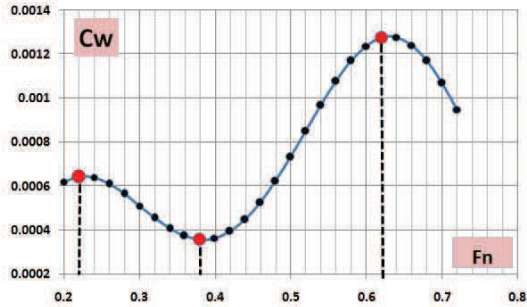


Figure 12: Diagram of wave making resistance in snorkel depth [27,28]

9-2-7- Review 1

This chapter, offered the evaluation of the critical Froude numbers of wave making system of the submarines at surface condition. According to studies conducted in this chapter, based on Figure 13, the results can be summarized as follows:

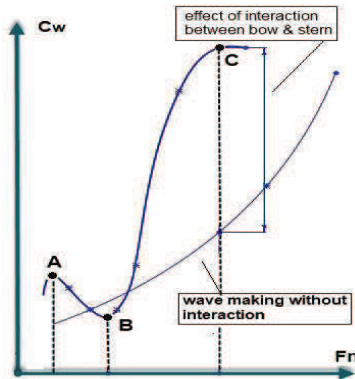
- 1- The usual value of the Froude number of naval submarines is in the range of 0.15 to 0.25.
- 2- The usual value of maximum surface speed is approximately in the range of 45-60% of maximum submerged speed with an average value equal to 55%.
- 3- The ratio of the resistance coefficients in surface and submerged conditions is proportional to the cube of the inversed speeds.
- 4- The form of submarine can affect the wave height, but have little effect upon the wave length.
- 5- The hump and hollow points and the wave length are strongly related to Froude numbers.
- 6- Critical Froude numbers of submarines can be suggested as follows: $(Fn)A=0.23\sim 0.25$, $(Fn)B=0.4$. The Froude number of 0.58 is inaccessible, but, if available, can be a major hump.

7- In the wave resistance diagram, the range of variations at critical points can be stated as:

$$\frac{(C_w)_B}{(C_w)_A} = 1.5 \sim 2.5 \quad , \quad \frac{(C_w)_C}{(C_w)_B} = 4 \sim 12.$$

8- In submarines, because the maximum Froude number is usually less than 0.25, then, for Froude numbers less than 0.2, the variations of the wave resistance coefficient versus Froude number can be estimated by a simple linear interpolation between the points (0, 0) and A. The error of this method can be less than 10%.

9- At critical Froude numbers of A, B and C, the general form of the interference between bow and stern wave systems is represented in Figure 14.



0.23~0.25	0.41~0.42	0.56~0.58	According to Ref.[30]	Submarine
0.22	0.38	0.62~0.64	According to formula of Ref.[27,28]	
0.3	0.34	0.46	According to Ref.[31]	
0.28	0.4	--	According to CFD	
0.25	0.28	--	According to model test	
0.31	0.34	0.51	According to Ref.[1]	Ship
0.31	0.38	0.53	According to Ref.[21]	
0.27	0.31	0.54	According to Ref.[22] Based on 0.9LBP	
0.25	0.29	0.51	According to Ref.[22] Based on LBP	
0.23~0.25	0.4	0.58	Expected for submarine	

Figure 13: Estimation of critical Froude number in submarine

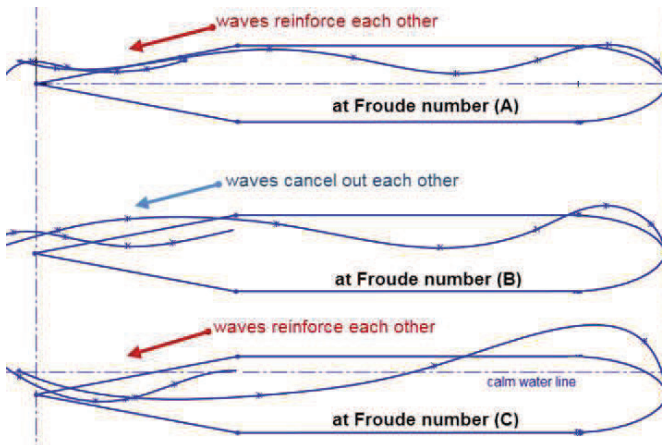


Figure 14: General form of interference of bow and stern waves in critical Froude numbers of A, B, C

9-3- Added Resistance of Submarine due to Deck Wetness at Surface Condition

9-3-1-Freeboard and reserve of buoyancy in submarines

One of the main reasons of deck wetness and bow flooding in submarines is low values of ROB (Reserve of Buoyancy) and as a result, low freeboard height. As mentioned in Refs.[8-11], the common values of ROB in submarines, according to the volume of Main Ballast Tanks (MBT), is

between 10 and 15%. These values of ROB resulted in an approximately freeboard between $0.1D$ and $0.17D$ as shown in Fig.1. It means a very low freeboard which can be flooded easily by bow wave making system. As shown in Fig.1, the pressure hull is watertight while space between the pressure hull and deck does not have this characteristic and has several flooding holes. Based on this fact, this space is named "free-flooding space". Since the deck is not watertight, the freeboard height is the distance from waterline to the top of the pressure hull. Usually, the height of the deck is considered so small that produce minimum resistance in submerged navigation mode. The whole bow part becomes wetted and flooded too. When deck wetness happens, a large amount of water can enter the free flooded spaces. It causes the added resistance due to the added wetted surface. Weight variation is very significant for submarine from floating and stability point of view. Apart from that, the dynamic properties of submarine are important too.

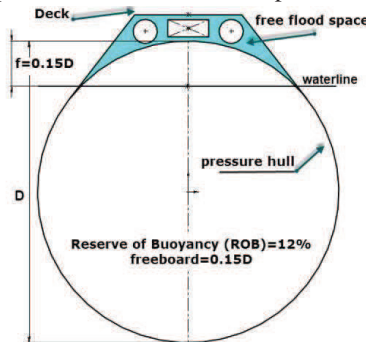


Figure 15: Free board, deck and free flooding space in submarine

9-3-2- Assumptions for the Model of CFD analysis

The base models that considered here, is an axis-symmetric body similar to torpedo, without any appendages because in this study, only bare hull, wants to be studied. It helps to half CFD modeling of the body and saving the time. Here, one model at two drafts is considered. The specifications of the model are presented in Tab.4 and Fig.16.

Table 4: Main assumptions of models

Model	V (m/s)	Fn	L (m)	D (m)	L/D	S (m ²)
A	1.4~7	0.2~1	5	0.6	8.33	7.87

The speed of models is considered so that the usual range of Froude numbers in submarines could be covered. Froude numbers less than 0.2 are not studied here. It is for this reason that the wave height would be too small so that the deck wetness does not occur and wave making resistance adopts a very low value.

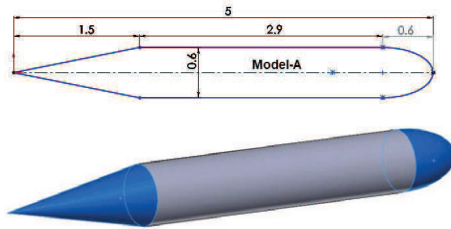


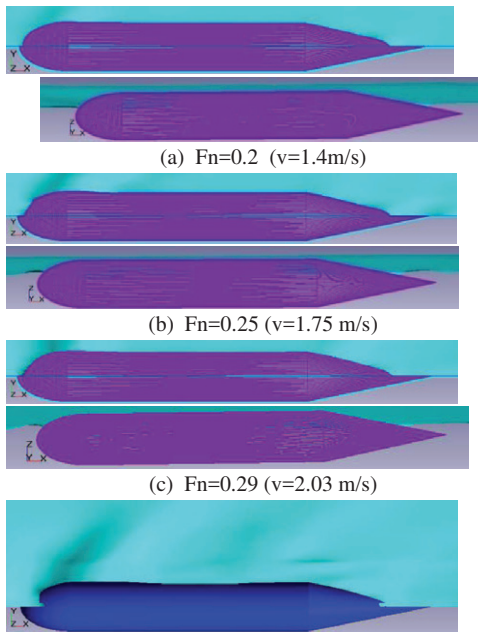
Figure 16: General configuration of the model

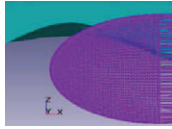
Two different drafts are considered; $h=0$ and $0.1m$. At draft $h=0$, the hull axis is located on the free surface level. This situation is equal to $ROB=50\%$, that is not according to the real demand of submarines. This case is considered only for evaluation of the extremes of the deck wetness. The draft of $0.1m$ is equivalent to $ROB=12\%$ that is related to the real naval submarines. This situation is consistent with the fact.

9-3-3- CFD Results at $h=0$

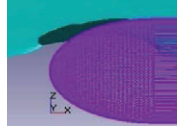
In this study, the model is analyzed in several Froude numbers of $0.2\sim 1$ at the draft $h=0$. In this draft, only half of the body is submerged. For evaluating the added resistance due to deck and bow wetness, and comparing the results, the model is analyzed in fully submerged condition without free surface effects.

Because of symmetry in the model and flow direction, only a quarter of submarine and domain is modeled. The results of bow wave profile at each Froude number are shown in Fig.17. Then, one-quarter of this resistance is compared to the resistance in free surface condition. It is for this reason that, at free surface condition only half of the body is being modeled and in this modeling only half of the model is submerged. It means that in the free surface condition, only a quarter part of the body is the wetted part. Frictional resistance is proportional to the wetted area. This portion of the draft is unusual in submarines, but here, it is considered for studying the frictional resistance. According to Fig.17-a,b, the bow wave appears at Froude numbers above 0.2. By increasing the Froude number (Fn), bow is partially flooded (Fig.17-c-d) until a value of Fn 0.35 is reached. At this value, the bow is completely flooded (Fig.17-e). At Froude number of 0.5, deck wetness is complete.

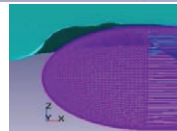




(d) $Fn=0.33$ ($v=2.31$ m/s)



(e) $Fn=0.35$ ($v=2.45$ m/s)

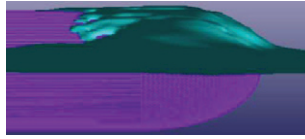


(f) $Fn=0.38$ ($v=2.66$ m/s)

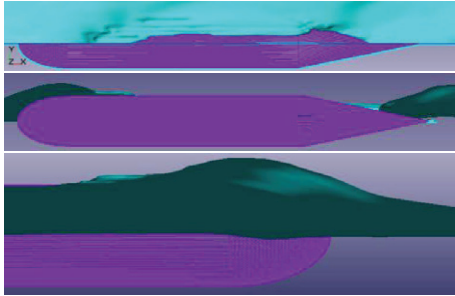


(g) $Fn=0.42$ ($v=2.94$ m/s)





(h) $Fn=0.46$ ($v=3.22$ m/s)



(i) $Fn=0.5$ ($v=3.5$ m/s)

Figure 17: Up view and side view of free surface at $h=0m$

Added resistance due to deck wetness is presented in Tab.5. This table shows the considered Froude number, related velocity, a quarter of the resistance in submerged mode (without free surface effects) and half of the resistance in free surface condition. The last column in tab. 5 is “difference”. This term is the difference in the frictional resistance between fully submerged mode and free surface condition and is defined as:

$$\begin{aligned}
 \text{Added frictional resistance (\%)} &= \frac{\left(\begin{array}{l} \text{half of frictional resistance in free surface} \\ - \text{quarter of frictional resistance in submerged} \end{array} \right)}{\text{quarter of frictional resistance in fully submerged}} \\
 &= \frac{\frac{1}{2} R_{f2} - \frac{1}{4} R_{f1}}{\frac{1}{4} R_{f1}} \times 100
 \end{aligned}$$

Table 5: Added frictional resistance due to deck wetness

Test condition		Fully Submerged (1)		Free Surface (2)		Difference (%)
		1/4 Rt	1/4 Rf	1/2 Rt	1/2 Rf	
Fn	V (m/s)					
0.2	1.4	10	6	21	6	0.0
0.25	1.75	15.3	9	37.2	9.2	2.2
0.27	1.89	18	11	49.4	11.4	3.6
0.29	2.03	20.4	12	65	13	8.3
0.31	2.17	23.1	13.6	86	14	2.9
0.33	2.31	26	15.1	103	17	12.6
0.35	2.45	29	16.9	120	21	24.3
0.38	2.66	34.5	19.7	165	24	21.8
0.4	2.8	37.7	21.7	115	26	19.8
0.42	2.94	41.3	23.6	125	30	27.1
0.46	3.22	49	28	186	36	28.6
0.5	3.5	57.5	32.5	203	34	4.6
0.54	3.78	66.5	37.5	235	40	6.7
0.57	3.99	74	41.5	267	44	6.0
0.6	4.2	81.7	45.7	250	47	2.8
0.65	4.55	95.2	53.2	290	59	10.9
0.71	5	114	64	305	73	14.1
0.8	5.6	141.8	78.3	403	85	8.6
0.9	6.3	178	97	519	99	2.1
1	7	218	118	581	124	5.1

As shown in Tab.5, the frictional resistance is increased in all speeds from 0 to 30 percent (approximately). In Froude number of 0.2, the added resistance is almost equal to zero because the bow and deck flooding is not happening. The increase in the added frictional resistance is not regular because of variation in wave profile in different Froude numbers. Again, it needs to be mentioned that the model is fixed and there is no change in the draft. It can affect the results in real floating condition and causes more resistance. Pressure resistance represents the resistance without viscosity. In free surface condition, the pressure resistance is equal to the summation of the wave resistance and the form resistance. Nevertheless, there is no wave resistance in fully submerged condition. Therefore, the pressure resistance is equal to the form resistance. The amount of the total, pressure and frictional resistance are shown in Fig.18 for fully submerged condition. It shows that total resistance includes 55% for frictional and 45% for pressure resistance.

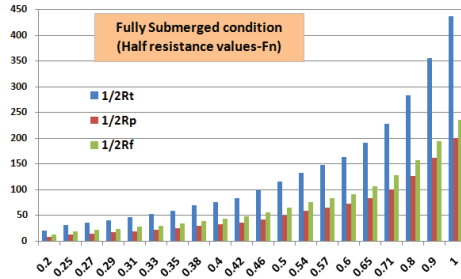


Figure 18: Resistance versus Froude numbers in fully submerged condition

The amount of the total, pressure and frictional resistance are shown in Fig.19 for free surface condition. It shows that the quota of frictional and pressure resistance depends on the Froude number. However, compared to the submerged condition, the frictional resistance in most of the speeds has been decreased, because of the bow and deck wetness.

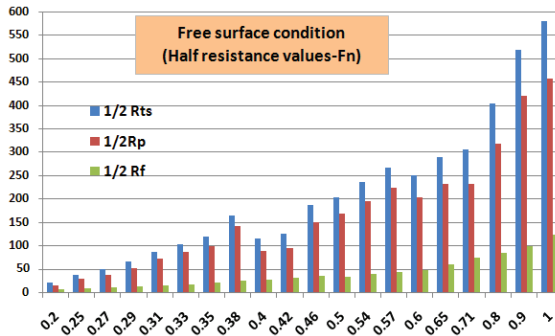


Figure 19: Resistance versus Froude numbers in free surface condition

9-3-4- CFD results at h=0.1m

In this part, the model is analysed in several Froude numbers of 0.2~0.27 at the draft h=0.1. This draft is in the range of real submarine draft and ROB. The results of bow wave profile at each Froude number are shown in Fig.20. This figure shows that at Froude number 0.2, the wave profile is visible. At Froude number of 0.27, the most part of the deck is flooded and fully deck wetness is happened.

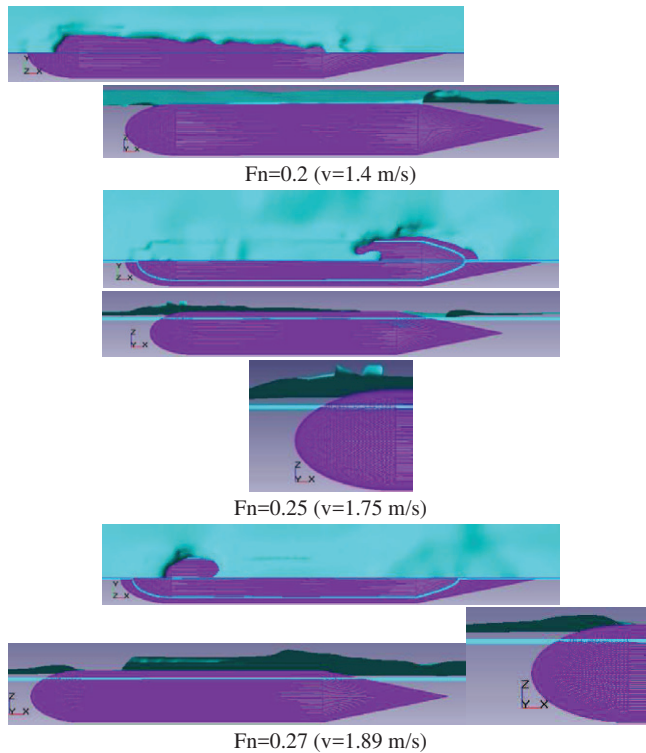


Figure 20: Up view and side view of free surface at $h=0.1m$

9-3-5- Review 2

This chapter studied the bow wave profile and deck wetness of submarines by CFD method. The bow wave and deck wetness depends on three main parameters: 1- draft 2- Speed (or the corresponding Froude number) 3-bow shape. In CFD modeling, two drafts ($h=0$ and $0.1m$) were modeled. For defining the draft, usual reserve of buoyancy (ROB) in submarines should be regarded. Common ROB in submarines is between 10 and 15 percent, according to the volume of Main Ballast Tanks (MBT). This ROB results in a freeboard that is approximately equal to $0.1D\sim 0.17D$. By increasing the speed and Froude number, the height of bow wave increases. The usual Froude number in naval submarines is in the range of $0.15\sim 0.25$. Usually, the maximum surface speed is approximately 45~60% of the maximum

submerged speed, and by an average of 55%. It means 55% speed loss, due to free surface effect and wave making resistance. At the draft $h=0$, the bow wave appears at Froude number above 0.2. By increasing the Froude number, bow is partially flooded until a value of Froude number 0.35 is reached. At this value, the bow is completely flooded. In Froude number of 0.5, deck wetness is occurred completely. At draft of 0.1m, at Froude number 0.2, wave profile is sensible. At Froude number 0.27, the most part of the deck is flooded, and fully deck wetness is happened.

Nomenclature

CFD	Computational Fluid Dynamics
C_T	Total resistance coefficient
C_{T1}	Total resistance coefficient (submerge)
C_{T2}	Total resistance coefficient (surface)
D	maximum diameter of the outer hull (m)
EFD	Experimental Fluid Dynamics
Fn	Froude number- $Fn = v/\sqrt{g.L}$
h	Submergence depth (m)
H*	non-dimensional depth
IHSS	Iranian Hydrodynamic Series of Submarines
L	overall length of hull (m)
LOA	Length overall or maximum length (m)
R	maximum radius of the outer hull (m)
Rt	Total resistance (N)
Rf	Frictional resistance (N)
R_{f0}	Flat plate frictional resistance (N)
Rp	Pressure resistance (N)
Rvp	Viscous resistance (N)
Rw	Wave resistance (N)
ROB	Reserve of Buoyancy (%)
	$ROB = \frac{\text{surface displacement}}{\text{submerge displacement}} * 100$
S	Wetted surface area (m ²)
v	Speed of submarine (m/s)
V1	Maximum submerged Speed (m/s)
V2	Maximum surfaced Speed (m/s)

References

- [1] Mohammad Moonesun, Yuri Mikhailovich Korol, Hosein Dalayeli, Mehran Javadi, Seyyed Hosein Moosavizadegan , Anna Brazhko, Wave making system in submarines at surface condition, Indian Journal of Geo-Marine Sciences, Vol. 45(1), January 2016, pp. 44-53.
- [2] Mohammad Moonesun, Mehran Javadi, S.H.Mousavizadegan, Hosein Dalayeli, Yuri Mikhailovich Korol, A.Gharachahi, Computational Fluid Dynamics Analysis on the Added Resistance of Submarine due to Deck Wetness at Surface Condition, Journal of Engineering for the Maritime Environment (Ins. Mechanical Engineering-Part M, SAGE), February 2016, pp.1-9.
- [3] Edward.V. Lewis, Principles of Naval Architecture, Vol.II; Resistance Propulsion and Vibration, The Society of Naval Architects and Marine Engineers, USA, 1988.
- [4] V.Bertram, Practical Ship Hydrodynamics, Butterworth-Heinemann Linacre House, Oxford OX2 8DP, page 65, 2000.
- [5] A.F.Molland, S.R.Turnock, D.A.Hudson, Ship Resistance and Propulsion, Cambridge University Press, page 14, 2011.
- [6] K.J.Rawson, E.C.Tupper, Basic Ship Theory-vol.2, Oxford OXD 8D2, page 685, 2001.
- [7] S.F.Hoerner, Fluid Dynamic Drag, USA, 1965.
- [8] Burcher R, Rydill L J, Concept in submarine design, The press syndicate of the University of Cambridge., Cambridge university press, pp. 295,1998.
- [9] Yuri.N.Kormilitsin, Oleg.A.Khalizev, Theory of Submarine Design, Saint Petersburg State Maritime Technical University, Russia, pp.185-221, 2001.
- [10] Ulrich Gabler, Submarine Design, Bernard & Graefe Verlag, 2000.
- [11] A group of authorities, Submersible vehicle system design, The society of naval architects and marine engineers, 1990.
- [12] Mehran.Javadi, M.D.Manshadi, S. Kheradmand, Mohammad Moonesun, Experimental investigation of the effect of nose profiles on resistance of a submarine in free surface motion, Journal of Marine Science and Application,2014.
- [13] Bao-ji Zhang, Shape optimization of bow bulbs with minimum wave-making resistance based on Rankine source method, Journal of Shanghai Jiaotong University, 17(1), 65-69, 2012.
- [14] Alvarez A, Bertram V, Gualdesi V, Hull hydrodynamic optimization of autonomous underwater vehicles operating at snorkeling depth. Jordan Journal of Ocean Engineering, 36(1), 105–112, 2009.
- [15] Desta Alemayehu, et al, Design Report Guided Missile Submarine SSG(X), Virginia Tech, page 75, 2006.
- [16] Grant.B.Thomton, A design tool for the evaluation of atmosphere independent propulsion in submarines, page 205, 1994.
- [17] O.F.Sukas, O.K.Kinaci, Sakir Bal, Computation of total resistance of ships and a submarine by a RANSE based CFD,2009.
- [18] H.A. Jackson, Submarine Design Notes, Massachusetts Institute of Technology,1982
- [19] H.Ghasemi, H.Shahifar, Computations of Wave - Making Drag for Underwater Vehicle, International Journal of Maritime Technology, 4 (6), pp:39-48, Iran, 2007 (published in Persian),
"http://www.ijmt.ir/browse.php?a_id=39&slc_lang=en&sid=1&ftxt=1 " .

Chapter 10:

Fully Submerged Depth for eliminating wave making resistance

10-1- Introduction

Submarines have two modes of navigation: surfaced mode and submerged mode. Conventional naval submarines are periodically obliged to transit near the surface of water for surveillance and recovery affairs such as: intake fresh air, charge the high pressure air capsules and start the diesel-generators for recharging the batteries. The process of charging the battery is the most time-consuming task at near surface depth or snorkel depth for usually 6~10 hours that depends on the specifications of electric power system and battery storage. Submarines have usually 220~440 battery cell that should be charged in the period of snorkeling. Minimizing the resistance of a submarine, transiting close to the ocean surface, is very important, because a submarine must save the energy for earlier charging the batteries and lesser need to stay at snorkel depth. If the submarine, waste a lot of energy for propulsion, it needs to stay more and more in snorkel depth. It is a very dangerous situation for a submarine because of the increase in the probability of detection. Common relative dimensions of sailing and mast, and depth in snorkel condition for real naval submarines are shown in Fig.1.

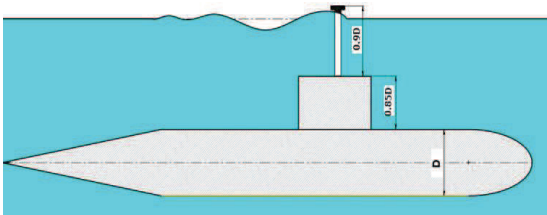


Figure 1: Relative snorkel depth in naval submarines

Some torpedoes are obliged to approach the free surface too. It depends on the operational demands and the type of torpedo, for example, cruising just beneath the sea surface for receiving the target information by radio electronic devices or satellite. In this condition, the submergence depth of torpedo should

be less than 2-3 meters equal to maximum permeability depth of electromagnetic wave into the water. For every submersible, the further resistance equals to the further power requirement and thus, lesser range and lesser duration of operation or endurance. In contrast to a surface vessel, a deeply submerged submarine, doesn't encounter the penalty of wave making resistance. Wave making resistance, in critical Froude numbers, can make up more than 50% of total resistance. When a submarine ascends from the deep depth to the near the surface of water, the free surface effects, causes a steep increase in the resistance because of appearance of wave making resistance. In surfaced mode of navigation, such as ships, the body interferes with free surface of water. In surface mode in calm water, the wave making resistance is a main part of resistance that depends on the Froude number. For a submarine at the deep depth of the water, there is not wave resistance because there is not a free surface. This depth is named "fully submerged depth". In every depth between surface mode and fully submerged mode, the movement of a submarine or torpedo, causes turbulence on the surface of water. This effect decreases by increasing the depth of submergence but there is a certain depth, which free surface effect and wave resistance is very little and ignorable. In all depths more than this depth, there is fully submerged condition. This chapter tries to define this "fully submerged depth". This depth is depended on the dimensions of a submarine. The fully submerged depth, in Refs.[1,2], is defined as a multiple of the outer diameter of submarine hull (D) but in Ref.[3], is defined as a multiple of the length of the submarine hull (L). Fully submerged condition in reference [3] is defined as half of submarine length ($h=L/2$) and in reference [1] is defined as $3D$ ($h=3D$) and in reference [9], this depth is suggested $5D$ ($h=5D$). In Refs.[11,12], M.Moonesun *et al* showed that, according to experimental tests in towing tank for short values of L/D for submarines, the depth, $h=5D$ can be a good suggestion but this depth can be lesser. Now, this chapter has concentrated the studies, to find out this depth for high values of L/D and short values of L/D , by CFD method. There are few published scientific articles about the hydrodynamic effects on a submerged body near a free surface, such as dynamics and maneuvering effects by K.Rhee, J.Choi, S.Lee [5], C.Polish, D.Ranmuthugala, J.Duffy, M.Renilson [6] and D.Neulist [7]. Resistance and wave making effects near the free surface are studied by E.Dawson, B.Anderson, S.V.Steel, M.Renilson, D.Ranmuthugala [8], S.Wilson-Haffenden [9] and S.V.Steel [10] which all of

them conducted by Australian Maritime Collage. For investigating the wave making resistance of a submarine below the free surface, before this book, Refs.[9,10] have been the main published articles which both are based on the DARPA SUBOFF submarine model in low Froude numbers. For these analyses, the base method is Experimental Fluid Dynamics (EFD) but to some extent, is reviewed by Computational Fluid Dynamics (CFD). This chapter wants to extend the studies about resistance of submersibles which travel near the free surface of calm water in low and high Froude numbers [11].

10-2- Main factors in near surface resistance

As a hydrodynamic point of view, for the resistance of a submerged body traveling close to the free surface of water, three parameters are important: 1) non-dimensional depth (H^*), that can be defined as: depth from the free surface to the top of axis-symmetric hull (h) divided on the diameter of hull (D), or by the other definition, " h " divided on the body length(L). 2) Froude number ($Fn = v/\sqrt{g \cdot L}$), as will be discussed. 3) The length on diameter ratio (L/D) of submarine because for very long bodies by L/D more than 15, length is a dominant parameter so non-dimensional depth (H^*) should be defined as a function of length(L). In this chapter, the usual values of L/D for naval submarines and torpedoes are considered as mentioned in Ref.[12], that is usually less than 15. Figure 2 shows the resistance coefficient (C_D) which decreases by increasing submergence depth because by increasing the depth, the wave making resistance, decreases.

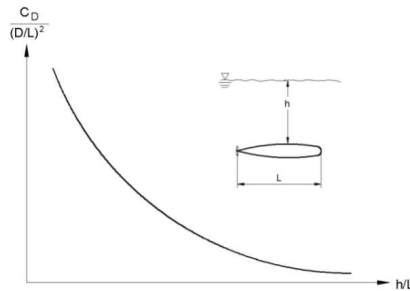


Figure 2: General variations of total Resistance coefficient versus submergence depth

It is obvious in Fig.5, that C_w , decreases by increasing the depth.

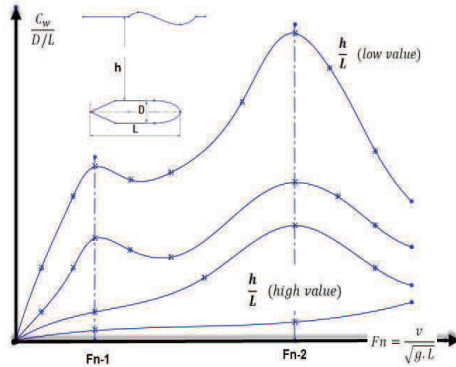


Figure 3: General variations of wave making resistance coefficient versus Froude number and depth of submergence

10-3- Assumptions for the Models

The base models that considered here, is an axis-symmetric body similar to torpedo, without any appendages because in this study, only bare hull, wants to be studied. It helps to quarterly CFD modeling of the body and saving the time. These are two models, with different values of L/D : 1)Model A: with normal value in submarines with $L/D=8.33$, $L=5\text{m}$ and $D=0.6\text{m}$. 2)Model B: as a long vehicle with $L/D=20$, $L=4\text{m}$ and $D=0.2\text{m}$. The specifications of two models are presented in Tab.1 and Fig.4.

Table 1: Main assumptions of models

Model	v (m/s)	Fn	L (m)	D (m)	L/D	S (m ²)
A	5	0.71	5	0.6	8	7.87
B	5	0.8	4	0.2	20	2.17

The speeds of models are constant and equal to 5 m/s but are so selected that the values of Froude number be more than the range of hump and hollow, i.e. more than 0.7.

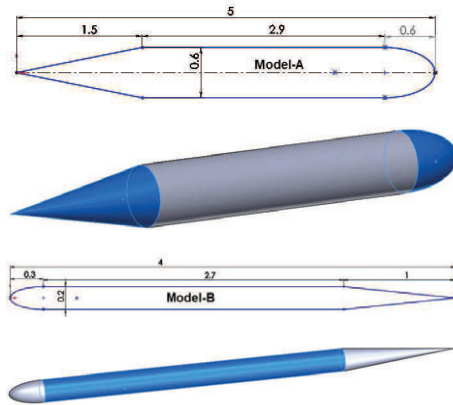


Figure 4: General configuration of the models

Each Model is evaluated in several depths as Table 2. H^* is defined as:

$$H^* = \frac{\text{submergence depth (h)}}{D} \quad (9)$$

The parameter "h", is the depth from the free surface to the top of the hull, as showed in Fig.3.

Table 2: Simulation depth of Models

Model-A		Model-B	
h		h	
0	0	0	0
0.5D	0.3	0.25D	0.05
D	0.6	0.6D	0.12
1.5D	0.9	1D	0.2
2.8D	1.7	1.5D	0.3
3.5D	2.1	2.5D	0.5
4.5D	2.7	3.5D	0.7
6.5D	3.9	4.5D	0.9
infinite	Without free surface	6.5D	1.3
		20D=L	4
		infinite	Without free surface

The domain as shown in Fig.5, has inlet (with uniform flow), Free outlet, Symmetry (in the four faces of the box) and Wall (for the body of submarine). Dimensions of cubic domain are constant for Model-A and B with 50m length (that frontal distance of the model is 12.5 m), 6m beam and 10m height (7m

for water depth and 3m for air). Pay attention to that only half of the body is modeled because of axis-symmetric shape, and the domain is for that. Meanwhile, the study has shown that the beam and height more than 10D in this study can be acceptable. The base model of analysis is "Free surface" with the method of "Volume of Fluid" and turbulence model is K-Epsilon and minimum y^+ is considered equal to 30. The considered fluid is fresh water in 20 degrees of centigrade and constant velocity of 5 m/s. Free surface modeling is shown in Fig.5.

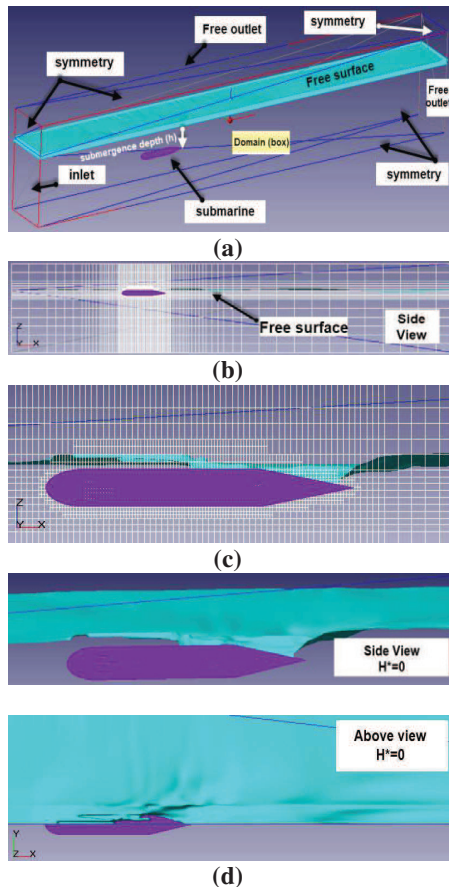


Figure 5: (a) Domain and structured grid (b) tiny cell around free surface (c) Very tiny cells near the wall for boundary layer modeling and keeping y^+ about 30 (d) Half

modeling because of axis-symmetry and free surface variations

10-4- CFD Results and Analysis

The modeling of these two models is represented:

Model-A) The geometrical specification of this model is presented in Tab.1. Total resistance in each depth is shown. Viscous resistance is constant at all depths because it is depended on the viscosity, velocity, form and wetted area which all of them are constant at all depths. By increasing the depth, total resistance, decreases until the fully submerged depth, that the free surface effect eliminates and total resistance, remains constant. To ensure that fully submerged condition is provided, a modeling without free surface is performed in Flow Vision, which can simulate the infinite depth modeling. Last row in Tab.3 shows the deeply submerged resistance that contains only viscous resistance. This value is constant at all depths, and only wave resistance, varies in every depth. As mentioned before:

Wave resistance= Total resistance - Viscous resistance.

Table 3: Resistance of Model-A in several depths

Depth	Rt (N)	Rv (N)	Rw (N)	Rr/Rt (%)
0	906	410	496	54.7
0.5D	864	410	454	52.5
D	500	410	90	18.0
1.5D	450	410	40	8.9
2.8D	434	410	24	5.5
3.5D	426	410	16	3.8
4.5D	410	410	0	0.0
6.5D	410	410	0	0.0
infinite	410	410	0	0.0

Diagrams of Fig.6, shows the values of the total, viscous and wave resistance in all depths. It is obvious that total resistance and wave resistance in $H^*=0$, are the largest values. By increasing the depth, wave resistance decreases and because of that, total resistance decreases. After a certain depth, wave resistance, eliminates completely and after this depth, total resistance remains constant. It is "fully submerged depth".

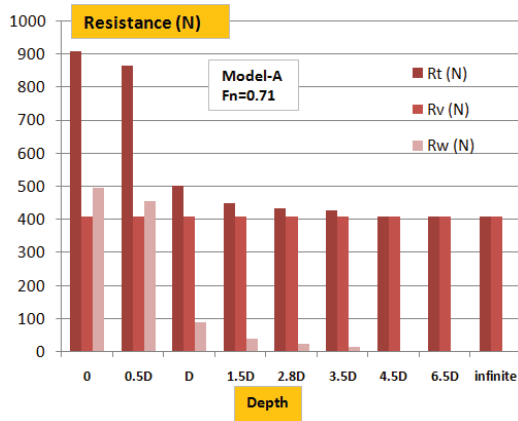


Figure 6: Diagrams of each part of resistance for Model-A

The variations of total resistance versus depth for Model-A, in Fig.7, shows that fully submerged depth is happened in $H^*=4.5$ or $h=4.5D$. A sharp decline in resistance is happened from just near surface ($H^*=0$) to the $H^*=1$ which wave resistance decreases by 80%. It is "Milestone depth". Milestone depth in Model-A is at $H^*=1$ or $h=D$ or $h=0.12L$.

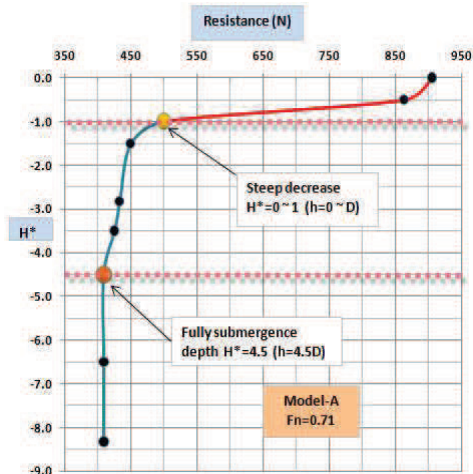


Figure 7: Variations of total resistance versus depth in Model-A

Model-B) This model is a long model with high values of L/D. The geometrical specification of this model is presented in Tab.1. By increasing the depth, total resistance, decreases until the fully submerged depth. To ensure that fully submerged condition is provided, a modeling without free surface is performed in Flow Vision and is shown in the last row in Tab.4.

Table 4: Resistance of Model-B in several depths

Depth	Rt (N)	Rv (N)	Rw (N)	Rr/Rt (%)
0	240	102	138	57.5
0.25D	218	102	116	53.2
0.6D	210	102	108	51.4
1D	182	102	80	44.0
1.5D	134	102	32	23.9
2.5D	110	102	8	7.3
3.5D	106	102	4	3.8
4.5D	102	102	0	0
6.5D	102	102	0	0
20D=L	102	102	0	0
infinite	102	102	0	0

As mentioned before, diagrams of Fig.8, shows the values of the total, viscous and wave resistance in all depths. Total resistance and wave resistance in $H^*=0$, are the largest values. By increasing the depth, wave resistance decreases.

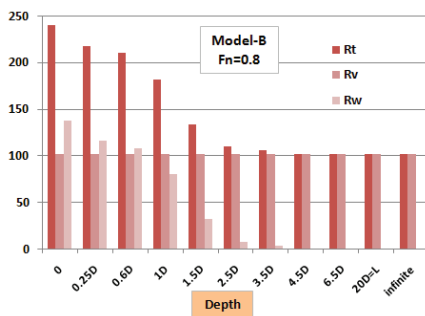


Figure 8: Diagrams of each part of resistance for Model-B

The variations of total resistance versus depth for Model-B, in Fig.9, shows that fully submerged depth is happened in $H^*=4.5$ or $h=4.5D$. A sharp decline in resistance (Milestone depth) is happened at $H^*=2.5$ which wave resistance

decreases by 95%. Milestone depth in Model-B is at $H^*=2.5$ or $h=2.5D$ or $h=0.125L$.

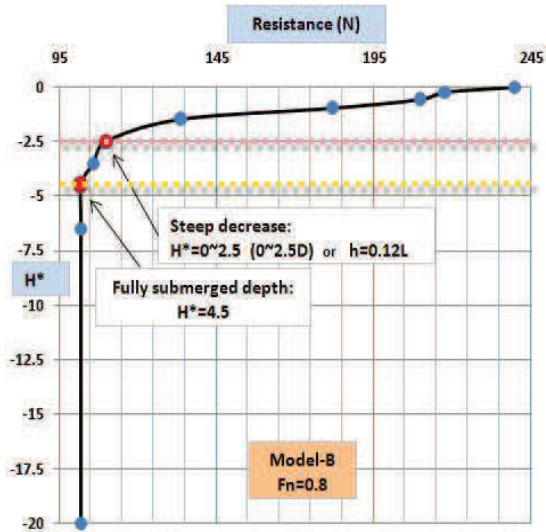


Figure 9: Variations of total resistance versus depth in Model-B

In comparison to the results of Model- A and B these can be derived that: 1) Model-A has a normal value of L/D but Model-B is a long vehicle with large values of L/D . 2) Froude numbers of Models A and B are 0.71 and 0.8 respectively that show high Froude number condition of modeling. Froude numbers in Refs.[16-18] is in the range of 0.13~0.66 that meant low Froude numbers in the range of the hump and hollow of the wave resistance diagram. 3) Fully submerged depth for both models are equal to $4.5D$ for high Froude numbers. It is independent from the L/D value of the model. This value in Refs.[8-10] for low Froude number is earned equal to $2.8D$ (or $3.3D$ from the free surface to the centre line of the body). 4) Milestone depth for both models is obtained equal to $0.125L$. It seems that "Milestone depth" can't be stated as a function of " D ", but as a function of " L " because this value is dependent on the L/D ratio. For long vehicles, it happens later. For model-A equal to $1D$ and for model-B equal to $2.5D$ but the criterion of $0.125L$ can be used for all values of L/D .

10-5- Review

General result of this chapter is graphically shown in Fig.10 and for high Froude numbers (more than 0.7) such as torpedoes and high speed submarines, these can be stated as:

- 1) Flow Vision software can be used for free surface modeling.
- 2) In submergence depth, there are two important depths: "Milestone depth" that wave resistance decreases more than 80% and "Fully submerged depth" that wave resistance is eliminated completely.
- 3) First advice for submarines and torpedoes is moving in the depth more than fully submerged depth, or at least, in the depth between milestone depth and fully submerged depth. Generally, the more depth is equal to less resistance.
- 4) The ratio of L/D is important in the statement of Milestone depth but is not an essential parameter.
- 5) Froude number is an important parameter for the evaluation of submergence depth. The characteristics are different for ordinary values ($Fn < 0.5$) and high values ($Fn > 0.7$).
- 6) Fully submerged depth for high Froude numbers equals to $4.5D$.
- 7) Milestone depth for high Froude numbers is equal to $0.125L$.

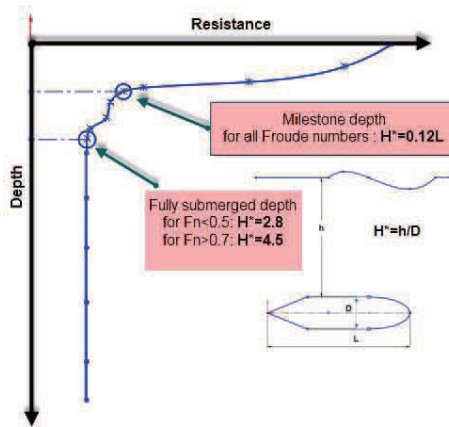


Figure 10: Milestone and Fully submergence depth in high and low Froude numbers

Nomenclature

C_f	Friction resistance coefficient
C_w	Wave making resistance coefficient
C_R	Residual resistance
C_t	Total resistance coefficient
CF	Computational Fluid Dynamics
D	
D	maximum diameter of the outer hull (m)
EF	Experimental Fluid Dynamics
D	
Fn	Froude number- $Fn = v/\sqrt{g.L}$
h	Submergence depth (m)
H*	non-dimensional depth
IHS	Iranian Hydrodynamic Series of Submarines
S	
L	overall length of hull (m)
N	Semi period number
R	maximum radius of the outer hull (m)
Rt	Total resistance (N)
Rv	Viscous resistance (N)
Rw	Wave resistance (N)
S	Wetted surface area (m ²)
v	Speed of submarine (m/s)
ρ	Water density (kg/m ³)
λ	Wave length (m)

References

- [1] P.N.Joubert, "Some aspects of submarine design: part 1: Hydrodynamics", Australian Department of Defence, 2004.
- [2] P.N.Joubert, "Some aspects of submarine design: part 2: Shape of a Submarine 2026", Australian Department of Defence, 2004.
- [3] Burcher R, Rydill L J, "Concept in submarine design", (The press syndicate of the University of Cambridge., Cambridge university press), 1998, pp. 295.
- [4] Yuri.N.Kormilitsin, Oleg.A.Khalizev, "Theory of Submarine Design", Saint Petersburg State Maritime Technical University, Russia, 2001, pp.185-221.
- [5] Ulrich Gabler, "Submarine Design", Bernard & Graefe Verlag, 2000.
- [6] L.Greiner, "Underwater missile propulsion : a selection of authoritative technical and descriptive papers", 1968.
- [7] A group of authorities, "Submersible vehicle system design", The society of naval architects and marine engineers, 1990.
- [8] H.A.Jackson, "Submarine Design Notes",1980.
- [9] Bertram V, "Practical Ship Hydrodynamics", (Elsevier Ltd., UK), 2000, pp. 369.
- [10] Rawson K J, Tupper E C, "Basic Ship Theory", (Jordan Hill., Oxford), 2001, pp. 731.
- [11] M.Moonesun, M.Javadi, P.Charmdooz, U.M.Korol, "evaluation of submarine model test in towing tank and comparison with CFD and experimental formulas for fully submerged resistance", Indian Journal of Geo-Marine Science, vol.42(8), December 2013, pp.1049-1056.
- [12] M.Moonesun, " Introduction of Iranian Hydrodynamic Series of Submarines (IHSS)", Journal of Taiwan Society of Naval Architects and Marine Engineers, ISSN 1023- 4535, Vol.33, No.3, pp.155-162, 2014.
- [13] K.Rhee, J.Choi, S.Lee, "Mathematical model of wave forces for the depth control of a submerged body near the free surface", International offshore and polar engineering conference, Canada, 2008
- [14] C.Polish, D.Ranmuthugala, J.Duffy, M.Renilson, "Characterisation of near surface effects acting on an underwater vehicle within the vertical plane", Australian Maritime College, 2011.
- [15] D Neulist, Experimental Investigation into the Hydrodynamic Characteristics of a Submarine Operating Near the Free Surface, Australian Maritime College, Launceston (2011).
- [16] E.Dawson, B.Anderson, S.V.Steel, M.Renilson, D.Ranmuthugala, "An experimental investigation into the effects of near surface operation on the wave making resistance of SSK type submarine", Australian Maritime College, 2011.
- [17] S Wilson-Haffenden, "An Investigation into the Wave Making Resistance of a Submarine Travelling Below the Free Surface", Australian Maritime College, Launceston, 2009.
- [18] S Van Steel, "Investigation into the Effect of Wave Making on a Submarine Approaching the Free Surface", Australian Maritime College, Launceston, 2010.
- [19] M.Moonesun, Y.M.Korol, Davood Tahvildarzade, "Optimum L/D for Submarine Shape", The 16th Marine Industries Conference (MIC2014), Bandar Abbas, Iran, 2014.

Chapter 11: Fully Submerged Depth at Waves

11-1- Minimum immersion depth for minimizing the submarine motions under regular waves

11-1-1- Introduction

Water wave is an orbital wave in which particles moves in the orbital path. These waves transmit energy along the interface between two fluids of different density. Circular orbital motion dies out quickly below the surface. At some depth below the surface, the circular orbits become so small that movement is negligible. This depth is called the "Wave Base". Wave base can be regarded equal to one-half the wavelength ($\lambda/2$) measured from still water level (Fig.1). Only wave length controls the depth of the wave base, so the longer the wave, the deeper the wave base. The decrease of orbital motion with depth has many practical applications. For instance, submarines can avoid large ocean waves simply by submerging below the wave base. Even the largest storm waves will go unnoticed if a submarine submerges to only 150 meters [1]. Floating bridges and floating oil rigs are constructed so that most of their mass is below wave base, so they will be unaffected by wave motion. In fact offshore floating airport runways have been designed using similar principles. Additionally, seasick scuba divers find relief when they were submerged into the calm, motionless water below wave base [1]. Therefore, deep water defines as depth more than $\lambda/2$. The hydrodynamic forces of ocean surface wave on the submerged bodies are studied in some different fields of engineering such as: 1) Offshore engineering: wave effects on the vertical and horizontal fixed cylinders such as the structural members of platform leg. Many extended studies have been performed to analyzing diffraction around a submerged fixed cylinder. Thus Dean (1948) [2], used a linearized potential theory, for showing the reflection effects. Ursell (1949) [3] and later Ogilvie (1963) [4] presented the formulation of wave steepness up to the second order. Chaplin (1984) [5] measured the nonlinear force on a fixed horizontal cylinder beneath waves by an experimental method. He analyzed the influence of the Keulegan-Carpenter number on the harmonics of the applied force. 2) Wave Energy Converter (WEC): wave effects on the moored or prescribed motions of cylinders of energy converter just near the surface. It is either interesting in

offshore engineering for moored semi-submersibles [6-10]. Wu (1993) presented a formulation for calculating the forces exerted on a submerged cylinder undergoing large-amplitude motions. The free surface condition is linearized and the body surface condition is satisfied on its instantaneous position. The solution for the potential is stated as multi-pole expansion. Wu obtained results for a circular cylinder in purely vertical motion and clockwise circular motion in a wave field (Wu, 1993).

3) Submarine and submersible design: wave effects on the non-moored free submerged body near the free surface and at the snorkel depth. The aim of this chapter is the third category. This chapter aimed to recommend a safe depth for calm and stable movement of a submarine. This safe depth is not equal to wave base necessarily. For this study, a torpedo shaped submersible is analyzed in several depths accompanying by regular surface wave. By increasing the depth, the reduction of submarine movements is evaluated. The results of this research can be used for AUVs, research submersibles and submarines. General discussions and specifications about submersible and submarine hydrodynamics and dynamics is represented in [11-14]. In the field of submarine hydrodynamic near the free surface effect or in snorkel depth (or periscope depth) three general categories could be considered:

- 1) Resistance: by focus on the wave making resistance of a submarine traveling below the free surface in still water (without ocean wave) is discussed in [15-22].
- 2) Dynamic in still water: by focus on the submarine dynamic equations and coefficients affected by free surface of water. General dynamic equations of marine vehicles and submarines are presented in [23,24] as the most famous and comprehensive references in these fields. Revised standard submarine equations of motion were represented in [25-27]. An interesting common study about submarine control, is designing a control system for a submarine running near the free surface or snorkel depth. Refs.[28-32] study the controller design and maneuvering in still water.
- 3) Dynamic under surface waves (seakeeping): by focus on the submarine dynamic equations under ocean wave exciting is assessed in Ref.[33-41]. Collective experimental helpful results for wave forces on submerged bodies are presented in [42] for several different wave conditions. M.Moonesun et.al. have performed a study about submarine dynamics under regular waves by Flow-3D software and CFD method in Ref.[44] and under irregular waves by Maxsurf-Dynamics software and Panel method in Ref.[45].

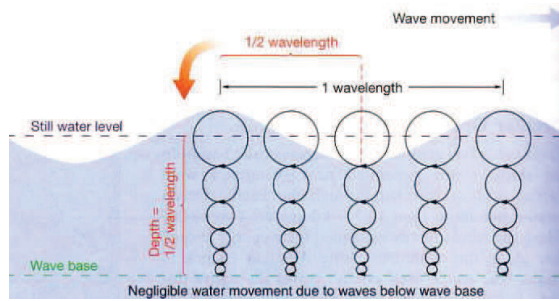


Figure 1: Orbital motion in waves [1]

Finally after the literature survey, it can be stated that approximately all references are based on potential flow for inviscid fluid. For modeling the 3D object and calculating their hydrodynamic coefficient, some methods such as strip theory and conformal mapping should be used which are basically incompatible with the submerged body (without water plane area). Other activities for adjusting these potential flow solutions to submerged bodies such as [33] has clarified that, this manner can be useful only in the early stages of design. In the early stage of design, some estimated and approximated values are sufficient. For the next stages and earning the better careful results and exactly modeling the 3D form of submarine, numerical prediction of CFD method can be a good selection. Some specially explanation of numerical methods for modeling the submarine near the free surface is presented in [32]. These methods are more time consuming than analytical methods but have better results. Accordingly our study and manner of this chapter is focused on the CFD method. There are several CFD softwares which can model the ocean waves (regular and irregular waves) such as: Flow-3D, IOWA and OpenFOAM. This study uses Flow-3D software.

11-1-2- CFD Method of Study

The commercially available CFD package Flow-3D uses the finite-volume method to solve the RANS equations [43]. The computational domain is subdivided using Cartesian coordinates into a grid of variable-sized hexahedral cells. The average values for the flow parameters (pressure and velocity) for each cell, are computed at discrete times by staggered grid

technique (Versteeg and Malalasekera 1995). The free surface is computed using a modified volume-of-fluid (VOF) method [43].

11-1-3-Specifications of Model

In this study a torpedo shaped submersible (Persia110) is considered. The general form and dimensions of this model are shown in Fig.2. This model has 1 DOF, free to pitch. The model has a volume of 8.38 liter, total area of 0.36 m² and weight of 8.38 kg and transverse moment of inertia (I_{yy}) of 1.3 kg.m². This model is the same in several depths in CFD method and the same for validation experiment in towing tank marine laboratory.

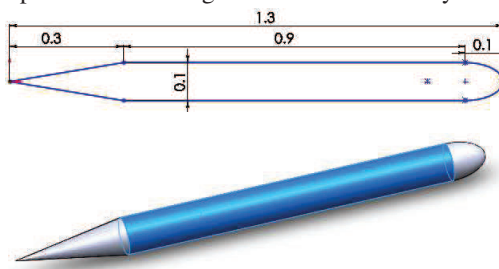
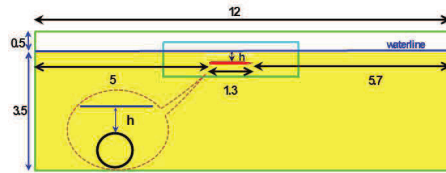


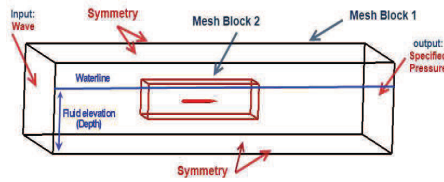
Figure 2: General configuration of the model Persia-110

11-1-4- Domain and Boundary Conditions

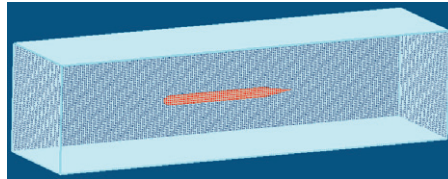
The general configurations and dimensions of domain are shown in Fig.3. The length and width are 12 and 2.6 meters. Depth is 4 meters (3.5 for draft and 0.5 for freeboard). The boundary conditions are: Input: wave, Output: Specified pressure and other sides are symmetry. The model is situated in different depths of "h" according to Fig.3.a. There are two mesh block: one block for the total domain with coarse meshes and other block for fine meshes around the object body. The accuracy of the shape of the body depends on the fine meshes (Fig.3.b,c). For producing the wave, the input boundary condition is "Wave". Flow-3D can produce regular and irregular waves. The produced wave and the situation of the object under the waves are shown in Fig.3.d.



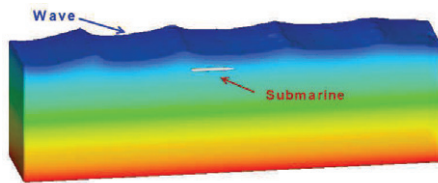
(a) Dimensions of Domain (in meter)



(b) Boundary conditions in domain



(c) Fine meshes in Mesh Block2



(d) Generated wave and position of submarine

Figure 3: Wave simulation by CFD tools (Flow-3D)

1) Meshes: As mentioned above, there are two mesh block. The dimensions of mesh block2 are: $4 \times 1 \times 1$ meters. By changing the location of the model, the situation of the mesh block 2 has been changed. In all conditions of analyses in this study, the mesh number considered 800.000 which are 300.000 for mesh block1 and 500.000 for mesh block 2. Therefore, mesh block 2 contains

fine meshes around the object. Generally it should be notified that in wave problem, it doesn't need for fine meshes for modeling the boundary layer because the frictional forces are very small compare to the wave pressure forces. All meshes are hexahedral and without skew. Aspect ratio is 1, expansion factor between mesh block 1 and 2 equals to 2 and inside every block is 1. Mesh planes are coincide in the adjacent meshes.

2) Wave Modeling: The defined Input boundary condition is a regular wave. General definition of regular wave is represented in Fig.4. Here these parameters are defined in Flow-3D: wave amplitude 0.18 meters, wave period 1 second and mean fluid depth (according to the depth of domain) is 3.5 meters and current velocity is regarded zero. Based on these definitions, deep water condition is compatible because $d/\lambda > 0.5$. For deep waters according to the formula of $\lambda = 1.56T^2$ the wave length is 1.56 meters. Wave speed according to $C = 1.25\sqrt{\lambda}$ is 1.56 m/s. The orbital radius of wave articles path(R) according to this formula is depended on the distance from water surface (h): $R = A \cdot e^{-kh}$. and $k = 2\pi/\lambda$. The variations of article radius versus depth were shown in Fig.1 and here can be stated as: 1) At the water surface, $h=0$ and $R=A$ which means at the surface, the radius of orbital movement of articles equals to wave amplitude. 2)At $h=\lambda/2$, there is $R=0.043A$. 3)At $h=\lambda$, there is $R=0.002A$. It is obvious that at the depth equal to $\lambda/2$, the circle radius is just 4% of the surface value and at the depth equal to λ , it is just 0.2% of the initial value at the surface. Therefore, at the depths more than $\lambda/2$ the wave will be damped out.

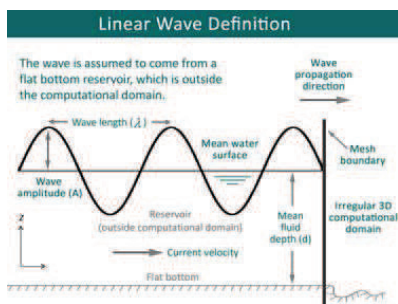


Figure 4: Linear wave definition

3) Simulation Time: for selecting the proper simulation time, the time history of variation of pitch angle was studied in 100 seconds (Fig.5). This diagram shows that there are two overshoot points (maximum and minimum) and except these values, other variations are smooth and inside a certain limit. These overshoots happen because of initial momentum of inertia. For saving the time, these overshoot points were eliminated and simulation time was considered 20 seconds.

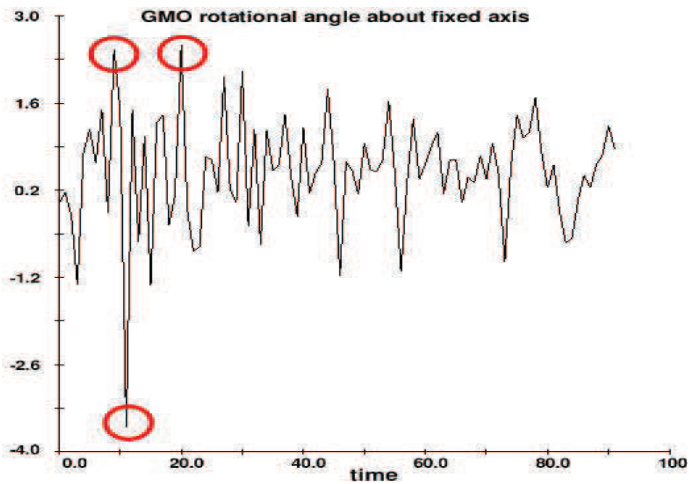


Figure 5: Evaluation of time history of pitch angle in 100 seconds for condition $h=D$

4) Domain Dimensions: in this problem, the specifications of wave are very important for determination of domain dimension.

Length: The considered wave length is about 1.56 meters. For better forming of wave before arriving to the object, more than two complete waves are considered in 5 meters. About the same value is considered after the object equal to 5.7 meters. By considering the 1.3 meter length of the object, the total length of domain is achieved 12 meters.

Breadth: The considered breadth equals to object length ($L=1.3m$) to each side and the total breadth is $2L$.

Breadth:As mentioned above, the wave base is approximately equal to $\lambda/2$. This study aims to evaluate the wave effects on the submarine at the depth of 2λ . For avoiding the bottom effects, the draft of domain is considered 3.5

meters. The wave amplitude (A) is 0.18 meter, thus the freeboard above water level is considered 0.5 meter. Therefore, the depth of domain is considered 4 meters.

Settings of simulation are abstracted in Tab.1.

Table 1: Settings of simulation

Elements	Boundary conditions	Descriptions	
Domain	Cubic	conditions	with free surface and linear wave - domain with inlet, outlet and symmetry - without heat transfer- without current velocity
		dimensions	L*B*D=12*2.6*4 m- draft 3.5 m
		grid	structured grid- hexahedral cells-without skew- two mesh block- more fine meshes in mesh block 2 around the object- Mesh number of 800.000, aspect ratio 1, expansion factor between blocks 2 and inside blocks 1.
		settings	Simulation time: 20 sec- Time step=0.005-0.013 sec
Fluid	-	Incompressible fluid (fresh water)- tempreture:20 deg- $\rho=999.841 \text{ kg/m}^3$ - turbulent modeling: Standard k- ϵ	
Object	GMO	Submarine, length:1.3m, Diameter:0.1, 1DOF free to pitch angle	
Input	Inlet	Linear wave, wave amplitude 0.18 m, wave period 1 sec, mean fluid depth 3.5 m	
Output	Outlet	Specified pressure (Specified fluid level: 3.5 m)	
Symmetry	Symmetry	In 4 faces	
Initial conditions		Fluid level: 3.5 m	

11-1-5- Considered Conditions for Analyses

For studying the wave effects on the submarine, several depths for submarine situation (h) are considered according to Fig.3.a and Table 2.

Table 2: Considered conditions for analyses

	Submarine depth (m)	Description (equivalent to)
1	0	Body tangent to free surface
2	0.05	R_s (or) 0.03λ
3	0.1	D_s (or) 0.06λ
4	0.15	$1.5D_s$ (or) 0.09λ
5	0.25	$2.5D_s$ (or) 0.16λ
6	0.35	$3.5D_s$ (or) 0.22λ
7	0.55	$5.5D_s$ (or) 0.35λ
8	0.75	$7.5D_s$ (or) 0.48λ
9	0.95	$9.5D_s$ (or) 0.61λ
10	1.6	$\cong \lambda$
11	2.4	$\cong 1.5\lambda$
12	3	$\cong 3\lambda$

11-1-6-Results and Discussion

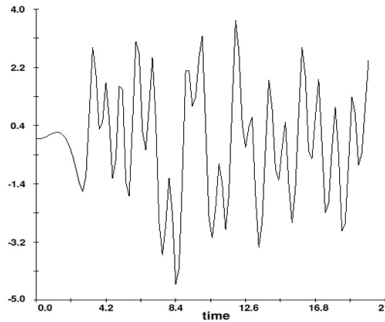
11-1-6-1-Method of Extracting the Results

According to the diagram of Fig.5, there is a disordered and irregular variation of pitch angle versus time. Usually in sea keeping studies, Root Mean Square (RMS) analysis is used. Therefore, here the RMS value of pitch angle is calculated in every depth, after eliminating the overshoot points. RMS is calculated as Eqn.9:

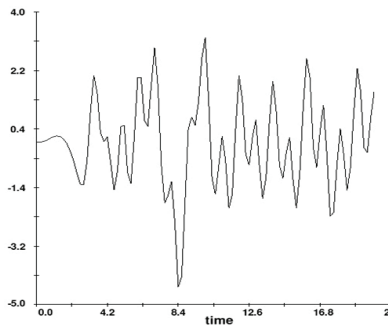
$$RMS = \sqrt{\frac{\theta_1^2 + \theta_2^2 + \dots + \theta_n^2}{n}} \quad (9)$$

11-1-6-2-Results

The time history of pitch angle in 12 conditions is analyzed. Fig.6 shows two samples of time history for $h=0.1$ and 0.35 meter. Table 2 represents the results for each depth. The percentage of decrease in last column is based on comparison to $h=0$ therefore; $\text{average} = ((h_0 - h_i) / h_0 * 100)$. It should be notified that the static pitch angle of this submarine is 0.34 degree.



(a) $h=0.1$, RMS=1.67 deg



(b) $h=0.35$, RMS=1.22 deg

Figure 6: time history of pitch angle

11-1-6-3-Discussion and Analysis

It is obvious that by increasing in the depth, the wave effect decreases and pitch angle approaches to static trim angle. The last column of Tab.3 can smoothly describe the percentages of reduction in pitch angle. In depth of 0.03λ there is 33% reduction and in depth of 0.06λ there is 51% reduction.

Intense gradient of pitch angle will be continued until the depth of 0.09λ which experiences 59% reduction. After this depth, there is a gentle variation. Values of RMS at the depths of λ , 1.5λ and 2λ are equal to static trim angle which meant no effect of waves on the submarine. Almost around the depth of $\lambda/2$ the wave effect is negligible. The reason of this phenomenon is based on the principle of "wave base" which described in Introduction. It meant that if a submarine dive to the depth more than $\lambda/2$, doesn't experience the wave effects. For long swell waves, the value of $\lambda/2$ may be more than the collapse depth of the submarine and be impossible. In this condition, if submarine dives to the depth about 0.1λ , it can avoid the 60% of movements and shakes. For instance, in a swell wave (which is very similar to regular waves) with a period of 15 seconds, the wave length is 351 meters. The half wave length is about 175 meters which may be dangerous depth for a submarine and it can be catastrophic. Despite that, if submarine dives to the depth of 0.1λ equal to about 35 meters, can navigate in very calm and more stable conditions.

Table 3: RMS values for considered conditions

	depth (m)	depth (λ)	RMS (degree)	Percentage of Decrease (%)
1	0	0	3.43	0
2	0.05	0.03	2.29	33
3	0.1	0.06	1.67	51
4	0.15	0.09	1.42	59
5	0.25	0.16	1.38	60
6	0.35	0.22	1.22	64
7	0.55	0.35	1	71
8	0.75	0.48	0.82	76
9	0.95	0.61	0.44	87
10	1.6	1	0.1	97
11	2.4	1.5	0.03	99
12	3	2	0	100

11-1-7- Review 1

In conclusion, the results could be abstracted in the Fig.7 which fairly shows the gradient of movements versus depth of submergence. Depth of $\lambda/2$ could be considered as the absolutely calm depth but the depth of 0.1λ could be recommended as an operational safe and approximately calm depth for submarines.

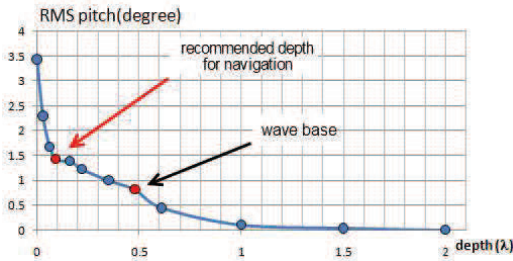


Figure 7: gradient of RMS pitch versus submergence depth of submarine

11-2- Evaluation of Submarine Motions under Irregular Ocean Waves by Panel Method

11-2-1- Theory of the Study

There are two main methods in the numerical methods of the study based on the Potential flow: Strip Theory and Panel Method. The Strip Theory is well known and applicable for surface crafts and ships but it has no applicability for submerged bodies. The reason for this can be ascribed to a Conformal Mapping basis which requires a water plane area. So in order to study the dynamics of submerged bodies like submarines by the potential flow, only the Panel Method is applicable. The main disadvantage of this method is an almost zero forward speed. Table.1 shows the main differences between the Strip Theory and the Panel Method [47]. This study is accomplished via Maxsurf Motions. In order to simulate the submerged submarine at viscous fluid and at non zero speed, only CFD methods based on solving RANS equations are utilized. This method is more accurate but more time consuming as regards solving and more complicated in terms of programming.

Table 4: Comparison between Strip theory and Panel method

method	Speed (Fn)	Motion	Applicable
Strip theory	0~0.7	Heave, Roll, Pitch	slender body
Panel method	0~0.1	all 6 DOF	all bodies

11-2-2-The Model Specifications

The overall shape of the submarine is provided in Figs [8,9]. It has the general shape of a naval submarine with a sailing mast on the top of the hull and a snorkel mast for snorting depth. The model submarine has a weight of 134.5 tons and a length of 29 meters. It is a small-sized naval submarine. The main advantage of the present research is that it addresses small and medium submarines because they can't submerge to very high depths, equalling to "wave base". Therefore our focus is on finding a real accessible calm depth for submarines of this type. To explain more, such submarines have a maximum dive depth of 100 meters. In a wave length of 300 meters, "the wave base" is 150 meters which is a lot more than the maximum dive depth of a submarine. At this stage, we try to determine the minimum logical, calm and safe depth for small and medium submarines.

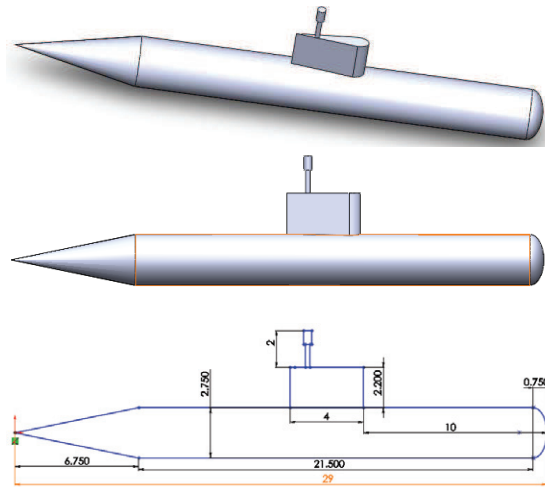


Figure 8: General form of modeled naval submarine

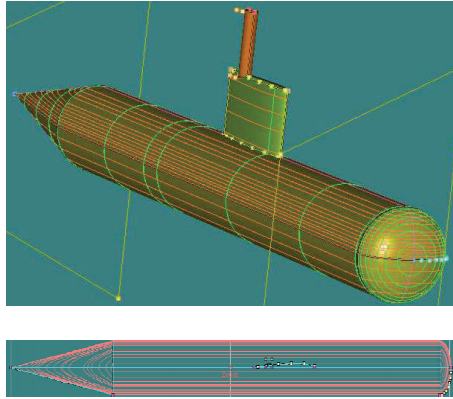


Figure 9: 3D model with body lines in Maxsurf

The mass distribution for dynamic modelling is presented in Tab.5.

Table 5: mass distribution of the simulated model

Total mass (t)	LCG (m)	VCG (m)	Rxx (m)	Ryy (m)	Rzz (m)
134.5	3	1.237	1.1	7.25	7.25

The LCG=LCB is considered from a mid-ship section. The vertical center of gravity (VCG) is considered from base line at the bottom of the cylindrical hull. The longitudinal radius of gyration (R_{xx}) is considered 40%BOA and $R_{yy}=R_{zz}=25\%LOA$. The hydrostatic properties of the model are listed in Tab.6.

Table 6: hydrostatic properties of the model

	Measurement	Value	Units
1	Displacement	134.5	t
2	V/Volume (displaced)	131.266	m ³
3	Draft Amidships	5.500	m
4	Immersed depth	5.436	m
5	WL Length	0.400	m
6	Beam max extents b	0.207	m
7	Wetted Area	464.377	m ²
8	Max sect. area	6.710	m ²
9	Waterpl. Area	0.080	m ²
10	Prismatic coeff. (Cp)	46.907	
11	Block coeff. (Cb)	267.854	
12	Max Sect. area coeff.	5.886	
13	Waterpl. area coeff.	0.963	
14	LCB length	3.044	from a
15	LCF length	2.544	from a
16	LCB %	761.093	from a
17	LCF %	635.989	from a
18	KB	1.416	m
19	K/G fluid	1.237	m
20	BMT	-0.041	m
21	BML	0.000	m
22	GMT corrected	0.137	m
23	GML	0.179	m
24	KMit	1.374	m
25	KML	1.416	m
26	Immersion (TPc)	0.001	tonne/c
27	MTC	0.006	tonne
28	RM at 1deg = GMT/Di	0.322	tonne
29	Length:Beam ratio	1.928	

11-2-3- Irregular wave specifications and wave spectrum

This study uses JONSWAP energy spectrum as a base for nonlinear wave. After analyzing the data collected during the Joint North Sea Wave Observation Project ,JONSWAP, Hasselmann et al. (1973), found that the wave spectrum is never fully developed. It continues to develop through non-linear, wave-wave interactions even for very long durations and distances. Hence, an extra and somewhat artificial factor was added to the Pierson-Moskowitz spectrum in order to improve the fit to their measurements. The JONSWAP spectrum is thus a Pierson-Moskowitz spectrum multiplied by an extra peak enhancement factor γ .

$$S_j(\omega) = \frac{\alpha g^2}{\omega^5} \exp\left[-\frac{5}{4}\left(\frac{\omega_p}{\omega}\right)^4\right] \gamma^r$$

$$r = \exp\left[-\frac{(\omega - \omega_p)^2}{2\sigma^2\omega_p^2}\right]$$

Wave data collected during the JONSWAP experiment were used to determine the values for the constants in the above equations:

$$\alpha = 0.076 \left(\frac{U_{10}^2}{Fg} \right)^{0.22}$$

$$\omega_p = 22 \left(\frac{g^2}{U_{10}F} \right)^{1/3}$$

$$\gamma = 3.3$$

$$\sigma = \begin{cases} 0.07 & \omega \leq \omega_p \\ 0.09 & \omega > \omega_p \end{cases}$$

where F is the distance from a lee shore, called the fetch, or the distance over which the wind blows with constant velocity. Therefore, based on JONSWAP, the characteristics for irregular waves are shown in Table 7.

Table 7: Characteristics of JONSWAP irregular wave

Significant wave height (m)	Modal period (s)	Average period (s)	Zero-up crossing period (s)
2	9.95	8.37	7.87

The submergence depth should be stated as wave length (λ). For deep water the formula $\lambda = \frac{g}{2\pi} T^2$ could be applied where the wave length equals 100 meters. The headings of 0, 45, 90, 135 and 180 degrees are considered in the encounter frequencies of 0.2~2 (rad/s) for 10 frequencies. The speeds of 1,3,5,7,9 knots are considered for calculating the encounter frequency but generally the Panel method is applicable for very small speeds and Froud numbers of 0~0.1.

11-2-4- Modeling by Panel Method and results

The simulation is performed for 11 different drafts and depths. The depth is considered between the top side of the cylindrical part of the hull and the still water surface. The descriptions for each depth are presented in Table 8.

Table 8: descriptions of surfaced or submerged depth

Depth (m)	description
4.2	at surface draft
3.9	Waterline tangent to the main hull
0	at snorkel depth
-1	Depth, 1 meter ($\lambda/100$)
-3	Depth, 3 meters ($\lambda/33$)
-5	Depth, 5 meters ($\lambda/20$)
-8	Depth, 8 meters ($\lambda/12.5$)
-12	Depth, 12 meters ($\lambda/8.3$)
-16	Depth, 16 meters ($\lambda/6.25$)
-25	Depth, 25 meters ($\lambda/4$)
-50	Depth, 50 meters ($\lambda/2$)

The general form of Meshing the body in Panel Method at surfaced and submerged conditions is shown in Fig.10. At surface conditions, the body is meshed up to the surface draft.

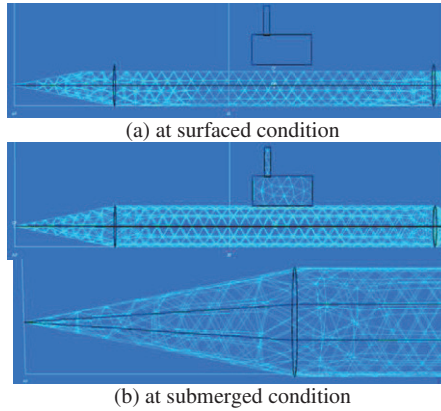
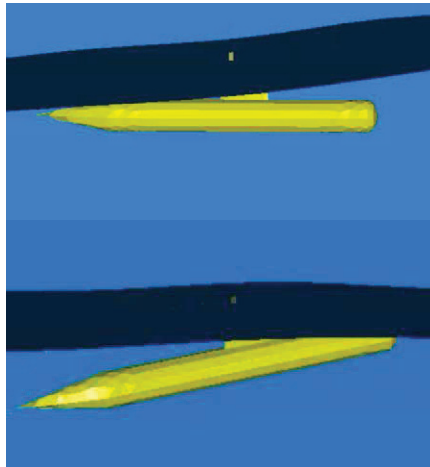
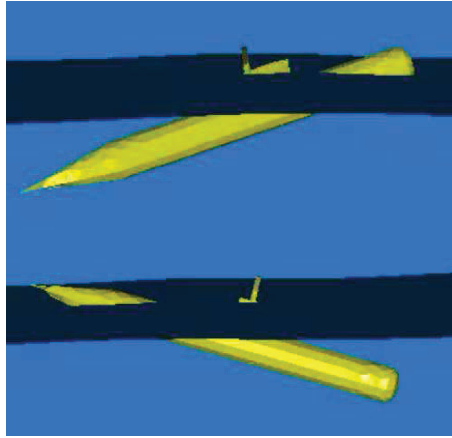


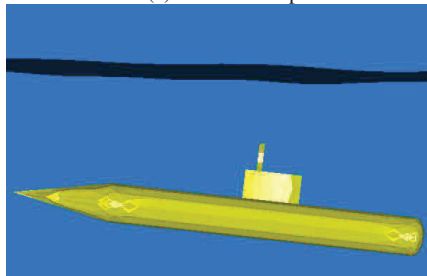
Figure 10: Meshing the body in Panel Method

The visualized results of simulations for submarine motions and irregular wave surface are shown in Fig.11. As it can be seen, by increasing the depth of submergence, a decrease in motion amplitude occurs.

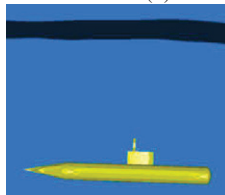




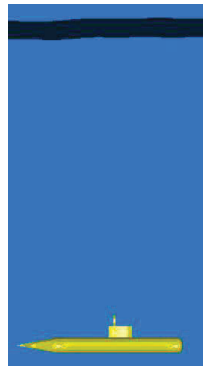
(a) at snorkel depth



(b) at a depth of 5m



(c) at a depth of 16m



(d) at a depth of 50m

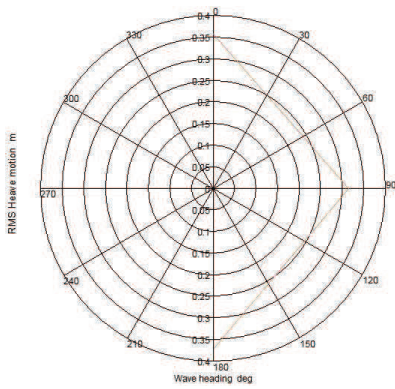
Figure 11: Dynamic simulation of submarine under non-linear wave (JONSWAP spectrum)

Table 9 provides the sample result at snorkel depth and encountered wave angle of 180 degrees at JONSWAP spectrum with a significant wave height of 2 meters, a time period of 10 seconds and a wave length of 100 meters.

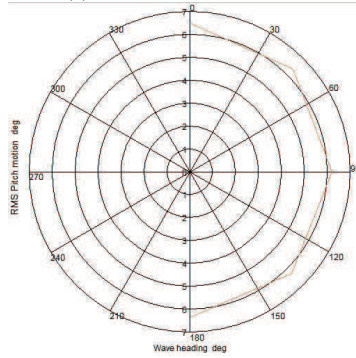
Table 9: Sample result at snorkel depth and encountered wave angle of 180

9 kn 180 deg JONSWAP: 9.995 s, 2 m					
9 kn; 180 deg; JONSWAP: 9.995 s, 2 m					
	Item	m0	units	RMS	units
1	Modal period	9.990	s	--	
2	Characteristic wave height	2.000	m	--	
3	Spectrum type	JONSWAP			
4	Wave heading	180.0	deg	--	
5	Vessel Speed	9.000	kn	--	
6	Vessel displacement	76.187	m ³		Monohull
7	Vessel GMt	0.179	m	--	
8	Vessel trim	0.0	deg	--	
9	Vessel heel	0.0	deg	--	
10	Transom method	n/a for Panel Met		--	
11	Wave force method	n/a for Panel Met		--	
12	Added res. method	n/a for Panel Met		--	
13	Pitch gyradius	7.250	m	--	
14	Roll gyradius	1.100	m	--	
15	Yaw gyradius	7.250	m	--	
16	Wave spectrum	0.261	m ²		0.501 m
17	Encountered wave spectrum	0.251	m ²		0.501 m
18	Added resistance	-1.400	kN	--	
19	Surge motion	0.800	m ²		0.894 m
20	Sway motion	0.000	m ²		0.003 m
21	Heave motion	0.168	m ²		0.410 m
22	Roll motion	0.00030	deg ²		0.017 deg
23	Pitch motion	37.67	deg ²		6.14 deg
24	Yaw motion	0.00003	deg ²		0.0055 deg
25	Surge velocity	0.638	m ² /s ²		0.799 m/s
26	Sway velocity	0.158	m ² /s ²		0.397 m/s
27	Heave velocity	0.158	m ² /s ²		0.397 m/s
28	Roll velocity	0.00000	(rad/s) ²		0.00034 rad/s
29	Pitch velocity	0.01132	(rad/s) ²		0.10640 rad/s

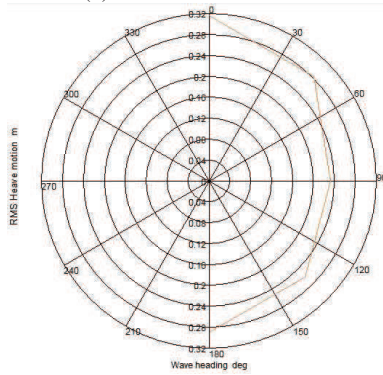
As it is usual in marine applications, the results of seakeeping modeling are shown in the form of polar diagrams. The polar diagrams are easy to understand for any headings. In this diagram, the heading angle is shown from 0 to 180 degrees and the RMS values for every seakeeping parameter (e.g. heave) are given in several radiuses. The polar diagram for each depth of submergence of submarine is shown in Fig.12.



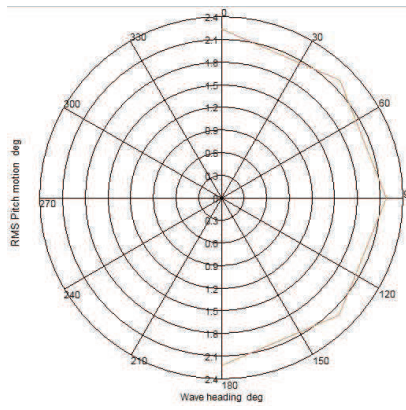
(a) RMS Heave at 3 meters



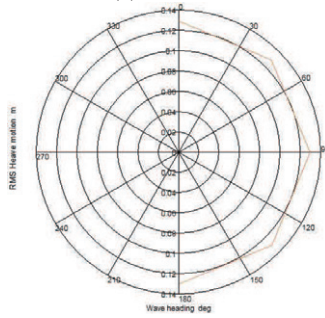
(b) RMS Pitch at 5 meters



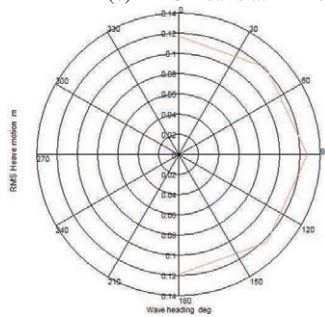
(c) RMS Heave at 5 meters



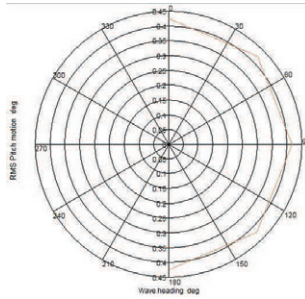
(d) RMS Pitch at 12 meters



(e) RMS Heave at 12 meters



(f) RMS Heave at 25 meters



(g) RMS Pitch at 25 meters

Figure 12: Polar diagram at several depths

The total results for the main headings of 0, 90 and 180 degrees are provided in Tab.10.

Table 10: Results for the main headings of 0, 90 and 180 degrees

h (m)	Heading					
	0		90		180	
	Pitch (deg)	Heave (m)	Pitch (deg)	Heave (m)	Pitch (deg)	Heave (m)
4.2	18.5	2.7	18.9	3.3	16.5	3.17
3.9	6.7	1	8.42	1.1	6.6	0.82
0	8.25	0.41	5.72	0.43	6.14	0.41
-1	11.6	0.76	11.55	0.71	12.2	0.82
-3	6.9	0.36	6.9	0.31	7.1	0.37
-5	6.5	0.31	6.17	0.23	6.3	0.29
-8	3.8	0.17	3.7	0.13	3.7	0.16
-12	2.24	0.13	2.17	0.13	2.21	0.13
-16	1.27	0.125	1.24	0.135	1.26	0.13
-25	0.43	0.12	0.41	0.13	0.42	0.12
-50	0.06	0.06	0.05	0.07	0.05	0.06

For instance, two diagrams for two conditions are presented in Fig.7: 1) RMS pitch angle at the heading of 180 degree and different depths and 2) RMS heave at the heading of 180 degree and different depths. These diagrams illustrate a descending trend when increasing the depth. But there are some distortions and inconsistencies at the depths near the water surface. The reason can be attributed to two factors: 1) at surface conditions or near surface depths, there are some huge forces and moments bringing about large values of heave and pitch motions; in large motions, panel method is not valid. However, The meshing of the submarine body is executed up until the waterline level as is shown in Fig.10-a. Therefore, at large motion amplitudes,

the main body can jump out of water or dive in water while there is no any meshing inside the water for the non meshed area on the body. These two parameters indicate that we can ignore the results of surface and near surface depths (first three depths). By studying other cases, it becomes clear that by increasing the depth, a fast decrease in RMS values occurs. This decreasing trend shows that at a depth of 8 meters ($\lambda/12.5$), RMS Pitch is only 30% of a 1-meter depth ($\lambda/100$). Also, at the depth of 8 meters ($\lambda/12.5$), RMS heave is only 20% of a 1-meter depth ($\lambda/100$). This is one main result of the present study which shows the depth about 0.1λ can be recommended as an operationally calm, stable, and safe for naval or research submarines. Depth of 50 meters ($\lambda/2$ equal wave base depth) is absolutely calm and depth; however, it may be inaccessible for small and medium submarines. A logical and accessibly recommended depth for all submarine types is 0.1λ .

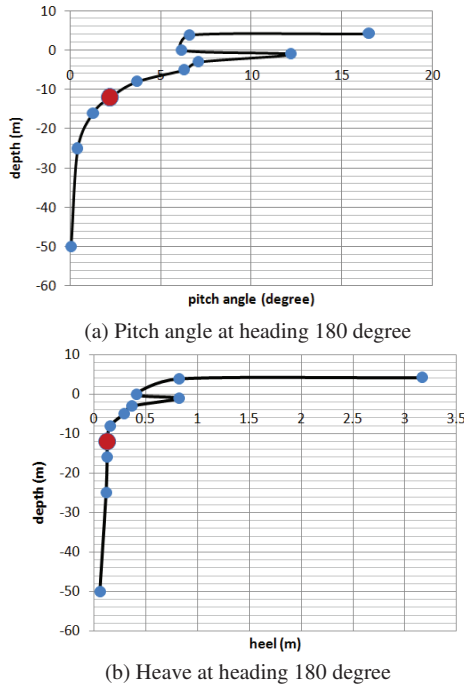
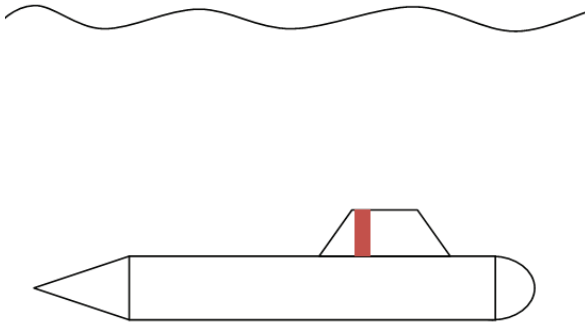


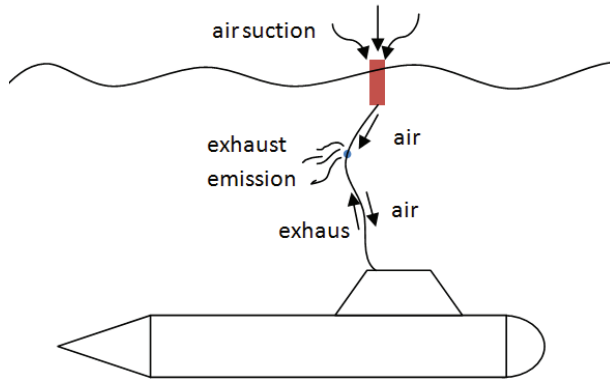
Figure 13: RMS values of motions at different depths.

11-3- Moon-Korol system

The "Moon-Korol" system or "Snorting Buoy" is an innovative engineering plan which was unveiled in 2013 and then was registered in Ukraine and Iran. The main advantage of this system is enabling the Small and medium submarines to snorting in rough ocean waves. Now a day, small and medium submarines cannot perform the snorting operation in rough and stormy sea because they have weak stability and seakeeping specifications. This defect was covered by this innovative plan. The Moon-Korol system, first time was designed for installing on medium size submarines of Iranian Navy. The main Advantages of Snorting Buoy is: 1- Small and medium submarines are capable of snorting in rough ocean waves. 2- Fewer movements at snorting operation. 3- Fewer dangers against aerial bombing attack. 4- Better SONAR hearing due to fewer waves ambient noise. 5- Capable of near zero forward speed at snorting operation. As shown in Fig.14, this buoy is mounted inside the sailing and will be released at safe depth beneath the sea water level. This safe depth, as mentioned above, should not be less than 0.1λ . The inside arrangement of Snorting Buoy is presented in Fig.15.



(a) Moon-Korol is mounted in after side of the sailing



(b) Moon-Korol is released to sea level for fresh air suction and exhaust emission

Figure 14: Schematic of Moon-Korol snorting system

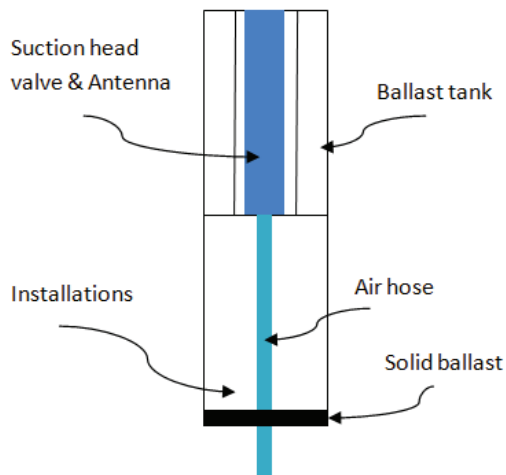


Figure 15: Inside arrangement of Snorting Buoy: ballast tank is used

for floating the buoy and solid ballast (lead) for providing stability and upright standing

Nomenclature

λ	Wave length (m)
θ	Pitch angle (degree)
A	Wave amplitude (m)
AUV	Autonomous Underwater Vehicle
CFD	Computational Fluid Dynamics
d	Depth of water (m)
Ds	Diameter of submarine body
DOF	Degree Of Freedom
GMO	General Moving Object
h	Distance from top of the object (submarine) to the water surface (m)
IHSS	Iranian Hydrodynamic Series of Submarines
L	Length of object (submarine)
R	orbital radius of wave articles path (m)
Rs	Radius of submarine body
RMS	Root Mean Square
VOF	Volume Of Fluid

References

- [1] Thurman, Harold V.; Trujillo, Alan P. "Essentials of Oceanography", Edition 5, Prentice Hall, 2001, pp.240-243.
- [2] Dean, WR (1948). "On the Reflexion of Surface Waves by a Submerged Circular Cylinder," ProcCamb Phil Soc, Vol 44, pp 483-491.
- [3] Ursell, F (1949). "Surface Waves in the Presence of a Submerged Circular Cylinder, I and II," ProcCamb Phil Soc, Vol 46, pp 141-158.
- [4] Ogilvie, TF (1963). "First- and Second-Order Forces on a Cylinder Submerged Under a Free Surface," J Fluid Mech, Vol 16, pp 451-472.
- [5] Chaplin, JR (1984). "Nonlinear Forces on a Horizontal Cylinder Beneath Waves," J Fluid Mech, Vol 147, pp 449-464.
- [6] Etienne Guerber, Michel Benoit, Stéphan T. Grilli, Clément Buvat, Modeling of Fully Nonlinear Wave Interactions with Moving Submerged Structures, Proceedings of the Twentieth (2010) International Offshore and Polar Engineering Conference Beijing, China, June 20-25, 2010, pp.529-536.
- [7] Wu, GX (1993). "Hydrodynamic Forces on a Submerged Circular Cylinder Undergoing Large-amplitude Motion," J Fluid Mech, Vol 254, pp 41-58.
- [8] Evans, DV, Jeffrey, DC, Salter, SH, and Taylor, JRM (1979). "Submerged Cylinder Wave Energy Device: theory and experiment," Applied Ocean Research, Vol 1, No 1, pp 3-12.
- [9] D Dessi, A Carcaterra, and G Diodati, Experimental investigation versus numerical simulation of the dynamic response of a moored floating structure to waves, Proceedings of the Institution of Mechanical Engineers, Part M: Journal of Engineering for the Maritime Environment, September 1, 2004; vol. 218, 3; pp. 153-165.
- [10] S H Salter, J R M Taylor, and N J Caldwell, Power conversion mechanisms for wave energy, Proceedings of the Institution of Mechanical Engineers, Part M: Journal of Engineering for the Maritime Environment, June 1, 2002; vol. 216, 1; pp. 1-27.
- [11] P.N.Joubert, "Some aspects of submarine design: part 1: Hydrodynamics", Australian Department of Defence, 2004.
- [12] P.N.Joubert, "Some aspects of submarine design: part 2: Shape of a Submarine 2026", Australian Department of Defence, 2004.
- [13] Moonesun.M, Korol.Y.M, Dalayeli.H, CFD analysis on the bare hull form of submarines for minimizing the resistance, International Journal of Maritime Technology (IJMT), Vol.3, 2014, p.1-13.
URL http://www.ijmt.ir/browse.php?a_code=A-10-450-1&slc_lang=en&sid=1
- [14] Renilson.M, Submarine Hydrodynamics, Springer, 2015, pp.45-89.
- [15] D Neulist, Experimental Investigation into the Hydrodynamic Characteristics of a Submarine Operating Near the Free Surface, Australian Maritime College, Launceston (2011).
- [16] E.Dawson, B.Anderson, S.V.Steel, M.Renilson, D.Ranmuthugala, "An experimental investigation into the effects of near surface operation on the wave making resistance of SSK type submarine", Australian Maritime College, 2011.

- [17] S Wilson-Haffenden, "An Investigation into the Wave Making Resistance of a Submarine Travelling Below the Free Surface", Australian Maritime College, Launceston, 2009.
- [18] S Van Steel, "Investigation into the Effect of Wave Making on a Submarine Approaching the Free Surface", Australian Maritime College, Launceston, 2010.
- [19] C.Polish, D.Ranmuthugala, J.Duffy, M.Renilson, "Characterisation of near surface effects acting on an underwater vehicle within the vertical plane", Australian Maritime College, 2011.
- [20] A.Alvarez, V. Bertram, L. Gualdesi, Hull hydrodynamic optimization of autonomous underwater vehicles operating at snorkeling depth, *Ocean Engineering* 36 (2009) 105–112.
- [21] Shiyang Wang, Lixin Cui, Chao Wang, Sheng Huang, Resistance performance of submarine under different traveling stations, Harbin Engineering University Harbin, China.
- [22] M.Moonesun ,Y.M.Korol,"Minimum Immersion Depth for EliminatingFree Surface Effect on Submerged Submarine Resistance", *Turkish Journal of Engineering, Science and Technology (TUJEST)*, vol.3, No.1, pp.36-46, 2015.
- [23] Fossen.T.I, *Guidance and Control of Ocean Vehicles*, John Wiley and Sons Ltd, 1999.
- [24] Fossen.T.I, *Handbook of Marine Craft Hydrodynamics and Motion Control*, John Wiley and Sons Ltd, 2011.
- [25] J.Feldman, Revised standard submarine equations of motion, Naval Ship Research and Development Centre, Wash. DC, Tech. Rep.DTNSRDC-SPD-0393-09.
- [26] J.B.Spencer, *Stability and Control of Submarines, Parts I-IV*, Reprint of the Royal Naval Scientific Service, vol.23, pp.187-205, 265-281,327-345.
- [27] M.Gertler, G.R.Hagen, *Standard Equations of Motion for Submarine Simulation*, Naval Ship Research and Development Centre, Wash. DC, Tech. Rep. RNSRDC2510.
- [28] R.J.Richards, D.P.Stoten, *Depth Control of a Submersible Vehicle*, *Int.Shipbuilding Progress*, vol.81, pp.30-39, 1981.
- [29] M.Grimble, G.van der Molen, E.Liceaga-Castro, *Submarine Depth and Pitch Control*, *IEEE Conf.Contr.Appl.* Vancouver, Canada, 1993.
- [30] C.J.Daniel, R.J.Richards, *A Multivariable Controller for Depth Control of a Submersible Vehicle*, *Inst. of Meas. and Cont. Conf. on Application of Multivariable System*, 1982.
- [31] YanglingHao, Donghui Shen, ZhilanXiong, *Design of Submarine Near Surface Depth Controller*, *IEEE, 5th World Congress on Intelligent Control and Automation*, 15-19 June, 2004, China, pp.4530-4533.
- [32] M.J.Griffin, *Numerical Prediction of the Maneuvering Characteristics of Submarines Operating Near the Free Surface*, MIT, PhD thesis, 2002.
- [33] G.W.Johnston, S.P.Foster, *Frequency Domain Prediction of Submarine Motion in Waves (SUBMO)*, vol.1, National Defence Research and Development, Canada, 1991.
- [34] K.Rhee, J.Choi, S.Lee, "Mathematical model of wave forces for the depth control of a submerged body near the free surface", *International offshore and polar engineering conference*, Canada, 2008
- [35] Wang.X, Sun.Y, Hong.W, *Catastrophe of submarine near surface motion*, *IEEE* 1-4244-2386-6, 2008.

- [36] Ni.S.Y, Zhang.L, Dai.Y.S, Hydrodynamic Forces on a Moving Submerged Body in Waves, International Shipbuilding Progress, vol.41, pp.95-111.
- [37] T.B.Booth, Optimal depth control of an underwater vehicle under a seaway, RINA Symp, Naval Submarines, London, 1983, pp.17-19.
- [38] E.Lisegaga Castro, M.Molen, Submarine H_{∞} depth control under wave disturbances, IEEE Transactions on Control Systems Technology, Vol.3, No.3,pp.338-346, 1995.
- [39] Musker.A.J, Loader.P.R, Butcher.M.C, Simulation of a submarine under waves, International shipbuilding progress, 1988, vol. 35, pp. 389-410.
- [40] Dogan.P.P, Optimum stabilization of a near surface submarine in random seas, Cambridge, MIT, AD651821, 1967.
- [41] João LD Dantas, Jose J da Cruz, and Ettore A de Barros, Study of autonomous underwater vehicle wave disturbance rejection in the diving plane, Proceedings of the Institution of Mechanical Engineers, Part M: Journal of Engineering for the Maritime Environment, May 2014; vol. 228, 2: pp. 122-135., first published on November 28, 2013.
- [42] Henry.Ch.J, Milton.M, Kaplan.M, Wave forces on Submerged Bodies, Davidson Laboratory, Stevens Institute, 1961.
- [43] http://www.flow3d.com/resources/tech_paper/res_tp_main.html
- [44] Mohammad Moonesun¹, Firouz Ghasemzadeh, Yuri Korol, Valeri Nikrasov, Alexi Yastreba, Alexander Ursolov, Asghar Mahdian, Technical Notes on the Near Surface Experiments of Submerged Submarine, International Journal of Maritime Technology, IJMT Vol.5/ Winter 2016 (41-54).
- [45] Mohammad Moonesun^{1,2}, Asghar Mahdian¹, *Olha Korneliuk², Yuri Korol³, Alexander Bandarinko³, Nikrasov Valeri³, Evaluation of Submarine Motions under Irregular Ocean Waves by Panel Method, SAGE journal, In press.
- [46] http://www.flow3d.com/resources/tech_paper/res_tp_main.html
- [47] Maxsurf Motions, User Manual (Maxsurf 20), 2013.

Chapter 12:

Underwater Model Test of Submarine in Towing Tank

12-1- Scaling method for underwater hydrodynamic model test of submarine

12-1-1-Introduction

In every experimental test in towing tank, water tunnel and wind tunnel, in the first step, the speed of the model should be developed to the full-scale vessel (ship or submarine). In the second step, the obtained resistance of the model should be developed. For submarine, there are two modes of movement: surface and submerged mode. There is not any problem in surface mode because, according to Froude's law, the ratio of speed of the model to the full-scale vessel is proportional to the square root of lengths (length of the model on the length of the vessel) [1-3]. This leads to a reasonable speed and is not so much for the model that is applicable in the laboratory.

$$(F_r)_M = (F_r)_S \quad V_M = V_S(\sqrt{L_M/L_S})$$

For example, for a submarine at surface mode with a speed of 10 m/s and a scale of 1:100, the required speed of the model in towing tank will be 1m/s that is easily possible. The main problem is in submerged mode (fully submerged). At submerged mode, Froude equation cannot be used because of absence of free surface effects and waves. In the depth of water, there is frictional and viscous pressure resistance and there is not wave resistance [4,5]. Furthermore, the use of Reynold's equation is impracticable because model speed will be too large and impossible to provide [6].

$$(Re)_M = (Re)_S \quad V_M = V_S(L_S/L_M)$$

For example, for a submarine with a speed of 10 m/s and a scale of 1:100, the required speed of the model in towing tank will be 100 times of main submarine, which means 1000 m/s that is actually impossible. The related dynamic effects are evaluated in [7-11]. A popular and well known classification in marine engineering for total resistance (R) is the summation of wave resistance, viscous pressure resistance (R_{vp}) and friction resistance (R_f) [12,13,14]. There is not wave resistance for fully submerged submarine. Total resistance coefficient (C_d), friction resistance coefficient (C_f), viscous pressure resistance coefficients (C_{vp}) are defined as:

$$C_d = \frac{R}{0.5\rho A_w V^2} \quad C_f = \frac{R_f}{0.5\rho A_w V^2} \quad C_{vp} = \frac{R_{vp}}{0.5\rho A_w V^2}$$

Which V is the velocity in (m/s), and A_w is wetted area surface in m^2 .

There are three important notes about critical Reynolds and resistance coefficients that are described below.

Note 1: Reynolds of model and submarines do not have to be exactly equal. Main aid of Reynold's equation is to ensure from the existence of a turbulent flow on the surface of the model because the flow regime on real submarines is turbulence. Critical Reynolds is different from 300,000 to about 1000,000 that depend on another condition such as roughness of model, initial flow turbulence, vibration and heat transfer. Here is an important note that says, "providing turbulent flow can be done by many parameters not only by the Reynolds". By providing these parameters that mentioned above, the required critical Reynolds decreases steeply. For example, by setting a wire or pin on the bow of model, turbulence can be happened at critical Reynolds less than 500,000. Thus, we can be sure that the flow on the model is turbulent even in low Reynolds. Apart from that, providing Reynolds equal to one millions is not difficult and is not out of access because the kinematic viscosity coefficient is about 0.000001 that it means, for example, in a model with 1 meter length, and speed of 1 m/s the Reynolds equals to one millions.

Note 2: Variation of the curves of frictional resistance coefficient and viscous pressure resistance coefficient after critical Reynolds (turbulent current) is almost horizontal, and shows the constant coefficient. Total resistance in fully submerged mode is equal to frictional resistance plus viscous pressure resistance. Schematic curve of variation is shown in Figures 1 and 2. The diagram of variations of frictional resistance coefficients versus Reynold's number for pipes is presented in all fluid dynamic books as "Moody diagram" thus it is an accepted obvious origin. This chapter wants to prove that this origin can be extended to be used in fully submerged resistance of submarine. For this purpose C_f and C_{vp} diagrams versus Reynolds are plotted for three analyses. These diagrams will show that "after a special Reynolds, these coefficients are almost constant".

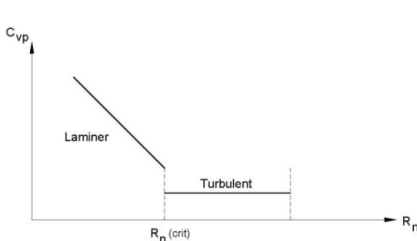


Figure 1: Schematic variations of the viscous pressure resistance coefficients versus Reynold's number

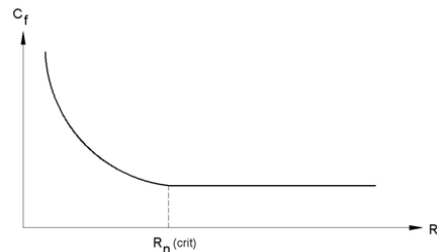


Figure 2: Schematic variations of the frictional resistance coefficients versus Reynold's number

Note 3: The variations of resistance coefficients versus Reynold's number are independent of the geometry and the shape of objects. For proving this concept, the three samples have the different shape from each other.

In the next section, the results of analysis of three studied cases are presented that contains two cases by CFD method and one case by experimental test in towing tank.

Many extensive studies have been done about resistance (drag) in aerospace engineering such as Ref [16], but none of them didn't any suggestion for developing the model test results to main object for submerged vehicles. Critical Reynolds depends on the shape of object, velocity and environment. There are main differences between specifications of marine and aerial vehicles such as sharp nose, sub and super sonic speed and compressibility of air. Our focus in this chapter is finding a critical Reynolds for developing the result of the model to the main vehicle for marine crafts. The references [6,14-17] are the main references of this chapter.

12-1-2- connection of model and strut

12-1-2-1- At deeply submerged depth

As mentioned in chapter 10, for modeling the deeply submerged depth and eliminating the wave making of the main body, the height of the strut should be more than $4.5D$. Maximum height of strut should not be more than $7D$ because of vibrations imposed by the strut. Towing tank depth and bottom effect may be another limitation. Therefore, the acceptable range of strut height is $4.5D \sim 7D$. The model should be tested inverted for: 1- reducing the interference between strut and sailing. 2- reducing the wave making effect of sailing (Fig.3).

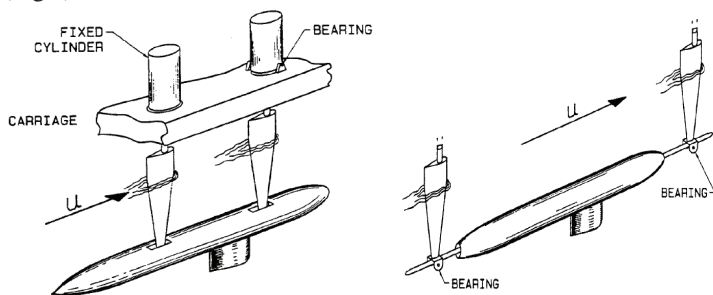


Figure 3: Deeply submerged model test [15]

12-1-2-2- At snorkel depth

The estimation of resistance and power at snorkel depth is vital for submarine operation because the submarine is charging the batteries. In this condition, real and exact estimation of power is necessary for calculation of Indiscretion Ratio (IR). For estimating the snorting time, needs to know total power includes hotel load and propulsion power. At snorkel depth, there is a stockish mast with a large diameter for intaking the fresh air. For more real test condition, the strut can be connected exactly at the position of the mast with the same scaled diameter (Fig.4). Pay attention to the upright condition of the sailing (not inverse) similar to real condition. If there are some inappropriate vibrations, the second strut can be situated at the after part of the body (Fig.4).

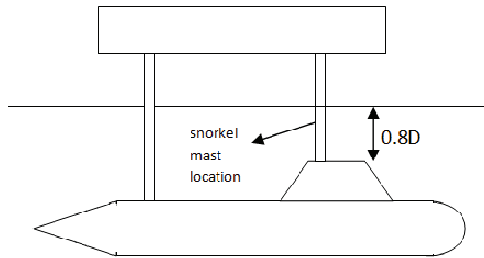
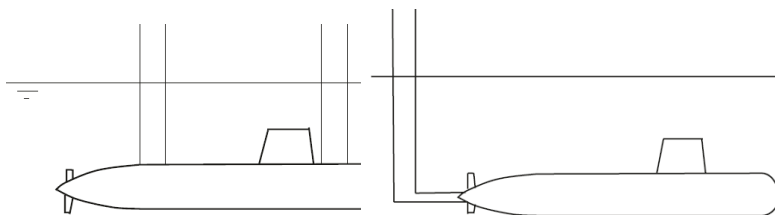


Figure 4: Model test at snorkel condition

Other positions of connections are shown in Fig.5 [14].



(a) Two strut system

(b) Aft sting system

Figure 5: Other position of connections [14]

In two strut system there is the problem of interference between strut wake flow and sailing flow which may cause inaccurate results for resistance but

fewer vibrations. The aft sting system is better for wake interference but worse for vibrations. Another approach for determining the resistance of a deeply submerged submarine is to make use of a wind tunnel [14] (Fig.6) . The advantages of the wind tunnel are: 1) It may be possible to obtain a higher Reynolds number in a wind tunnel than a towing tank 2) There is not free surface effect and wave making resistance. 3) Better flow visualization.

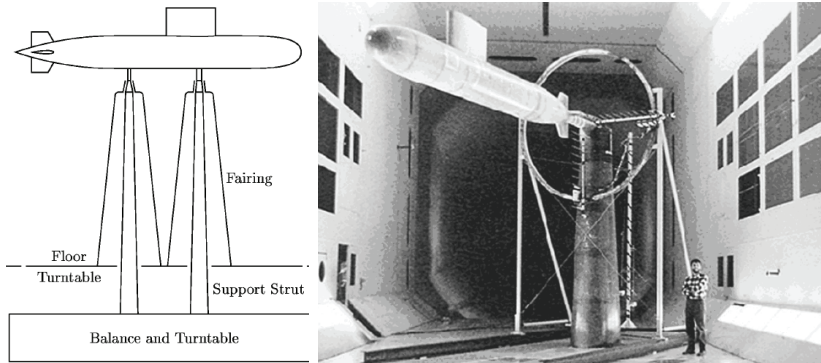


Figure 6: Submarine model test in towing tank (Two strut arrangement) [15]

12-1-3- Case Study

Case 1: CFD analysis for a submarine

The dimensions of the submarine are presented in Figure 7, and The modeling in Flow Vision is shown in Figure 8. Wetted area is 29.27 m^2 and the specifications of fresh water are considered. According to Iranian Hydrodynamic Series of Submarines (IHSS) the code of this shape is: IHSS.1001565-30108025. Therefore, the foil section of the tower is NACA0025.

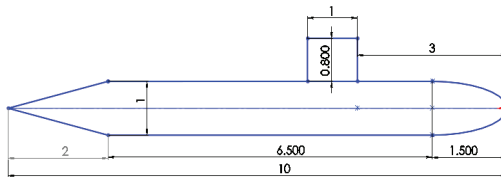


Figure 7: Dimensions of the model in case 1

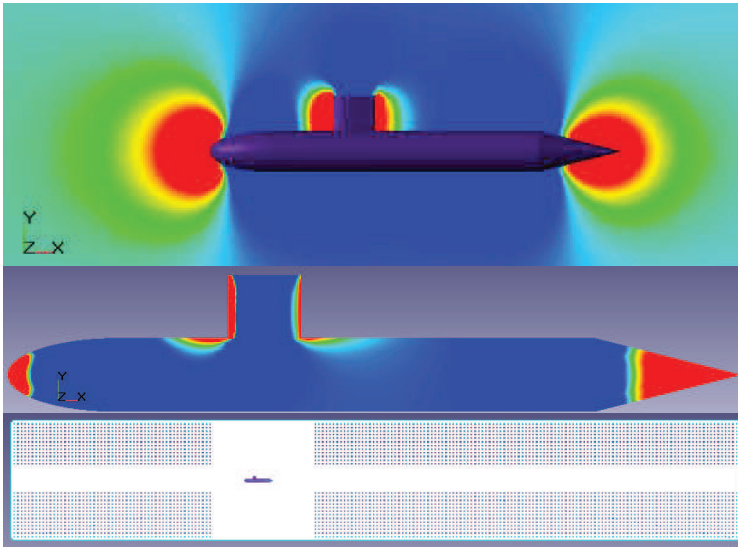


Figure 8: Modeling of case 1 in the Flow Vision software

Results are presented in Table 1, and the diagram is shown in Figures 9 and 10.

Table 1: Total resistance coefficient of case 1 by CFD method

V (m/s)	Resistance (N)	Rn	Cd
1	182.5	10000000	0.012470106
1.5	305.17	15000000	0.009267585
2	524.84	20000000	0.008965494
2.5	800.91	25000000	0.008756105
3	1136	30000000	0.008624682
5	2742	50000000	0.007494363
7	5544	70000000	0.007730978
9	9309	90000000	0.007852814
11	13738	110000000	0.007757922
13	18995	130000000	0.007679976
15	25034	150000000	0.007602475
17	31951	170000000	0.007554294

Table 2: Viscous pressure resistance coefficient of case 1 by CFD method

V (m/s)	Resistance (N)	Rn	Cd
1	99.3	10000000	0.006785104
1.5	106.48	15000000	0.003233648
2	187.8	20000000	0.003208063
2.5	292.11	25000000	0.00319355
3	456	30000000	0.00346202
5	1245	50000000	0.003402802
7	2575	70000000	0.003590777
9	3717	90000000	0.003135558
11	5562	110000000	0.003140891
13	7762	130000000	0.003138298
15	10274	150000000	0.00312007
17	13195.8	170000000	0.003119932

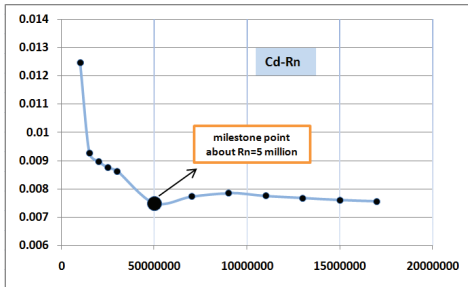


Figure 9: The diagram of variations of total resistance coefficients versus Reynold's numbers in case 1

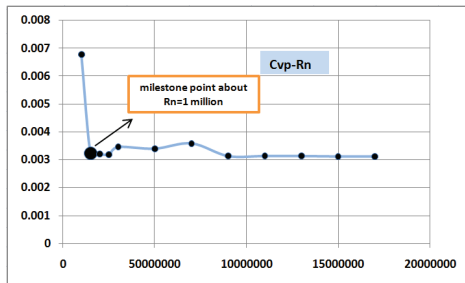


Figure 10: The diagram of variations of viscous pressure resistance coefficients versus Reynold's numbers in case 1

Study on the results shows that for the total resistance coefficient, there is a millstone in Reynolds 5 millions because after this point, the variations are less than 5% (in maximum) that meant almost constant resistance coefficient after this Reynolds. The diagram of variations of viscous pressure resistance coefficients versus Reynolds, shows a millstone after Reynolds 1 millions. In both above-mentioned diagrams, there is a local hump around Reynolds 8 millions.

Case 2: CFD analysis for a torpedo

The specifications of the model are shown in Figure 11. All modeling conditions are as mentioned in case 1. Wetted area is 7.87 m² and the specifications of fresh water are considered. According to Iranian Hydrodynamic Series of Submarines (IHSS) the code of this shape is: IHSS.8336058.

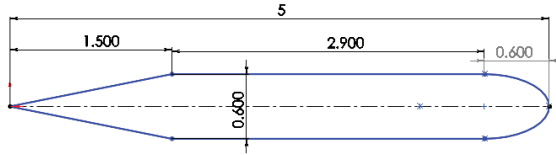


Figure 11: Dimensions of model in case 2

Results are presented in Table 3, and the diagram is shown in Figure 12 and 13.

Table 3: Total resistance coefficient of case 2 by CFD method

V (m/s)	Resistance (N)	Rn	Cd
0.05	0.092	250000	0.00935197
0.2	1.33	1000000	0.008449809
0.5	6.78	2500000	0.006891995
1	23.83	5000000	0.006055909
2	89.1	10000000	0.005660737
4	342	20000000	0.00543202
6	756	30000000	0.005336722
8	1297	40000000	0.005150095
10	1970	50000000	0.005006353
12	2836	60000000	0.005004941
14	3803	70000000	0.004930892
16	4950	80000000	0.004913834
18	6250	90000000	0.004902191
20	7595	100000000	0.004825286
26	13124	130000000	0.004933723

Table 4: Viscous pressure resistance coefficient of case 2 by CFD method

V (m/s)	Resistance (N)	Rn	Cd
0.05	0.042	250000	0.00426938
0.2	0.65	1000000	0.00412961
0.5	3.18	2500000	0.00323253
1	11.1	5000000	0.00282084
2	43.7	10000000	0.00277637
4	179.8	20000000	0.00285578
6	397.5	30000000	0.00280601
8	713.4	40000000	0.00283275
10	1094	50000000	0.00278018
12	1598	60000000	0.00282013
14	2156	70000000	0.00279543
16	2835	80000000	0.00281429
18	3650	90000000	0.00286288
20	4401	100000000	0.00279606
26	7750	130000000	0.00291347

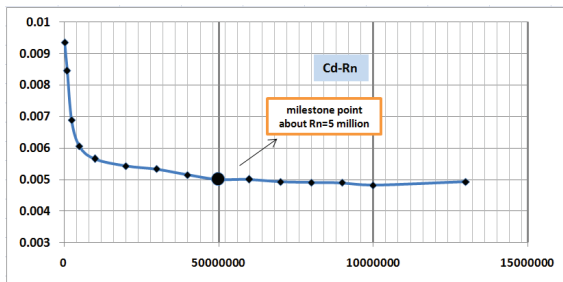


Figure 12: The diagram of variations of total resistance coefficients versus Reynold's numbers in case 2

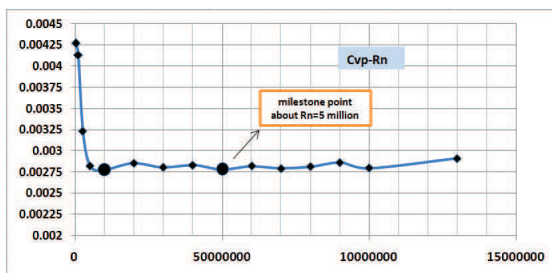


Figure 13: The diagram of variations of viscous pressure resistance coefficients versus Reynold's numbers in case 2

Study on the results shows that for the total resistance coefficient, there is a millstone in Reynolds 5 millions because after this point, the variations are less than 4% (in maximum) that meant almost constant resistance coefficient after this Reynolds. The diagram of variations of viscous pressure resistance coefficients versus Reynolds, shows a millstone after Reynolds 1 and 5 millions. Such as mentioned formerly in case 1, here in both diagrams, there is a local hump around Reynolds 9 millions.

Case 3: model tests in towing tank

Experiments were conducted in the marine laboratory of Isfahan University of Technology (IUT) in Iran. The towing tank has 108(m) length, 3 (m) width and 2.2 (m) depth. The basin is equipped with a trolley that can operate in through 0.05-6 m/s speed that moves by two 7.5 KW electro-motors with ± 0.02 m/s accuracy. The system is prepared with a proper frequency encoder, i.e., 500 pulses in a minute, which decreases the uncertainty of measurements. The dynamometer was calibrated by calibration weights. A three degree of freedom dynamometer is used for force measurements. Data are recorded via an accurate data-acquisition system. The dynamometer is equipped with 100 N load cells. An amplifier set is used to raise signals of load cells and to reduce the noise sensitivity of the system. The experiment is conducted with a submarine model that is made by wood materials according to ITTC recommendations. Tango nose submarine is a type of submarine that has been tested in underwater mode. All data are filtered to eliminate the undesirable acceleration, primary and terminative motion of trolley. The trolley was controlled in a wireless system from control room of lab. For each run, at least 750 samples in 15 seconds were collected and the ensemble averaged. Schematic of the model and the overall test stand is shown in Figure 14.

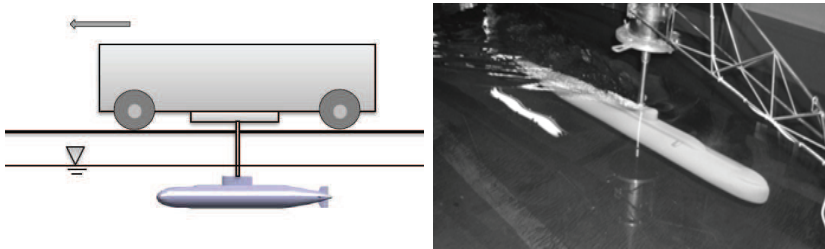


Figure 14: Schematic shape of the test stand

Dimensions of studied submarine in this chapter are shown in Table 5 with parallel middle body form. Relation L/D is equal to 8.88. Hull bow has Tango shape and stern is conical. Main submarine has a deck with 28 meters of length, 0.4 meters of height and 1 meter of the beam. In addition; it has a conning tower of 3.2 meters length and 3 meters of height on top of the main hull. Maximum submerged speed is 14 knots, and the wetted surface area is 450 square meters. All dimensions of this submarine have been scaled by 1:32.

Table 5: Main Submarine Dimensions (meter)

Overall length (m)	32
Hull diameter (m)	3.6
Displacement (t)	235
Bow length (m)	5
Cylinder length (m)	21
Conical stern length (m)	6
Conical stern Angle (deg)	16.7

Table 6: Results of model test in towing tank

V	Rn	Cd
0.2	200000	0.0065
0.5	500000	0.004293
0.6	600000	0.004119
0.7	700000	0.004201
0.8	800000	0.004177
0.9	900000	0.004047
1	1000000	0.004
1.1	1100000	0.003999
1.2	1200000	0.004011
1.3	1300000	0.003949
1.4	1400000	0.003883
1.5	1500000	0.003842

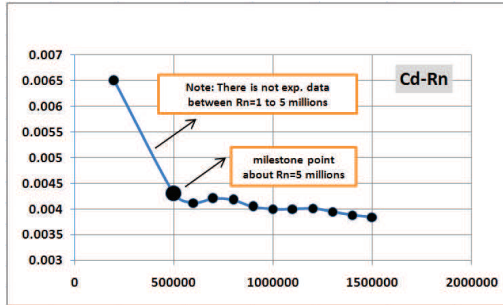


Figure 15: The diagram of variations of resistance coefficients versus Reynold's numbers for model test in towing tank

By study on the experimental results, it is shown that for the total resistance coefficient, there is a millstone in Reynolds 5 millions because after this point, the variations are less than 5.1% (in maximum) that meant almost constant resistance coefficient after this Reynolds. In experimental results, such as mentioned for CFD results, there is a local hump around Reynolds 7-8 millions.

12-1-4- Analysis and Conclusion

In this chapter, a practical solution was presented for solving an old problem about developing the results of the experimental model to the full-scale submarine in fully submerged mode. In every experimental test, in the first step, the speed of the model should be developed to full-scale submarine. In the second step, the obtained resistance of the model should be developed. The main problem is providing the speed of the model in the laboratory, based on Reynold's similarity. It leads to a very high and impossible speed for model. Based on the findings of this chapter, if the Reynolds of submarine at submerged test be more than 5,000,000 it can be actually supposed that total resistance coefficient of the model and full-scale submarine is equal ($C_{TS}=C_{Tm}$) for every speed in the region of the mentioned Reynolds. It means that the both problems for finding "corresponded speed" and "related resistance coefficient" were simultaneously solved. For Reynold's number 5,000,000, the error of this assumption can be less than 5 percent. If providing this Reynolds be difficult, setting some wire or pin on the bow, can be used for providing turbulent flow. Furthermore, many other ways to providing turbulent flow can be used. In every method that we be confident about turbulent flow, the total resistance coefficient is constant in every related speed. For example, in case 3, for full-scale submarine with length 32 meters, in every speed greater than 0.16 m/s, the Reynold's number is more than

5,000,000 thus the flow regime is certainly turbulent. According to the model test results, in all speeds larger than 0.5 m/s the Reynolds are more than 5,000,000 with constant total resistance coefficients equal to 0.004. Therefore, for full-scale submarine for every speed more than 0.16 m/s, we can suppose that total resistance coefficient is constant and equal to 0.004. It should be noted that the maximum speed of the model which was tested was only 1.5 meters that are easily possible for doing.

Another interesting subject, is unexpected local hump in the resistance coefficient diagram in Reynold's number of about 7-9 millions. This phenomenon is seen in both CFD and experimental results but now, there is not any scientific reason for that.

We can summarize the findings of this chapter as below (Fig.15):

- 1- Total resistance coefficient after Reynolds 5,000,000 is almost constant.
- 2- There is not any need for high speed for model test in towing tank because "corresponding speed" (such as in ship model and based on Froude's law) doesn't define here. On the other hand, Reynold's similarity for finding "corresponding speed" is an unnecessary process.
- 3- There is a local hump in the resistance coefficient diagram in Reynold's number of 7-9 millions.

12-2- Technical notes on the near surface experiments of submerged submarine

12-2-1- Model

In this study a torpedo shaped submersible (Persia110) is considered. The general form and dimensions of this model is shown in Fig.16. This model is fixed and doesn't have DOF. This model is the same in CFD method and experiments in towing tank. The model has a volume of 8.38 liters, total area of 0.36 m², wetted area in the surface draft of 0.26 m² and weight of 8.38 kg. Surface draft is equal to 80mm from beneath the hull and 20mm freeboard. The ratio of L/D is 13 which is inside the range of usual L/D of large naval submarines.

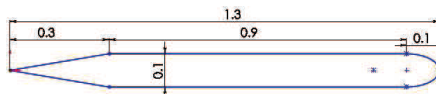


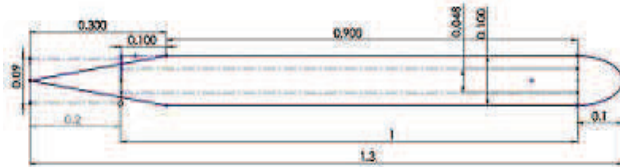


Figure 16: General configuration of the model dimensions of Persia-110 [in meter]

The material density of the model should be near the density of water for earning the natural buoyancy in submerged condition. Fiberglass and wood could not be a good selection because of imposing a stiff positive buoyancy on the dynamometer. Kapralon could be a excellent suggestion because of: 1) density of 1.01~1.15. For adjusting the density to the water density, the internal part of the model could be carved according to Fig.17) water tight material 3)easy carving properties. 4) cylindrical traditional form which is similar to the body shape of submarine (Fig.17) and 5)smooth surface.



(a) Traditional cylindrical form of Kapralon



(b) Carving the interior part of Persia-110

Figure 17: Kapralon material for body construction

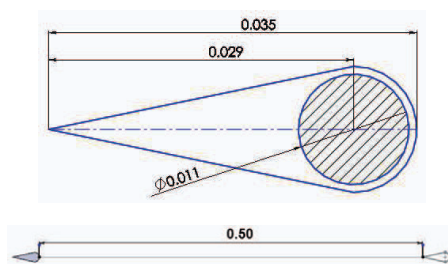
For conducting the test, two general conditions are considered: 1) surface draft of 90mm. 2) near the surface: depth of 100mm from water level to the top of the body (equal to depth of the strut). Froude numbers are considered according to Tab.7. As mentioned above, the usual range of Froude number of submarines are between 0.2 to 0.24 but here, a wider range is studied. In submerged test, the extracted values more than 1 m/s have encountered a problem because of the severe vibrations in high speeds in struts. Therefore, the diagrams of underwater test are represented for values less than 1 m/s.

	V(m/s)	Fn
1	0.196	0.05
2	0.296	0.08
3	0.393	0.11
4	0.492	0.14
5	0.604	0.17
6	0.705	0.20
7	0.803	0.22
8	0.899	0.25
9	0.996	0.28
10	1.397	0.39
11	1.598	0.45
12	1.801	0.50

12-2-2- Strut

The cross section of the strut is a foil shape as shown in Fig.18-a. Distance between struts is 0.5 meter. More studies have shown that this foil section could not be a good design because of resistance and vibrations. The reason is the existence of free surface effects and the role of wave making resistance. In

the wind tunnel, because of absence of free surface, symmetric NACA00 foil sections usually are used. Two struts with foil shape form impose about 45% of total resistance. Inversed foil shape struts imposes about 35% resistance. Figure 18-b shows a recommended shape of cross section of the strut similar to water plane of ships which two struts of them, impose approximately 25% of total resistance. If a one strut arrangement could be used, it would have a resistance less than 20%. Therefore, the foil section such as Fig.18-a can be the worst selection which should be avoided. A reasonable acceptable range of resistance of struts could be about 30% of total resistance.



(a) Struts of Persia-110

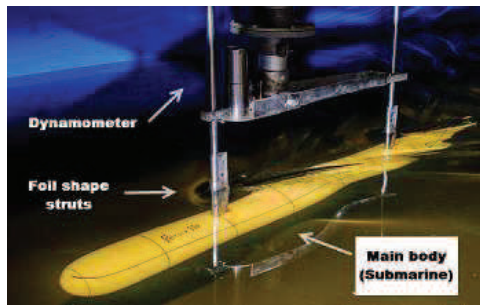


(b) Recommended foil section of strut

Figure 18: Cross section of struts

12-2-3- Towing Tank

Experimental tests have been performed on the model Persia-110 in the towing tank of Admiral Makarov University, which has 33(m) length, 2.5 (m) width and 1.3 (m) draft (Fig.19). The basin is equipped with a trolley that able to operate in 0.05-6 m/s speed with ± 0.02 m/s accuracy. A three degree of freedom dynamometer is used for force and moment measurements. The dynamometer was calibrated by calibration weights and several case studies. The model is fixed without any DOF. The test is in still water and water inside the tank is fresh water.



(a) Marine laboratory of Admiral Makarov University



(b) Model Persia-110 according to specifications of Fig.2
Figure 19: Towing tank and model Persia-110

12-2-4-Experimental results

12-2-4-1- At surface draft

The experimental results at the surface draft are presented in Fig.20. It shows a range of 0.012~0.016 for the resistance coefficient in common Froude

numbers at the surface draft. All values of resistance coefficients in this chapter are based on wetted area.

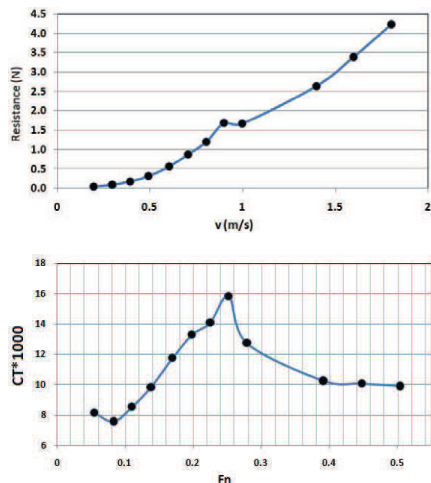


Figure 20: Resistance and resistance coefficient of persia-110 at surface draft

12-2-4-2- At snorkel draft

Estimating the resistance of the bare hull of submarine at snorkel depth (100mm) is to some extent more difficult than the surface draft. For extracting the submarine resistance, in first stage, submarine with struts are tested. In second stage, only the struts are tested. The results are shown in Tab.8. At first glance it seems that submarine resistance could be achieved from subtraction of second and third columns of Table 8 but it can't be a right estimation. It is because of the existence of induced resistance of tips of struts. For estimating this induced resistance we have to use CFD method.

Table 8: Resistance in depth of 100mm

V (m/s)	Sub & Struts (N)	Struts (N)
0.196	0.09	0.03
0.296	0.19	0.06
0.393	0.32	0.10
0.492	0.48	0.19
0.604	0.69	0.25
0.705	0.91	0.31
0.803	1.17	0.41
0.899	1.47	0.53
0.996	1.87	0.69

12-2-5- Estimation of induced resistance by CFD method

In this section the focus is on the estimation of induced resistance of struts. In this research, the dynamic pressure fluctuation has been investigated by a commercially available CFD solver, Flow-3D, developed by Flow ScienceInc. The modeling is done in one depth of 100mm from top of the body to the water level. The considered speeds are exactly according to the model test speed. The nine speeds are (m/s): 0.196, 0.296, 0.393, 0.492, 0.604, 0.705, 0.803, 0.899 and 0.996. In every speed three main parts are modeled: 1) submarine and struts 2) only submarine 3) only struts (Figure 21):

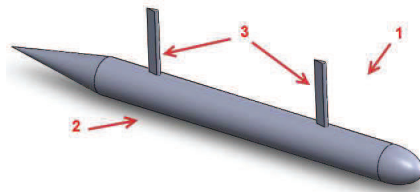
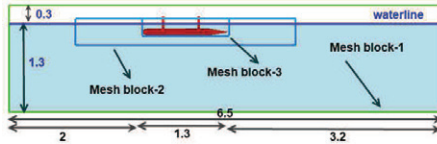


Figure 21: Three main conditions of Modeling

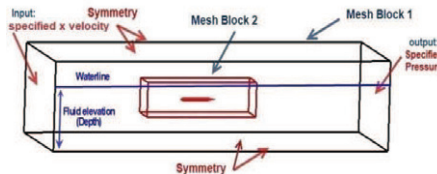
The general configurations and dimensions of domain are shown in Fig.22. The length and width are 6.5 and 2.6 meters. Depth is 1.6 meters (1.3meters draft). The boundary conditions are: Input: specified velocity, Output: Specified pressure and other sides are symmetry. The model is situated in depths of 100mm according to Fig.22.a,b. There are three mesh block: one block for the total domain with coarse meshes and other two blocks for fine meshes around the struts and object body. The accuracy of the modeled shape of the struts and body depends on the fine meshes because of small dimensions of struts (Fig.22.c,d). The other settings of CFD modeling are presented in Table 9.

Table 9: Settings of CFD simulation

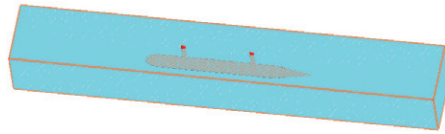
Elements	Boundary conditions	Descriptions	
Domain	Cubic	conditions	with free surface - domain with inlet, outlet and symmetry - without heat transfer- with current velocity equal to considered submarine speed
		dimensions	$L*B*D=6.5*2.6*1.6$ m- draft 1.3 m
		grid	structured grid- hexahedral cells-without skew- three mesh block- more fine meshes in mesh block 3 around the struts and main body- Mesh numbers: 1000.000 in mesh block1, 1000.000 in mesh block2, 500.000 in mesh block3, aspect ratio 1 in each block, expansion factor 1 in each block, expansion factor between blocks less than 2.
		settings	Simulation time: 10 sec- Time step=0.0003-0.0005 sec
Fluid	-	Incompressible fluid (fresh water)- temprature:20 deg- $\rho=999.841$ kg/m ³ - turbulent modeling: Standard k- ϵ	
Object	GMO	Submarine, length:1.3m, Diameter:0.1, DOF =0	
Boundaries	Inlet	Specified velocity (different for each submarine speed), mean fluid depth 1.3 m	
	Outlet	Specified pressure (Specified fluid level: 1.3 m)	
	Symmetry	In 4 faces	
Initial conditions		Fluid level: 1.3 m, velocity (m/s): equals to specified velocity in Inlet	



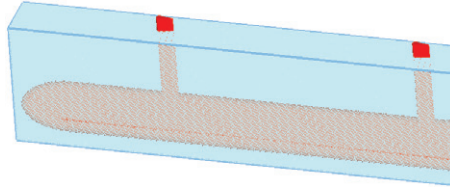
(a) Dimensions of Domain (in meter)



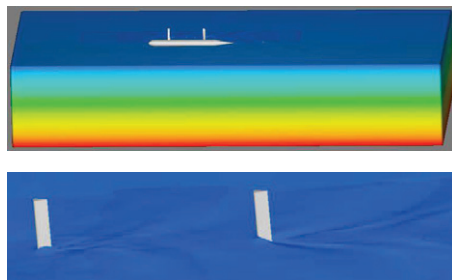
(b) Boundary conditions in domain



(c) Fine meshes in Mesh Block2



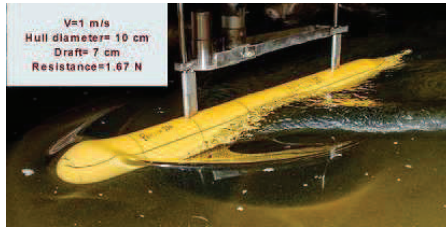
(d) Very fine meshes in Mesh Block 3



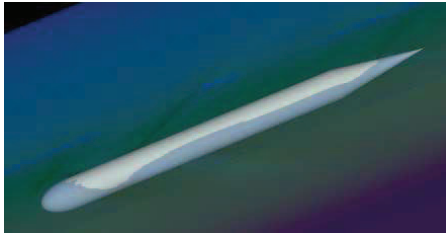
(e) Free surface modeling

Figure 22: Domain and Boundary Conditions in Flow-3D

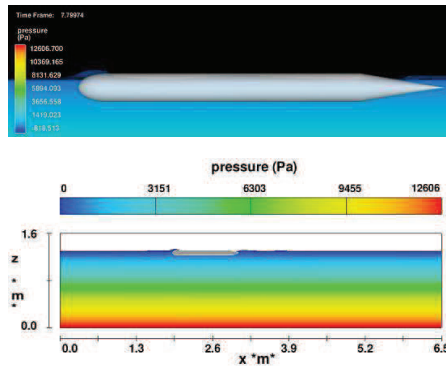
For validating the results of Flow-3D modeling, one of the results of experimental tests has been considered on the model Persia-110 (Fig.23). The experiment was performed in surface condition at the draft of 8 cm and speed of 1 m/s. The CFD modeling (Fig.23) was adjusted exactly according to the experimental conditions. Comparison of Fig 23-a and Fig 23-b shows a excellent agreement between experimental and CFD results. The form of free surface has a good compatibility. The resistance of the model in CFD method is shown in Fig.24 and the comparison with the resistance in these conditions is represented in Tab.10.



a) Test in the surface draft of 7 cm and speed of 1 m/s



(b) CFD modeling in the same conditions of experiment



(c) General configuration of analysis in Flow-3D for the model

Figure 23: Comparison of the results of the experiment and CFD method (Flow-3D)

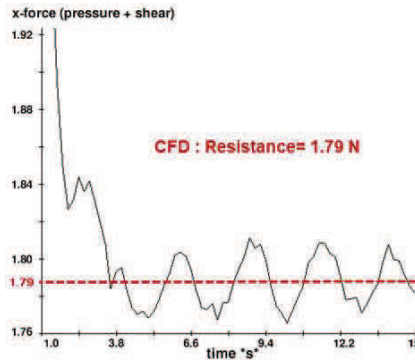


Figure 24: Total resistance in CFD method for case study validation

Table 10: Comparison of resistance

Resistance in experiment	1.67 (N)
Resistance in CFD	1.79 (N)
Difference	6.6 %

The difference of about 6.6 percentages is reasonable and acceptable. This validation case clearly shows the capability of a CFD tool, Flow-3D to reasonably predict the hydrodynamic problems of incompressible flow. The results of CFD modeling for resistance are presented in Tab.11. Column 1 shows the resistance of submarine with strut (R_T) and column 2, shows the resistance only for the strut (R_S) plus induced resistance (R_i) of the strut. The column 3 is the difference of column 1 and 2 which should be equal to the resistance of the body of submarine (R_B). It could be written as: $R_T = (R_S + R_i) + R_B$. Induced resistance usually happens because of tip vortex effects of struts, which is an undesirable parameter and should be eliminated from the results. It meant that for achieving the net resistance of submarine hull, the induced resistance should be eliminated. As induced resistance is dependent on the struts, for a fair estimation, it can be stated as a percentage of the resistance of the strut. Column 4 shows the resistance of submarine without struts. Column 3 is smaller than column 4, because of existence of tip induced resistance of alone struts. When the struts stand on the body in experiment or CFD, the tip vortex would be eliminated. For solving the problem, by omitting the induced resistance in column 2, the values in column 3 will be increased

and will be closer to values of column 4. As the result, the comparison of column 2 and 5 clarifies the role of induced resistance as approximately 70% of alone strut resistance (column 2) i.e: $R_i=0.7(R_s+R_i)$. Consequently, the modified results are applied on Tab.7. Application of this correction shows a good compatibility between column 3 and 4 in Tab.12.

Table 11: Initial CFD results of resistance

	(1)	(2)	(3)=(1)-(2)	(4)	(5)=(4)-(3)
V (m/s)	R_T (N)	R_s+R_i (N)	Difference (N)	R_B (N)	R_i (N)
0.2	0.20	0.02	0.18	0.22	0.04
0.3	0.30	0.04	0.27	0.29	0.02
0.39	0.41	0.11	0.29	0.38	0.09
0.49	0.54	0.18	0.37	0.50	0.13
0.60	0.75	0.26	0.49	0.70	0.21
0.71	0.98	0.34	0.64	0.90	0.26
0.80	1.27	0.45	0.82	1.19	0.37
0.9	1.61	0.55	1.06	1.44	0.38
1	2.10	0.68	1.42	1.95	0.53

Table 12: Modified CFD results of resistance

		(1)	(2)	(3)=(1)-(2)	(4)
	V (m/s)	Sub & Strut (N)	Modified Strut results (N)	Difference (N)	Submarine Only (N)
1	0.2	0.20	0.01	0.20	0.22
2	0.3	0.30	0.01	0.29	0.29
3	0.39	0.41	0.03	0.37	0.38
4	0.49	0.54	0.05	0.49	0.50
5	0.6	0.75	0.08	0.67	0.70
6	0.71	0.98	0.10	0.88	0.90
7	0.8	1.27	0.13	1.13	1.19
8	0.9	1.61	0.17	1.44	1.44
9	1	2.10	0.20	1.90	1.95

12-2-6- Discussion

Now the earned results of CFD modeling for the effect of induced resistance should be applied on the experimental results. Therefore, the induced resistance is eliminated by considering the 30% of initial values of strut resistance (Tab.13). The comparisons of the results of submarine bare hull resistance by CFD and experimental methods are presented in Fig.25. It shows some differences in low Froude numbers but a good adjustment in the usual range of Froude of submarines. In this range, the differences are between 7 to

9 percent. The reason of differences in low Froude numbers could be related to the laminar flow on the hull and absence of turbulator wire in CFD modeling. In experiments, there is a turbulator wire in the fore part of the body. For generalizing the results, resistance coefficients should be presented. These values are shown in Fig.26. In the usual Froude numbers (0.2~0.24) the resistance coefficient of bare hull of submarine with $L/D= 13$ (as usual in large submarines) at the surface draft is in the range of 0.012~0.016 and in snorkel depth (depth equal to D) is in the range of 0.009~0.01.

Table 13: Modified experimental results

V (m/s)	Sub & Strut (N)	Strut (N)	Modified strut results (N)	Submarine Bare hull (N)
0.196	0.09	0.03	0.01	0.08
0.296	0.19	0.06	0.02	0.17
0.393	0.32	0.10	0.03	0.29
0.492	0.48	0.19	0.06	0.42
0.604	0.69	0.25	0.08	0.62
0.705	0.91	0.31	0.09	0.82
0.803	1.17	0.41	0.12	1.04
0.899	1.47	0.53	0.16	1.31
0.996	1.87	0.69	0.21	1.67

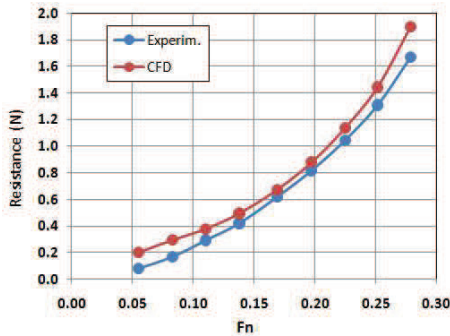


Figure 25: Comparison of the results of submarine bare hull resistance by CFD and experimental methods

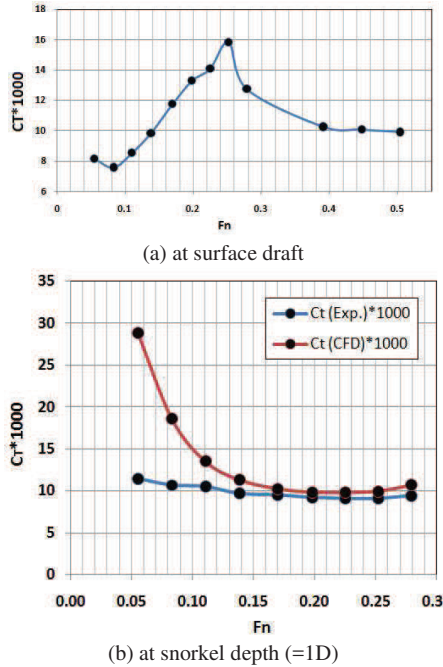


Figure 26: Resistance coefficients at surface draft and snorkel depth

12-2-7- Review

This chapter presented some technical notes for conducting the submarine model test in towing tank at near surface depth. Induced resistance between struts and hull is an important factor which should be evaluated exactly. This induced resistance could be considered 70% of resistance of alone struts with tip vortex effects. For a fair estimation, in the usual Froude numbers (0.2~0.24) the resistance coefficient at the surface draft is in the range of 0.012~0.016 and in snorkel depth (depth equal to D) is in the range of 0.009~0.01. The cross section of struts for underwater test should be similar to water plan of ships. Foil shaped symmetric NACA shapes couldn't be a good advice because of large resistance and vibrations. Kapralon material has good properties for the construction of the submarine body for underwater tests.

Nomenclature

A_w	Wetted area surface (m^2)
C_d	Total resistance coefficient
C_f	Frictional resistance coefficient
C_{vp}	Viscous pressure resistance coefficient
C_t	Total resistance coefficient based on wetted area. $C_t = R_t / (0.5 \rho A V^2)$
CFD	Computational Fluid Dynamics
D	maximum diameter of the outer hull [m]
DOF	Degree Of Freedom
Fn	Froude number - $Fn = V / \sqrt{g \cdot L}$
$(Fn)_M$	Froude number of model
$(Fn)_S$	Froude number of submarine
GMO	General Mobile Object
h	depth from water level to the top of the submarine body [m]
H^*	dimensionless depth (h/D)
IHSS	Iranian Hydrodynamic Series of Submarines
L	overall length of hull [m]
L_M	Total length of model (m)
L_S	Total length of submarine (m)
R_T	resistance of submarine with strut [N]
R_S	resistance only for strut [N]
R_B	resistance of body of submarine [N]
R_i	induced resistance [N]
$(Re)_M$	Reynolds of Model
R	Total resistance (N)
R_f	Frictional resistance (N)
R_{vp}	Viscous pressure resistance (N)
$(Re)_S$	Reynolds of submarine
V_M	Speed of model (m/s)
V_S	Speed of ship (m/s)

* Other parameters are shown on the figures or described inside the text.

References

- [1] K.J.Rawson, E.C.Tupper, Basic Ship Theory, Jordan Hill., Oxford, 2001.
- [2] H.A.Jackson, Submarine Design Notes, Massachusetts Institute of Technology,1982.
- [3] M.Moonesun, Handbook of Naval Architecture Engineering, Isfahan, Kanoon Pajohesh, 2009.
- [4] E.V.Lewis, Principles of Naval Architecture, Second Revision, Volume II • Resistance, Propulsion and Vibration, The Society of Naval Architects and Marine Engineers (SNAME), 1988.
- [5] V.Bertram, Practical Ship Hydrodynamics, UK, Elsevier Ltd, 2000.
- [6] M.Moonesun, M.Javadi, P.Charmdooz, U.M.Korol, "Evaluation of submarine model test in towing tank and comparison with CFD and experimental formulas for fully submerged resistance", Indian Journal of Geo-Marine Science, vol.42(8), December 2013, pp.1049-1056.
- [7] Chong-Ku Hah. Lee-Young Lim, Jae-Seok Ki, "Hydrodynamic evaluation for developing the inflatable kayak", Journal of the Korean Society of Marine Engineering, Vol. 37, No. 6 pp. 623~630, 2013.
- [8] Min-Su Kim, Kang-Su Lee, "Hydrodynamic force calculation and motion analysis of OC3 Hywind floating offshore platform", Journal of the Korean Society of Marine Engineering, Vol. 37, No. 8 pp. 953~961, 2013.
- [9] Dong.Jin.Yeo, Key.Pyo.Rhee, "A Study on the Sensitivity Analysis of Submersibles' Maneuverability", Journal of the Society of Naval Architects of Korea, Volume 42, Issue 5, pp.458-465, 2005.
- [10] Yong.Ku.Shin, Seung-Keon Lee, "A Study on the Modeling of Hydrodynamic Coefficient for the Emergency Maneuver Simulation of Underwater Vehicle", Journal of the Society of Naval Architects of Korea , Volume 42, Issue 6, pp.601-607, 2005.
- [11] Dong Jin Yeo, Hyeon Kyu Yoon, Yeon Gyu Kim, Chang Me Lee, "A Research on the Mathematical Modeling for the Estimation of Underwater Vehicle's Tail Plane Efficiency", Journal of the Society of Naval Architects of Korea, Volume 42, Issue 3, pp.190-196, 2005.
- [12] V.Bertram, Practical Ship Hydrodynamics, Butterworth-Heinemann Linacre House, Oxford, page 65, 2000.
- [13] A.F.Molland, S.R.Turnock, D.A.Hudson, Ship Resistance and Propulsion, Cambridge University Press, page 14,2011.
- [14] Renilson, M., (2015), Submarine Hydrodynamics, Springer.
- [15] M.Mckay, The standard submarine model: a survey of static hydrodynamic experiments and semiempirical predictions, Defence R&D Canada, 2003.
- [16] S.F.Hoerner, Fluid Dynamic Drag, USA, 1965.
- [17] Monesun, M., Korol, Y.M., Tahvildarzade,D. and Javadi,M. (2014), Practical scaling method for underwater hydrodynamic model test of submarine, Journal of the Korean Society of Marine Engineering, Vol. 38, No. 10 pp. 1217~1224, URL: <https://sites.google.com/site/jkosme76/archives/back-issues>.

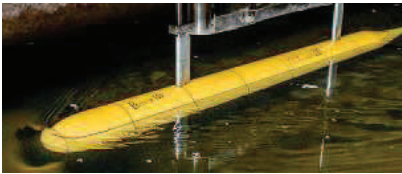
Appendix A: Wave form in surface draft



$V=0.2 \text{ m/s}$ ($F_n=0.05$)



$V=0.3 \text{ m/s}$ ($F_n=0.08$)



$V=0.39 \text{ m/s}$ ($F_n=0.11$)



$V=0.49$ ($F_n=0.14$)



$V=0.6 \text{ m/s}$ ($F_n=0.17$)



$V=0.7 \text{ m/s}$ ($F_n=0.2$)



$V=0.8 \text{ m/s}$ ($F_n=0.22$)



$V=0.9 \text{ m/s}$ ($F_n=0.25$)



V= 1 m/s (Fn=0.28)



V= 1.4 m/s (Fn=0.39)



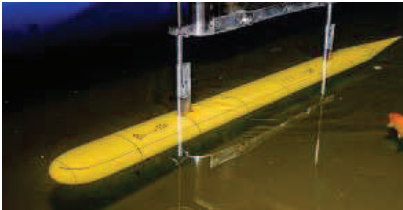
V= 1.6 m/s (Fn=0.45)



V= 1.8 m/s (Fn=0.5)



Appendix B: Wave form in snorkel draft: 100mm



V=0.2 m/s (Fn=0.05)



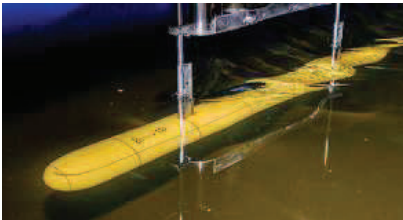
V=0.3 m/s (Fn=0.08)



V=0.39 m/s (Fn=0.11)



V= 0.49 (Fn=0.14)



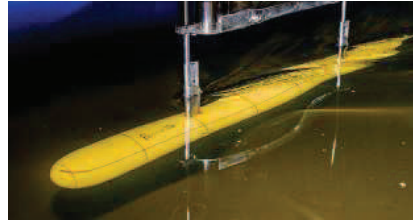
V= 0.6 m/s (Fn=0.17)



V= 0.7 m/s (Fn=0.2)



V= 0.8 m/s (Fn=0.22)



V= 0.9 m/s (Fn=0.25)



V= 1 m/s (Fn=0.28)



V= 1.4 m/s (Fn=0.39)



V= 1.6 m/s (Fn=0.45)



V= 1.8 m/s (Fn=0.5)

Appendix C: Wave form of strut at draft: 100mm



V=0.2 m/s



V=0.3 m/s



$V=0.39$ m/s



$V=0.49$ m/s



$V=0.6$ m/s



$V=0.7$ m/s



$V=0.8$ m/s



$V=0.9$ m/s



$V=1$ m/s

Chapter 13: Bottom effect on the submarine moving close to the sea bottom

13-1- Introduction

In some operations that may be defined for submarines and submersibles, they must be able to navigate, close to the sea bottom safely. These operations are such as; tracking and inspecting the marine pipelines and cables on the sea bottom by unmanned underwater vehicles (UUV), keep away from the sea surface for getting stealth in shallow seas by naval submarines and other offshore research activities[1,2]. Moving close to sea bottom, induces wall effects on hydrodynamic forces; resistance and lift. It can change the dynamic stability and maneuvering of submarine significantly, and can cause hit to sea bottom and serious damage to the submarine. Therefore, it seems that sea bottom effect on submarines, should be studied carefully. At present, the research on underwater sailing near the sea bottom is comparatively rare. Bystron and Anderson (1998) made a model test, and concluded that the vertical force and trimming moment show linear features obviously with the dimensionless change of distance between the hull and the sea bottom [3]. Bao-Shan Wu, *et al* (2005) [4] and Xiao-xu DU, *et al* (2014) [5], have investigated the hydrodynamic characteristics of submarine moving close to the sea bottom with CFD methods. In the above literature, it seems that there is not the comprehensive study about the subject so, there are some problems, that this chapter tries to cover them, such as; accurate safe depth from the bottom, nonlinear formula for the relations between the forces and the distance from the sea bottom, variations of frictional and pressure resistance. Currently, there are mainly two principal methods to calculate hydrodynamic parameters, including model test and numerical simulation. Model test method is very accurate but costs too much and has a long cycle, so it is usually limited by the budget. The numerical simulation method, by a high quality commercial simulation software and powerful computers, can be a reliable, accurate and inexpensive method. Therefore, it seems, computational fluid dynamics (CFD) method, is more and more in practice. Refs [6,7] are the technical references that describe the notes of naval submarine hydrodynamics. Collective studies about submarine hydrodynamics are gathered in IHSS [8]. Some restrictions about submarine operation, near the sea bottom are described in Refs.[9,10]. Some conditions of submarine hydrodynamic modeling are discussed in Refs[11,12]. Main reference of this chapter is [13].

13-2-Specifications of the Model

The base model that is considered here, is an axis-symmetric body similar to torpedo, without any appendages because in this research, only bare hull,

wants to be studied. It helps to half CFD modeling of the body and saving the time. The total length of is 5m, diameter 0.6m, wetted surface area 7.87m^2 , fineness ratio (L/D) of 8.33. The specifications of the model are presented in Fig.1. The speed of the model is constant and equal to 4 m/s. The length, diameter and speed of the model are selected similar to the common unmanned underwater vehicles (UUV) and autonomous underwater vehicle (AUV). Most of the UUVs and AUVs have the length between 4~6 meters and the range of speed of 3~6 knots (approximately 1.5~3 m/s). Selected speed for the model is a little more than that, for approaching to the limits of effects.

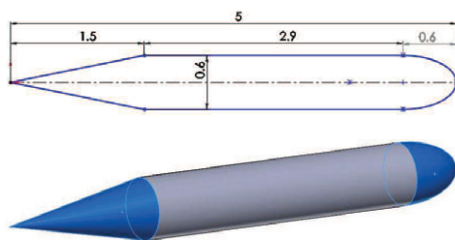


Figure 1: General configuration of the models

13-3- CFD Method of Study

This analysis is performed by Flow Vision (V.2.3). For modeling these cases in this chapter, Finite Volume Method (FVM) is used. A structured mesh with cubic (hexahedral) cell has been used to map the space around the submarine. Transition of laminar layer to the turbulent layer in boundary layer, and flow separation is a very important factor in resistance calculations. Two significant parameters in CFD, for modeling the boundary layer, are Y^+ and mesh numbers, which should be selected correctly. For modeling the boundary layer near the solid surfaces, the selected cell near the object is tiny and very small compared to the other parts of domain. For selecting the proper quantity of the cells, for one certain depth ($H^*=0.5$) and $v=4\text{m/s}$, seven different amount of meshes were selected and the results of lift force were compared insofar as the results remained almost constant after 1.1 millions meshes, and it shows that the results are independent of meshing (Fig.2). In all modeling the mesh numbers are considered more than 1.4 millions.

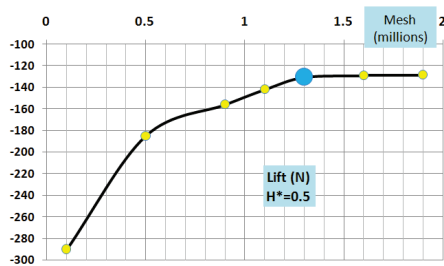
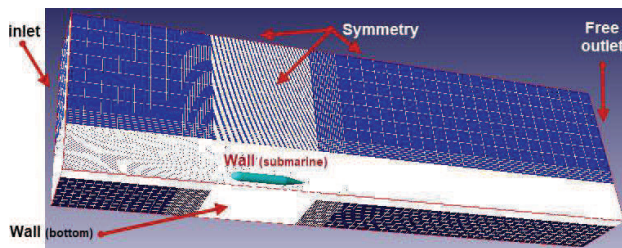


Figure 2: Mesh independency evaluations

For the selection of suitable iteration, it was continued until the results were almost constant with variations less than one percent, which shows the convergence of the solution. In the most cases, the iterations are continued to more than 1000. In this domain, there is inlet (with uniform flow), Free outlet, Symmetry (in the four faces of the box) and Wall (for the body of submarine and for the sea bottom). Dimensions of cubic domain are 40m length (equal to 8L), 5m beam and 11m height (more than 2L or 18D). Pay attention to that only half of the body is modeled because of axis-symmetric shape and symmetry of flow current, and the domain is for that. Here, there are little meshes in far from the object. The forward distance of the model is equal to 3L and after distance is 4L in the total length of 8L (Fig.3). The turbulence model is K-Epsilon, turbulent scale is considered 0.1m and y^+ is considered 30~100. The considered flow is incompressible fluid (fresh water) in 20 degrees centigrade and constant velocity of 4 m/s. Settings of the simulation are collected in Tab.1.



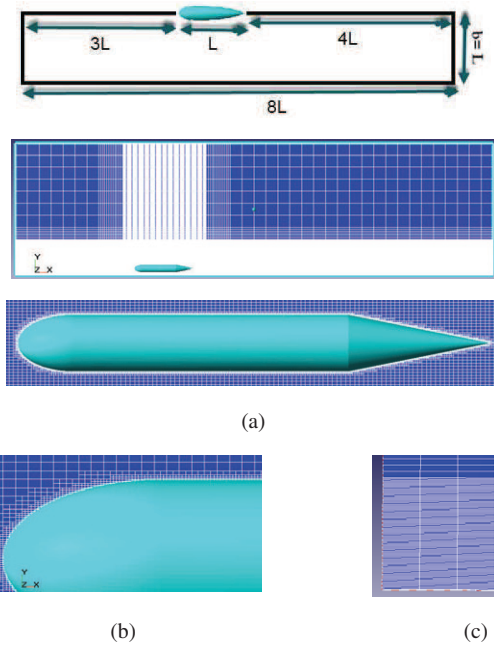


Figure 3: (a) Domain and structured grid (b) Very tiny cells near the wall for boundary layer modeling and keeping y^+ about 30 (c) Half modeling because of symmetry

Table 1: Settings of the simulation

Elements	Boundary conditions	Descriptions	
Domain	Box	conditions	Fully submerged modeling (without free surface)- half modeling-domain with inlet, outlet, symmetry and wall- Without heat transfer.
		dimensions	40*5*11 m- length before and after model=15 & 20m
		grid	structured grid- hexahedral cells- tiny cell near wall- Meshes more than 1.4 millions.
Fluid	-	settings	Iterations more that 1000- Time step=0.01sec. Incompressible fluid- Reynolds number, constant and equal to 20 million for all depths- turbulent modeling: Standard k-ε- fresh water- temprature:20 deg- $\rho=999.841 \text{ kg/m}^3$.
Object	Wall		Bare hull of submarine- value $30 < y^+ < 100$ - roughness=0- no slip
Input	Inlet		Velocity=4m/s- constant- normal (along x)- in 1 face
Output	Free outlet		Zero pressure- in 1 face
Boundaries	Symmetry		In 3 faces
	Wall		For modeling the bottom- no slip condition

13-4- Bottom effect on the pressure field around a submarine

When a body moves through a fluid (with or without viscosity), there is a pressure field over the body. Longitudinal diffraction of pressure between the fore and after parts of the body, produces pressure resistance. Vertical diffraction of pressure between the upper and lower parts of the body, produces lift force. Total resistance in fully submerged condition, is the summation of frictional and pressure resistance. Resistance and lift forces, are the dominant hydrodynamic forces on the body which can produce hydrodynamic moments. Figure 4, shows a sample submarine in the fully submerged pressure field without wall effect of the sea bottom. It is the general form of pressure distribution around a submarine. In the stagnation point, at the bow tip, there is a high positive pressure area. At the end of the stern, there is another positive pressure area, but is not so stiff positive pressure. In the bow and stern shoulders, there are negative pressure areas, as shown in Fig.4. Moderate pressure area, encompasses the most parts on the middle cylindrical part of the submarine. In Fig.4, usually $P_1 > P_2$, and it is the reason of pressure resistance.

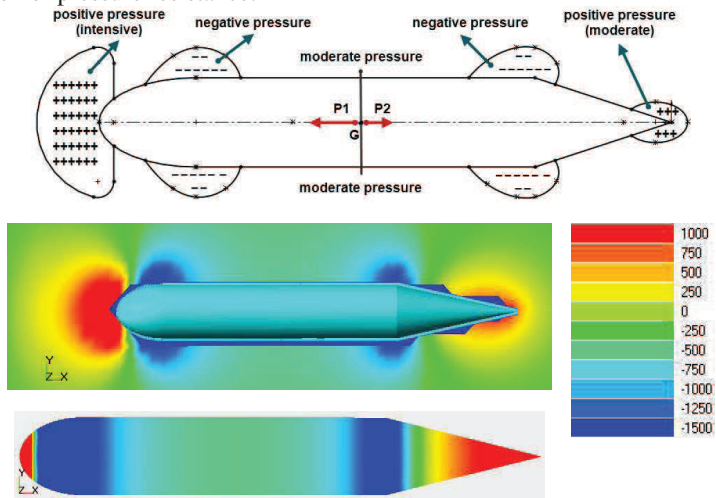


Figure 4: Pressure field around a submarine (far from the sea bottom)

This field is a free pressure field, but when a submarine approaches to the sea bottom, the velocity and pressure fields, are changed. Equation 1 represents the Bernoulli formula:

$$P + \rho gh + \frac{1}{2} \rho v^2 = \text{constant} \quad (1)$$

According to Bernoulli equation and Law of mass conservation, by closing to the bottom, the fluid underneath the body, gets higher velocity and therefore, gets lower pressure. Thereafter, the axis-symmetry condition of pressure domain will be changed. This condition is shown in Fig.5. The result of change in the pressure field is changing the pressure resistance and lift force. The lower part of the hull has lower pressure than upper part, which results in suction area. It leads to attraction force to the bottom and can cause the collision incident.

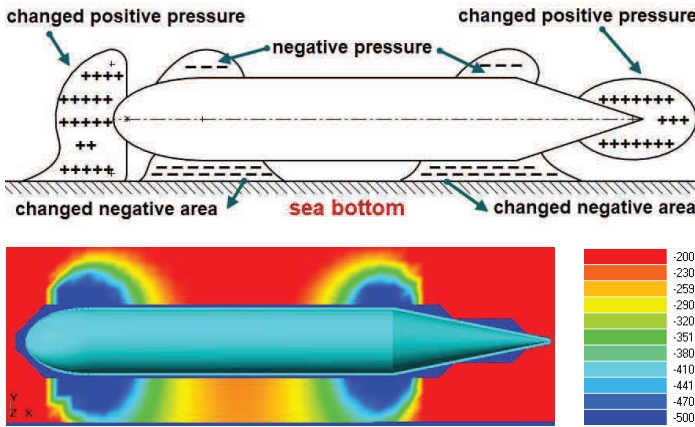


Figure 5: Negative pressure (suction) area at the effect of the sea bottom

13-5- CFD Results Analysis

The results of analysis are represented in Tab.2 and Fig.6. For analyzing the bottom effect, several distances of submarine to the sea bottom are considered. This distance (h), is measured from beneath of submarine hull to the sea bottom. For generalizing the analysis, the non-dimensional distance ($H^*=h/D$) is considered for discussions. Lift and resistance coefficients are calculated as (for example C_t): $C_t = \frac{R_r}{\frac{1}{2} \rho A v^2}$, which A is wetted surface area and equal to $7.87m^2$.

Table 2: Values of resistance and lift in distance from sea bottom

h (m)	$H^*=h/D$	Rt (N)	Rp (N)	Rf (N)	Lift(F_L) (N)	Ct *10000	Cp *10000	Cf *10000	CL *10000
0.1	0.16	266.8	91	175.8	-315	42.38	14.45	27.92	-50.03
0.2	0.33	270.8	94.4	176.4	-193.4	43.01	14.99	28.02	-30.72
0.3	0.5	271.2	95.2	176	-130.6	43.07	15.12	27.95	-20.74
0.6	1	271.6	95.8	175.8	-54.2	43.14	15.22	27.92	-8.61
0.9	1.5	270.4	96	174.4	-27.4	42.95	15.25	27.70	-4.35
1.2	2	269.6	96.4	173.2	-16.2	42.82	15.31	27.51	-2.57
1.5	2.5	269.6	96.4	173.2	-9.2	42.82	15.31	27.51	-1.46
1.8	3	269.6	96.4	173.2	-6	42.82	15.31	27.51	-0.95
2.4	4	269.6	96.4	173.2	-1.6	42.82	15.31	27.51	-0.25
3	5	269.6	96.4	173.2	0	42.82	15.31	27.51	0.00
3.6	6	269.6	96.4	173.2	0	42.82	15.31	27.51	0.00
5.4	9	269.6	96.4	173.2	0	42.82	15.31	27.51	0.00

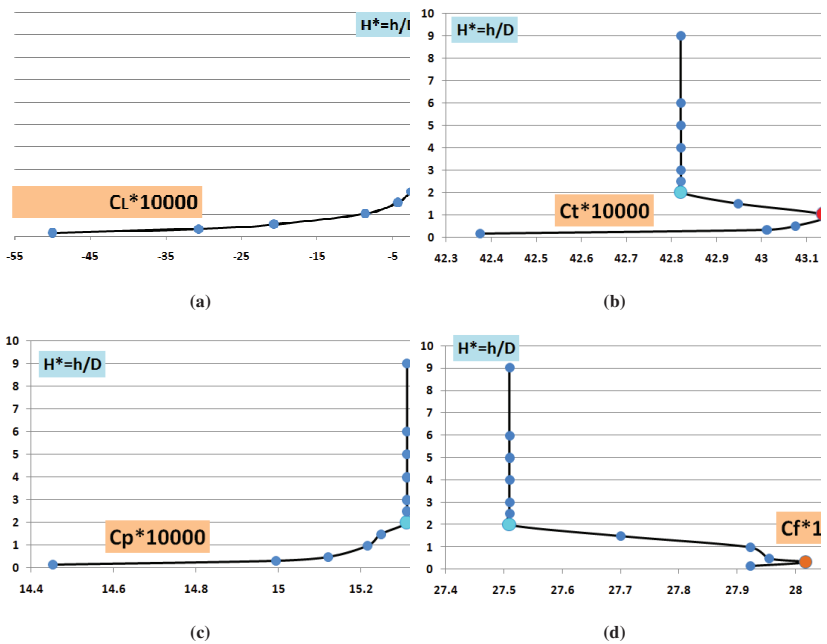


Figure 6: Variation of hydrodynamic coefficients versus distance from sea bottom

13-6- Analysis of lift force

As discussed before, the lift force is the result of difference of the pressure in upper and lower part of the hull. Whenever submarine moves close to sea bottom, according to Bernoulli rule, a low-pressure area appears in lower part of the body. While the submarine keeps out from the sea bottom, the lift force reduces exponentially (Fig.6-a). The equation of this curve is extracted by Curve Expert software (Fig.7). Therefore, this equation can be expressed as:

$$C_L * 10000 = \frac{92 - 16.65H^{0.5}}{1 + 4.37H^0 + 3.42(H^0)^2} \quad (2)$$

Another equation can be fitted to them. It is exponential equation:

$$C_L * 10000 = \frac{-23}{1 - 1.23e^{-1.08H^0}} \quad (3)$$

The lift force, experiences a lot of variations because of the effect of the sea bottom. The variation of lift force is zero (at far from the sea bed) to the stiff negative pressure (close to sea bottom), and can change the pitching moment consumedly. Un-controlled change in pitch angle, can cause a crash to sea bottom.

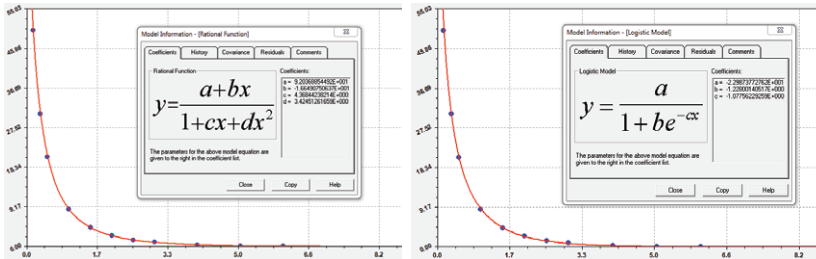


Figure 7: Fit the best curves to the variation of C_L versus H^*

13-7- Analysis of resistance force

The results of this simulation show that, wall effect of sea bed on the resistance is not notable compare to the variations of lift force. The range of this variation is less than 1%, because vice versa the channels, in the sea, there is not beam or cross limitation, therefore, there are not huge changes in speed

and resistance. Total force is the summation of frictional and pressure resistance. Their variations are shown in Fig.6-b,c,d.

Pressure resistance: Pressure resistance decreases by an increase in the distance (Fig.6-c). The reason is that, when a submarine approaches to the sea bottom, the pressure distribution changes, and high pressure region in the front part of the body decrease. Then, the difference between the front and after part of the body will be decreased. Therefore, pressure resistance will be decreased. According to Fig.6-c, in distance $H^*=2$, the wall effect on the pressure resistance can be ignored.

Frictional resistance: Frictional resistance has a maximum point. According to Fig.6-d, in distance $H^*=2$, the wall effect on the frictional resistance can be ignored. While get close to the sea bottom, the frictional resistance will be increased because, according to the law of conservation of mass, by decrease in distance, the velocity of the fluid will be increased. Frictional resistance depends on the velocity; therefore the friction will be increased. By get closer to sea bottom, after a special depth, the frictional resistance will be decreased another time, because of the growth of the turbulent boundary layer. In the model of this chapter, this depth is $H^*=0.25$. For finding out this distance, the thickness of boundary layer should be calculated. In this model by the length of 5m and speed of 4m/s, the Reynolds number is approximately 20 million that meant the turbulent flow over the hull. For turbulent flow, the thickness of boundary layer (δ) is calculated as Eqn.3. In the middle of the body ($x=2.5m$), $\delta = 3.2cm$. By accounting the boundary-layer thickness of the bottom, the distance between the bottom and hull at $x=2.5m$, that is occupied is $\delta=6.4cm$, and at $x=5m$, there is $\delta=12.8cm$. At the $H^*=0.16$, the distance is $h=10cm$. It meant an unfree fluid flow which results in fall of fluid speed and frictional resistance.

$$\frac{\delta}{x} = \frac{0.37}{(Re)^{\frac{1}{4}}} \quad (3)$$

Total resistance: Total resistance has a maximum point. According to Fig.6-b, in distance $H^*=2$, the wall effect on the frictional resistance can be ignored. While get close to the sea bottom, the total resistance will be increased but after $H^*=1$, it will be decreased. The reason of this variation is the different between frictional and pressure resistance, which are inverse to each other, as discussed before. Generally, the configuration of the total resistance curve,

depends on the dimensions of the submarine. If frictional resistance be dominant, the diagram has a downward trend but if pressure resistance be dominant, the diagram has an upward trend.

13-8- Review

In conclusion, about sea bottom effect, it can be said that:

- 1- The variation of lift force is more important than resistance force. This range is about 1% for resistance but may be several times in lift force.
- 2- At depth more than $H^*=5$, the bottom effect on the lift force can be ignored.
- 3- At depth more than $H^*=2$, the bottom effect on the total, frictional and pressure resistance can be neglected.
- 4- Necessarily, by getting close to the sea bottom, the resistance does not decrease.
- 4- Maximum resistance can be expected at $H^*=1$.
- 5- At depth very close to the sea bottom, the boundary-layer thickness has a dominant effect.

Nomenclature

C_f	Frictional resistance coefficient
C_L	Lift coefficient
C_p	Pressure resistance coefficient
C_t	Total resistance coefficient
D	maximum diameter of the outer hull (m)
h	Distance from sea bottom (m)
H^*	$=h/D$ (relative distance from sea bottom)
IHSS	Iranian Hydrodynamic Series of Submarines
L	Overall length of hull (m)
Re	Reynolds number
R_f	Frictional resistance (N)
R_p	Pressure resistance (N)
R_t	Total resistance (N)
x	Longitudinal distance from the bow end (m)

References

- [1] D.R.Yoerger, M.Jakuba, A.M.Bradley, "Techniques for deep sea near bottom survey using an autonomous underwater vehicle", *Robotics Research in Springer Tracts in Advanced Robotics*, vol.28, pp.416-29,2007.
- [2] C.Y.Lin, J.Zhu, "Numerical computation of added mass of submarine maneuvering with small clearance to sea- bottom", *Ship Engineering Journal*;25(1):26-9, 2003 [in Chinese].
- [3] L.Bystron, R.Anderson, "The submarine underwater maneuvering. submarine technology research and development", *The 5th International Conference on Submarines Selection*. China Ship Scientific Research Center, pp.132-43,2000.
- [4] Bao-Shan Wu, Fu Xing, Xiao-Feng Kuang, Quan-Ming Miao, "Investigation of Hydrodynamic characteristics of Submarine Moving Close to the Sea Bottom with CFD Methods", *Ship Mechanics*, vol 9-3, pp: 19-28, 2005.
- [5] Xiao-xu DU, H.Wang, C.zhi Hao, Xin-liang Li, "Analysis of hydrodynamic characteristics of unmanned underwater vehicle moving close to the sea bottom", *Defence Technology* 10, pp:76-81, 2014.
- [6] P.N.Joubert, "Some aspects of submarine design: part 1: Hydrodynamics", Australian Department of Defence, 2004.
- [7] P.N.Joubert, "Some aspects of submarine design: part 2: Shape of a Submarine 2026", Australian Department of Defence, 2004.
- [8] M.Moonesun, "Introduction of Iranian Hydrodynamic Series of Submarines (IHSS)", *Journal of Taiwan society of naval architecture and marine engineering* , Vol.33, No.3, pp.155-162, 2014.
- [9] R.Burcher, L.J.Rydill, "Concept in submarine design", The press syndicate of the University of Cambridge., Cambridge university press, pp. 295,1998.
- [10] Yuri.N.Kormilitsin, Oleg.A.Khalizev, "Theory of Submarine Design", Saint Petersburg State Maritime Technical University, Russia, pp.185-221, 2001.
- [11] M.Moonesun, M.Javadi, P.Charmdooz, U.M.Korol, "evaluation of submarine model test in towing tank and comparison with CFD and experimental formulas for fully submerged resistance", *Indian Journal of Geo-Marine Science*, vol.42(8), pp.1049-1056, December 2013.
- [12] M.Moonesun, K.Y.Mikhailovich, D.Tahvildarzade, M.Javadi, "Practical scaling method for underwater hydrodynamic model test of submarine", *Journal of the Korean Society of Marine Engineering*, Vol. 38, No. 10 pp. 850~857, 2014.
- [13] Mohammad Moonesun, Yuri Mikhailovich Korol, Nikrasov Valeri, Anna Brazhko, Alexander Ursolov, Bottom effect on the submarine moving close to the sea bottom, *Journal of Scientific and Engineering Research*, 2016, 3(1):106-113.

Chapter 14: AUV Moving Inside a Water Pipeline

14-1- Axi-Symmetric Movement

14-1-1- Introduction

Water or petroleum pipelines are extended all over the world with millions of kilometers long. A severe breakdown of a pipeline can lead to large costs and also lead to pollution and accidents. Hence routine inspection and maintenance of the pipelines are necessary for their trouble-free performance. Water supply is a basic public service and therefore, inspection tasks cannot compromise on the continuity or quality. Unnikrishnan [1] presented an inspection system which is capable of operating when the pipeline is in-service. Today several different pipeline inspection robots exist which are presented by Moghaddam [2], Harry [3], Bahmanyar [4], Muramatsu [5], Roh [6,7] and Dadkhah [8]. The pipeline inspection robots presently are used by the contact with the walls for motion and positioning in the centre of the pipe (Okamoto[9]). Figure 1 (Unnikrishnan [1]) shows the Autonomous Underwater Vehicle (AUV) inside a pipeline. This is a simple AUV with conical ends, but today modern AUVs have usually torpedo shape. The aim for developing this inspection system is to enable non-destructive and non-disruptive inspection of water pipelines. Main references of this chapter are Refs.[10,11].

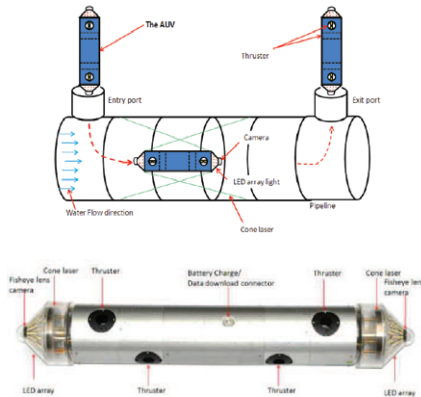
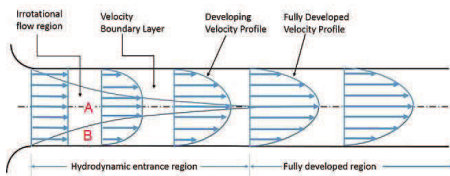


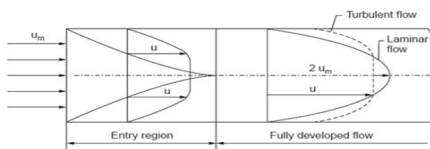
Figure 1: Schematic of pipeline inspection System and sample AUV (PICTAN) (Unnikrishnan[1])

Recently torpedo shaped ocean-going AUVs (Najjaran [12] and Jorg [13]) have been modified to inspect large pipelines. These vehicles have been used to inspect very huge pipelines having a diameter of more than 2 meters. It is important for the pipeline internal inspection robots to be able to enter and leave the pipeline with the least disruption or damage to the existing pipe systems. The larger the pipeline network, the greater the amount of inspection needs to be carried out. Hence autonomous and free operation is ideal for long distance inspection. Therefore, Autonomous Underwater Vehicles (AUV) are ideal tools for pipeline internal inspection (Unnikrishnan [1]). The flow field around a submarine inside a pipe or ducted space is different from the free stream. The proximity to the interior boundary of the hull induces wall effect on the fluid flow. In such cases, the boundary layer develops all over the circumference. The initial development of the boundary layer is similar to that occurring over the flat plate. At some distance from the entrance, the boundary layers merge and further changes in velocity distribution become impossible. The velocity profile beyond this point remains unchanged. The distance up to this point is known as the entry length which is about $0.04Re \times d$. The flow beyond this said to be fully developed. The velocity profiles in the entry region and the fully developed region are shown in Fig.2-a. The flow was observed to be laminar until a Reynolds number value of about 2300. The Reynolds number is calculated on the basis of the diameter (ud/ν). In the pipe flow, it is not a function of the length. As long as the diameter is constant, the Reynolds number depends upon the velocity for a given flow. Hence the value of velocity determines the nature of the flow in pipes for a given fluid. The value for the flow Reynolds number is decided by the diameter and the velocity. As shown in Fig.2-a, Region (A) is the non-viscous flow that is not affected by the boundary layer but Region (B) is the boundary layer region. The development of boundary layer in the turbulent region is shown in Fig.2-b. In this case, there is a very short length in which the flow is turbulent. This length, x , according to (Pritamashutosh[14]), can be calculated using the relation $x/D = 4.4Re^{1/4}$. After this length, the flow within the boundary layer turns turbulent. A very thin laminar sub-layer near the wall in which the velocity gradient is linear is present all through. After some length the boundary layers merge and the flow becomes fully developed. The entry length in turbulent flow is about 10 to 60 times the diameter (Seif [15]). The

velocity profile in the fully developed flow remains constant and is generally flatter compared to laminar flow where it is parabolic. Now it should be clear that, the flow through the pipe is different from that of a free stream. When an AUV moves inside a pipe, it experiences wall effects, especially in low diameter pipes. This causes an increase in resistance. The narrower the pipe diameter, the more the resistance. This added resistance should be calculated accurately, since it is necessary for the determination of vehicle speed, power demand, range and duration of operation. Another important parameter is the AUV diameter. According to the pipe diameter, the diameter of the AUV should be specified to obtain the minimum resistance.



(a)



(b)

Figure 2: (a) Boundary layer and velocity distribution inside a pipe in laminar flow (b) Difference in laminar and turbulent flow [15]

14-1-2- Specifications of the Model and pipe

The base model that is considered here is an axis-symmetric AUV similar to that of a torpedo, having no appendages since in the research is to study only the bare hull. This helps to halve CFD modeling of the body which would save time. The total length of the model is 2m, the diameter 0.25m, the wetted surface area 1.35m², the volume 0.08m³ and the fineness ratio (L/D) is 8. The specifications of the model are presented in Figure 3.

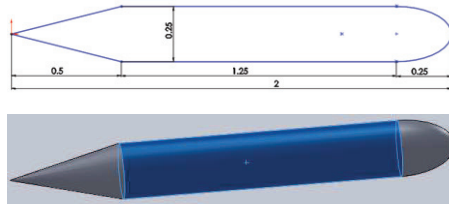


Figure 3: General configuration of the models

Inside dimensions of the model are constant, but the diameter of the tube (d) changes. For this study, according to Figure 4 and Table 1, ten different pipe diameters are considered ($d/D=1.22, 1.41, 1.58, 1.73, 2, 3, 4, 10, 12$ and 13). The ratio of the water section area (A_2) to the section area of the model (A_1) is crucial. Some of the d/D values are considered according to A_2/A_1 . The values of $d/D=1.22, 1.41, 1.58$ and 1.73 are respectively equivalent to $A_2/A_1=0.5, 1, 1.5$ and 2 respectively. Three different speeds are considered; $1, 3$ and 10m/s . These speeds are considered so that all Reynolds number (ud/ν) values exceed 2300 . This provides fully turbulent flow inside the pipe. The usual speed of AUVs inside the tube is in the range of $1\sim 3\text{m/s}$ but the speed of 10m/s is considered for high speed vehicles such as the ejection of torpedo from the torpedo tube.

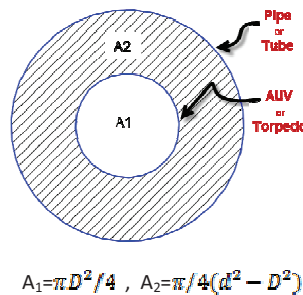


Figure 4: Cross section area of AUV and pipe (hatched area: water between AUV and pipe)

Table 1: Description of considered conditions

D (m)	d/D	A_2/A_1
0.304	1.22	0.5
0.36	1.41	1
0.394	1.58	1.5
0.432	1.73	2
0.5	2	2.9
0.75	3	7.8
1	4	14.7
2.5	10	97.1
3	12	140.3
3.25	13	164.8

14-1-3- CFD Method of Study

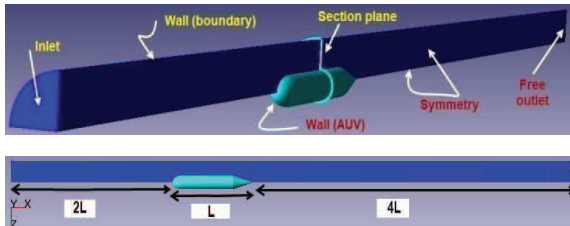
This analysis is performed by Flow Vision (V.2.3) software based on CFD method and solving the RANS equations. Based on the traditional Finite Volume concept and modern C++ implementation, Flow Vision is still very different from the competition. The Flow Vision workflow is more flexible and focused on solving physical problems rather than mesh generation. Meshing in Flow Vision is completely automatic and forms an integral part of a solver, which results in many benefits and unique capabilities. The Flow Vision development started in the late 90's at Russian Academy of Science and is continued since 1999 in the Capvidia group. Today Flow Vision evolved to the third generation product addressing wide range of applications often unique and not supported by traditional CFD products. Co-simulation with SIMULIA Abaqus has been pioneered for over 12 years resulting in powerful solution for heavily coupled FSI (Fluid Structure Interaction) problems as e.g. simulation of tires hydroplaning. High-level scalability of Flow Vision parallel solver minimizes computational time scaling complex R&D simulations to practical engineering tasks. The multi-parameter optimization automates design processes to deliver optimal solutions which are impossible to get through traditional engineering practices (FVweb[16]).

14-1-3-1- Condition "A"

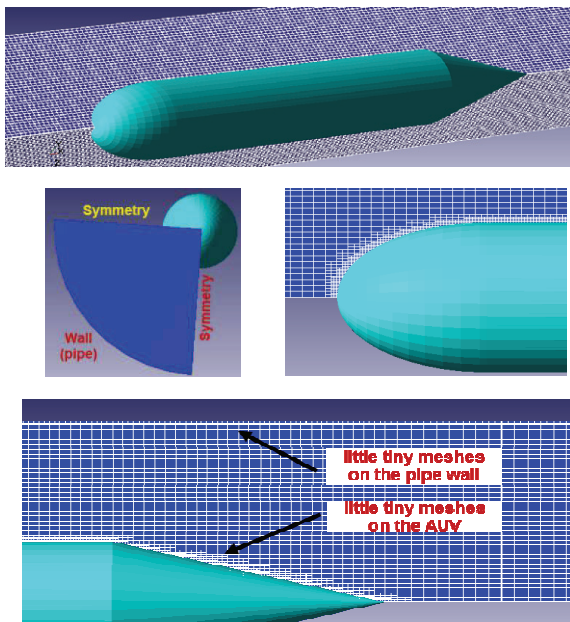
This analysis is performed by Flow Vision (V.2.3) software based on CFD method and solving the RANS equations. Generally, the validity of the software results has been confirmed by several experimental test cases. The software, nowadays, is accepted as a practicable and reliable software in CFD activities. For the purpose of modeling these cases, Finite Volume Method (FVM) is employed. A structured mesh with cubic (hexahedral) cells has been used to map the space around the AUV. Transition of laminar layer to the turbulent layer in boundary layer, and flow separation are very important factors in resistance calculations. Y^+ and mesh numbers which to be selected with great care, are two significant parameters for modeling the boundary layer in CFD. For modeling the boundary layer near the solid surfaces, the selected cell near the object is very small compared to the other parts of the domain. Because of axis-symmetric shape and axis-symmetry of the flow current only a quarter of the body and the domain are modeled (Fig.5). In this domain, there is an inlet (with uniform flow), a free outlet, a symmetry (in the two faces of the symmetric plane) and a wall (for the body of AUV and for the pipe interior boundary). Domain length is equal to $7L$ ($2L+L+4L$) with several different diameters. The study assumes that the water inside the pipe is calm and having no speed and only the AUV moves. The turbulence model is K-Epsilon, turbulent scale is considered $0.1m$ and Y^+ is considered $30\sim 100$. The fluid is considered incompressible (fresh water) at 20 degrees centigrade and velocity of $1, 3, 10m/s$. Settings of the simulation are collected in Table 2. Selection of the proper "time step" in each iteration, depends upon three parameters: speed, model length and mesh numbers along the main direction of movement, since the transfer of network is to be stopped on each section. For example, if $v=1m/s$, then the boundary layer will pass $2m$ length of the body in 2 seconds. The direction of velocity is along the axis, and for every 1 cm, one station of mesh is considered, that is 200 longitudinal station along the body (not all the domain). For stopping the steam (flow) in each station, the time step is $2/200=0.01$ seconds. On the other hand, the minimum time step required is

$$\left(\frac{\text{body length/speed}}{\text{longitudinal station numbers on the body}} \right)$$

In order to select the suitable iteration amount, the boundary layer should be considered in such a way that it could travel to the whole domain, from the beginning to the end. As an example, if the full length of the domain be 21m, and $v=3\text{m/s}$, it needs 7 seconds to traverse the total length, and if "Time step=0.01sec" is considered, a minimum number of $7 \div 0.01=700$ iterations is needed. These conditions are collected in Table 2.



(a)



(b)

Figure 5: Condition A: (a) Domain and general dimensions (b) structured grid and Very fine cells near the wall for boundary layer modeling

14-1-3-2- Condition "B"

To analyze the pipe wall effect upon the resistance, it is needed to simulate the free stream, that is, no pipe and no wall effect. The domain and the simulation are shown in Figure 6. In this domain, there is an inlet (with uniform flow), a free outlet, a symmetry (in the four faces of the box) and a wall (for the submarine body). The domain is a box with dimensions of 12^*2^*2 m (or $6L^*16R^*16R$). Mesh number is two millions.

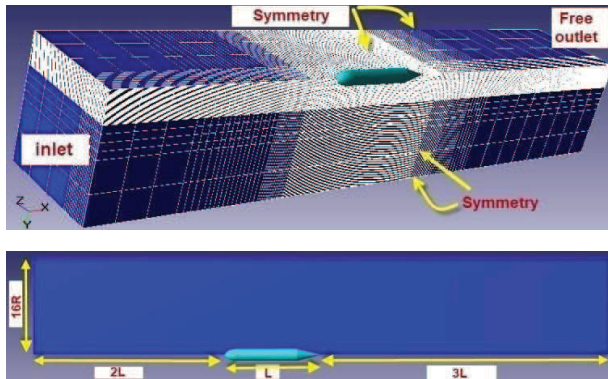


Figure 6: Condition B: Free stream modeling (without pipe wall effects)

14-1-3-3- Condition "C"

As mentioned above, the main assumption is that the water inside the pipe is calm and only the AUV moves, but if we regard that there is an initial water speed inside the pipe, the entrance length should be taken into account. To determine the forward distance, more "hydrodynamic entrance length" from the beginning of the pipe is required. As discussed before, the entry length in turbulent flow is about 10 to 60 times the diameter, and the turbulent flow occur after Reynolds number(ud/ν) exceeds 2300. More turbulent flow induces lesser entrance length. At this point, this condition is studied only in one case: $d/D=4$ and $v=1,3,10\text{m/s}$. It is supposed that the AUV is constant and

only the water moves. The flow is turbulent, and the entrance length (forward distance) is minimally considered to be equaling "10d". Thus, the length of the cylindrical domain is "10d+L+3L"(Figure 7). This domain has a diameter of 1m and a length of 18m (10+2+6). Here, the mesh number is more than 2.8 million and there are little meshes far from the object. Other simulation conditions are similar with the ones mentioned before.

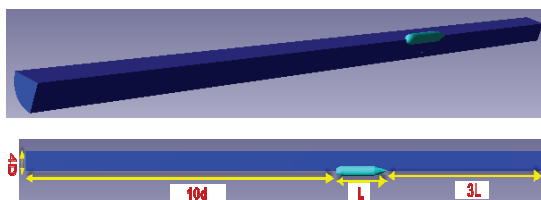


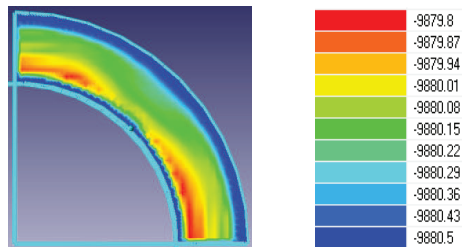
Figure 7: Condition C: Entrance length condition for $d/D=4$

Table 2: Settings of the simulation (inside the pipe)

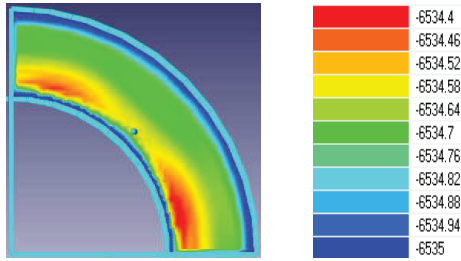
Elements	Boundary conditions	Descriptions
Domain	Cylinder (quarterly)	conditions Fully submerged modeling (without free surface)- quarter modeling- domain with inlet, outlet, symmetry and wall- Without heat transfer.
		dimensions A) length: $7L=2L+L+4L$ (distance before: $2L$ - distance after: $4L$) B) length: $6L=2L+L+3L$ (distance before: $2L$ - distance after: $3L$)* $16R*16R$
		grid C) length: $10d+L+3L$: distance before: $10d$ - distance after: $3L$ structured grid- hexahedral cells- fine cell near wall- Mesh numbers: A) more than 2.1 million B) 2 million C)2.8 million
Fluid	-	settings Iterations more than 700- Time step=0.01sec. Incompressible fluid (water)- Reynolds number, is different in each pipe- turbulent modeling: Standard k- ϵ - fresh water- tempreture:20 deg- $\rho=999.841 \text{ kg/m}^3$. Bare hull of AUV- value $30 < y^+ < 100$ - roughness=0- no slip Velocity=1,3,10m/s- normal (along x)- in 1 face Zero pressure- in 1 face
Object	Wall	
Input	Inlet	
Output	Free outlet	
Symmetry	Symmetry	In 2 faces
Boundaries	Wall	For modeling the pipe wall- no slip condition

14-1-4- CFD Results and Analysis

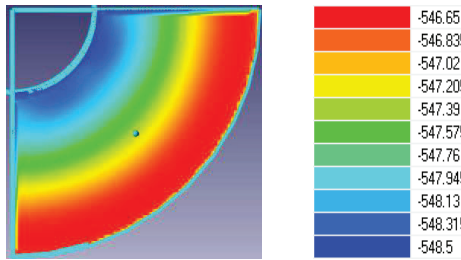
In this regard, two main factors should be discussed: 1)The pipe wall effects and 2)The fluid speed changes effects. Wall effect on the pipe causes some boundary layer effects on the fluid, and a zero speed just on the wall. Fluid speed change appears because of the limited cross section area between the body and the pipe. The minor distance between the body and the pipe, means minor cross section area (A_2). The fluid flux is constant, so the fluid speed should be increased. Increase in speed, according to Bernoulli's law, is equivalent to a decrease in pressure. For little values of A_2 , the change in the fluid speed owing to the flux is more than the effect of the boundary layer on the pipe wall. Figure 8, shows the variation of pressure, for several values of d/D , in the cross section of the pipe. As the figure clearly shows an increase in A_2 , induces an increase in average pressure of the fluid. Indeed, this comes as a result of a decrease in speed. In Fig.8a, the average pressure is -6530 (P_a) and in Fig.8d, it is 127 (p_a). In Fig.8a& 8b the form of pressure distribution is different from those of (c) and (d), because, as mentioned above, an increase in the pipe diameter brings about a decrease in the constant flux effect. In the next stage, the variation of resistance of the model (AUV) is discussed. The resistance for conditions A, B and C are represented. The total resistance (R_t) is the summation of the pressure resistance (R_p) and the viscous resistance (R_f). Here, the main factor causing a change in the resistance is the pressure resistance, because of it is wholly depended upon the pressure distribution over the body. In each stage, the total resistance and the pressure resistance are presented.



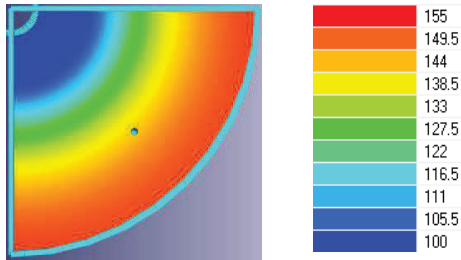
(a) $d/D=1.41$ ($A_2/A_1=1$), $P_{avg}= -9880$ pa



(b) $d/D=1.58$ ($A_2/A_1=1.5$), $P_{avg} = -6530$ pa



(c) $d/D=3$ ($A_2/A_1=7.8$), $P_{avg} = -547$ pa



(d) $d/D=10$ ($A_2/A_1=97.1$), $P_{avg} = 127$ pa

Figure 8: Pressure variation in several ratios of d/D

14-1-4-1- Condition "A" and "B"

The total resistance and the pressure resistance of AUV in several different diameters of tubes are presented in the Table 3 and Figure 9. These results are presented for three speeds of 1, 3 and 10m/s. Clearly at all speeds where $d/D < 1.41$ (or $A_2/A_1 < 1$), there is a jump in the resistance diagram. Therefore, it

can be suggested that in all pipes or torpedo tubes, the following should be considered $d/D > 1.41$ (or $A_2/A_1 > 1$). In swim out (self-propelled) system of torpedoes, in submarines, the torpedo diameter is 533mm and torpedo tube (launcher) is 640mm, which eventuate $A_1 = 0.223\text{m}^2$ and $A_2 = 0.0985\text{m}^2$. For easier ejection of torpedo from the tube, a minimum tube diameter of 750mm, can be recommended which provides $A_1 = A_2$. The main limitation for increasing the tube diameter is the architecture arrangement inside a submarine or naval ship, and the required volume of water to fill the space dimension between torpedo and the tube. This volume of water must be kept up in the submarine tanks, but in pipelines, there is no such restriction. The diameter of AUV can be designed according to the diameter of the pipe. The diagrams of Figure 10 show that, when $d/D = 1.41$, there is a mild variation in resistance. Logically, by increasing the pipe diameter, the decrease in resistance values is observed.

Table 3: Values of total resistance and pressure resistance

d/D	v=1ms		v=3ms		v=10ms	
	Rt (N)	Rp (N)	Rt (N)	Rp (N)	Rt (N)	Rp (N)
1.22	145.2	125.2	1110.8	963.6	12820	11624
1.41	34.8	26.4	258	198	2392	1838
1.58	22	15.6	160.8	114	1099.2	820
1.73	15.2	10	115.2	76	1075.2	715.6
2	10.4	6	78.4	46.4	741.2	445.6
3	7.2	4	50.4	26	490	266
4	6	3	46	23.6	444	238
10	6	3.36	37.6	16.8	358	172
12	4.6	2	36.8	17.2	352.4	166
13	4.6	2	36.6	16.8	348	158
infinite	4.6	2	36.6	16.8	348	158

At the speeds of 1m/s and 3m/s, the results after $d/D = 12$ remain constant. The values of " $d/D = \text{infinite}$ " is related to condition "B" which models the free stream condition. That is, after this limit, the added resistance and the pipe wall effect are negligible. This diameter is the "Critical diameter". At the speed of 10m/s, the critical diameter happens in $d/D = 13$. However, since there are no high speeds in pipes, one can conclude that $d/D = 12$ is related to the critical diameter.

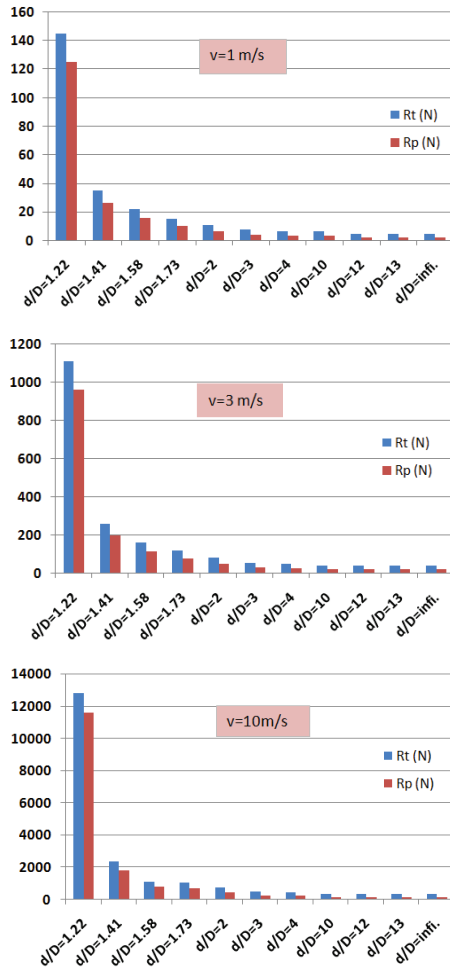


Figure 9: Total resistance and pressure resistance of AUV in several different d/D and speed

The ratio of pressure resistance to the total resistance is shown in Figure 10. As mentioned above, the pressure resistance has a unique role in the total resistance. This diagram shows that when the value of $d/D < 1.41$, the pressure resistance is about 90 percent of the total resistance. In the infinitive diameter

($d/D=\text{infin.}$), this value is about 45 percent. That is to say, the wall effect of the pipe has induced the pressure resistance to be twice as much. By increasing the diameter, the percentage of the pressure resistance decreases gradually.

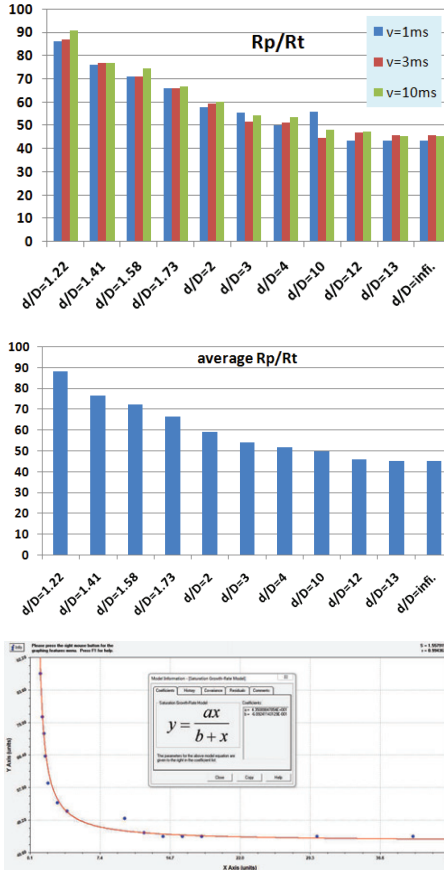


Figure 10: The ratio of pressure resistance to total resistance

To interpolate other values of d/D , the best curve is fitted to these points by Curve expert software (Figure 10). The extracted formula is as Eqn.7:

$$\frac{R_p}{R_T} = \frac{43.5 (d/D)}{-0.61 + (d/D)} \quad (7)$$

For a better understanding of the pipe wall effect on resistance, the ratio of total resistance to free stream resistance (condition C) is represented in Figure 11. The amount of $R_t/R_0=1$, shows that when the wall effect is deleted, free stream condition obtains.

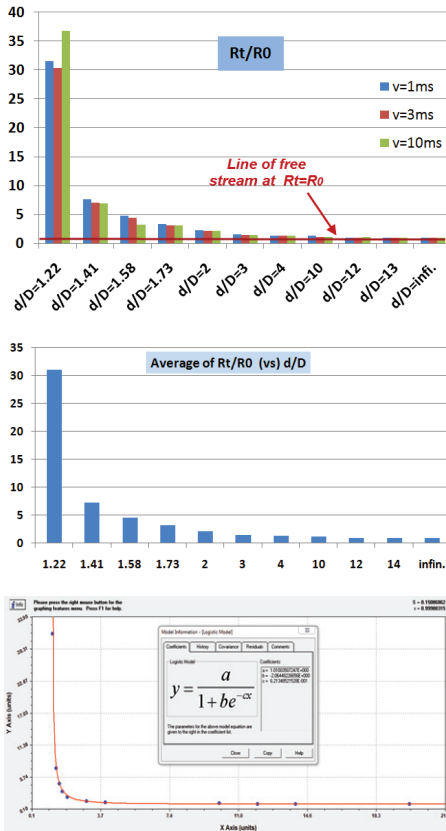


Figure 11: Ratio of total resistance to free stream resistance

To interpolate other values of d/D , the best fitted curve is shown in Figure 12, and the related formula is as Eqn.9:

$$\frac{R_T}{R_0} = \frac{1.01}{1 - 2.06e^{-0.62(d/D)}} \quad (9)$$

As mentioned before, the ratio of $d/D=12$ can be regarded for critical diameter, neglecting the added resistance and the pipe wall effect.

14-1-4-2- Condition "C"

The comparison between the results of condition A and C is presented in Table 4. The results show a decrease of about 5 percent in the total resistance, and 10~20 percent decrease in the pressure resistance. The reason for the decrease is a reduction in the fluid speed, coming about as a result of flow development and the boundary layer expansion after the entrance length. That is, if it is assumed that the fluid is not calm and it has an initial speed, then the entrance length should be regarded for developing the boundary layer taking into account an approximate five-percent decrease in the total resistance. In condition A, there is no entrance length, and the boundary layer is not developed. As a rule, in engineering problems, in order to inspect the pipelines, no initial flow speed is considered, for by conducting the inspections and repairs; the valves are closed.

Table 4: Comparison of results for $d/D=4$

	V=1m/s		v=3m/s		v=10m/s	
	Rt	Rp	Rt	Rp	Rt	Rp
Condition "A"	1.5	0.75	11.5	5.9	111	59.5
Condition "C"	1.4	0.6	10.9	5.1	107	53.3
Decrease percentage (%)	6.67	20	5.22	13.56	3.60	10.42

14-1-5- Review 1

To conclude, as regards the added resistance due to wall effect, for an AUV moving inside a pipe, the following can be mentioned: Pressure resistance play a major role in the total resistance. The ratio of $d/D=12$ can be regarded for the determination of the "critical pipe diameter" in which the added resistance is zero. The ratio of $d/D < 1.41$ (or $A_2/A_1 < 1$) causes a stiff increase

along with the resistance. Therefore, the values below this ratio is not recommended. In swim out system of torpedo launching, in the case of 533mm torpedoes, the minimum tube diameter of 750mm is recommended. If there is an initial water speed inside the tube, the entrance length and the developed boundary layer should be regarded.

14-2- Asymmetric Movement

The out of axis movement of AUV, is evaluated for two values: $d/D=4$ and 12. The parameter "e", shows the ratio of out of axis to the radius of pipe ($e=a/R$). The parameter "a" is calculated from the axis of the pipe (Fig.12). In the present study, four values of "e" are studied: $e=0, 0.25, 0.5, 0.75$.

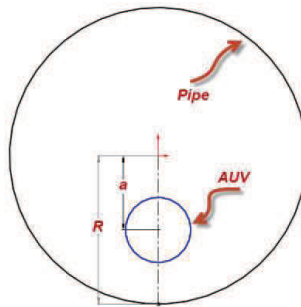


Figure 12: Out of axis movement of the AUV inside the pipe

In this part, the out of axis position of AUV in the pipe is analyzed. Here, the quarter-modeling can't be used. Therefore, the half domain modeling is utilized (Fig.13). Other conditions of modeling are that of Condition "A".

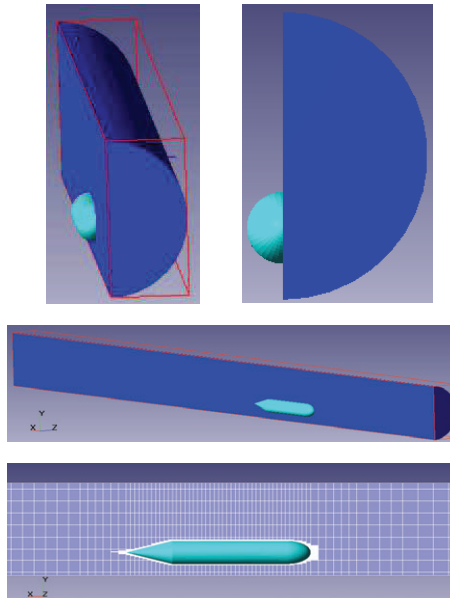
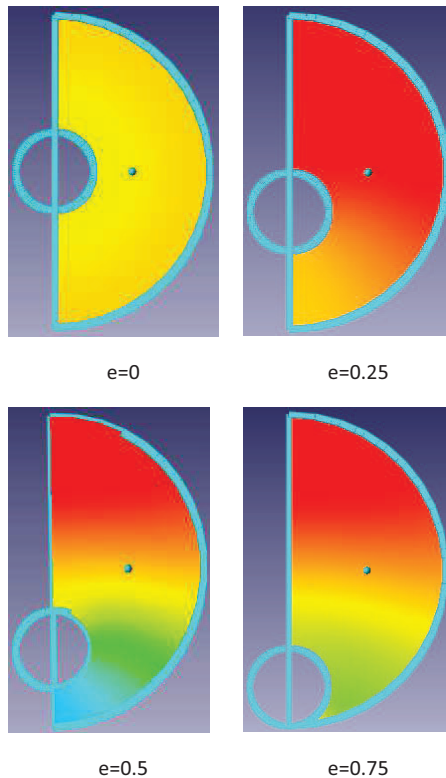


Figure 13: Out of axis modeling in Flow Vision

14-2-1- Pressure variation

In this case, there are two main factors: 1) The pipe wall effect of pipe. 2) The changes in flow speed. The pipe wall effect gives rise to boundary layer effects on the fluid, and a zero speed just on the wall. Fluid speed change appears due to the limited cross section area between the body and the pipe. The minor distance between the body and the pipe means minor cross section area (A_2). The flux of fluid is constant. Therefore the fluid speed should be increased. An increase in the speed, according to Bernoulli's law, is equivalent to a decrease in pressure. For little values of A_2 , the change in the fluid speed arising from the flux is more than the effect of boundary layer of the pipe wall. In the next stage, the variation in the resistance and lift force on the model (AUV) can be discussed. The resistance concerning conditions A, B and C are presented. The total resistance (R_t) is the summation of pressure resistance (R_p) and viscous resistance (R_f). Here, the main factor which changes the resistance, is pressure

resistance, because it is wholly depended upon the pressure distribution over the body. In each stage, the total and the pressure resistance are presented. The pressure variation in the condition of out of axis for the $d/D=4$ and speed of 3m/s for several amounts of "e" is shown in Fig.14. As the figure shows, at $e=0$, the pressure distribution is uniform and axis symmetric. Then the lift force is expected to be zero. By getting out of axis, the fluid velocity at the top of the body decreases and then, the pressure increases. At the low end of the body, these variations are inverse: the velocity increases and the pressure decreases. Therefore, there are visible changes in the lift force.



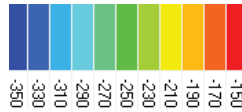
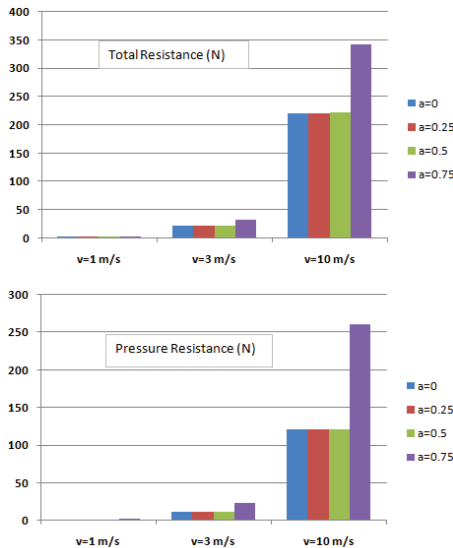


Figure 14: Pressure variation in several ratios of out of axis "e" for $d/D=4$ and $v=3\text{m/s}$.

The off-axis movement effect is studied for two amounts of $d/D=4$ and 12 , at the speeds of $1,3,10\text{m/s}$ for values of $e=0,0.25$ and 0.75 . The compared results are provided in the diagrams of Fig.15 and 16. For $d/D=4$, the variation of resistance in low and medium speeds is very little, but in $e=0.75$, it is considerable, as the body is very close to the pipe wall. The change in the lift force is very stiff owing to the asymmetric distribution of pressure, above and beneath the body. In every step of "e", an approximate 300 percent of increase is indicated, except in "e=0.75", which is different, because at this position, the body is tangent to the pipe wall. This results in different changes in the pressure domain.



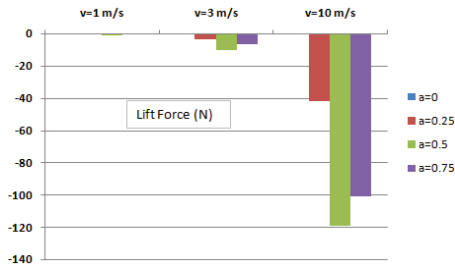
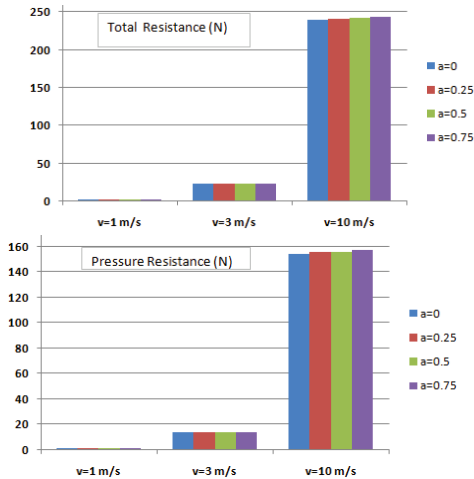


Figure 15: Diagram of hydrodynamic forces in $d/D=4$

As it was shown earlier, in $d/D=12$, a free stream at the center of the axis can be represented, but by getting out of the center of the pipe, the free stream is not valid. As before, the variation in the resistance of all speeds and all values of "e" is negligible. The change in the lift force is very stiff too. In every step of "e", an approximate 3-10 times increase in the lift force is observable.



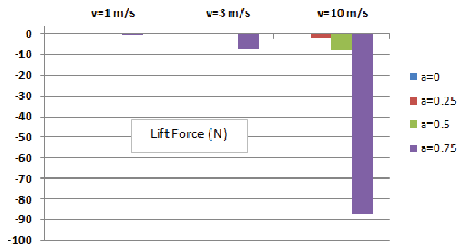


Figure 16: Diagram of hydrodynamic forces in $d/D=12$

It can be concluded that the out-of-axis movement has a little effect on the resistance, because the principal factor is the pressure resistance. The pressure resistance is a function of fluid velocity around the body, which is the function of the flux. By changing the location of AUV inside the pipe, the fluid flux remains constant. Therefore the changes in the pressure resistance and subsequently the total resistance is insignificant. The out-of-axis movement imposes a stiff variation in the lift force of the body. It is imperative to neutralize this negative lift force in order to prevent hitting to the wall and the consequent damage. For this purpose the hydroplanes of the AUV should be designed in such a way to produce inverse lift to neutralize the body lift force. That is, the hydroplanes should be so designed as to be able to produce such a big lift force. It is vital to keep the equilibrium and stability of an the AUV while operating inside a pipe.

14-2-2- Review 2

In conclusion, as regards the added resistance of an AUV moving inside a pipe, arising from the wall effect, the followings can be suggested:

- 1- The ratio of $d/D=12$ can be regarded for the determination of "the critical pipe diameter" which added resistance to be zero.
- 2- The ratio of $d/D < 1.41$ (or $A_2/A_1 < 1$) causes a stiff increase along with the resistance. Therefore, the values lower than this ratio are not recommended.
- 3- In the swim out launching system, for 533mm torpedoes, the minimum tube diameter of 750mm is recommended.

4- Pressure resistance has a crucial role in the total resistance of about 45-90 percent.

5- If there is an initial water speed inside the tube, the entrance length and the developed boundary layer have to be taken into account.

6- The fully developed condition of the stream- after the entrance length- provides about 5 percent decrease in the total resistance and a 10-20 percent decrease in the pressure resistance.

7- Out-of-axis movement of the AUV inside a pipe causes some change in the resistance force.

8-Out-of-axis movement of the AUV inside a pipe imposes a stiff increase in the lift force. Hydroplanes of AUV should be able to neutralize this body lift force.

Nomenclature

- A₁ Section area of the model
- A₂ Section area of water between model and pipe wall
- AUV Autonomous Underwater Vehicles
- C_f Frictional resistance coefficient
- C_p Pressure resistance coefficient
- C_t Total resistance coefficient
- CFD Computational Fluid Dynamics
- D Maximum diameter of AUV (m)
- d Diameter of pipe (m)
- IHSS Iranian Hydrodynamic Series of Submarines
- L Overall length of hull (m)
- l Overall length of pipe (m)
- P_{avg} Average Pressure of fluid between pipe and model (pa) (all pressures are relative = P-P_{atm})
- Re Reynolds number
- R_f Frictional resistance (N)
- R_p Pressure resistance (N)
- R_t Total resistance (N)
- R₀ Total resistance in free stream (without pipe wall stream) (N)

References

- 1- Unnikrishnan V. Painumgal, Blair Thornton, Tamaki Uray, Yoshiaki Nose, (2013), *Positioning and Control of an AUV inside a water pipeline for non-contact in-service Inspection*,
<http://www.mtsjournal.org/Papers/PDFs/130503-241.pdf>,
- 2- Majjid. M. Moghaddam, Alireza Hadi, (2005), *Control and Guidance of a Pipe Inspection Crawler (PIC)*, 22nd International Symposium on Automation and Robotics in Construction.
- 3- Harry T. Roman, Bruce A. Pellegrino, (1993), *Pipe Line Crawling Inspections: An Overview*, *IEEE Transactions on Energy Conversion*, Vol. 8, No.3, p.2196-2203.
- 4- Bahmanyar S, Yousefi-Koma A, Ghasemi H. (2011), *Development of a robot fish with experimental analysis*, 3; 7 (13) :49-65
URL http://www.ijmt.ir/browse.php?a_code=A-10-13-1&slc_lang=en&sid=1
- 5- M.Muramatsu, N. Namiki, R. Koyama, Y. Suga, (2000), *Autonomous Mobile Robot in Pipe for Piping Operations*, IEEE International Conference on Intelligent Robots and Systems, pp. 2166-2171.
- 6- Roh, S.G.; Ryew, S.M.; Yang, J.H.; Choi, H.R., (2001), *Actively steerable in-pipe inspection robots for underground urban gas pipelines*, IEEE International Conference on Robotics and Automation, vol.1, pp. 761 - 766.
- 7- Se-gon Roh, Hyouk Ryeol Choi, (2005), *Differential-drive in-pipe robot for moving inside urban gas pipelines*, IEEE Transactions on Robotics and Automation, Volume 21, Issue 1, pp. 1 - 17.
- 8- Dadkhah Khiabani E, M. Gharabaghi A R, Abedi K. (2013), *Investigation into the Effects of Buckle Arrestors on the Arresting of Dynamic Buckle Propagation in Pipelines*. 3; 8 (16) :19-31

URL http://www.ijmt.ir/browse.php?a_code=A-10-164-

[1&slc_lang=en&sid=1](#)

9- Okamoto, Jun, Julio C. Adamowskia, Marcos S.G. Tsuzukia, Fla vio Buiochia, Claudio S. Camerinib, (1999), *Autonomous system for oil pipelines inspection*, Mechatronics , Elsevier, pp. 731-743(13).

10- Mohammad Moonesun, Yuri Korol, Hosein Dalayeli, Asghar Mahdian, Anna Brazhko, Added resistance of an AUV moving inside a water pipeline due to wall proximity, International Journal of Maritime Technology, Vol.4/Summer2015 (1-9).

11- M. Moonesun, A. Mahdian, Y.M. Korol and A. Brazhko, Out of Axis Movement of an AUV inside a Water Pipeline, The Journal of Engineering Research (TJER), Vol. 14, No. 1, (2017) 10-22.

12- H.Najjaran, (2005), *IRC creating an underwater robotic vehicle to inspect inservice water mains*, Construction Innovation, vol. 10, no. 2.

13- Jorg Kalwa, (2012), *SeaCat AUV Inspects Water Supply Tunnel*, *Sea Technology Magazine* <http://www.seatechnology.com/features/2012/0812/seaCat.php>.

14- <http://pritamashutosh.wordpress.com/2014/02/06/flow-through-circular-conduits/>

15- M.S.Seif, (2012), *Fluid Mechanics*", Fadak publication, Iran.

16- *Flow Vision website*: <https://fv-tech.com/index.php/en/>

**More
Books!** 



yes
I want morebooks!

Buy your books fast and straightforward online - at one of the world's fastest growing online book stores! Environmentally sound due to Print-on-Demand technologies.

Buy your books online at
www.get-morebooks.com

Kaufen Sie Ihre Bücher schnell und unkompliziert online – auf einer der am schnellsten wachsenden Buchhandelsplattformen weltweit!
Dank Print-On-Demand umwelt- und ressourcenschonend produziert.

Bücher schneller online kaufen
www.morebooks.de

OmniScriptum Marketing DEU GmbH
Bahnhofstr. 28
D - 66111 Saarbrücken
Telefax: +49 681 93 81 567-9

info@omniscrptum.com
www.omniscrptum.com

OMNIScriptum 

